

# Photophysical Properties of Imine Metal Complexes

Thesis submitted for the degree of  
Doctor of Philosophy  
at the University of Leicester

by

Raissa Ibraimo Patia

Department of Chemistry  
University of Leicester

2018

# Title: Photophysical Properties of Imine Metal Complexes

Author: Raissa Ibraimo Patia

## ABSTRACT

A range of bis-cyclometallated Ir(III) complexes  $[\text{Ir}(\text{C}^{\wedge}\text{N})_2(\text{N}^{\wedge}\text{O})]$  containing different cyclometallated ( $\text{C}^{\wedge}\text{N}$ ) and ancillary ( $\text{N}^{\wedge}\text{O}$ ) ligands with *endo*- and *exocyclic* imine bonds have been synthesised. Additionally, Ir(III), Rh(III) and Ru(II) half-sandwich complexes with *exocyclic* imine bonds were also synthesised. All new compounds were characterised by  $^1\text{H}$  and  $^{13}\text{C}$  NMR spectroscopy, mass spectrometry and some compounds have been structurally characterised by X-ray crystallography. The photophysical properties of the complexes were also studied.

Chapter one introduces luminescent metal complexes particularly cyclometallated complexes of Ir(III) and some of their applications. Chapter two introduces the phenomenon of Aggregation Induced Emission (AIE) and Enhanced Phosphorescence in the Solid State (EPESS). Photophysical and computational studies of cyclometallated Ir(III) complexes  $[\text{Ir}(\text{C}^{\wedge}\text{N})_2(\text{N}^{\wedge}\text{O})]$  show EPESS and it arises due to distortion of the  $\text{N}^{\wedge}\text{O}$  chelate ring in the triplet excited state; not  $\pi$ -stacking nor restricted rotation as proposed previously.

Chapter three describes isomeric complexes containing a 5-membered chelate  $\text{N}^{\wedge}\text{O}$  ligand with an *exocyclic* imine. These do not show EPESS instead they undergo *trans-cis* photoisomerisation of the  $\text{C}=\text{N}$  bond. The isomerisation can be reversed thermally in some cases suggesting the complexes have potential applications as photoswitches. DFT studies suggest that the *trans* isomer is the most stable which agrees with the experimental data.

Chapter four describes the syntheses of Ir(III), Rh(III) and Ru(II) half-sandwich complexes with 5-membered chelating anionic  $\text{N}^{\wedge}\text{O}$  or neutral  $\text{N}^{\wedge}\text{N}$  ligands which have *exocyclic*  $\text{C}=\text{N}$  bonds. The nature of the ligand, the imine substituent and the metal centre all affect the photoisomerisation.

## Acknowledgements

Firstly, I would like to thank my supervisor, Prof D. L. Davies for his help, motivation, patience and guidance throughout this project. His support during my difficult times has been invaluable and I could have not asked for a more supportive and understanding supervisor.

I also want to thank Dr Barbara Villa-Marcos for the incredible support and friendship that has blossomed from my MChem year. Her presence in the department and our chats in the labs helped me be persistent and a better scientist. Her friendship has been invaluable during my research. I also want to thank Dr. Charles Ellul for his kind help and support while part of the DLD group.

My sincere thanks goes to Dr M. P. Lowe for his time, and assistance in the use of the fluorimeter. I would also like to thank our collaborators in the University of British Columbia, Vancouver, Prof. M. Wolf and Ashley Howarth and in the Università della Basilicata, Prof F. Lelj for the computational studies.

I would like to thank Dr G. A. Griffith for 2D NMR spectra, Mr. M. Lee for the mass spectra and Mr K. Singh for the X-Ray structure determinations.

I would also like to thank everyone I have worked with in the old inorganic lab on the first floor and the colleagues on the second floor lab that accommodated for us. I want to thank my inorganic ‘Chem Girls’ Mona, Amina and Martyna for being there for me in my hard and difficult days. I hope to carry on with our friendship even after we graduate. I also want to acknowledge the friends that I made during my first few years as an undergraduate chemist Zaheera, Aysha and Anand – who are still around even after several years!

My Pai and Mãe for being caring, kind and encouraging me to carry on studying throughout all the years of struggle. My crazy sisters Sana and Mariah who make me laugh and always understand my brain because we are the Power of Three! My mother in law who has been supportive and so generous!

I owe my loving and funny husband Riaz *ibn* Usman Patia a big thank you for the continuous encouragement when I thought I could not do it and for dragging me to the lab to complete my studies. His patience has been invaluable to me, and even after the loss of our dear daughter that I miss so much, he always told me to carry on.

*To Mushafai' & Idrees*

## Statement

This thesis is based on work conducted by the author in the Department of Chemistry at the University of Leicester, during the period between October 2013 and September 2017. All X-ray Crystallography was performed by Mr. Kuldip Singh.

Thanks go to Prof M. O. Wolf and its group and Prof Lej for collaborating on the work described in Chapter 2. Thanks to Ashlee Howarth for the synthesis of complexes and characterisation of complexes **2.24a-Ph** and **2.24b-Ph**.

Thanks to Prof Lej who performed DFT calculations on compounds mentioned in Chapter 3 and Chapter 4.

All the work described in the thesis is original unless otherwise stated. This work is not being presented for any other degree.

Signed: \_\_\_\_\_

Date: \_\_\_\_\_

*Raissa Ibraimo Patia*

## Abbreviations

### NMR

bd	broad doublet
bs	broad singlet
d	doublet
dd	doublet of doublets
ddd	doublet of doublet of doublets
m	multiplet
s	singlet
sept	septet
t	triplet
td	triplet of doublets
COSY	correlated spectroscopy
HSQC	heteronuclear single quantum correlation
NMR	nuclear magnetic resonance
NOE	nuclear Overhauser effect
NOESY	nuclear Overhauser effect spectroscopy
TOCSY	total correlation spectroscopy
ppm	parts per million
$\delta$	delta (NMR Chemical Shift)

### Other Techniques

ASAP	atmospheric solids analysis probe
DFT	density functional theory
ES-MS	electrospray mass spectrometry
FAB-MS	fast atom bombardment mass spectrometry
IR	infra-red
TD-DFT	time dependent-density functional theory

### Others

<i>fac</i>	facial
<i>mer</i>	meridional
h	hour
ISC	intersystem crossing

HOMO	highest occupied molecular orbital
LC	ligand centred
LLCT	ligand to ligand charge transfer
LUMO	lowest unoccupied molecular orbital
LEEC	light emitting electrochemical cells
MC	metal centred
MLCT	metal to ligand charge transfer
min	minute
ml	millilitre
MW	microwave
OLED	organic light emitting diode
PBS	phosphate-buffered saline
PMMA	poly(methyl methacrylate)
PSS	photostationary state
SOC	spin-orbit coupling
sh	shoulder

### **Chemical**

acac	anion of pentane-2,4-dione
bipy	2,2'-bipyridine
Cp*	Pentamethylcyclopentadienyl anion
Cym	cymene
DCM	dichloromethane
DMSO	dimethylsulfoxide
dppi	1,2-diphenylpyreno[4,5-d]imidazole
Dipp	2,6-diisopropyl phenyl
<sup>i</sup> Pr	isopropyl
Mes	mesityl
phen	phenanthroline
Ph	phenyl
ppy	2-phenylpyridine
ppz	1-phenylpyrazole
THF	tetrahydrofuran

TMS	trimethylsilane
<i>t</i> Bu	<i>t</i> -butyl

## Table of Contents

<b>Chapter 1: General Introduction .....</b>	<b>1</b>
1.1 Luminescence.....	1
1.2 Luminescent d <sup>6</sup> Transition Metals .....	2
1.3 Cyclometallated Ir(III) Complexes .....	4
1.3.1 Tris-Cyclometallated Ir(III) Complexes [Ir(C <sup>^</sup> N) <sub>3</sub> ] .....	5
1.3.2 Heteroleptic Bis-Cyclometallated Ir(III) Complexes .....	7
1.3.3 Tuning Emission in [Ir(C <sup>^</sup> N) <sub>2</sub> (X <sup>^</sup> Y)] <sup>n+</sup> (n = 0, +1).....	10
1.4 Applications of Ir(III) Complexes.....	18
1.5 Overview .....	24
1.6 Bibliography.....	25
<b>Chapter 2: Enhanced Phosphorescence Emission in the Solid State (EPESS) in Ir(III) complexes .....</b>	<b>31</b>
2.1 Aggregation-Induced Emission.....	31
2.1.1 Restricted Intramolecular Rotation (RIR) .....	32
2.1.2 Restricted Intramolecular Vibration (RIV) .....	32
2.1.3 Restricted Intramolecular Motions (RIM).....	33
2.1.4 Aggregation Induced Emission in Transition Metal Complexes .....	34
2.2 Results and Discussion.....	42
2.2.1 Synthesis and Characterisation of [Ir(C <sup>^</sup> N) <sub>2</sub> (N <sup>^</sup> O)] (N <sup>^</sup> O = salicylimine) ...	42
2.2.2 Photophysical Investigation of [Ir(C <sup>^</sup> N) <sub>2</sub> (N <sup>^</sup> O)] (N <sup>^</sup> O = salicylimine) .....	54
2.2.3 Computational Studies.....	59
2.2.4 Conclusion .....	63
2.3 Bibliography.....	64
2.4 Appendix .....	68

<b>Chapter 3: Bis-Cyclometallated Ir(III) Complexes with exocyclic Imine Bonds....</b>	<b>70</b>
3.1 Introduction .....	70
3.1.1 Photoisomerisation of C=C bonds.....	70
3.1.2 Photoisomerisation of N=N bonds .....	75
3.1.3 Photoisomerisation of C=N bonds.....	80
3.2 Results and Discussion.....	86
3.2.1 Synthesis and Characterisation of Exocyclic Imine Complexes [ $\text{Ir}(\text{C}^{\wedge}\text{N})_2(\text{N}^{\wedge}\text{O})$ ] .....	86
3.2.3 Photophysical Properties of [ $\text{Ir}(\text{C}^{\wedge}\text{N})_2(\text{N}^{\wedge}\text{O})$ ] Complexes.....	98
3.2.4 Computational Studies.....	100
3.2.4 Conclusion.....	103
3.3 Bibliography.....	105
3.4 Appendix .....	109
<b>Chapter 4: Photoisomerisation in Half-Sandwich Complexes .....</b>	<b>114</b>
4.1 Introduction .....	114
4.1.1 Photoisomerisation of N=N Bonds in Half-Sandwich Complexes .....	114
4.1.2 Photoisomerisation in C=N Bonds in Half-Sandwich Complexes.....	117
4.2 Results and Discussion.....	120
4.2.1 Synthesis, Characterisation and Photoisomerisation Studies of $\text{N}^{\wedge}\text{O}$ Complexes .....	120
4.2.2 Synthesis, Characterisation and Photoisomerisation Studies of $\text{N}^{\wedge}\text{N}$ Complexes .....	131
4.2.3 Computational Studies.....	134
4.2.4 Conclusion.....	136
4.3 Bibliography.....	140
<b>Chapter 5: Conclusions and Future Work .....</b>	<b>142</b>

<b>Chapter 6: Experimental.....</b>	<b>144</b>
6.1 General information and materials.....	144
6.2 Experimental procedures for Chapter 2 .....	147
General procedure for synthesis of $[\text{Ir}(\text{C}^{\wedge}\text{N})_2\text{N}^{\wedge}\text{O}]$ ( $\text{N}^{\wedge}\text{O}$ = salicylimine) .....	147
Complex <b>2.24a-<sup>i</sup>Pr</b> .....	147
Complex <b>2.24a-Mes</b> .....	148
Complex <b>2.24a-Dipp</b> .....	149
Complex <b>2.24b-<sup>i</sup>Pr</b> .....	150
Complex <b>2.24b-Mes</b> .....	151
Complex <b>2.24b-Dipp</b> .....	152
6.3 Experimental procedures for Chapter 3 .....	153
General procedure for synthesis of $[\text{Ir}(\text{C}^{\wedge}\text{N})_2(\text{N}^{\wedge}\text{O})]$ ( $\text{N}^{\wedge}\text{O}$ = <i>exocyclic imine</i> )...	153
Complex <b>3.27a-Ph</b> .....	153
Complex <b>3.27a-Mes</b> .....	155
Complex <b>3.27a-Anisyl</b> .....	156
Complex <b>3.27a-C<sub>6</sub>F<sub>5</sub></b> .....	157
Complex <b>3.27a-Cinnamyl</b> .....	158
Complex <b>3.27b-Ph</b> .....	159
Complex <b>3.27b-Mes</b> .....	161
Complex <b>3.27b-Anisyl</b> .....	162
Complex <b>3.27b-C<sub>6</sub>F<sub>5</sub></b> .....	163
Complex <b>3.27b-Cinnamyl</b> .....	164
6.4 Experimental procedures for Chapter 4 .....	165
General Procedure for the Synthesis of Half-sandwich complexes with $\text{N}^{\wedge}\text{O}$	
Ligands .....	165
Complex <b>4.15a-Mes</b> .....	166

Complex <b>4.15b-Mes</b> .....	167
Complex <b>4.15c-Mes</b> .....	168
Complex <b>4.15a-Anisyl</b> .....	169
Complex <b>4.15b-Anisyl</b> .....	170
Complex <b>4.15c-Anisyl</b> .....	171
Complex <b>4.15a-Cinnamyl</b> .....	172
General Procedure for the synthesis of half-sandwich complexes with N <sup>^</sup> N ligands. .....	172
Complex <b>4.16a-Mes</b> .....	173
Complex <b>4.16c-Mes</b> .....	174
Complex <b>4.16a-Anisyl</b> .....	175
Complex <b>4.16c-Anisyl</b> .....	176
6.5 Bibliography.....	177
<b>Crystallography Data for Chapter 2:.....</b>	<b>179</b>
Crystal data and structure refinement for <b>2.24a-iPr</b> .....	179
Crystal data and structure refinement for <b>2.24a-Dipp</b> .....	180
Crystal data and structure refinement for <b>2.24b-Dipp</b> .....	181
<b>Crystallography Data for Chapter 3:.....</b>	<b>182</b>
Crystal data and structure refinement for <b>3.27a-Ph</b> .....	182
Crystal data and structure refinement for <b>3.27b-Ph</b> .....	183
Crystal data and structure refinement for <b>3.27a-Mes</b> .....	184
Crystal data and structure refinement for <b>3.27b-Mes</b> .....	185
Crystal data and structure refinement for <b>3.27b-Anisyl</b> .....	186
<b>Crystallography Data for Chapter 4:.....</b>	<b>187</b>
Crystal data and structure refinement for <i>trans</i> - <b>4.15a-Cinnamyl</b> .....	187

Crystal data and structure refinement for <i>trans</i> - <b>4.15c-Mes</b> .....	188
Crystal data and structure refinement for <i>cis</i> - <b>4.15c-Mes</b> .....	189
Crystal data and structure refinement for <i>trans</i> - <b>4.15c-Anisyl</b> .....	190
Crystal data and structure refinement for <i>cis</i> - <b>4.15c-Anisyl</b> .....	191
<b>Postgraduate Activities</b> .....	<b>192</b>
Internal Seminars .....	192
Internal Symposia .....	192
External Symposia .....	193

## Chapter 1: General Introduction

### 1.1 Luminescence

Luminescence is the emission of light from electronically excited states. Depending on the nature of the excited state, emission can result in fluorescence or phosphorescence. These processes can be illustrated by using the Jablonski diagram (Figure 1.1).

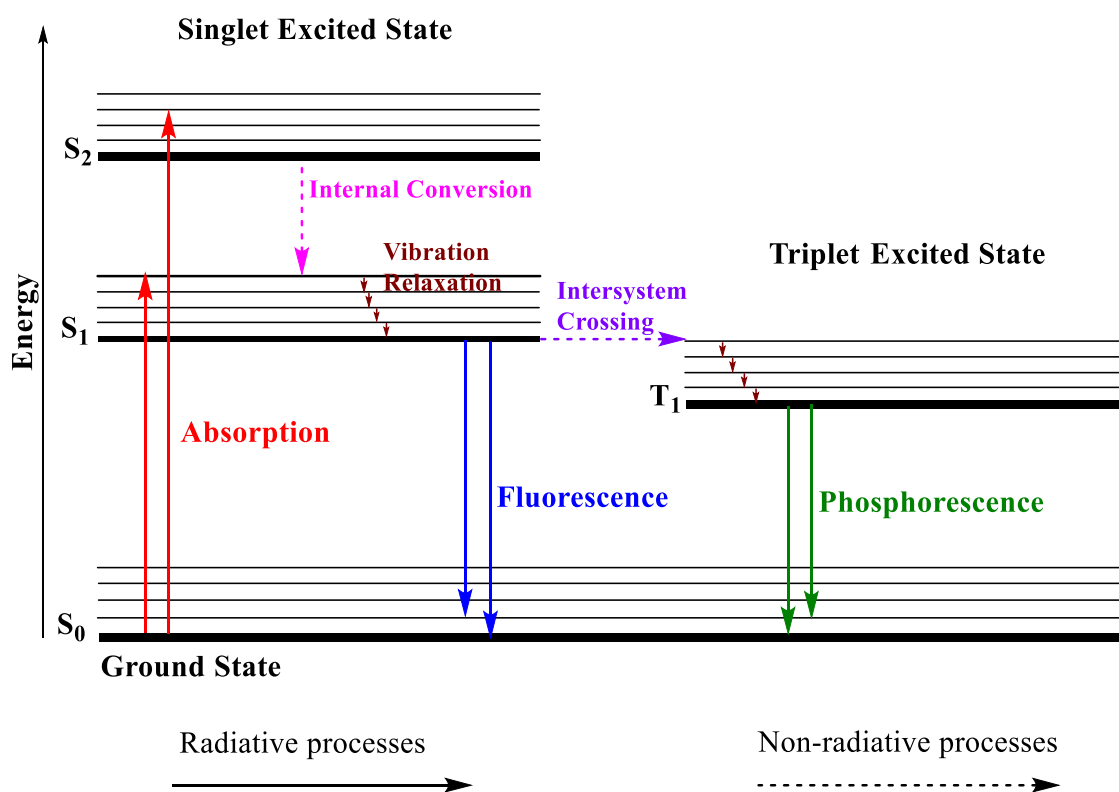


**Figure 1.1:** The Jablonski diagram.

The diagram shows two types of processes: radiative processes and non-radiative processes. The radiative processes include: absorption, fluorescence and phosphorescence. The first process is the absorbance of a photon by a molecule. A molecule is excited from the ground state to an excited state. Fluorescence is an emission process and is most often observed between the first excited state and the ground state for any particular molecule. It is an emission from a *singlet* excited state where the excited electron is paired with an electron in the ground state, therefore it is spin-allowed. This photon emission process occurs rapidly with its typical lifetime being between  $10^{-9}$  -  $10^{-7}$  seconds. On the other hand, phosphorescence is the emission from a *triplet* excited state to the ground state. The excited electron has the same spin orientation as the electron in the ground state orbital therefore, the return to the ground

state is *spin-forbidden* and the rate of emission is slow, resulting in longer lifetimes ( $10^{-3}$  to 1 s). The triplet excited state is long-lived so it has a far greater chance of being deactivated than the singlet excited state. This is because there are some deactivation (quenching) processes that compete with phosphorescence and can prevent the long-lived emission from occurring. Examples of these processes are:<sup>1,2</sup>

- Internal Conversion is an intramolecular process by which a molecule passes to a lower energy electronic state *without* emission of radiation. If vibrational energy levels strongly overlap electronic energy levels, a possibility exists that the excited electron can transition from a vibrational level in one electronic state to another vibrational level in a lower electronic state. Internal conversion can occur because of the overlap of the vibrational and electronic energy states.
- Vibrational Relaxation occurs when excess vibrational energy is lost in collisions between molecules of excited species and the solvent. Since this is a very fast transition, it is extremely likely to occur immediately following absorbance. This relaxation occurs between vibrational levels. So, generally, electrons will not change from one electronic level to another through this method.
- Intersystem Crossing (ISC) is a *forbidden* transition and is when the spin of the excited electron is flipped and changes spin multiplicity from an excited singlet state to an excited triplet state.

## 1.2 Luminescent $d^6$ Transition Metals

To assist in an explanation of luminescence in  $d^6$  transition metal complexes, Figure 1.2 shows the localised molecular orbital model of the excited states. This figure shows the orbitals and spectroscopic states diagram for a low spin  $d^6$  octahedral complex ( $ML_6$ ).<sup>3,4</sup> Transition metal complexes have partially filled  $d$ -orbitals and the order and occupancy of these orbitals determine their emissive properties. The octahedral crystal field splits the five degenerate  $d$  orbitals by delta ( $\Delta$ ) into a triply degenerate  $t$  level and a doubly degenerate  $e$  level. This is due to the two  $e$  orbitals that are directly pointing towards the six ligands and the remaining  $t_2$  orbitals point between the ligands.<sup>3</sup> The consequences of this splitting are due to the electrostatic interactions between the filled ligand orbitals and electrons placed in different  $d$  orbitals, therefore an electron placed in an  $e$  orbital has higher energy than one placed in a  $t_2$  orbital. This is important because it is determined by the crystal field strength of the ligands and the central metal ion. All spins are paired therefore the ground state ( $S_0$ ) is a singlet. The lowest excited states are

derived from promoting an electron to one of the unoccupied orbitals. The state classification is determined by the original and final orbitals.

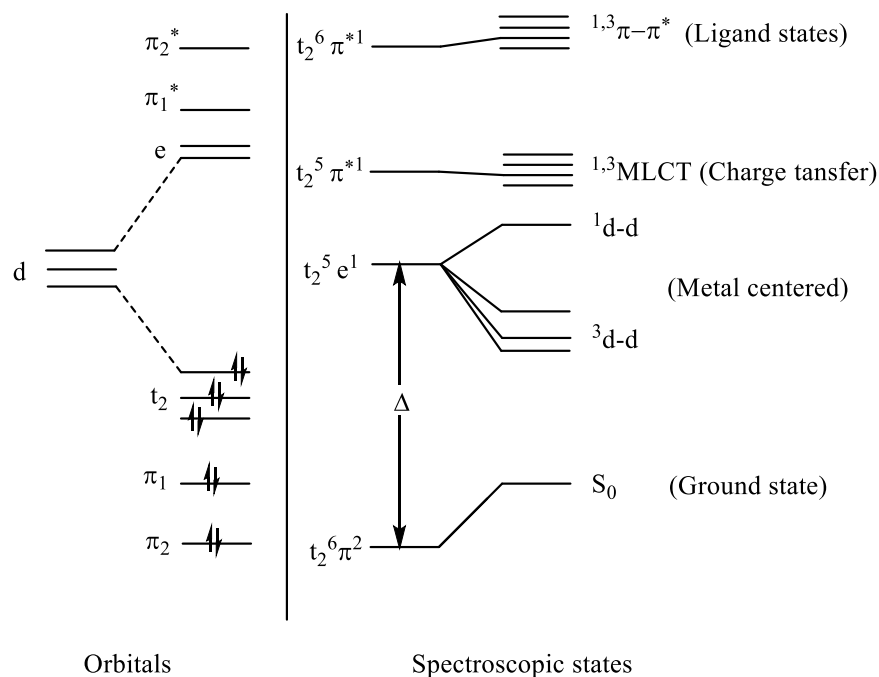


**Figure 1.2:** Simplified orbital and state diagrams for  $d^6$  metal in an octahedral environment.<sup>3</sup>

There are three types of excited states:<sup>3</sup>

(a) Metal centred (MC) d-d excited states arise from promoting a bonding electron from the  $t_{2g}$  level to the  $e_g^*$  level and give rise to weak absorption bands and therefore have small extinction coefficients. The d-d states need to be above the emitting levels (LC and MLCT) to prevent thermal excitation that could lead to excited state decay and photochemical instability.

(b) Ligand centred (LC)  $\pi-\pi^*$  states derive from promoting a bonding  $\pi$ -electron to an antibonding  $\pi^*$  level. These transitions are often very intense and are localised on the ligands.

(c) Metal-to-ligand-charge transfer (MLCT) states involve promoting an electron from a metal orbital to a ligand orbital or ligand to metal charge transfer states (LMCT) which involve promoting an electron from a ligand to a metal orbital. These transitions have significant absorptions in the visible region with high extinction coefficients.<sup>3,4</sup>

For a metal complex to be luminescent, it has to meet certain criteria:<sup>3,5</sup>

- (i) the lowest excited state must be either a charge transfer (CT) or ligand  $\pi$ - $\pi^*$ , this avoids photochemical instability associated with unstable d-d excited states,
- (ii) spin-orbit coupling must be high to permit radiative decay to compete more effectively with non-radiative decay
- (iii) the crystal field must be strong enough to raise the d-d state above the MLCT state, to avoid thermal excitation to a d-d state.

The quantum efficiency of transition metal complexes is dependent on the radiative and non-radiative relaxation of the excited states. Non-radiative relaxation occurs on a much faster time scale than radiative transitions.<sup>3</sup> The relative levels of the MLCT,  $\pi$ - $\pi^*$  and d-d states also determine the sensitivity of excited state decay times to temperature. If the d-d states are close to the MLCT or  $\pi$ - $\pi^*$  level, then they are thermally accessible. By increasing the temperature, the lifetime decreases due to the thermal population of the d-d states which is followed by rapid non-radiative decay.<sup>3</sup> Therefore, the d-d states need to be thermally inaccessible from the emitting MLCT or  $\pi$ - $\pi^*$  states. For example, in complex  $[\text{Ru}(\text{bipy})_3]^{2+}$  (**1.1**) (Figure 1.3) the Ru  $t_{2g}$  orbitals are the highest occupied molecular orbitals (HOMO) and the lowest unoccupied molecular orbital (LUMO) resides on the bipy ligand<sup>6</sup> with MLCT as the lowest electronic transition.<sup>7</sup>

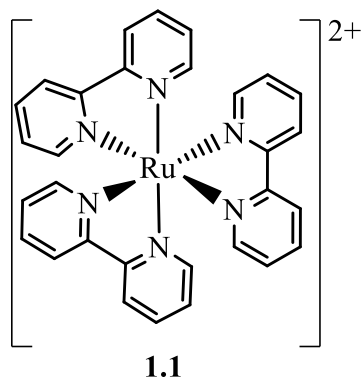


**Figure 1.3:** Luminescent  $[\text{Ru}(\text{bipy})_3]^{2+}$  complex.

### 1.3 Cyclometallated Ir(III) Complexes

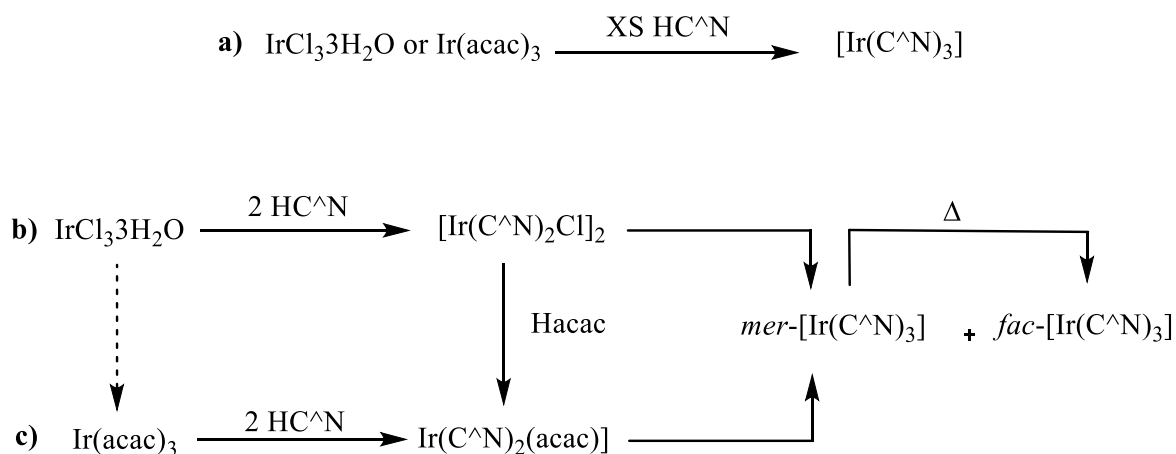
The last decade has seen a rapid increase in the number of publications regarding luminescent cyclometallated Ir(III) complexes. These complexes have been used in a range of applications including OLEDs<sup>8-12</sup>, LEECs<sup>13-16</sup>, solar cells<sup>17</sup>, luminescent sensors<sup>18-22</sup>, photocatalysis<sup>23</sup> and bioimaging.<sup>24-28</sup> Cyclometallated Ir(III) complexes are ideal for these applications due to high photo-luminescent quantum yields and ability to tune the emission properties by synthetic modifications.<sup>29</sup> There are two main types

of tris-bidentate Ir(III) complexes in the literature; homoleptic  $[\text{Ir}(\text{C}^{\wedge}\text{N})_3]$  and  $[\text{Ir}(\text{X}^{\wedge}\text{Y})_3]$  and heteroleptic  $[\text{Ir}(\text{C}^{\wedge}\text{N})_2(\text{X}^{\wedge}\text{Y})]$  and  $[\text{Ir}(\text{C}^{\wedge}\text{N})(\text{X}^{\wedge}\text{Y})_2]$ . However, there are not many examples of the type  $[\text{Ir}(\text{C}^{\wedge}\text{N})(\text{X}^{\wedge}\text{Y})_2]$ , and  $[\text{Ir}(\text{X}^{\wedge}\text{Y})_3]$  due to the difficulty in their synthesis and purification. Hence, the majority of known luminescent Ir(III) complexes are  $[\text{Ir}(\text{C}^{\wedge}\text{N})_3]$  and  $[\text{Ir}(\text{C}^{\wedge}\text{N})_2(\text{X}^{\wedge}\text{Y})]$ .

### 1.3.1 Tris-Cyclometallated Ir(III) Complexes $[\text{Ir}(\text{C}^{\wedge}\text{N})_3]$

Tris-cyclometallated Ir(III) complexes  $[\text{Ir}(\text{C}^{\wedge}\text{N})_3]$  can be prepared directly by reacting either  $\text{IrCl}_3 \cdot 3\text{H}_2\text{O}$ <sup>30, 31</sup> or  $\text{Ir}(\text{acac})_3$ <sup>30, 32</sup> with an excess of the cyclometallating ligand in glycerol at reflux temperatures (Scheme 1.1a) or in two steps by isolation of the intermediate bis-cyclometallated complexes  $[\text{Ir}(\text{C}^{\wedge}\text{N})_2(\text{acac})]$ <sup>33</sup> or  $[\text{Ir}(\text{C}^{\wedge}\text{N})_2\mu\text{-Cl}]_2$ <sup>34, 35</sup> (Scheme 1.1b and 1.1c). The dimers  $[\text{Ir}(\text{C}^{\wedge}\text{N})_2\mu\text{-Cl}]_2$  are easily prepared in high yields (> 85%) from  $\text{IrCl}_3 \cdot 3\text{H}_2\text{O}$ ,<sup>35, 36</sup> and can be reacted with Hacac to form  $[\text{Ir}(\text{C}^{\wedge}\text{N})_2(\text{acac})]$ .<sup>37, 38</sup> This route is much more efficient than going *via*  $[\text{Ir}(\text{acac})_3]$  which itself is prepared from  $\text{IrCl}_3 \cdot 3\text{H}_2\text{O}$  but only in low yield (< 20%).<sup>39</sup> Preparing  $[\text{Ir}(\text{C}^{\wedge}\text{N})_3]$  in two steps from  $\text{IrCl}_3 \cdot 3\text{H}_2\text{O}$  gives higher yields (75-80%) in comparison to the one step method (45-60%).<sup>31</sup> Also, the one pot method uses a much larger excess of the cyclometallating ligand as solvent (up to 60 times)<sup>31</sup> compared with only 2-3 times excess in each step during the two step procedure.<sup>37, 38</sup> Hence, the two-step method starting from  $\text{IrCl}_3 \cdot 3\text{H}_2\text{O}$  is the preferred method (Scheme 1.1b).<sup>33</sup>

Tris-cyclometallated Ir(III) complexes  $[\text{Ir}(\text{C}^{\wedge}\text{N})_3]$  can adopt either a facial (*fac*) or meridional (*mer*) structure which have all N,N-*cis* and one N,N-*trans* configuration, respectively (Figure 1.4). The *fac* isomer forms preferentially at high temperatures (> 200 °C) and the *mer* isomer forms at lower temperatures (< 150 °C).<sup>33</sup> It was also found that at high temperatures the *mer* isomer converts in to the *fac* isomer, suggesting that the *fac* isomer is the thermodynamic product and the *mer* isomer is the kinetic product. Additionally, hydroxy-bridged dimers  $[\text{Ir}(\text{C}^{\wedge}\text{N})_2\mu\text{-(OH)}]_2$ , have been used for the selective synthesis of *mer*- $[\text{Ir}(\text{C}^{\wedge}\text{N})_3]$  complexes at 100 °C.<sup>40</sup>



**Scheme 1.1:** Synthetic routes of tris- and bis-cyclometallated Ir(III) complexes.

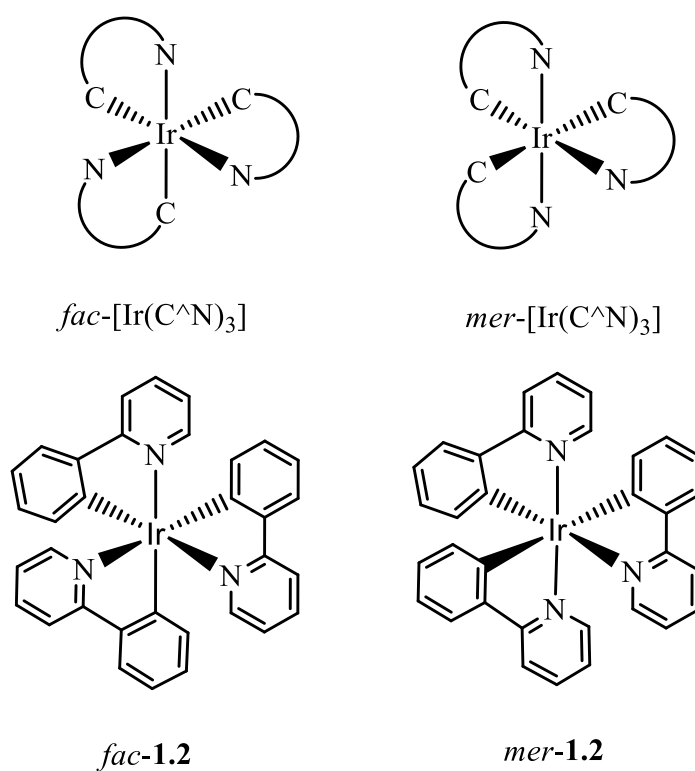


**Figure 1.4:** Structure of *fac*- and *mer*-1.2.

Watts and co-workers<sup>41</sup> were the first group to synthesise *fac*- $[\text{Ir}(\text{ppy})_3]$  (**1.2**), then later, Konno and Sasaki<sup>42</sup> used microwave irradiation to synthesise *fac*-**1.2** from  $\text{IrCl}_3 \cdot 3\text{H}_2\text{O}$  with a large excess of Hppy ligand. Thompson described the photophysical and electrochemical differences between *fac* and *mer* isomers; (i) the *mer* isomer can easily observe a one-electron oxidation in comparison to the *fac* isomer (ii) the *mer* isomer is the kinetically favoured product so it can be converted thermally to the *fac* isomer and (iii) the *mer* isomer has a broader and more red emission in comparison to the *fac*

isomer.<sup>33</sup> Marian and co-workers carried out computational studies to investigate the photophysics of *fac*-**1.2**.<sup>43</sup> Their findings showed that the electronic ground state of *fac*-**1.2** is C<sub>3</sub> symmetric, but in the singlet excited state the pseudo-Jahn-Teller interaction leads to a distortion and breaking of the C<sub>3</sub> symmetry.<sup>43</sup> The studies also showed that the HOMO resides on the Ir and Ir-C  $\sigma$ -bond while the LUMO resides on the pyridyl ring of ppy ligand. Substantial electronic spin-orbit coupling and a small energy gap make ISC an ultrafast process in *fac*-**1.2**; the rate of ISC (S<sub>1</sub> to T<sub>1</sub>) was calculated to be  $k_{\text{ISC}} = 6.9 \times 10^{12} \text{ s}^{-1}$  hence, fluorescence ( $1 \times 10^6 \text{ s}^{-1}$ ) could not compete with the much faster ISC, therefore a phosphorescence is observed rather than fluorescence.<sup>43</sup> These results agree with previous experimental studies of a sub-picosecond ISC process and a triplet quantum yield close to unity<sup>44, 45</sup> and that the emission of tris-cyclometallated complexes comes from a mixture of ligand centred,<sup>3</sup> ( $\pi$ - $\pi^*$ ) and MLCT excited states.<sup>46</sup>

47

### 1.3.2 Heteroleptic Bis-Cyclometallated Ir(III) Complexes

Thompson and co-workers were the first group to use *fac*-**1.2** as a green phosphorescent dopant in OLED's.<sup>12</sup> This led to an interest in developing new cyclometallated Ir(III) complexes. Thereafter, different bis-cyclometallated Ir(III) complexes (**1.3**) (Figure 1.5) were developed with two cyclometallated C<sup>^</sup>N ligands and one X<sup>^</sup>Y ancillary ligand which have useful photophysical properties such as: (i) large Stokes shift, (ii) high spin-orbit coupling, (iii) long lifetimes, and (iv) high quantum yields.

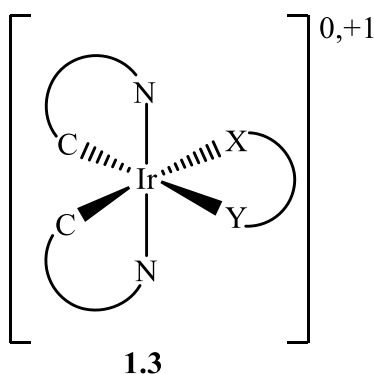
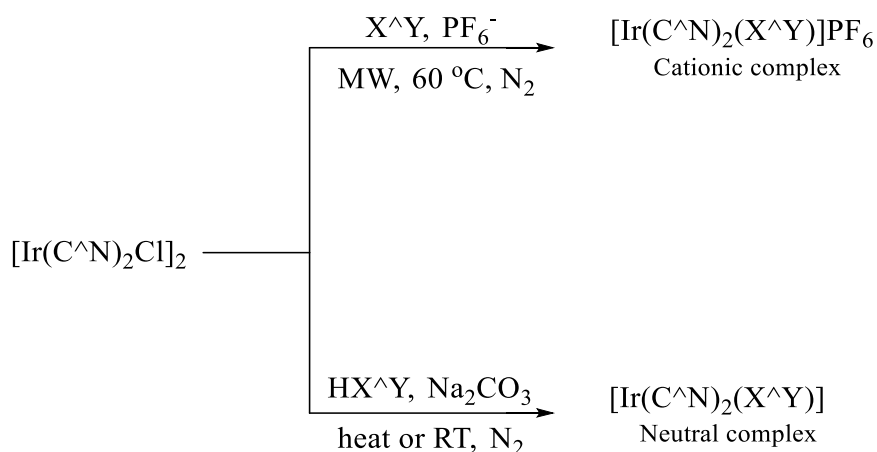


**Figure 1.5:** Structure of bis-cyclometallated Ir(III) complex with general formula



The most common luminescent Ir(III) complexes have two C<sup>^</sup>N ligands and one X<sup>^</sup>Y ancillary ligand. A neutral X<sup>^</sup>Y ligand gives a cationic complex,  $[\text{Ir}(\text{C}^{\wedge}\text{N})_2(\text{X}^{\wedge}\text{Y})]^+$ , whilst an anionic X<sup>^</sup>Y ligand gives a neutral complex  $[\text{Ir}(\text{C}^{\wedge}\text{N})_2(\text{X}^{\wedge}\text{Y})]$ . Dimeric





**Scheme 1.3:** a) Microwave method for the synthesis of  $[\text{Ir}(\text{C}^{\wedge}\text{N})_2\mu\text{-Cl}]_2$  dimers; b) Scheme showing the synthesis of  $[\text{Ir}(\text{C}^{\wedge}\text{N})_2(\text{X}^{\wedge}\text{Y})][\text{PF}_6]$  and  $[\text{Ir}(\text{C}^{\wedge}\text{N})_2(\text{X}^{\wedge}\text{Y})]$ .

In theory, complexes  $[\text{Ir}(\text{C}^{\wedge}\text{N})_2(\text{X}^{\wedge}\text{Y})]^{n+}$  ( $n = 0, +1$ ) can exist in three different geometrical isomers (**I**, **II** or **III**) (Figure 1.6a). However, the vast majority of reported complexes have structure (**I**).<sup>18, 19, 25</sup> In this case, the two carbon atoms are *cis* to each other and the nitrogen atoms are *trans* to each other and the complex exists as two optical isomers:  $\Lambda$  and  $\Delta$  (Figure 1.6b).

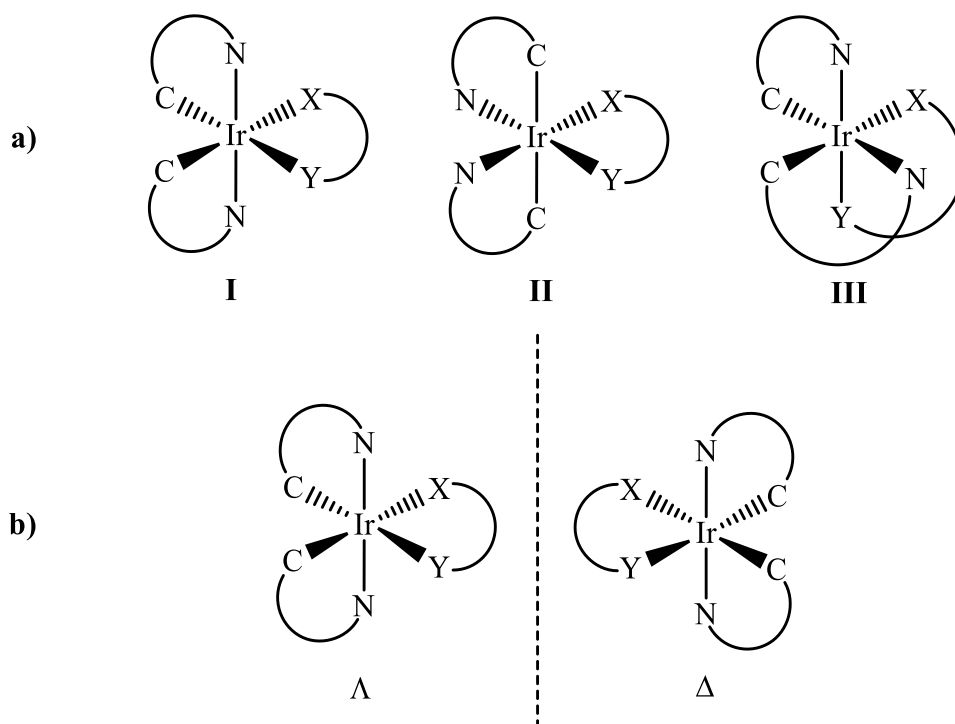


**Figure 1.6:** a) Geometrical isomers of  $[\text{Ir}(\text{C}^{\wedge}\text{N})_2(\text{X}^{\wedge}\text{Y})]$ ; b) optical isomers of structure **I**.

### 1.3.3 Tuning Emission in $[\text{Ir}(\text{C}^{\wedge}\text{N})_2(\text{X}^{\wedge}\text{Y})]^{n+}$ ( $n = 0, +1$ )

Changing the cyclometallating  $\text{C}^{\wedge}\text{N}$  and/or  $\text{X}^{\wedge}\text{Y}$  ligands can change the emission wavelength over the whole visible spectrum from blue to red and even into the near infrared.<sup>51-54</sup> This can be achieved by changing the donor atoms or changing the degree of conjugation on the ligands<sup>55, 56</sup> or by adding different substituents on the ligand.<sup>36</sup> Examples are discussed below starting with changing  $\text{C}^{\wedge}\text{N}$  ligands then moving on to changing  $\text{X}^{\wedge}\text{Y}$  ligands.

Figure 1.7 shows the tuning in emission by changing the cyclometallating  $\text{C}^{\wedge}\text{N}$  ligand in complexes **1.4a-l**.<sup>37, 57 58</sup> Adding the fused benzene to **1.4a** leads to a slight red shift in emission from 520 nm to 525 nm for complex **1.4a** and **1.4b**, respectively. A similar, change for complexes **1.4c** and **1.4d** also causes the emission to redshift from 546 nm to 557 nm for **1.4c** and **1.4d**, respectively. Complex **1.4e** with simple phenylpyridine shows an emission band at 516 nm. However, complexes **1.4f-h**, with increased conjugation from the quinolone or isoquinoline groups show red shifts in emission. The position of the fused ring in complexes **1.4f-h** also has an effect, thus **1.4h** has the most redshifted emission in comparison to **1.4f** and **1.4g**. Changing the phenyl (**1.4e**) to a thiophene (**1.4i**) leads to a red shift in emission from 516 nm to 562 nm. A similar effect is seen comparing **1.4d** with **1.4j** (557 to 593 nm). Then, changing the N-donor pyridine in **1.4i** to benzothiazoline in **1.4j** leads to a red shift from 562 to 593 nm, respectively. Changing the C-donor from a thiophene (**1.4j**) to a naphthyl group in the *alpha* position (**1.4k**) shows a small redshift in emission from 593 nm to 606 nm, respectively whilst with a *beta*-naphthyl group (**1.4l**) the emission wavelength is virtually the same, only 1 nm different between **1.4j** and **1.4l**. When comparing **1.4d** (with phenyl) and **1.4k** and **1.4l** (naphthyl), the *alpha* position has a greater redshift in emission at 606 nm than *beta* position at 594 nm in comparison to the phenyl at 557 nm (**1.4d**). When comparing the oxazoline (**1.4b**) and thiazoline (**1.4d**), there is a difference in emission by changing the atom in the heterocycle from O to S. It was found that **1.4b** has an emission  $\lambda_{\text{max}}$  at 525 nm in comparison to 557 nm for complex **1.4d**. A similar effect is found comparing **1.4a** with **1.4c**. Hence the substitution of an oxygen atom (**1.4a** and **1.4b**) by a sulphur atom (**1.4c** and **1.4d**) in the chromophores leads to a redshift in the emission because of the higher polarizability of sulphur over oxygen in the ligand. By changing the position and the number of the heteroatoms and the size of the heterocycle in the cyclometallating ligand, the nature of the emitting excited state also changes giving rise

to different emission wavelengths. Overall, the emission with higher energy is observed with **1.4e** ( $\lambda_{\text{max}} = 516 \text{ nm}$ ) while **1.4h** has the lowest energy emission ( $\lambda_{\text{max}} = 622 \text{ nm}$ ).

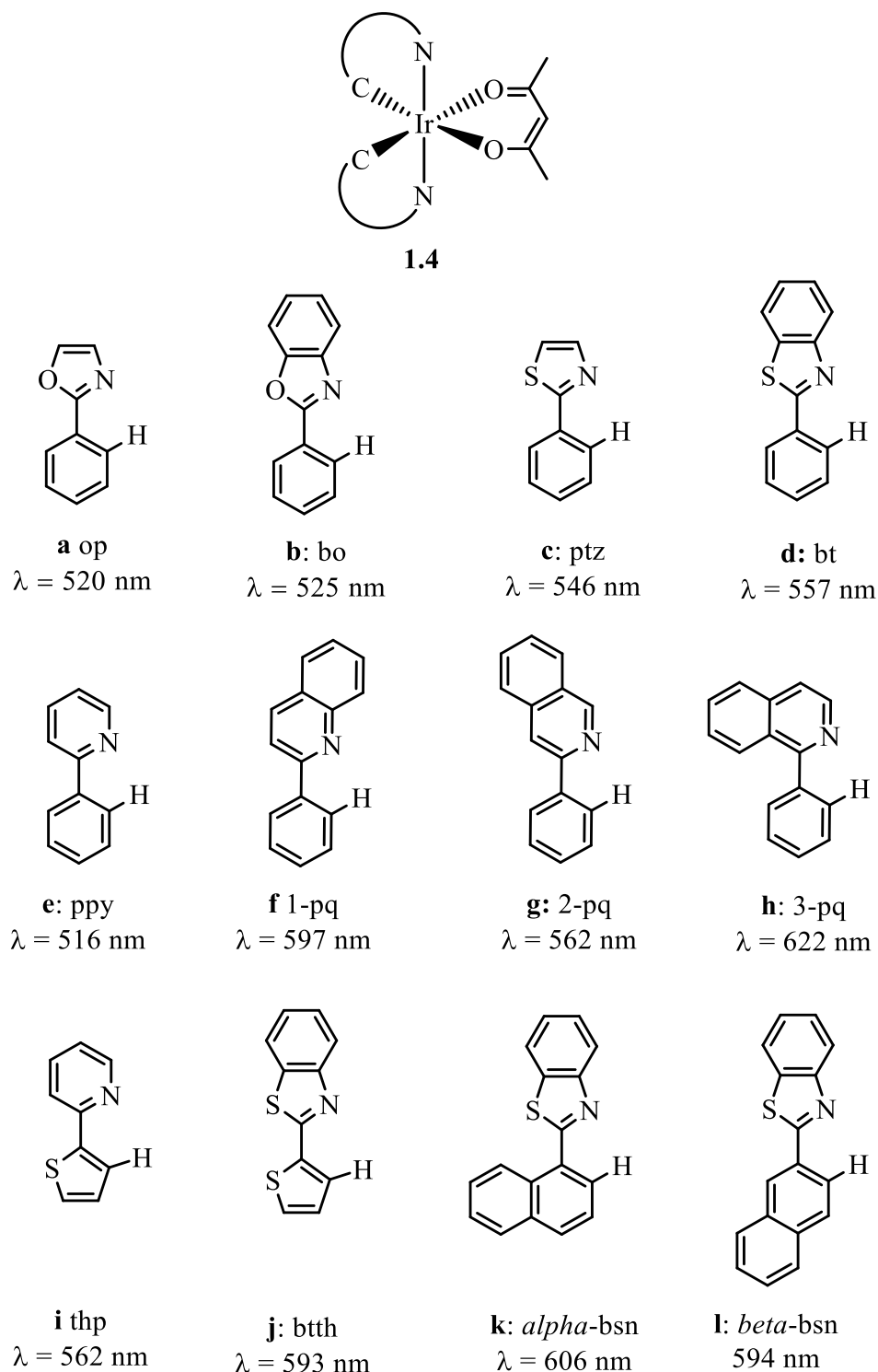


**Figure 1.7:** Structure of  $[\text{Ir}(\text{C}^{\wedge}\text{N})_2(\text{acac})]$  (**1.4a-l**)<sup>37, 57, 58</sup> with various cyclometallated ligands.

In neutral complexes, both the HOMO and the LUMO can involve either the  $\text{C}^{\wedge}\text{N}$  and/or the  $\text{X}^{\wedge}\text{Y}$  ligand, hence it can be difficult to adjust the energy of just the HOMO

or the LUMO without having any effect on the other. A way to disrupt the communication between the pyrazole and the phenyl ring was to introduce a methylene linker giving a non-conjugated C^N ligand (**1.5**) (Figure 1.8).<sup>59</sup> This destabilizes the  $\pi^*$  orbitals of the non-conjugated C^N ligand, causing a blue shift in emission ( $\lambda_{em} = 437, 460$  (sh) nm) compared with **1.6**<sup>60</sup> ( $\lambda_{em} = 457$  nm) with a conjugated C^N ligand.

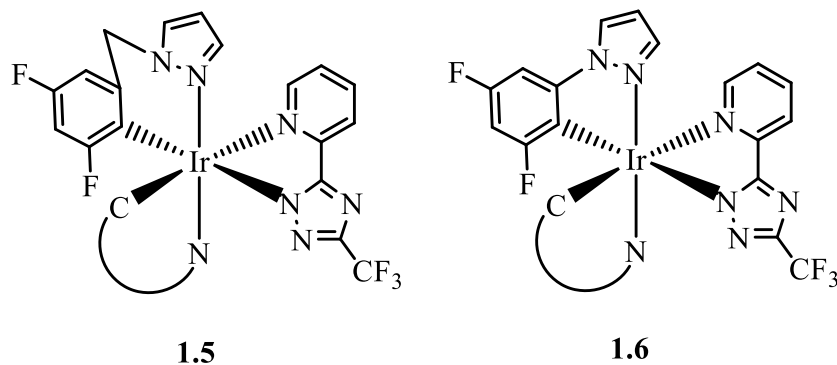


**Figure 1.8:** Structure of complex **1.5** with non-conjugated C^N ligand (left) and complex **1.6** with conjugated C^N ligand (right).

Theoretical studies were performed on complexes  $[\text{Ir}(\text{C}^{\wedge}\text{N})_2(\text{N}^{\wedge}\text{N})]^+$  (**1.7a-c**) (Figure 1.9) to study the effects of incorporating azole rings in the C^N ligands, and of the number of nitrogen atoms forming the azole ring, on the emission properties.<sup>61</sup> In complexes **1.7a-c**, the calculated HOMO is mainly composed of a mixture of Ir(III)  $d$ - $\pi$  orbitals and phenyl  $\pi$  orbitals of the cyclometalating ligands, whilst the LUMO is localised on the  $\pi^*$  orbital of the bipy ligand with a very small contribution from the metal. Compared to  $[\text{Ir}(\text{ppy})_2(\text{bipy})]^+$ , the substitution of the pyridine ring in the C^N ligands by an azole leads to a stabilisation of the HOMO as the number of nitrogen atoms in the azole ring increases, because the HOMO mostly resides in the C^N ligands which is where the structural change is observed. This suggests that the increase in the HOMO-LUMO gap energy is predicted to give a blue shift in emission with the increase of number of nitrogen atoms. The calculated emission values are in good correlation with the available experimental data, which supports the reliability of the theoretical results.<sup>62, 63</sup>

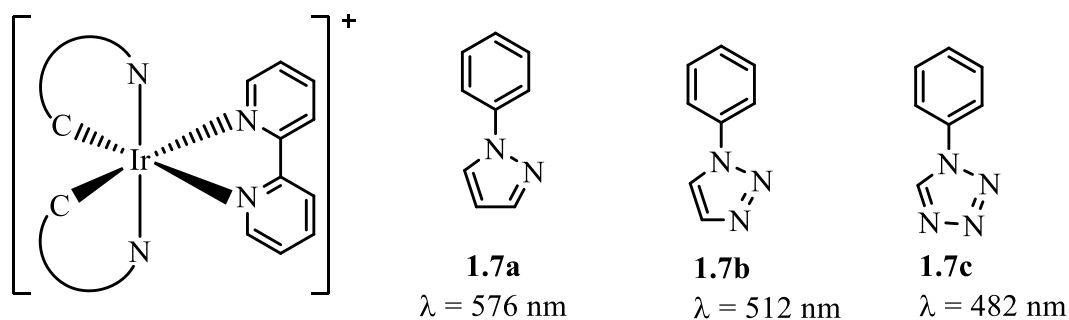


**Figure 1.9:** Structures of complexes **1.7a-c** with different azole rings in the cyclometallated C<sup>N</sup> ligand.

The next example shows the effect of different substituents in the phenyl part of the cyclometallated ligand (*para* position in relation to the metal) in complexes of general formula  $[\text{Ir}(\text{R-ppz})_2(\text{bipy})][\text{PF}_6]$  (**1.8a-e**). (Figure 1.10).<sup>36</sup> The  $\lambda_{\text{max}}$  for **1.8b** (R = Me) and **1.8c** (R = OMe) are 587 and 615 nm respectively, red shifted in comparison to 557 nm for **1.8a** (R = H). On the other hand, the  $\lambda_{\text{max}}$  of complexes **1.8d** (R = CF<sub>3</sub>) and **1.8e** (R = NO<sub>2</sub>) are 504 and 497 nm respectively, showing a blue shift in emission in comparison to 557 nm for complex **1.8a** (R = H). Hence, the nature of the substituents on the phenyl part of the C<sup>N</sup> ligand has a clear effect on the emission wavelength. DFT calculations show that electron-donating groups destabilise the HOMO, decreasing the HOMO-LUMO energy gap and therefore giving a red shifted emission.<sup>36</sup> On the other hand, electron withdrawing groups stabilise the energy of the HOMO which increases the HOMO-LUMO energy gap giving a blue-shifted emission. The position of the R group in the relation to metal was also studied and showed that when R is *para* to the metal it has a greater effect on the emission wavelength in comparison to the *meta* position. This is because in the *meta* position there is a only very small contribution of this carbon atom to the HOMO whereas the *para* position has a more significant contribution to the HOMO.<sup>36</sup>

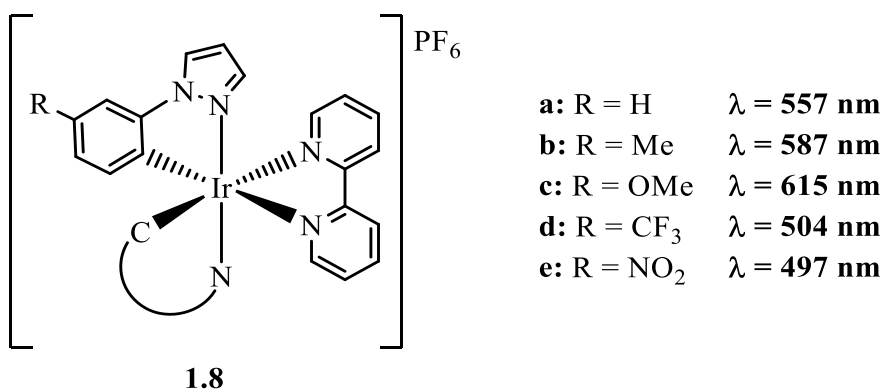


**Figure 1.10:** [Ir(R-ppz)<sub>2</sub>(bipy)][PF<sub>6</sub>] (**1.8a-e**) complexes with different substituents in the *para* position of the C<sup>N</sup> ligand.

The examples above described the effect of emission using different C<sup>N</sup> ligands. The following examples will describe the effect on emission by changing the X<sup>Y</sup> ancillary ligand with different anionic and neutral ligands. The emission wavelength of neutral and cationic complexes in heteroleptic Ir(III) complexes [Ir(ppy)<sub>2</sub>(X<sup>Y</sup>)]<sup>n</sup> (n = 0, +1) (**1.4e**, **1.9a-d**) (Figure 1.11) have considerably different emission wavelengths due to the difference in the localisation of the HOMO and LUMO for each complex. For example, the emission for neutral complexes **1.4e** and **1.9a** is 516 nm<sup>38</sup> and 505 nm<sup>64</sup>, respectively, whilst for cationic complexes **1.9b**, **1.9c** and **1.9d** the emission wavelength is 585 nm<sup>65</sup>, 582 nm<sup>66</sup> and 497 nm<sup>67</sup>, respectively. In neutral complexes, when X<sup>Y</sup> = acac (**1.4e**), the LUMO is mainly localised on the pyridyl ring of ppy ligand, whilst in **1.9a** the LUMO resides mainly on the pic ligand and partially on the pyridyl ring of the ppy ligand.<sup>50</sup> Predicting where the HOMO and LUMO is localised in neutral complexes becomes difficult without the use of DFT. In the cationic complexes (**1.9b** and **1.9c**), the HOMO resides mainly on the Ir and the phenyl part of the C<sup>N</sup> ligand whilst the LUMO is now mainly localised on the diimine ligand.

The cationic diimine complexes (**1.9b** and **1.9c**) have a smaller HOMO-LUMO gap than neutral complexes (**1.4e** and **1.9a**), due to the lower energy  $\pi^*$  orbitals of bipy leading to a lowering in the LUMO energy hence their emission is red shifted in comparison to the neutral complexes. In contrast, the emission of complex **1.9d** ( $\lambda_{\text{max}} = 497 \text{ nm}$ ) is significantly blue shifted compared to **1.9b**, and **1.9c** and even slightly blue shifted in comparison to neutral complexes **1.4e** and **1.9a**. This is due to the saturated diamine ligand in complex **1.9d** having no  $\pi^*$  orbitals hence the LUMO is back on the

C<sup>^</sup>N ligand. Overall, the emission data agrees with DFT calculations that the excited states vary according to the nature of the X<sup>^</sup>Y ligand.<sup>50</sup>

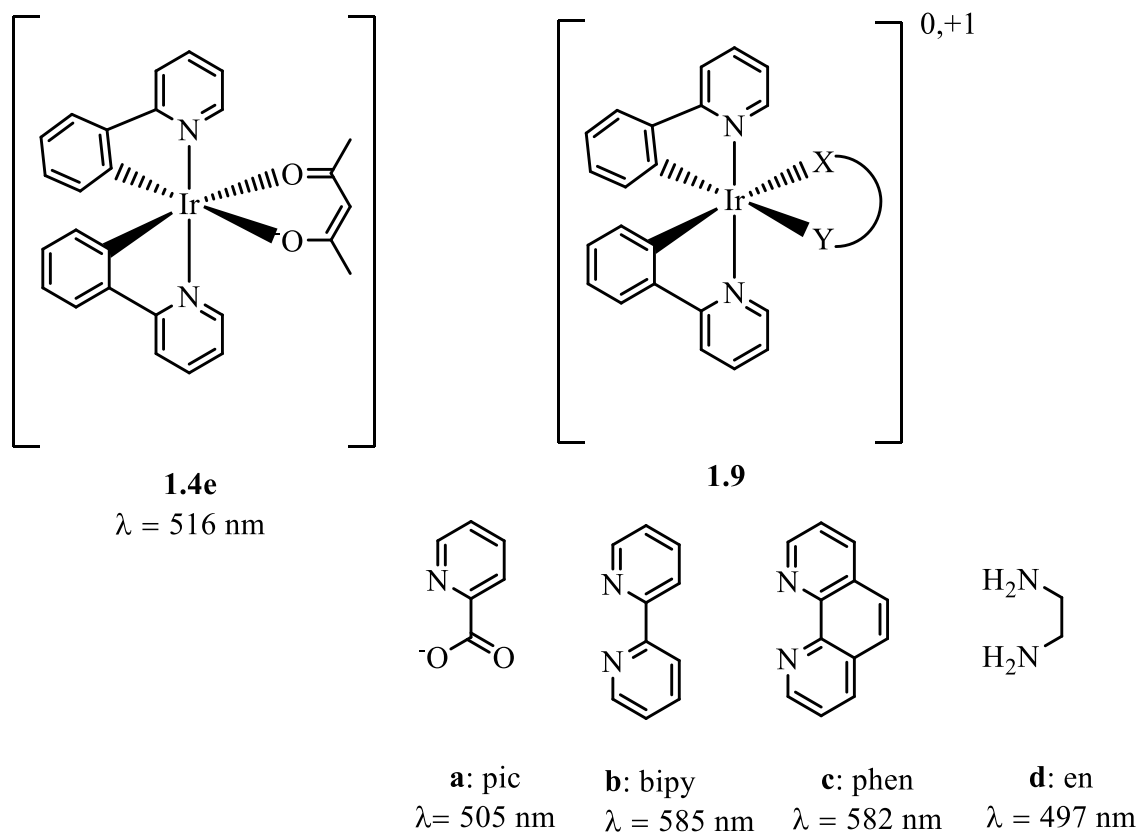


**Figure 1.11:**  $[\text{Ir}(\text{ppy})_2(\text{X}^{\wedge}\text{Y})]^n$  ( $n = 0, +1$ ) complexes with different X<sup>^</sup>Y ligands.

As discussed previously changing the degree of conjugation in the C<sup>^</sup>N ligand has an effect on the emission wavelength (Figure 1.7). Similar effects are seen by changing the degree of conjugation on the X<sup>^</sup>Y ligand, as seen in complexes  $[\text{Ir}(\text{piq})_2(\text{N}^{\wedge}\text{N})]\text{PF}_6$  (**1.10a-f**) (Figure 1.12).<sup>68</sup> For these complexes the HOMO is localised on the C<sup>^</sup>N ligand and partially on the Ir centre whilst the LUMO is localised in the N<sup>^</sup>N ligand. By increasing the conjugation of the N<sup>^</sup>N ligand the emission can be red shifted from 588 nm (**1.10a**) to 732 nm (**1.10f**). The increased conjugation leads to a decrease in the energy level of LUMO which consequently decreases the HOMO-LUMO gap leading to lower energy emission.<sup>68</sup>

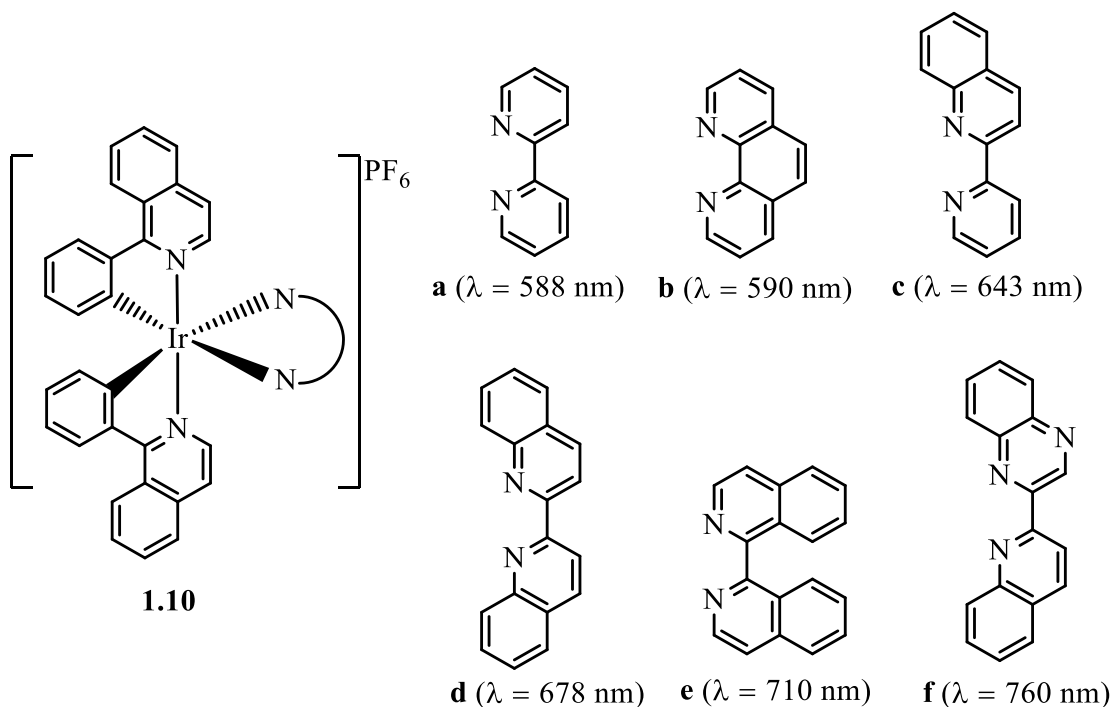


**Figure 1.12:** Structures of  $[\text{Ir}(\text{piq})_2(\text{N}^{\wedge}\text{N})]\text{PF}_6$  complexes by varying the conjugation on the  $\text{N}^{\wedge}\text{N}$  ligand.

More recently, Sun and co-workers synthesised cationic complexes  $[\text{Ir}(\text{dppi})_2(\text{N}^{\wedge}\text{N})]\text{PF}_6$  (**1.11a-f**) (Figure 1.13).<sup>69</sup> Complexes **1.11c**, **1.11e** and **1.11f** show red shifts in emission bands by increasing the conjugation with respect to the parent complex **1.11a**. Interestingly, complex **1.11b** shows a blue shift in comparison to complexes **1.11a**, **1.11d** and **1.11f**.<sup>69</sup> DFT calculations show that the HOMO is localised in the cyclometallated dppi ligand and Ir centre, while the LUMO is localised on the  $\text{N}^{\wedge}\text{N}$  ligand. The unusual blue-shift in emission is due to the occurrence of benzannulation in complex **1.11b**, the LUMO symmetry of **1.11a** at the annulation site matches the HOMO symmetry of 1,3-butadiene.<sup>69</sup> The LUMO–HOMO interactions raise the LUMO energy in **1.11b** and thus cause the blue-shifted emission band. A similar occurrence is observed from **1.11c** to **1.11d**.

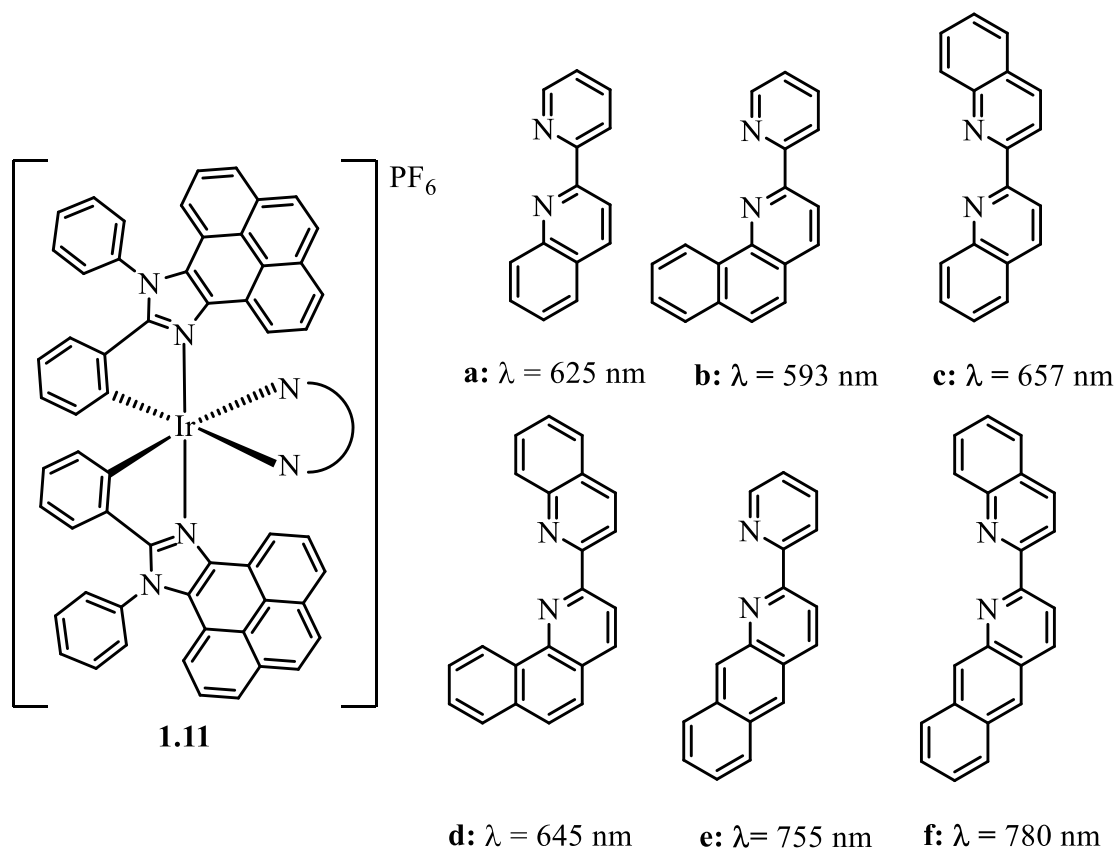


**Figure 1.13:** Structure of  $[\text{Ir}(\text{dppi})_2(\text{N}^{\wedge}\text{N})]\text{PF}_6$  complexes (**1.11a-f**) with different degrees of conjugation on the  $\text{N}^{\wedge}\text{N}$  ligand.

Theoretical studies were performed on complexes  $[\text{Ir}(\text{C}^{\wedge}\text{N})_2(\text{N}^{\wedge}\text{N})]^+$  (**1.12a-c**) (Figure 1.14) to study the effects of incorporatingazole rings in the  $\text{C}^{\wedge}\text{N}$  and/or  $\text{N}^{\wedge}\text{N}$  ligands, and of the number of nitrogen atoms forming theazole ring, on the emission properties.<sup>61</sup> The results are compared with those of the reference complex  $[\text{Ir}(\text{ppy})_2(\text{bipy})]^+$ . In complexes **1.12a-c**, the calculated HOMO is mainly composed of a mixture of Ir(III)  $d$ - $\pi$  orbitals and phenyl  $\pi$  orbitals of the cyclometallating ligands whilst the LUMO is again on the  $\text{N}^{\wedge}\text{N}$  ligand. Hence, DFT studies predict the main effect of an increase in the number of nitrogen atoms in the  $\text{N}^{\wedge}\text{N}$  ligand will be to decrease the energy of the LUMO. With the HOMO relatively unchanged this should lead to a reduction in the HOMO-LUMO energy gap and a predicted red shift in the emission.

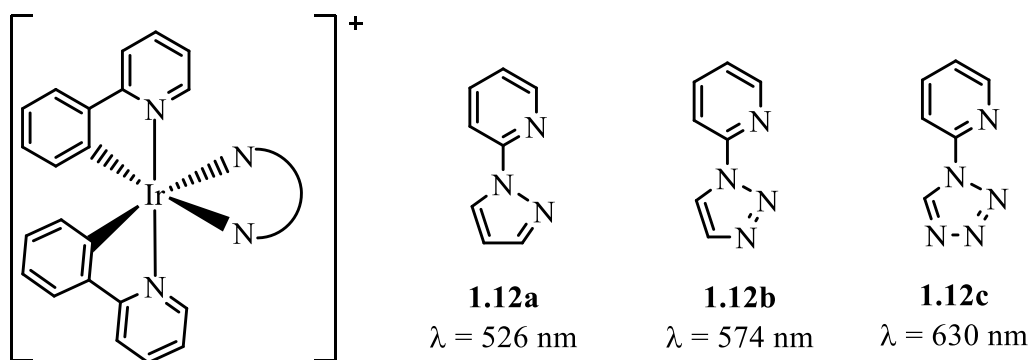


**Figure 1.14:** Theoretical studies carried out on  $[\text{Ir}(\text{C}^{\wedge}\text{N})_2(\text{N}^{\wedge}\text{N})]^+$  (**1.12a-c**) complexes with predicted emission wavelength.

Furthermore, Thompson compared the emission of complexes **1.4e** and **1.13a-c** containing different  $\beta$ -diketonates (Figure 1.15). All complexes (**1.4e**, **1.13a-c**) showed phosphorescent emission at 516 nm. However, complexes **1.4e** and **1.13a** give reasonable quantum yields ( $\Phi$  0.31 and 0.33, respectively) whilst complexes **1.13b** and **1.13c** have very low quantum efficiencies ( $\Phi < 0.01$ ).<sup>37</sup> In complex **1.13b** and **1.13c**, the excited states are localised mainly on the bza and dbm ligand, respectively which leads to very weak phosphorescence. In complexes **1.4e** and **1.13a** the lowest triplet energy is below that of their respective  $\beta$ -diketonate ligands giving rise to strong phosphorescence emission.

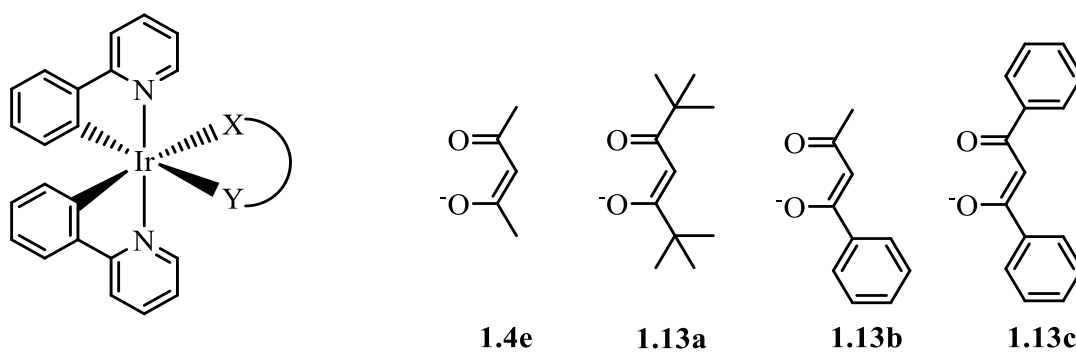


**Figure 1.15:** Structures of  $[\text{Ir}(\text{ppy})_2(\text{O}^{\wedge}\text{O})]^+$  complexes (**1.4e** and **1.13a-c**) containing different  $\beta$ -diketonate ligands.

#### 1.4 Applications of Ir(III) Complexes

As mentioned previously, luminescent Ir(III) complexes have many desirable photophysical properties such as high quantum yields, tuneable emission wavelength and life times, and large Stokes shifts. Tuning emission wavelengths was discussed above. Emission lifetimes of  $> 100$  ns can be used to discriminate the background fluorescence of bio-molecules ( $\tau = 1-10$  ns) from the emission of the complex ( $\tau = 0.1-$

10  $\mu$ s), by using a time delay before detection which is difficult for organic fluorophores owing to their shorter lifetimes. The Stokes shift is the difference between the band maxima of the absorption and emission arising from the same electronic transition; therefore, a large Stokes shift helps to isolate the excitation and emission wavelengths. As a result of a combination of these properties cyclometallated Ir(III) complexes have been used as OLEDs,<sup>9, 37, 70</sup> photo-sensitizers in solar energy conversion,<sup>71, 72</sup> photocatalysts,<sup>73, 74</sup> luminescent sensors<sup>22</sup> and biological labels<sup>24, 75</sup> and some of these are discussed in more detail below.

In 1999, complex *fac*-[Ir(ppy)<sub>3</sub>] (**1.2**) was used in an OLED for the first time<sup>12</sup> and since then, cyclometallated complexes have been widely studied and used in fabrication of light emitting devices.<sup>47, 51, 76</sup> OLED technology enables thin, efficient and bright displays that can be flexible and transparent and are therefore ideal for large displays, such as televisions.<sup>9</sup> Cyclometallated Ir(III) complexes are typically used as emitters in OLEDs because they possess the following characteristics:<sup>9</sup>

- i) Chemically, electrically and thermally stable.
- ii) Highly efficient triplet phosphorescence emission and high radiative decay rate.
- iii) Phosphorescent wavelength is relatively easily tuned to give blue to red emission.

Complexes *fac*-**1.2** and **1.14** have been used as green and red coloured light-emitting devices, respectively.<sup>9</sup> Complex **1.15** is one of the most well-known blue emitters<sup>77</sup> (Figure 1.16).

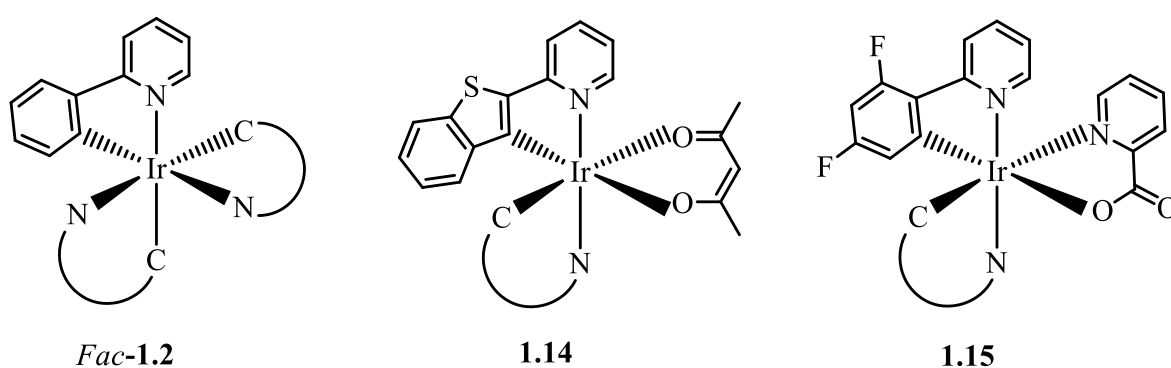


**Figure 1.16:** Structures of complexes *fac*-**1.2**, **1.14** and **1.15**.

Cyclometallated Ir(III) complexes also have been demonstrated to work efficiently as absorbers for solar cell applications.<sup>78</sup> Dye-sensitized solar cells (DSSCs) are considered a real solution for harnessing the energy of the sun and converting it into

electrical energy. Cyclometallated Ir(III) complexes can be good candidates for potential use as DSSCs due to their high quantum yields, as observed for cationic complex **1.16** (Figure 1.17).<sup>79</sup>

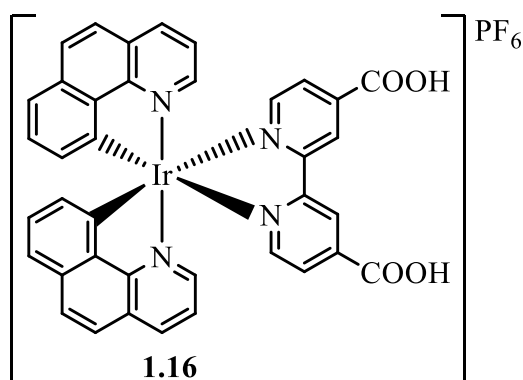
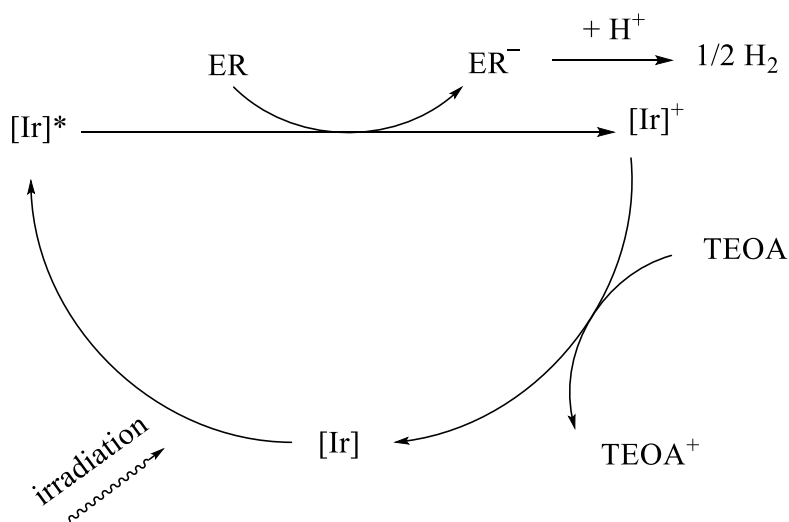


**Figure 1.17:** Cationic complex **1.16** used as DSSC.

In addition, solar energy can also be used in catalysis. This is very desirable as it does not require the use of non-renewable resources. Since the studies carried by MacMillan<sup>80</sup>, Yoon<sup>81</sup> and Stephenson,<sup>82</sup> visible-light photoredox catalysis has been an influential strategy in novel and useful reactions under mild conditions. In 2005, Bernhard and co-workers<sup>83</sup> used  $[\text{Ir}(\text{ppy})_2(\text{phen})]^+$  as a photosensitiser for the production of  $\text{H}_2$  gas from photocatalytic reduction of water (Scheme 1.4). The  $[\text{Ir}]$  corresponds to the photosensitiser and ER is the electron relay  $[\text{Co}(\text{bipy})_3]^{2+}$ . It takes two cycles through the pathway shown below to generate 1 equiv of  $\text{H}_2$  gas. TEOA (triethanolamine) serves as a two-electron reductant to reduce the photosensitiser.



**Scheme 1.4:** Simplified mechanism to produce  $\text{H}_2$  using  $[\text{Ir}]$  as the photosensitiser.

Cyclometallated Ir(III) complexes can also be used for biological applications such as the detection of thiol-containing amino acids like homocysteine (Hcy) and cysteine (Cys). The levels of Hcy in the plasma is an indicator of cardiovascular disorders and Alzheimer's,<sup>84</sup> while deficiency of Cys is associated with slow growth and liver damage.<sup>85</sup> Therefore, there is great interest in detecting these molecules in biological systems. Li and co-workers<sup>86</sup> designed complex  $[\text{Ir}(\text{pba})_2(\text{bpy})]\text{PF}_6$  (**1.17**) (Figure 1.18) with aldehyde groups on the cyclometallated C^N ligand to selectively react with Hcy and Cys to form cyclic thiazinane and thiazolidine groups, respectively. The emission colour of complex **1.17** in the presence of the amino acid changed from yellow to red suggesting that presence of the amino acid has an effect on the emission.

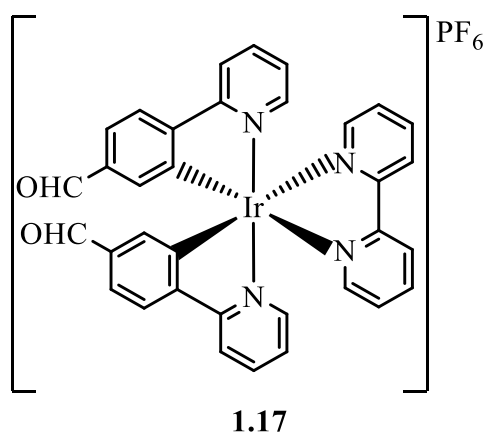


**Figure 1.18:** Structure of complex **1.17** with aldehyde groups on the cyclometallated C^N ligand.

Furthermore, Ir(III) cyclometallated complexes have also been proposed for applications in photodynamic therapy. Demas first reported about the dioxygen quenching of Ir(III) complexes and proposed an interpretation based on the formation of singlet oxygen, which was proved by photo-oxygenation of trimethylethylene.<sup>87, 88</sup> The mechanism of singlet oxygen photo-generation has been widely investigated especially in view of the interest of singlet oxygen for therapeutical applications.<sup>89, 90</sup> Ir(III) cyclometallated complexes show high luminescence in degassed solution, with increased quantum yields in comparison to non-degassed solutions. In the presence of oxygen (aerated solutions) quantum yields and lifetimes can be quenched by a factor of even 60 times compared to the values in degassed solutions.<sup>91</sup> Sensors in biological systems have also been explored by Wong and co-workers where they described the luminescent switch-on probe  $[\text{Ir}(\text{ppy})_2(\text{H}_2\text{O})_2]^+$  (**1.18**) (Figure 1.19) for histidine/histidine rich proteins and demonstrate its utility in protein staining.<sup>92</sup> The

complex is weakly emissive in PBS but in the presence of histidine, it displays a 180-fold increase in emission intensity. **1.18** has weakly bound H<sub>2</sub>O ligands, so the switch-on emission is due to the covalent bond between **1.18** and the imidazole moiety of histidine through ligand substitution. The use of organic solvents is not required for the optimal sensing of amino acids/proteins as it is readily soluble and stable in aqueous staining solutions.

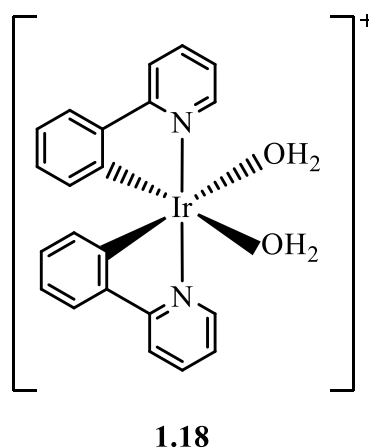


**Figure 1.19:** Cationic complex **1.18** with two H<sub>2</sub>O ligands.

The cationic Ir(III) complexes show a number of superiorities: exclusive staining in the cytoplasm, low cytotoxicity and reduced photo-bleaching thus rendering iridium complexes as excellent candidates for bio-imaging and cellular studies.<sup>75</sup> In 2008, Li and co-workers<sup>27</sup> reported for the first time cationic Ir(III) complexes (**1.19** and **1.20**) for living cell staining (Figure 1.20). Whilst both complexes showed exclusively staining in the cytoplasm of incubated HeLa cells, complex **1.19** gave bright green emission and complex **1.20** gave bright red emission. The good cell penetration was achieved by having cationic complexes rather than neutral complexes and their lipophilicity was achieved by the presence of fluorine groups on the cyclometallated C<sup>N</sup> ligand.

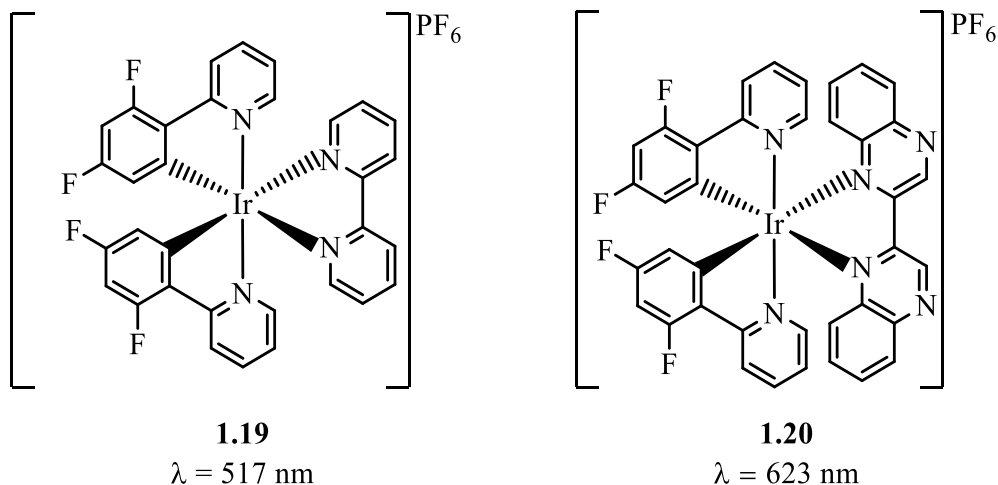


**Figure 1.20:** Complexes **1.19** and **1.20** used for staining in the cytoplasm.

Near-infrared (NIR) dyes have attracted attention for their potential applications in optical imaging *in vivo*, and medical diagnosis.<sup>24, 93</sup> Therefore, there is significant interest in tuning the emission wavelength to the NIR, as infrared light can penetrate tissue more readily with low toxicity. Many organic dyes (for example BODIPYs)<sup>94</sup> are used as NIR fluorophores for bioimaging applications, but transition metal complexes offer potential alternatives to fluorescent organic molecules. NIR phosphorescent Ir(III) complexes are advantageous with respect to fluorescent compounds in their compatibility with time-gated bioimaging techniques that eliminate background fluorescence. Complexes **1.21a-b** (Figure 1.21) exhibit exclusive staining in the cytoplasm with good cell membrane permeability under excitation at 488 nm.<sup>95</sup>

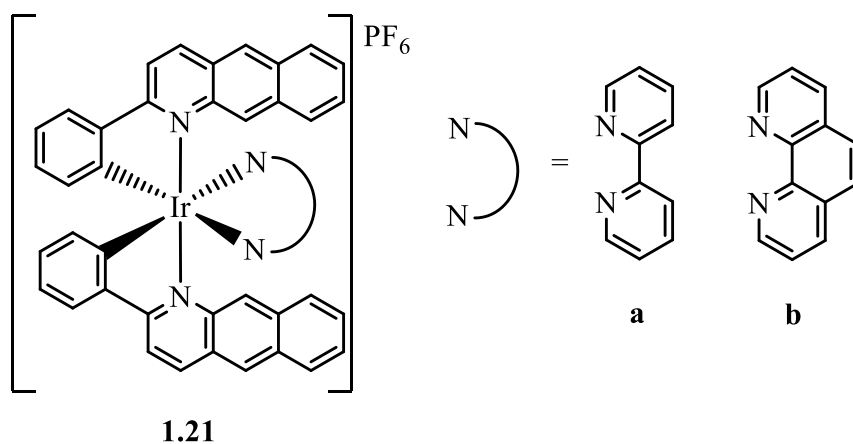


**Figure 1.21:** NIR complexes **1.21a-b** used in live cell imaging.

## 1.5 Overview

In summary, the emission wavelength of cyclometallated Ir(III) complexes  $[\text{Ir}(\text{C}^{\wedge}\text{N})_2(\text{X}^{\wedge}\text{Y})]^{n+}$  ( $n = 0, 1$ ) can be tuned through the entire visible region and into the near infrared by varying either the  $\text{C}^{\wedge}\text{N}$  ligand and/or the  $\text{X}^{\wedge}\text{Y}$  ligand including the degree of conjugation, presence and location of heteroatoms and addition of substituents on either of the ligands. The tuning of the emission wavelength occurs through modifications of the HOMO and LUMO orbitals. Since the position of the HOMO and the LUMO can vary depending on the particular ligands it is not possible to provide a general rule. Owing to their rich photophysical and electrochemical properties, these complexes will continue to be used in diverse applications such as emissive dopants in OLEDs, as sensors and as biological labels discussed previously. In addition cyclometallated Ir(III) complexes have the advantage of longer emission lifetimes compared with most organic fluorophores. This means there is potential for these complexes to be used in lifetime imaging microscopy.

In Chapter 2, the synthesis and characterisation of cyclometallated Ir(III) complexes with general formula  $[\text{Ir}(\text{C}^{\wedge}\text{N})_2(\text{N}^{\wedge}\text{O})]$  with 6-membered  $\text{N}^{\wedge}\text{O}$  chelate ligands are described. The absorption and emission wavelengths will be described and a new mechanism for Enhanced Phosphorescence Emission in the Solid State (EPESS) will also be discussed. In Chapter 3, the synthesis and characterisation of complexes with the same general formula  $[\text{Ir}(\text{C}^{\wedge}\text{N})_2(\text{N}^{\wedge}\text{O})]$  where the  $\text{N}^{\wedge}\text{O}$  ligands form a 5-membered chelate ring will be described. The effect of ring size and EPESS will also be discussed. Chapter 4 describes the syntheses of Ir(III), Rh(III) and Ru(II) half-sandwich complexes with 5-membered chelating anionic  $\text{N}^{\wedge}\text{O}$  or neutral  $\text{N}^{\wedge}\text{N}$  ligands which have *exocyclic*  $\text{C}=\text{N}$  bonds. The nature of the ligand, the imine substituent and the metal centre will all affect the photoisomerisation.

## 1.6 Bibliography

1. D. Frackowiak, *J Photoch Photobio B*, 1988, **2**, 399-408.
2. J. Zimmermann, A. Zeug and B. Roder, *Phys. Chem. Chem. Phys.*, 2003, **5**, 2964-2969.
3. J. N. Demas and B. A. Degraff, *Anal. Chem.*, 1991, **63**, A829-A837.
4. J. N. Demas and B. A. DeGraff, *J. Chem. Educ.*, 1997, **74**, 690-695.
5. V. Fernandez-Moreira, F. L. Thorp-Greenwood and M. P. Coogan, *Chem. Commun.*, 2010, **46**, 186-202.
6. V. Balzani, A. Juris, M. Venturi, S. Campagna and S. Serroni, *Chem. Rev.*, 1996, **96**, 759-834.
7. L. Spiccia, G. B. Deacon and C. M. Kepert, *Coord. Chem. Rev.*, 2004, **248**, 1329-1341.
8. Y. Chi and P.-T. Chou, *Chem. Soc. Rev.*, 2010, **39**, 638-655.
9. I. Omae, *Coord. Chem. Rev.*, 2016, **310**, 154-169.
10. X. Yang, G. Zhou and W.-Y. Wong, *Chem. Soc. Rev.*, 2015, **44**, 8484-8575.
11. C. Fan and C. Yang, *Chem. Soc. Rev.*, 2014, **43**, 6439-6469.
12. M. A. Baldo, S. Lamansky, P. E. Burrows, M. E. Thompson and S. R. Forrest, *Appl. Phys. Lett.*, 1999, **75**, 4-6.
13. K. J. Suhr, L. D. Bastatas, Y. Shen, L. A. Mitchell, G. A. Frazier, D. W. Taylor, J. D. Slinker and B. J. Holliday, *Dalton Trans.*, 2016, **45**, 17807-17823.
14. A. K. Pal, D. B. Cordes, A. M. Z. Slawin, C. Momblona, E. Ortí, I. D. W. Samuel, H. J. Bolink and E. Zysman-Colman, *Inorg. Chem.*, 2016, **55**, 10361-10376.
15. D. Tordera, A. Pertegas, N. M. Shavaleev, R. Scopelliti, E. Orti, H. J. Bolink, E. Baranoff, M. Gratzel and M. K. Nazeeruddin, *J. Mater. Chem.*, 2012, **22**, 19264-19268.
16. A. F. Henwood and E. Zysman-Colman, *Top. Curr. Chem.*, 2016, **374**, 36.
17. Y.-J. Yuan, Z.-T. Yu, D.-Q. Chen and Z.-G. Zou, *Chem. Soc. Rev.*, 2017, **46**, 603-631.

18. Z. Liu, W. He and Z. Guo, *Chem. Soc. Rev.*, 2013, **42**, 1568-1600.
19. Q. Zhao, F. Li and C. Huang, *Chem. Soc. Rev.*, 2010, **39**, 3007-3030.
20. C. Liu, H. Yu, X. Rao, X. Lv, Z. Jin and J. Qiu, *Dyes and Pigments*, 2017, **136**, 641-647.
21. D.-L. Ma, S. Lin, W. Wang, C. Yang and C.-H. Leung, *Chem. Sci.*, 2017, **8**, 878-889.
22. M. C. DeRosa, D. J. Hodgson, G. D. Enright, B. Dawson, C. E. B. Evans and R. J. Crutchley, *J. Am. Chem. Soc.*, 2004, **126**, 7619-7626.
23. Y. You and W. Nam, *Chem. Soc. Rev.*, 2012, **41**, 7061-7084.
24. K. K.-W. Lo and K. Y. Zhang, *RSC Adv.*, 2012, **2**, 12069-12083.
25. Q. Zhao, C. Huang and F. Li, *Chem. Soc. Rev.*, 2011, **40**, 2508-2524.
26. Q. Zhao, M. Yu, L. Shi, S. Liu, C. Li, M. Shi, Z. Zhou, C. Huang and F. Li, *Organometallics*, 2010, **29**, 1085-1091.
27. M. Yu, Q. Zhao, L. Shi, F. Li, Z. Zhou, H. Yang, T. Yi and C. Huang, *Chem. Commun.*, 2008, 2115-2117.
28. Q. Zhao, Y. Liu, Y. Cao, W. Lv, Q. Yu, S. Liu, X. Liu, M. Shi and W. Huang, *Adv. Opt. Mater.*, 2015, **3**, 233-240.
29. A. J. Wilkinson, H. Puschmann, J. A. K. Howard, C. E. Foster and J. A. G. Williams, *Inorg. Chem.*, 2006, **45**, 8685-8699.
30. K. Dedeian, P. I. Djurovich, F. O. Garces, G. Carlson and R. J. Watts, *Inorg. Chem.*, 1991, **30**, 1685-1687.
31. R. Ragni, E. A. Plummer, K. Brunner, J. W. Hofstraat, F. Babudri, G. M. Farinola, F. Naso and L. De Cola, *J. Mater. Chem.*, 2006, **16**, 1161-1170.
32. V. V. Grushin, N. Herron, D. D. LeCloux, W. J. Marshall, V. A. Petrov and Y. Wang, *Chem. Commun.*, 2001, 1494-1495.
33. A. B. Tamayo, B. D. Alleyne, P. I. Djurovich, S. Lamansky, I. Tsyba, N. N. Ho, R. Bau and M. E. Thompson, *J. Am. Chem. Soc.*, 2003, **125**, 7377-7387.
34. A. R. McDonald, M. Lutz, L. S. von Chrzanowski, G. P. M. van Klink, A. L. Spek and G. van Koten, *Inorg. Chem.*, 2008, **47**, 6681-6691.

35. M. Lepeltier, H. Le Bozec, V. Guerchais, T. K.-M. Lee and K. K.-W. Lo, *Organometallics*, 2005, **24**, 6069-6072.
36. D. L. Davies, M. P. Lowe, K. S. Ryder, K. Singh and S. Singh, *Dalton Trans.*, 2011, **40**, 1028-1030.
37. S. Lamansky, P. Djurovich, D. Murphy, F. Abdel-Razzaq, H.-E. Lee, C. Adachi, P. E. Burrows, S. R. Forrest and M. E. Thompson, *J. Am. Chem. Soc.*, 2001, **123**, 4304-4312.
38. S. Lamansky, P. Djurovich, D. Murphy, F. Abdel-Razzaq, R. Kwong, I. Tsyba, M. Bortz, B. Mui, R. Bau and M. E. Thompson, *Inorg. Chem.*, 2001, **40**, 1704-1711.
39. M. A. Bennett and T. R. B. Mitchell, *Inorg. Chem.*, 1976, **15**, 2936-2938.
40. K. A. McGee and K. R. Mann, *Inorg. Chem.*, 2007, **46**, 7800-7809.
41. K. A. King, P. J. Spellane and R. J. Watts, *J. Am. Chem. Soc.*, 1985, **107**, 1431-1432.
42. K. Hideo and S. Yoshiyuki, *Chem. Lett.*, 2003, **32**, 252-253.
43. M. Kleinschmidt, C. v. Wüllen and C. M. Marian, *J. Chem. Phys.*, 2015, **142**, 094301.
44. K.-C. Tang, K. L. Liu and I. C. Chen, *Chem. Phys. Lett.*, 2004, **386**, 437-441.
45. G. J. Hedley, A. Ruseckas and I. D. W. Samuel, *Chem. Phys. Lett.*, 2008, **450**, 292-296.
46. M. G. Colombo, T. C. Brunold, T. Riedener, H. U. Gudel, M. Fortsch and H.-B. Büergi, *Inorg. Chem.*, 1994, **33**, 545-550.
47. T. Sajoto, P. I. Djurovich, A. B. Tamayo, J. Oxgaard, W. A. Goddard and M. E. Thompson, *J. Am. Chem. Soc.*, 2009, **131**, 9813-9822.
48. T. M. Monos, A. C. Sun, R. C. McAtee, J. J. Devery and C. R. J. Stephenson, *J. Org. Chem.*, 2016, **81**, 6988-6994.
49. S. Sprouse, K. A. King, P. J. Spellane and R. J. Watts, *J. Am. Chem. Soc.*, 1984, **106**, 6647-6653.

50. T. Fei, X. Gu, M. Zhang, C. Wang, M. Hanif, H. Zhang and Y. Ma, *Synth. Met.*, 2009, **159**, 113-118.
51. A. Tsuboyama, H. Iwawaki, M. Furugori, T. Mukaide, J. Kamatani, S. Igawa, T. Moriyama, S. Miura, T. Takiguchi, S. Okada, M. Hoshino and K. Ueno, *J. Am. Chem. Soc.*, 2003, **125**, 12971-12979.
52. Y. Y. Zhou, J. Y. Zhuang, W. M. Su and X. M. Wang, *Eur. J. Inorg. Chem.*, 2015, 5571-5576.
53. K. Hasan, A. K. Bansal, I. D. W. Samuel, C. Roldan-Carmona, H. J. Bolink and E. Zysman-Colman, *Sci. Rep.*, 2015, **5**.
54. P. Sun, K. Wang, B. Zhao, T. Yang, H. Xu, Y. Miao, H. Wang and B. Xu, *Tetrahedron*, 2016, **72**, 8335-8341.
55. Z. Li, P. Cui, C. Wang, S. Kilina and W. Sun, *J. Phys. Chem. C*, 2014, **118**, 28764-28775.
56. C. H. Yang, K. H. Fang, W. L. Su, S. P. Wang, S. K. Su and I. W. Sun, *J. Organomet. Chem.*, 2006, **691**, 2767-2773.
57. C. Yao, B. Jiao, X. Yang, X. Xu, J. Dang, G. Zhou, Z. Wu, X. Lv, Y. Zeng and W.-Y. Wong, *Eur. J. Inorg. Chem.*, 2013, **2013**, 4754-4763.
58. C. L. Li, Y. J. Su, Y. T. Tao, P. T. Chou, C. H. Chien, C. C. Cheng and R. S. Liu, *Adv. Funct. Mater.*, 2005, **15**, 387-395.
59. Y. H. Song, Y. C. Chiu, Y. Chi, Y. M. Cheng, C. H. Lai, P. T. Chou, K. T. Wong, M. H. Tsai and C. C. Wu, *Chem. Eur. J.*, 2008, **14**, 5423-5434.
60. C.-H. Yang, S.-W. Li, Y. Chi, Y.-M. Cheng, Y.-S. Yeh, P.-T. Chou, G.-H. Lee, C.-H. Wang and C.-F. Shu, *Inorg. Chem.*, 2005, **44**, 7770-7780.
61. P. Pla, J. M. Junquera-Hernandez, H. J. Bolink and E. Orti, *Dalton Trans.*, 2015, **44**, 8497-8505.
62. A. B. Tamayo, S. Garon, T. Sajoto, P. I. Djurovich, I. M. Tsyba, R. Bau and M. E. Thompson, *Inorg. Chem.*, 2005, **44**, 8723-8732.
63. R. D. Costa, E. Ortí, H. J. Bolink, S. Graber, S. Schaffner, M. Neuburger, C. E. Housecroft and E. C. Constable, *Adv. Funct. Mater.*, 2009, **19**, 3456-3463.

64. B. Beyer, C. Ulbricht, D. Escudero, C. Friebe, A. Winter, L. González and U. S. Schubert, *Organometallics*, 2009, **28**, 5478-5488.
65. F. Neve, M. L. Deda, F. Puntoriero and S. Campagna, *Inorg. Chim. Acta*, 2006, **359**, 1666-1672.
66. Y. You, S. Cho and W. Nam, *Inorg. Chem.*, 2014, **53**, 1804-1815.
67. S. P.-Y. Li, T. S.-M. Tang, K. S.-M. Yiu and K. K.-W. Lo, *Chem. Eur. J.*, 2012, **18**, 13342-13354.
68. Q. Zhao, S. Liu, M. Shi, C. Wang, M. Yu, L. Li, F. Li, T. Yi and C. Huang, *Inorg. Chem.*, 2006, **45**, 6152-6160.
69. B. Liu, L. Lystrom, S. Kilina and W. Sun, *Inorg. Chem.*, 2017, **56**, 5361-5370.
70. E. Baranoff, J.-H. Yum, M. Graetzel and M. K. Nazeeruddin, *J. Organomet. Chem.*, 2009, **694**, 2661-2670.
71. T. Bessho, E. Yoneda, J.-H. Yum, M. Guglielmi, I. Tavernelli, H. Imai, U. Rothlisberger, M. K. Nazeeruddin and M. Grätzel, *J. Am. Chem. Soc.*, 2009, **131**, 5930-5934.
72. G. Tan, P. Liu, H. Wu, S.-C. Yiu, F. Dai, Y.-H. Feng, X. Liu, Y. Qiu, Y. H. Lo, C.-L. Ho and W.-Y. Wong, *J. Organomet. Chem.*, 2016, **812**, 280-286.
73. Y. Kuramochi and O. Ishitani, *Inorg. Chem.*, 2016, **55**, 5702-5709.
74. C. Yang, F. Mehmood, T. L. Lam, S. L.-F. Chan, Y. Wu, C.-S. Yeung, X. Guan, K. Li, C. Y.-S. Chung, C.-Y. Zhou, T. Zou and C.-M. Che, *Chem. Sci.*, 2016, **7**, 3123-3136.
75. Y. You, *Curr. Opin. Chem. Biol.*, 2013, **17**, 699-707.
76. T. Hofbeck and H. Yersin, *Inorg. Chem.*, 2010, **49**, 9290-9299.
77. R. J. Holmes, S. R. Forrest, Y.-J. Tung, R. C. Kwong, J. J. Brown, S. Garon and M. E. Thompson, *Appl. Phys. Lett.*, 2003, **82**, 2422-2424.
78. T. B. Fleetham, Z. Wang and J. Li, *Inorg. Chem.*, 2013, **52**, 7338-7343.
79. C. Dragonetti, A. Valore, A. Colombo, S. Righetto and V. Trifiletti, *Inorg. Chim. Acta*, 2012, **388**, 163-167.
80. D. A. Nicewicz and D. W. C. MacMillan, *Science*, 2008, **322**, 77-80.

81. M. A. Ischay, M. E. Anzovino, J. Du and T. P. Yoon, *J. Am. Chem. Soc.*, 2008, **130**, 12886-12887.
82. J. M. R. Narayanam, J. W. Tucker and C. R. J. Stephenson, *J. Am. Chem. Soc.*, 2009, **131**, 8756-8757.
83. J. I. Goldsmith, W. R. Hudson, M. S. Lowry, T. H. Anderson and S. Bernhard, *J. Am. Chem. Soc.*, 2005, **127**, 7502-7510.
84. S. Seshadri , A. Beiser , J. Selhub , P. F. Jacques , I. H. Rosenberg , R. B. D'Agostino , P. W. F. Wilson and P. A. Wolf *N. Engl. J. Med.*, 2002, **346**, 476-483.
85. S. Shahrokhian, *Anal. Chem.*, 2001, **73**, 5972-5978.
86. L. Xiong, Q. Zhao, H. Chen, Y. Wu, Z. Dong, Z. Zhou and F. Li, *Inorg. Chem.*, 2010, **49**, 6402-6408.
87. J. N. Demas, E. W. Harris, C. M. Flynn and D. Diemente, *J. Am. Chem. Soc.*, 1975, **97**, 3838-3839.
88. J. N. Demas, E. W. Harris and R. P. McBride, *J. Am. Chem. Soc.*, 1977, **99**, 3547-3551.
89. P. R. Ogilby, *Chem. Soc. Rev.*, 2010, **39**, 3181-3209.
90. O. Oter and A.-C. Ribou, *J. Fluoresc.*, 2009, **19**, 389-397.
91. M. S. Lowry, W. R. Hudson, R. A. Pascal and S. Bernhard, *J. Am. Chem. Soc.*, 2004, **126**, 14129-14135.
92. D.-L. Ma, W.-L. Wong, W.-H. Chung, F.-Y. Chan, P.-K. So, T.-S. Lai, Z.-Y. Zhou, Y.-C. Leung and K.-Y. Wong, *Angew. Chem., Int. Ed.*, 2008, **47**, 3735-3739.
93. V. J. Pansare, S. Hejazi, W. J. Faenza and R. K. Prud'homme, *Chem. Mater.*, 2012, **24**, 812-827.
94. S. Luo, E. Zhang, Y. Su, T. Cheng and C. Shi, *Biomaterials*, 2011, **32**, 7127-7138.
95. G. Zhang, H. Zhang, Y. Gao, R. Tao, L. Xin, J. Yi, F. Li, W. Liu and J. Qiao, *Organometallics*, 2014, **33**, 61-68.



aggregates are formed and restrict the motion and induce AIE leading to a large increase in intensity of emission. Since the discovery of AIE in organic molecules, different mechanisms have been proposed to explain the phenomenon.

### 2.1.1 Restricted Intramolecular Rotation (RIR)

The mechanistic model proposed as the main cause of the AIE phenomenon is RIR in the solid state.<sup>5</sup> Many AIE molecules contain molecular rotors such as rotatable aromatic rings. When fully solvated, the rotation of the aromatic rotors of AIE molecules consume the excited-state energy, allowing the energy of an excited state to quickly decay non-radiatively. Upon aggregation, intermolecular interactions between AIE molecules restrict the rotations of the rotors, causing the molecules to decay via radiative channels. For example, compound **2.3** (Figure 2.2) has a naphthyl core structure and phenyl rotors and it shows an AIE effect. The emission is enhanced in THF/water mixtures, where water is the *poor* solvent.<sup>6</sup>

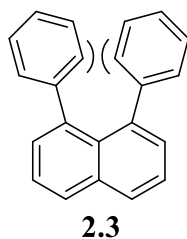


**Figure 2.22:** Compound **2.3** shows AIE.

### 2.1.2 Restricted Intramolecular Vibration (RIV)

Tang and co-workers studied other organic molecules that exhibit the AIE phenomenon but which lacked any rotors.<sup>7</sup> Hence, the AIE effect cannot be explained through the proposed RIR mechanism, therefore other parameters were considered. Compound **2.4** shows AIE due to the RIR principle as described above, but for compounds **2.5** and **2.6** where the rotors are fixed and are not able to rotate, AIE is also observed (Figure 2.3). In compounds **2.5** and **2.6**, a RIV mechanism was proposed where the in-plane/out-of-plane vibrational (twisting) motions would dissipate the excited-state energy causing non-radiative pathways to diminish the emission. Experimental and computational studies showed that the twisting motions were the cause of the non-radiative decay of the excited-state energy. It was concluded that the restriction of these vibrational motions in the solid state resulted in the turn-on emission of compound **2.5** and **2.6**.<sup>7</sup> Other RIV motions include bending, flapping, stretching, wagging, and rocking motions.<sup>8</sup>

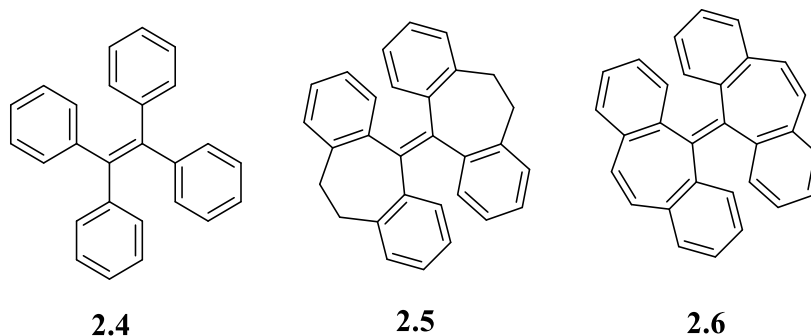


**Figure 2.3:** Organic compounds that show AIE effect.

### 2.1.3 Restricted Intramolecular Motions (RIM)

The RIM mechanism is the combination of the RIR and RIV mechanisms that is present in the same molecule. The fundamental idea of RIM is that the RIR and RIV mechanisms are not mutually exclusive but instead can work together to bring about the AIE phenomenon. Figure 2.4 shows compounds **2.7** and **2.8** that are non-luminescent when dissolved in THF but become emissive in THF/water mixtures because the water causes precipitation of the compounds. Their AIE activity was attributed to the phenyl ring rotations and the vibrations of the cyano unit, as these aid in the dissipation of the excited state energy.<sup>8-10</sup>

Alternatively, to test the theory of RIM in **2.7** and **2.8**, the moieties that introduce RIR (aryl groups) and RIV (cyano groups) could be removed. By doing this, the AIE effect could be measured against having the aryl or the cyano groups versus both moieties present, and understand if one component is more crucial than the other. DFT studies were not performed in these molecules therefore it is not clear if both RIR and RIV are equally essential for AIE to be observed in **2.7** and **2.8**.

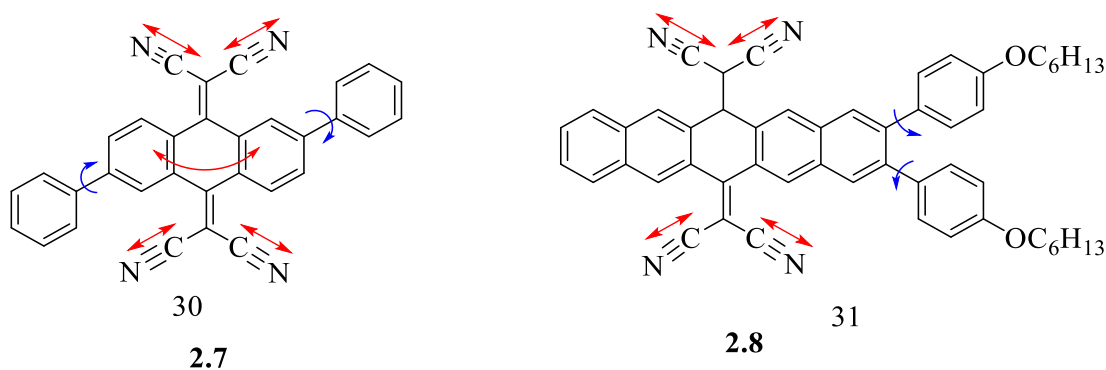
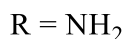
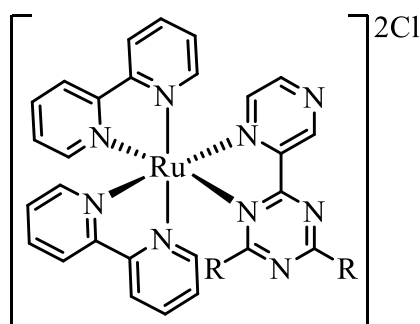


**Figure 2.4:** Organic molecules that show AIE effect.

### 2.1.4 Aggregation Induced Emission in Transition Metal Complexes

Using a metal centre allows the use of a wide range of ligand combinations therefore predicting the origin of AIE is more difficult. Indeed, more mechanisms may be possible for metal complexes (see below). The next section will describe the AIE effect in some transition metal complexes and the proposed origin(s) for this effect. Heavy transition metal complexes can undergo ISC due to high-spin orbit coupling which aids the emission to be of triplet nature i.e. – phosphorescence. Hence, another term that has been used in conjunction with AIE in heavy transition metal complexes is EPESS (Enhanced Phosphorescence Emission in the Solid State). Similar to organic molecules, the metal complex is non- or weakly emissive in solution but its emission is enhanced when aggregates are formed.<sup>2, 5, 11</sup>

Ji and co-workers reported the first polypyridyl Ru(II) complex (**2.9**) to be AIE active (Figure 2.5).<sup>12</sup> In MeCN solution, complex **2.9** showed weak luminescence, but the emission was enhanced with increasing amounts of toluene. The authors did not determine the origin of AIE in **2.9** although, Tang<sup>2</sup> suggested that as there are no groups able to freely rotate in solution, the quenching of emission in **2.9** was assigned to be the vibrational motions of bipy and the N^N ancillary ligand. However, further studies would need to be carried out to confirm this.



**2.9**

**Figure 2.5:** The first Ru(II) polypyridyl complex to show AIE effect.

Li and co-workers found that complex **2.10** (Figure 2.6) is non-emissive in solution (DCM) but the emission is enhanced upon addition of a *poor* solvent (hexane).<sup>13</sup> The group proposed that RIR was the cause of AIE in **2.10**;<sup>13</sup> in addition, Tang, suggested it was due to RIR of the four diphenyl groups and the vibrational motions of the dibromo-1,10-phenanthroline groups together which quenched the emission in

solution.<sup>8</sup> Computational studies would need to be carried out to confirm this mechanism.

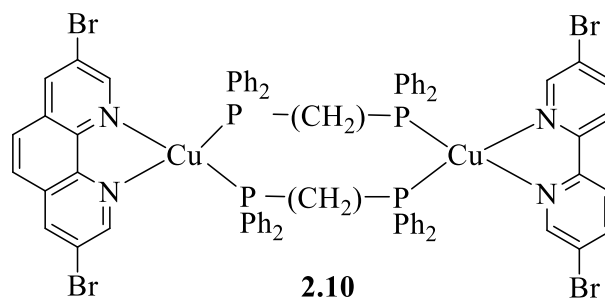
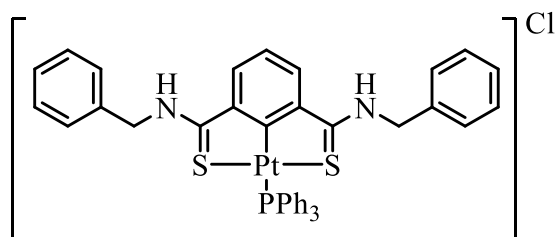


**Figure 2.6:** Complex **2.10** is AIE active.

Kanbara and co-workers found that when complex **2.11** (Figure 2.7) is precipitated from  $\text{CHCl}_3$ /hexane mixtures, the emission intensity is significantly enhanced compared to when it is dissolved in  $\text{CHCl}_3$  solution.<sup>14</sup> The group suggested that the rotational motions of the phenyl groups in the  $\text{PPh}_3$  unit and benzyl moieties contribute to a negligible emission in solution. The emission enhancement is attributed to the RIM effect where the intramolecular motions of the phenyl and benzyl groups are restricted in the solid state, leading to radiative pathways and hence making **2.11** emissive in the solid state.<sup>14</sup> The authors showed that the thioamide groups form hydrogen bonding interactions with the counteranion ( $\text{N-H}\cdots\text{Cl}$ , 2.45 Å) and postulated that this aided the formation of aggregates which suppressed the molecular motion and giving rise to emission in the solid state.<sup>14</sup> Neither Tang nor Kanbara carried out computational studies to investigate this or study the effect of other counter anions and its effect on AIE.



**2.11**

**Figure 2.7:** Pt(II) complex **2.11** showing AIE activity.

Yam and co-workers showed that in THF solution, complex **2.12** (Figure 2.8) has a weak emission but the emission is enhanced with THF/water mixtures.<sup>15</sup> Similarly, complex **2.13** is non-emissive in MeCN, however increasing the volume percentage of PBS (phosphate buffer saline) in mixtures with MeCN results in enhancement in the

emission intensity.<sup>16</sup> In both cases, details of the cause of AIE effect was not given however Tang suggested that AIE was due to RIR of the phenyl and triazole moieties (in **2.12**) and RIR of the phenyl and carbazolyl groups (in **2.13**).<sup>8</sup>

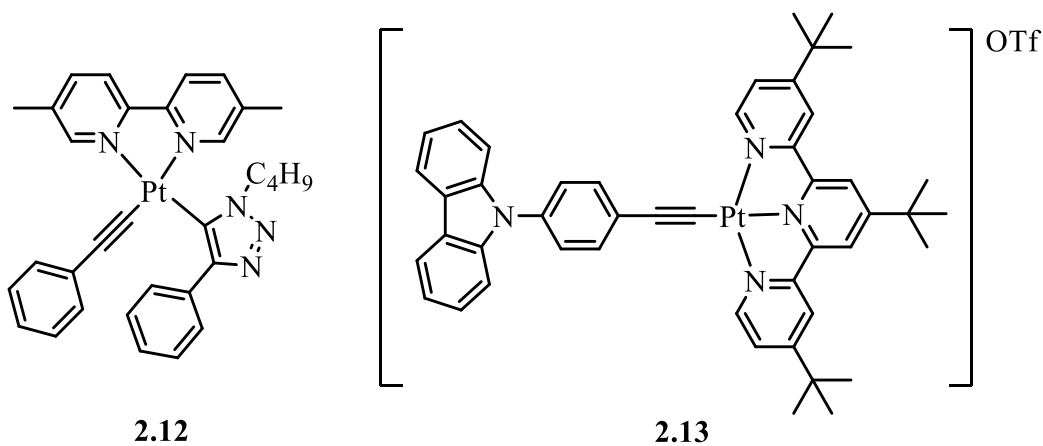


**Figure 2.8:** Other Pt(II) complexes showing AIE activity.

Cyclometallated Pt(II) complexes are known to be strongly emissive in solution when their excited states are dominated by the ppy ligand and the metal centre.<sup>17</sup> Therefore, [Pt(ppy)(N<sup>^</sup>O)] complexes where N<sup>^</sup>O = salicylimine ligand (**2.14-Ph** and **2.14-Bu**)<sup>18, 19</sup> (Figure 2.9) were expected to show emission in solution. Instead, both complexes are non-emissive in solution but are emissive in the solid state. Complex **2.14-Ph** has the possibility for intramolecular rotation around the N-phenyl bond, and complex **2.14-Bu** has the possibility of rotation around the N-C single bond of the propyl group. Computational studies showed that in solution complexes **2.14-Ph** and **2.14-Bu**, the HOMO and LUMO are dominated by the N<sup>^</sup>O ligand and metal centre with no contribution from the ppy ligand.<sup>18</sup> Additionally, a significant structural distortion in the excited state for the chelating six-membered cycle between Pt and the N<sup>^</sup>O ligand was observed in solution. In the solid state, both HOMO and LUMO are localised on the ppy and N<sup>^</sup>O ligand and the chelating six-membered cycles between Pt and N<sup>^</sup>O ligand are almost coplanar. This ligand distortion in solution is responsible for the inefficient emission and giving rise to non-radiative decay, whilst in the solid state the distortion is restricted allowing the ppy ligand to participate in the excited state and therefore giving rise to radiative decay. Hence, in complexes **2.14-Ph** and **2.14-Bu** the emission in solution is quenched due to significant distortions of the N<sup>^</sup>O ligand leading to non-radiative decay.<sup>18, 19</sup>

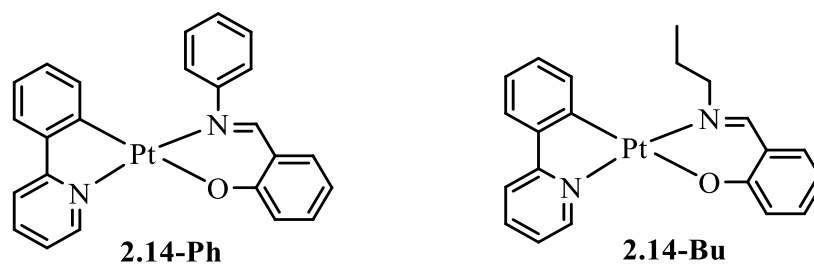


**Figure 2.9:** AIE active Pt(II) cyclometallated complexes.

The first examples of cyclometallated Ir(III) complexes reported as AIE (or EPESS) active are shown in Figure 2.10 and 2.11.<sup>20-22</sup> The cause of EPESS in  $[\text{Ir}(\text{ppy})_2(\text{N}^{\wedge}\text{O})]$  has been disputed in the literature, where two different mechanisms were proposed (i) restricted intramolecular rotations of substituents on the bidentate ancillary ligand  $\text{N}^{\wedge}\text{O}$ <sup>21</sup> (**2.14a-d**) (ii)  $\pi$ -stacking of cyclometallating 2-phenylpyridine ligands.<sup>20, 22, 23</sup> The two mechanisms are discussed in more detail below.

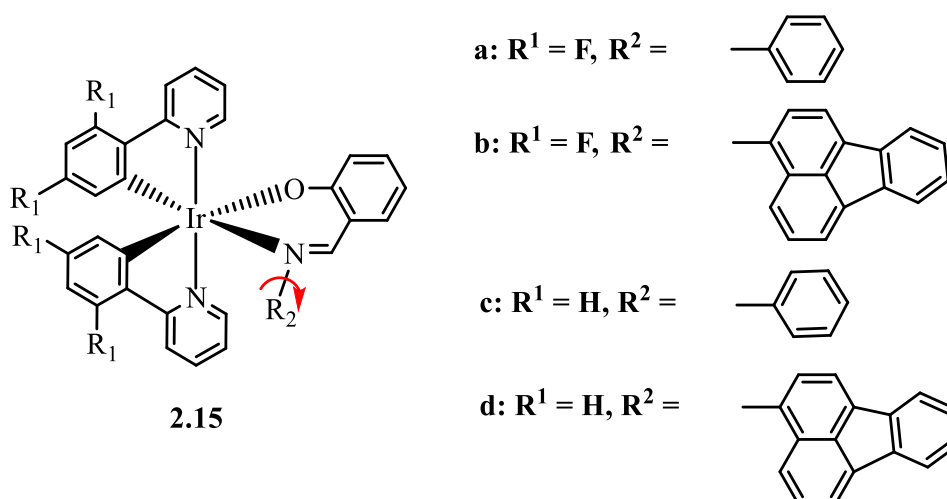


**Figure 2.10:** Complexes **2.15a-d** show EPESS.

Park and co-workers showed that complexes **2.15a-d** (Figure 2.10) are non-emissive in solution (DCM) but in neat films and in various polymer films strong emission is observed.<sup>21</sup> Using a combination of low temperature emission and TD-DFT studies, they concluded that the rotation around the N-aryl bond in solution gives rise to a non-radiative decay pathway causing these complexes to be non-emissive in solution.<sup>21</sup> It was proposed that this pathway is slowed down or shut-off in the solid state giving rise to the observed strong emission. On the other hand, Li and co-workers showed that

complexes **2.16b** and **2.16c** are EPESS active whilst complex **2.16a** is not EPESS active, showing emission in solution and in the solid state (Figure 2.11).<sup>22</sup> The group proposed that the energy of the emissive <sup>3</sup>MLLCT state is below a non-emissive triplet ligand (<sup>3</sup>L) when the  $\pi$ -stacking of the ppy ligands is present in the solid state. By lowering the emissive <sup>3</sup>MLLCT state below the low-lying, non-emissive <sup>3</sup>L state complex **2.16b** and **2.16c** have intense emissions in the solid state in comparison to solution.<sup>22</sup> Additionally, the group also showed that complexes **2.16d** and **2.16e** with no rotatable substituents are also EPESS active.<sup>20</sup> This finding led to uncertainties on the proposed mechanism by Park of the need of restricted intramolecular rotation for EPESS to be observed. X-Ray crystallography was used to show that complexes **2.16d** and **2.16e** also have  $\pi$ - $\pi$  interactions in the solid state agreeing with Li's theory of  $\pi$ -stacking.<sup>20</sup>

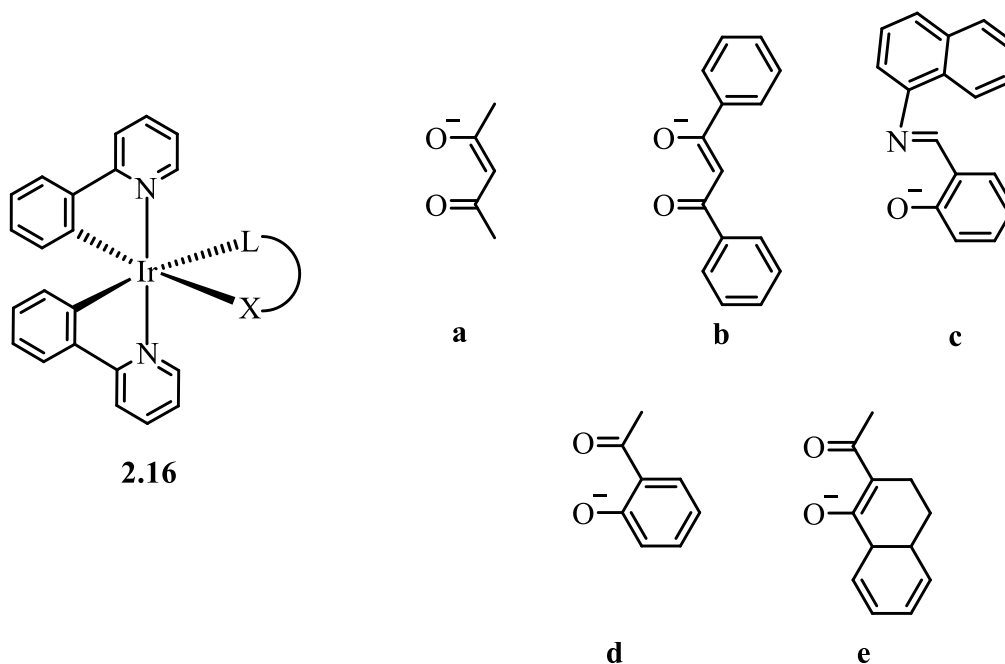


**Figure 2.11:** All complexes are EPESS active except for **2.16a**.

As mentioned above, complexes **2.15a-d** showed strong emission in polymer films,<sup>21</sup> however,  $\pi$ -stacking interactions are less likely to occur in this case due to low loading in the polymer. This is inconsistent with the interpretation put forward by Li that  $\pi$ - $\pi$  stacking is the cause of EPESS.<sup>20, 22</sup>

Liao and co-workers reported the first cationic Ir(III) complex (**2.17**) (Figure 2.12) with neutral N^N ancillary ligand to be EPESS active.<sup>24</sup> In MeCN solution, emission is not observed whilst in a mixture of MeCN:H<sub>2</sub>O the emission is observed. The results

suggested that the restricted intramolecular rotation is responsible for the emission in the solid state in **2.17**.

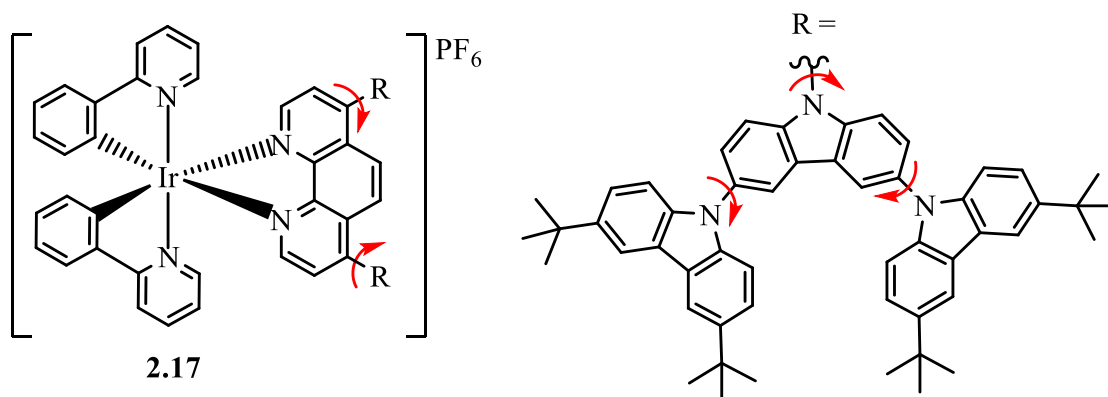


**Figure 2.12:** The first cationic cyclometallated Ir(III) complex (**2.17**) to show EPESS.

The same group later reported<sup>25</sup> that complex **2.18a** is emissive in solution and in the solid state, whilst complex **2.18b** and **2.18c** are weakly emissive in MeCN solution and highly emissive in MeCN:H<sub>2</sub>O mixtures (Figure 2.13). In complex **2.18a**, the HOMO is localised on the cyclometallated ligand and the Ir centre, whilst in **2.18b** and **2.18c** the HOMO is mainly localised on the indole and carbazole groups, respectively. In all three complexes the LUMO is identical residing primarily on the pyridine and 1,2,4-triazole groups of the ancillary ligands. The excited state of **2.18b** and **2.18c** shows large structural motion leading to non-radiative decay and no emission in solution whilst in the solid state, the motion is suppressed leading to radiative decay and emission is observed. Their findings showed that the emissive state for **2.18a** is mainly <sup>3</sup>MLCT/<sup>3</sup>LLCT character hence its emissive in both solution and the solid state. However, **2.18b** and **2.18c** have <sup>3</sup>ILCT character hence show weak emission in solution.<sup>25</sup>

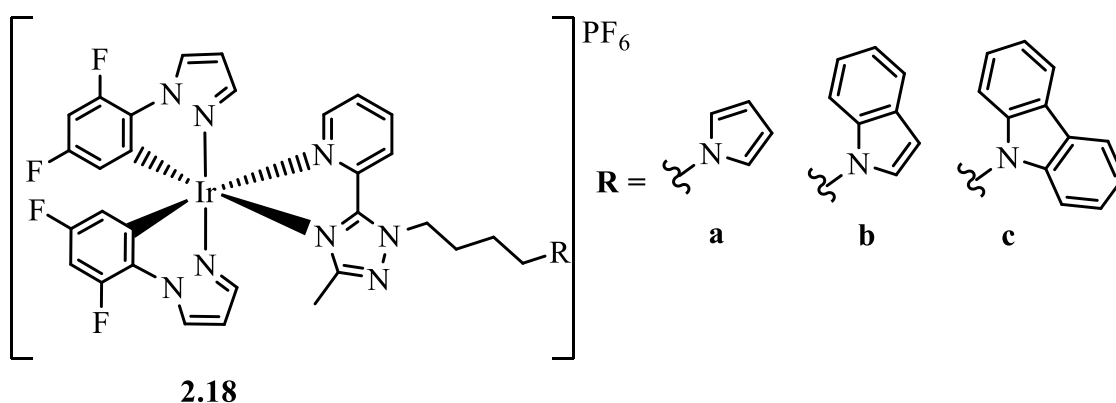


**Figure 2.13:** Complexes **2.18a-c** show different AIE properties by changing the R group.

Neutral complexes **2.19a-c** and **2.20a-b**, with one bidentate and four monodentate ligands, show weak emission in solution but when aggregates are formed using mixtures of THF:H<sub>2</sub>O, the emission is enhanced.<sup>26</sup> Dynamic light scattering (DLS) and scanning electron microscope (SEM) measurements were used to confirm the presence of aggregation and small particle formation. Hence, these complexes are AIE active. Furthermore, a viscous solvent (polyethylene glycol) was also used to study the emission properties and it was found as the concentration of polyethylene glycol increases the emission intensity increases. The authors suggested that in **2.19a-c** and **2.20a-b** (Figure 2.14) the hindrance of the rotationally active part on increasing the viscosity of the solution may be responsible for the increase of luminescence intensity in aggregated samples. Furthermore, in **2.19a-c** and **2.20a-b**, the reduced emission in solution was due to the rotation of the phenyl groups in the phosphine ligands whilst in the solid state and in the viscous solvent, these motions are hindered opening radiative pathways and emission is observed. Computational studies show that the HOMO is localised on the metal centre and on the non-pyridine rings of the cyclometallated ligand, with almost no participation of the phosphine ligands. More recently, the same group<sup>27</sup> showed that cationic complex **2.21** (Figure 2.14) also show enhanced emission in the solid state in comparison to solution. This phenomenon was also attributed as the restriction of intermolecular rotation of the phenyl rings in the phosphine ligands leading to radiative decay in the solid state.

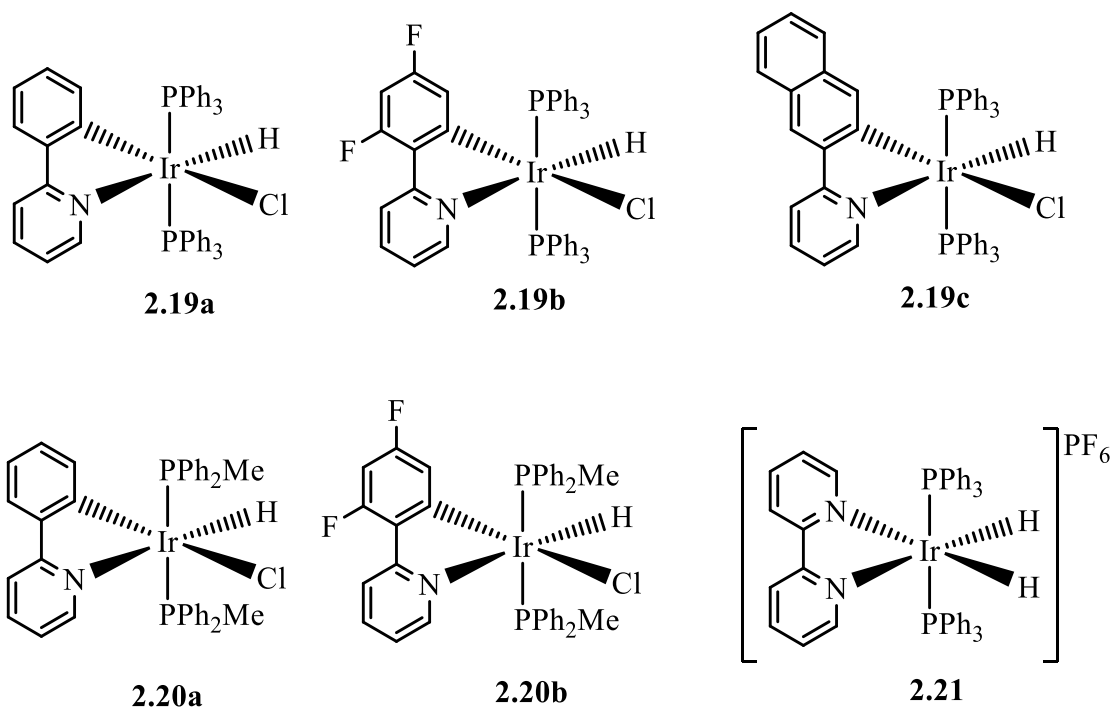


**Figure 2.14:** EPESS active complexes with phosphine ligands.

As shown above, there is disagreement on the mechanism of EPESS in Ir complexes and due to presence of different ligands elucidating the mechanism can become complex. Protection from O<sub>2</sub> in the solid state could also be a possible cause for weak emission in solution. Another factor that could lead to emission quenching in solution can be ligand dissociation. Tang's review does not mention this possibility as the cause of weak emission in metal complexes but then Elliot and co-workers<sup>28</sup> showed that when complex **2.22** (Figure 2.15) is irradiated in solution goes through ligand dissociation after photoexcitation. This could also be a potential quenching pathway in solution in cyclometallated Ir(III) complexes.

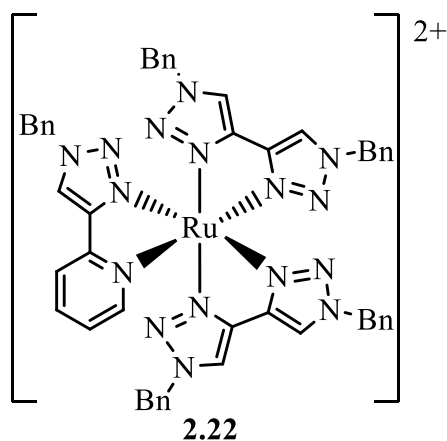


**Figure 2.15:** Complex **2.22** goes through ligand dissociation after photoexcitation.

## Aims and Objectives

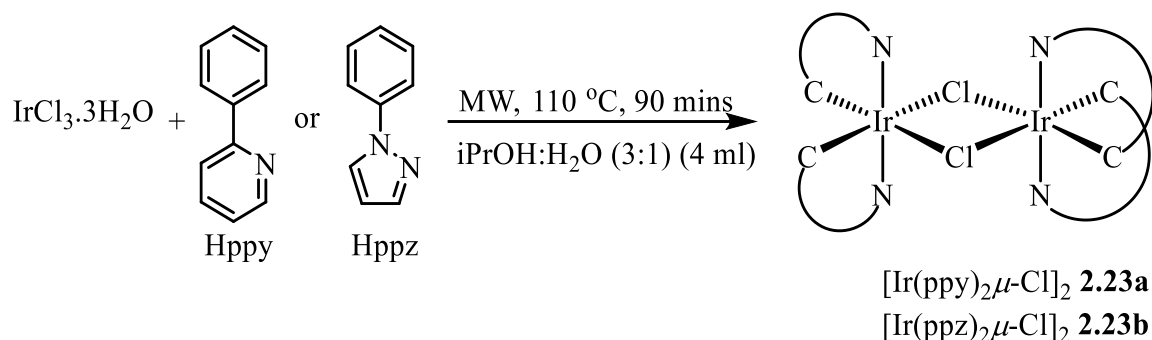
Most of the examples described show that some studies lack evidence for the cause of AIE in metal complexes and many studies lack further investigation to elucidate the poor emission in solution. There is disagreement between Park and Li, hence, the aim of this work was to study these and related complexes in more depth to understand more fully the mechanism of EPESS in such complexes. This chapter will contain a description of the synthesis and luminescent properties of  $[\text{Ir}(\text{C}^{\wedge}\text{N})_2(\text{N}^{\wedge}\text{O})]$  complexes and also the use of 1-phenylpyrazole (ppz) as a cyclometallating ligand since it has less propensity to  $\pi$ -stack than ppy ligands. In addition, large bulky N-aryl substituents on the imine will be used to try and ensure that rotation is not possible. Computational studies which were carried out by Professor F. Lelj (University of Potenza) are also included in this chapter to aid with the understanding of this phenomenon.

## 2.2 Results and Discussion

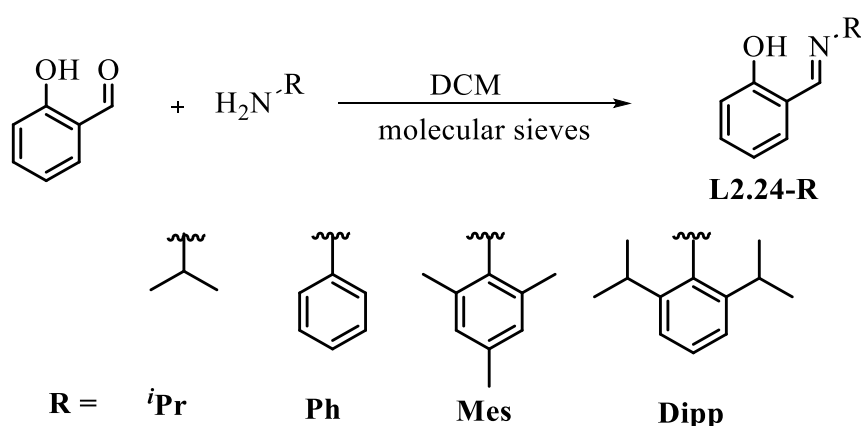
This section will describe the synthesis of the ligands and cyclometallated  $[\text{Ir}(\text{C}^{\wedge}\text{N})_2(\text{N}^{\wedge}\text{O})]$  complexes and their luminescent properties. Their EPESS ability will be tested followed by a discussion of the results obtained. This work was part of a collaborative project with Professor M. Wolf (UBC, Vancouver, Canada) and Professor F. Lelj (University of Potenza). Ligand **L2.24-Ph** and complexes **2.24a-Ph** and **2.24b-Ph** were prepared by A. J. Howarth (UBC) as well as its characterisation and the photophysical studies.<sup>29</sup>

### 2.2.1 Synthesis and Characterisation of $[\text{Ir}(\text{C}^{\wedge}\text{N})_2(\text{N}^{\wedge}\text{O})]$ ( $\text{N}^{\wedge}\text{O}$ = salicylimine)

The dichloro-bridged  $[\text{Ir}(\text{C}^{\wedge}\text{N})_2\mu\text{-Cl}]_2$  dimers (**2.23a-b**) were synthesised using a microwave reactor (Scheme 2.1).<sup>30</sup> The salicylimine ligands (**L2.24-R**) were synthesised using a typical condensation reaction with salicylaldehyde and the respective amine in the presence of molecular sieves in DCM (Scheme 2.2). All ligands are known in the literature.<sup>31-33</sup>



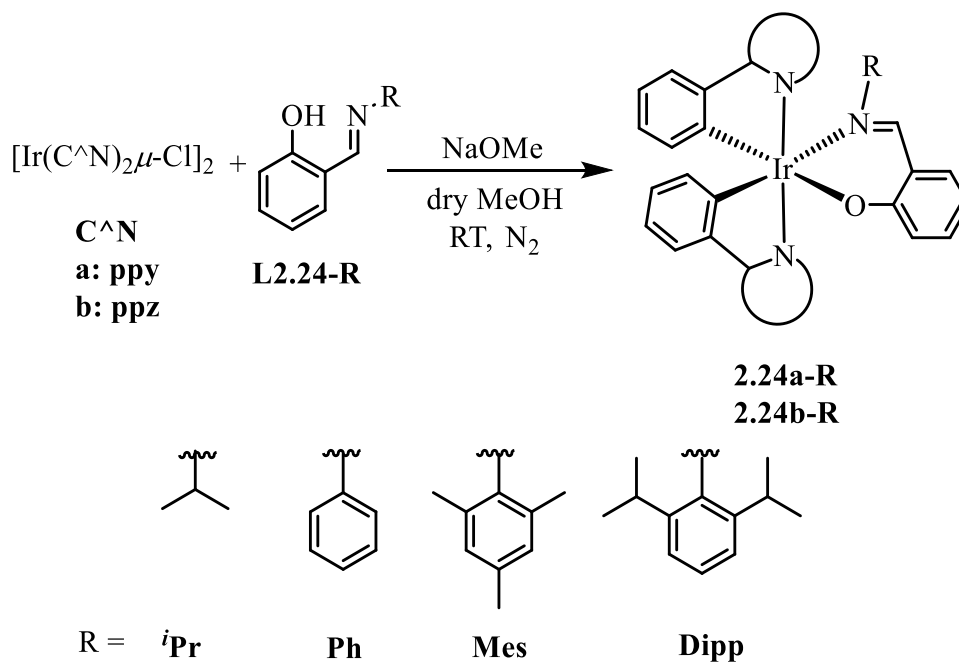
**Scheme 2.1:** Microwave reaction for the synthesis of Ir(III) dimers **2.23a-b**.



**Scheme 2.2:** Condensation reaction for the synthesis of ligands **L2.24-R**.

The  $^1\text{H}$  NMR and  $^{13}\text{C}$  NMR spectra of dimeric precursors **2.23a-b** agree with the literature, where the  $\text{C}^{\wedge}\text{N}$  ligands are chemically equivalent showing a  $\text{C}_2$  symmetry.<sup>30, 34</sup> The  $^1\text{H}$  NMR spectrum of ligand **L2.24-*i*Pr** shows the  $\text{N}=\text{CH}$  proton at  $\delta$  8.34 and the  $\text{N}^i\text{Pr}$  group appears as a 1H septet at  $\delta$  3.54 and a 6H doublet at  $\delta$  1.29. The  $^1\text{H}$  NMR spectrum of ligand **L2.24-Mes** shows a 1H singlet at  $\delta$  8.31 that corresponds to the  $\text{N}=\text{CH}$  proton, a 6H singlet at  $\delta$  2.17 that corresponds to the 2 x *ortho*-Me groups and a 3H singlet at  $\delta$  2.29 that corresponds to the *para*-Me. The aromatic protons in the mesityl group appear as a 2H singlet at  $\delta$  6.91. The  $^{13}\text{C}$  NMR spectrum shows a signal at  $\delta$  20.8 corresponding to the two *ortho*-Me groups and at  $\delta$  18.5 corresponding to the *para*-Me. This suggests that **L2.24-Mes** is rotating in solution. The  $^1\text{H}$  NMR spectrum of **L2.24-Dipp** shows a 1H singlet at  $\delta$  8.30 that corresponds to the  $\text{N}=\text{CH}$  proton and a 2H septet at  $\delta$  3.00 and a 12H doublet at  $\delta$  1.18. The  $^{13}\text{C}$  NMR spectrum shows peaks at  $\delta$  28.2 and 23.6 corresponding to the isopropyl  $\text{N}-\text{CH}$  and methyl groups respectively.

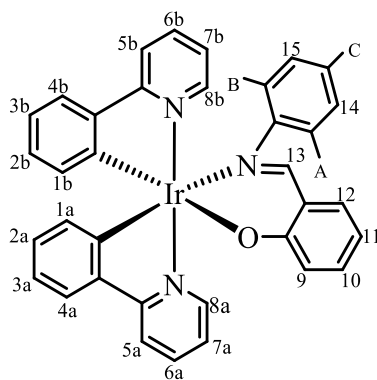
This suggests that the di-isopropyl R group in **L2.24-Dipp** is rotating in solution. Ligand **L2.24-Ph** was prepared by our collaborators in Canada.



**Scheme 2.3:** Synthesis of complexes **2.24a-R** and **2.24b-R**.

Note, complex **2.24a-Ph** was previously prepared by Park *et al.* (see complex **2.15c** earlier in Figure 2.10). Ir(III) dimers **2.23a-b** and N<sup>^</sup>OH ligands **L2.24-R** (2.2 equiv) in the presence of NaOMe (2.2 equiv) in dry methanol were used to form products **2.24a-R** and **2.24b-R** (61-81%) (Scheme 2.3).

The <sup>1</sup>H NMR spectra of products **2.24a-R** and **2.24b-R** showed that the C<sub>2</sub> symmetry of the dimers was lost upon complexation of the unsymmetrical N<sup>^</sup>O ligand, therefore the two C<sup>^</sup>N ligands become chemically inequivalent giving double the number of proton peaks. As an example, the assignment of complex **2.24a-Mes** (Figure 2.16) is explained in detail using parts of the TOCSY, NOESY, COSY and HSQC spectra in Figures 2.17-2.22.



**2.24a-Mes**

**Figure 2.16w:** Numbering system for complex **2.24a-Mes**.

Figure 2.17 shows the TOCSY spectrum for complex **2.24a-Mes** identifying two cyclometallated phenyl rings, two pyridine rings, one mesityl group, and one phenol ring.

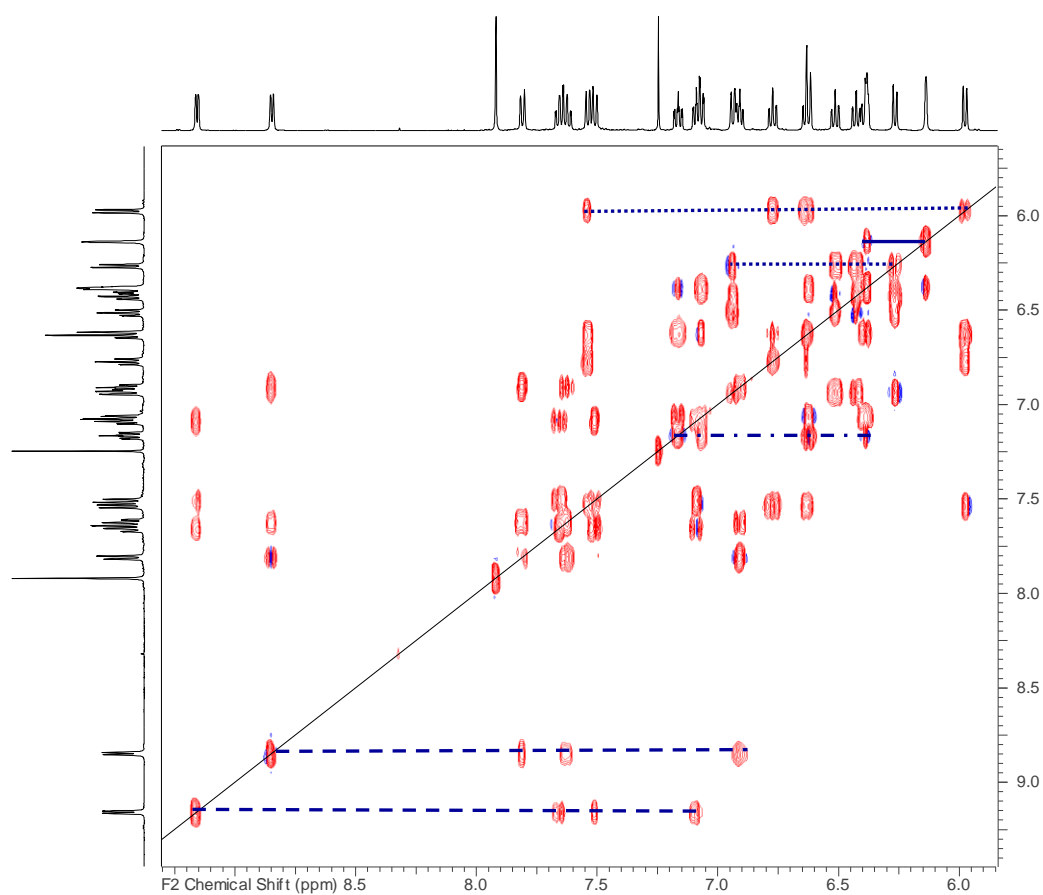


**Figure 2.17:** TOCSY spectrum of complex **2.24a-Mes** showing the identification of two cyclometallated phenyl rings (·····), two pyridine rings (-----) one mesityl group (—), and one phenol ring (-·-·-·-).

The TOCSY and the NOE spectra help identify the linkage between the pyridine and phenyl rings in the cyclometallated ligand. The identification of the C<sup>N</sup> ligand *a* and *b* were established using the NOE spectrum of the alkyl area. In complex **2.24a-Mes**, the mesityl group appears as three 3H singlets at  $\delta$  1.21, 1.93, 2.05 and the two aromatic protons as a singlet at  $\delta$  6.14 and under a multiplet at  $\delta$  6.39. The inequivalence of the methyl groups suggests that the mesityl group is fixed (i.e. not rotating) when complexed to the metal, unlike in the free ligand. The 3H singlet at  $\delta$  1.93 shows a NOE with pyridine proton H<sup>8a</sup> at  $\delta$  8.85 and phenyl proton H<sup>1b</sup> at  $\delta$  6.27, and this is assigned as an *ortho*-Me as the *para*-Me is too far away to show these correlations. Therefore, signal at  $\delta$  1.93 is assigned as Me<sup>A</sup> as it shows the NOE correlation only with H<sup>14</sup> at  $\delta$  6.14 and not with H<sup>15</sup> at  $\delta$  6.39 (under a multiplet). Consequently, protons H<sup>5a</sup>, H<sup>6a</sup> and H<sup>7a</sup> were identified using the COSY spectrum. Me<sup>C</sup> at  $\delta$  2.05 is the *para*-Me as it shows a NOE with both H<sup>14</sup> and H<sup>15</sup> (Figure 2.19). By process of elimination, signal at  $\delta$  1.21 corresponds to Me<sup>B</sup> as it only shows a NOE with H<sup>15</sup> and not with H<sup>14</sup> confirming that it is an *ortho*-Me and also shows a weak NOE with H<sup>8b</sup>. Pyridine proton H<sup>5a</sup> at  $\delta$  7.81 shows a NOE with H<sup>4a</sup> at  $\delta$  7.54 on the attached phenyl and therefore protons H<sup>1a</sup>, H<sup>2a</sup> and H<sup>3a</sup> were also identified by COSY spectrum. The protons from cyclometallated ligand *b* were assigned by looking at the NOE correlations between H<sup>5b</sup> and H<sup>4b</sup>; consequently, the remaining protons from ligand *b* were assigned using the COSY spectrum.

In the aromatic region, the most upfield doublets are usually the protons that correspond to the H<sup>1a</sup> and H<sup>1b</sup> of the phenyl ring in C<sup>N</sup> ligands due to current ring effects, as noted previously.<sup>30, 35</sup> H<sup>1b</sup> at  $\delta$  6.27 was found to be slightly more downfield than H<sup>1a</sup> at  $\delta$  5.98. This could be because H<sup>1b</sup> is closer to the mesityl group than H<sup>1a</sup> and may be affected by a ring current of the mesityl. The imine proton H<sup>13</sup> is easily identified as a singlet at  $\delta$  7.92. H<sup>13</sup> shows an NOE with H<sup>12</sup> at  $\delta$  7.07 that corresponds to a phenol proton and Me<sup>B</sup> at  $\delta$  1.21. The remaining phenol protons H<sup>9</sup>, H<sup>10</sup> and H<sup>11</sup> were assigned using the COSY spectrum.

It is important to note that the Chemdraw picture of **2.24a-Mes** is not an accurate representation of the 3D structure. Therefore, a 3D model kit was used where the mesityl group is not flat, instead it is likely to be parallel to the phenyl part of the C<sup>N</sup> ligand *b* as seen similarly in the X-Ray structure of **2.24a-Dipp** (see Figure 2.25 below).

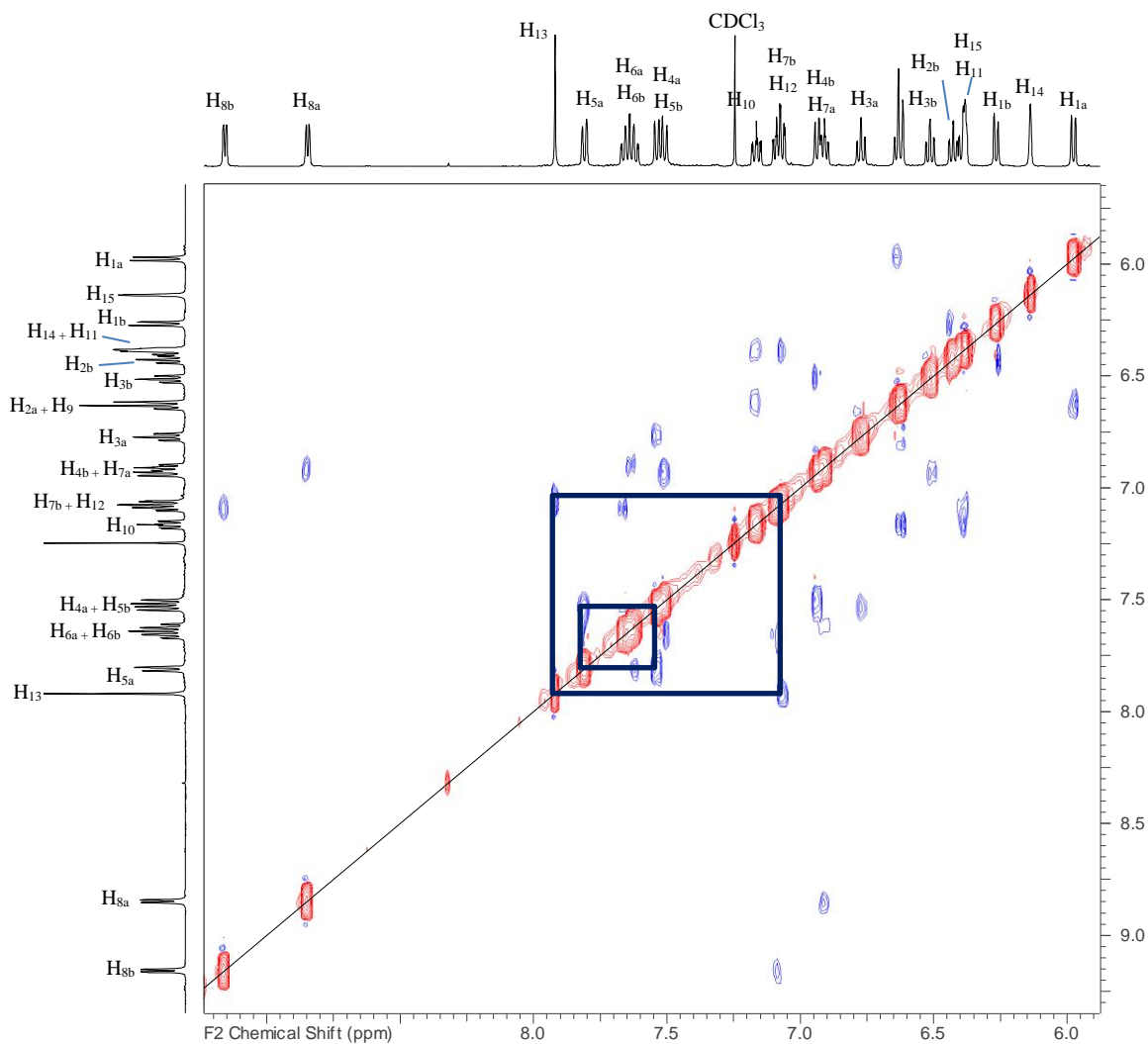


**Figure 2.18:** NOESY spectrum of complex **2.24a-Mes** showing some key NOEs in the aromatic region.

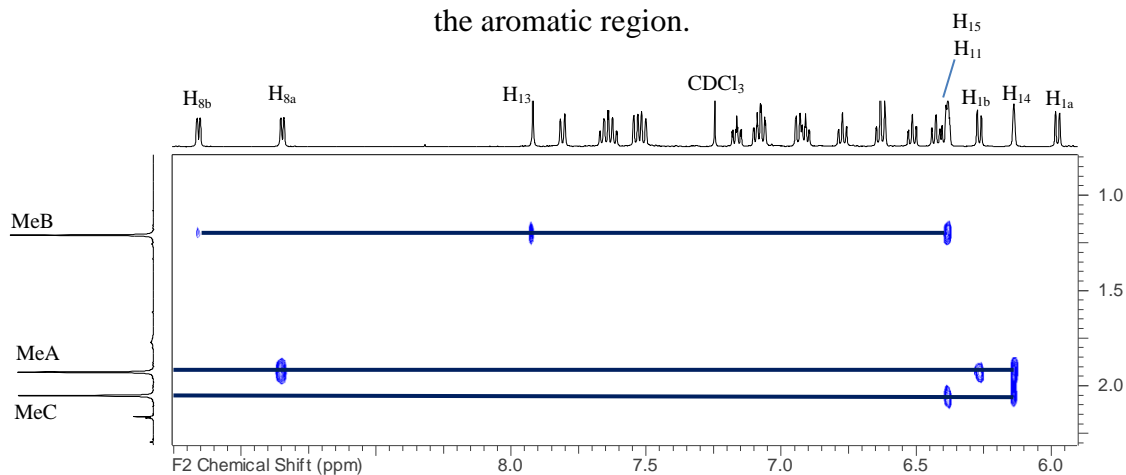


**Figure 2.19:** Partial NOESY spectrum of complex **2.24a-Mes** showing key NOEs in the alkyl region.

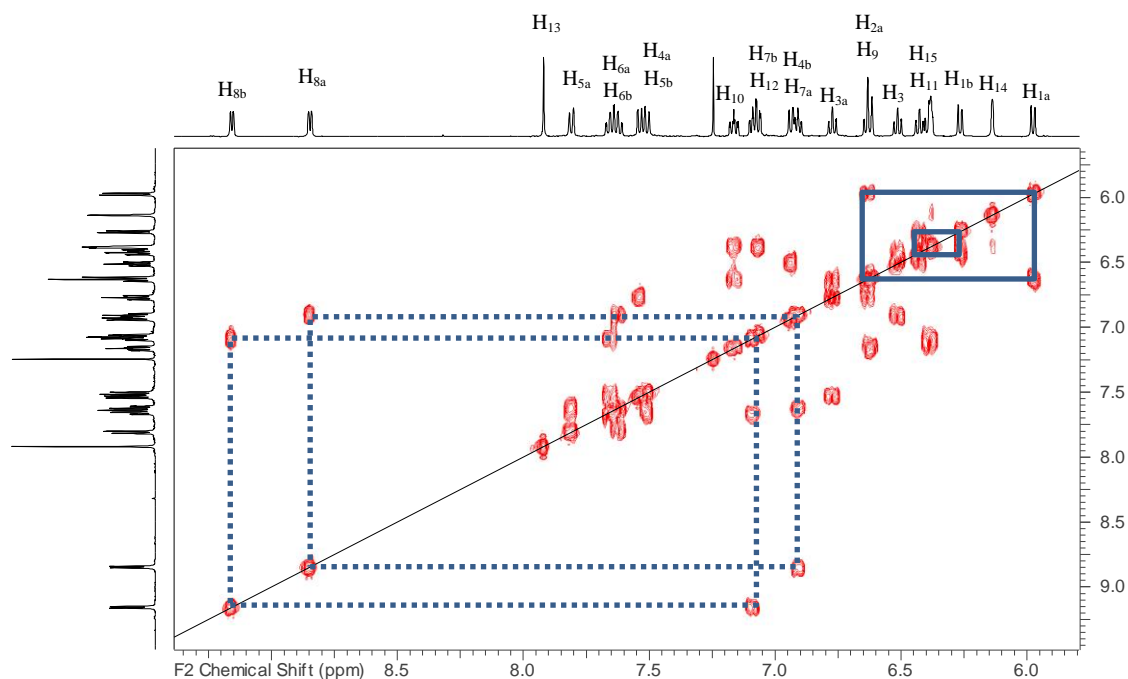


**Figure 2.20:** COSY spectrum of complex **2.24a-Mes** showing one bond correlations.

After assigning the protons in complex **2.24a-Mes**, the coupled carbons were determined using the HSQC spectrum. Figure 2.21 shows the couplings between the aromatic protons and its respective carbon peak, whilst Figure 2.22 shows the correlations in the alkyl region which further specifies the inequivalence of the methyl groups in the mesityl group. The MS(ASAP) showed a molecular ion peak at  $m/z$  740. The IR spectrum shows a  $\nu(\text{C}=\text{N})_{\text{imine}}$  stretch at  $1581\text{ cm}^{-1}$  in comparison to the free ligand at  $1631\text{ cm}^{-1}$  due to backbonding effect.

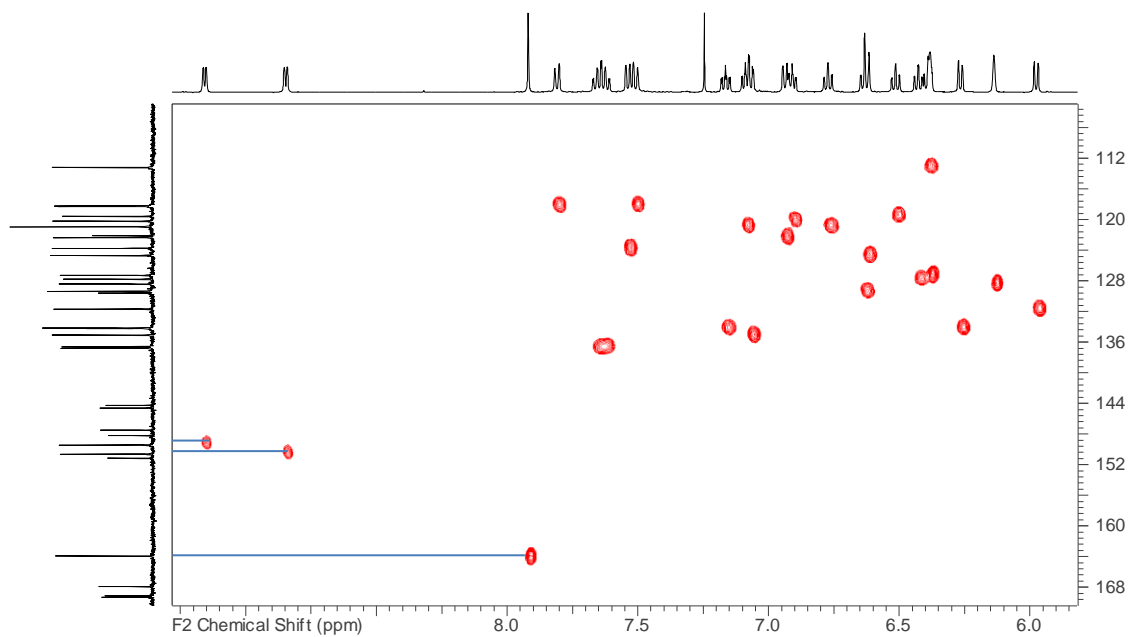


**Figure 2.21:** HMQC spectrum of complex **2.24a-Mes** showing some direct C-H bond couplings in the aromatic region.

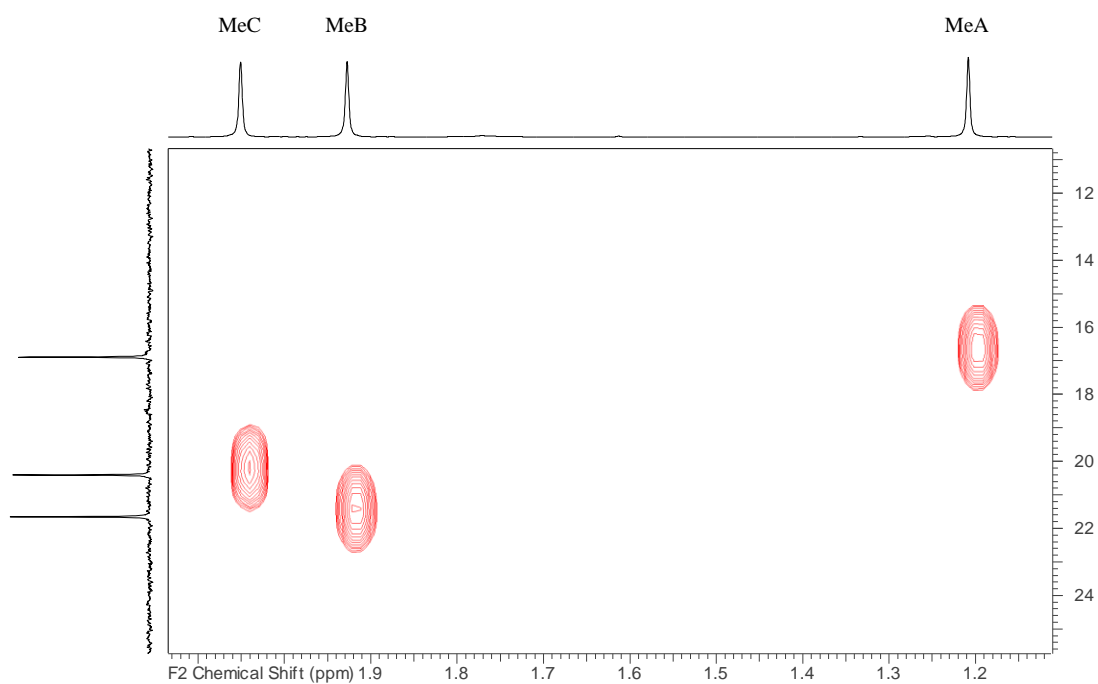
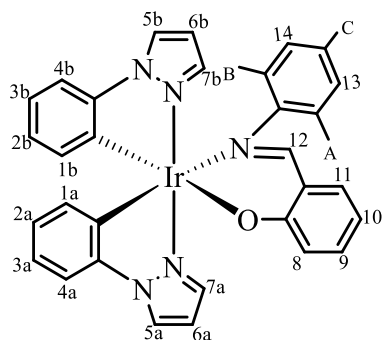


**Figure 2.22:** HMQC spectrum of complex **2.24a-Mes** showing direct C-H bond couplings in the alkyl region.



**2.24b-Mes**

**Figure 2.23:** Numbering system for complex **2.24b-Mes**.

The characterisation of complex **2.24b-Mes** (Figure 2.23) was carried out in a similar manner to **2.24a-Mes**. The TOCSY spectrum was used to identify the protons that correspond to the two pyrazole rings, the two phenyls from the C<sup>N</sup> ligand, the phenol and the mesityl signals. The mesityl group gives a 6H singlet at  $\delta$  2.04 and a 3H singlet at  $\delta$  1.43 possibly suggesting free rotation. However, the NOE spectrum (Figure 2.24) showed an NOE between the 3H methyl singlet at  $\delta$  1.43 and one *ortho* proton (H<sup>14</sup>) at  $\delta$  6.41 but not with H<sup>13</sup> at  $\delta$  6.21 and NOE with H<sup>5b</sup>, hence signal at  $\delta$  1.43 is *ortho*-Me<sup>B</sup> (pointing up). Therefore, the second *ortho*-Me (Me<sup>A</sup>) (pointing down) and the *para*-Me (Me<sup>C</sup>) have the same chemical shift. The 6H singlet at  $\delta$  2.04 shows a NOE to both *ortho* protons showing that it includes *para*-Me (Me<sup>C</sup>) but also an NOE with a phenyl proton H<sup>1b</sup> at  $\delta$  6.27 and pyrazole proton H<sup>5a</sup> at  $\delta$  7.68 and this is only possible if it is an *ortho*-Me as *para*-Me (Me<sup>C</sup>) would be too far away to correlate in space with H<sup>5a</sup>. Hence Me<sup>B</sup> is the 3H singlet and Me<sup>A</sup> and the *para*-Me (Me<sup>C</sup>) accidentally occur at the same chemical shift. Moreover, H<sup>5a</sup> shows an NOE with H<sup>4a</sup> at  $\delta$  7.10 and similarly H<sup>5b</sup> at  $\delta$  8.00 with H<sup>4b</sup> at  $\delta$  6.61. Consequently, the remaining protons on the C<sup>N</sup> ligand were identified using the COSY spectrum. The imine peak H<sup>12</sup> at  $\delta$  7.83 shows an NOE with phenol proton H<sup>11</sup> at  $\delta$  7.07, thus the remaining phenol protons were identified using the COSY spectrum. The fact that the two *ortho* methyl groups are inequivalent suggests the mesityl is fixed in solution as for **2.24a-Mes**.

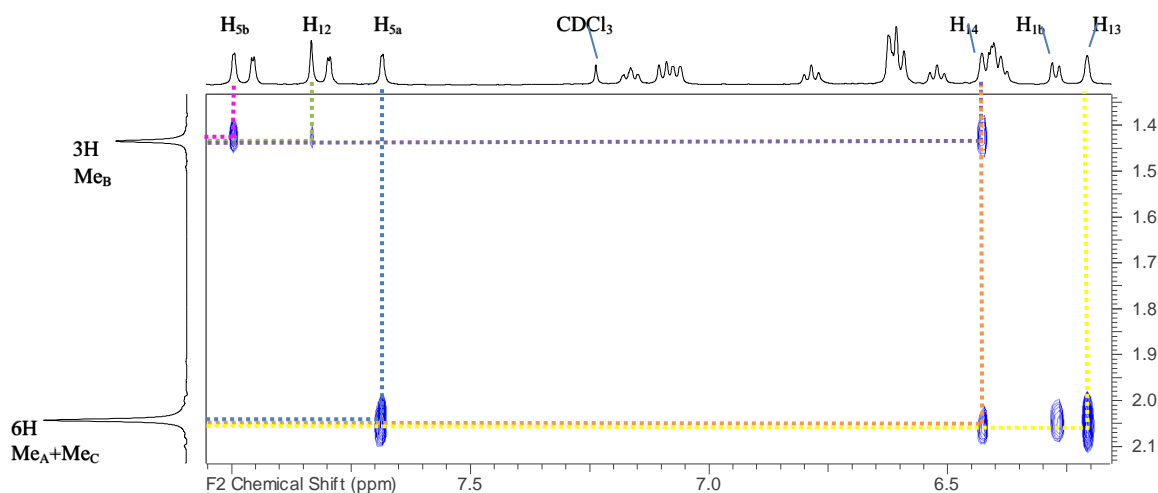


**Figure 2.24:** NOESY spectrum of complex **2.24b-Mes** showing some key NOEs in the aromatic region.

The  $^1\text{H}$  NMR spectra of complexes **2.24a-*i*Pr** and **2.24b-*i*Pr** show a 1H singlet due to the imine proton at  $\delta$  8.15 and 8.06, respectively. Complex **2.24a-*i*Pr** shows a 1H septet at  $\delta$  3.54 and two 3H doublets at  $\delta$  1.12 and 0.53 due to the *i*Pr group whilst in **2.24b-*i*Pr** the corresponding signals are at  $\delta$  3.72 (1H) and two 3H doublets at  $\delta$  1.18 and 0.55. When **L2.24-*i*Pr** is complexed to the Ir centre, mirror plane is lost and the methyls of the *i*Pr group become inequivalent giving two 3H doublets. The protons of the C<sup>N</sup> ligand in both complexes are also inequivalent and the characterisation was done following the method of **2.24a-Mes**. The high field aromatic protons in **2.24a-*i*Pr** appear at  $\delta$  6.15 and  $\delta$  6.36, whilst **2.24b-*i*Pr** H<sup>1a</sup> appears at  $\delta$  6.25 and H<sup>1b</sup> at  $\delta$  6.18. The characteristic high field protons are due to ring current effects.<sup>30, 35</sup> The mass spectra (HR ESI) shows a molecular ion at  $m/z$  664 for complex **2.24a-*i*Pr** and  $m/z$  642 for complex **2.24b-*i*Pr**, and the IR spectrum shows a  $\nu(\text{C}=\text{N})_{\text{imine}}$  stretch at  $1581\text{ cm}^{-1}$  and  $1598\text{ cm}^{-1}$ , respectively in comparison to the free ligand at  $1625\text{ cm}^{-1}$ .

In complex **2.24a-Dipp**, the  $^1\text{H}$  NMR spectrum shows two septets at  $\delta$  2.48 and 3.33 and four 3H doublets at  $\delta$  1.14, 0.89, 0.88, and 0.39 due to the isopropyl groups. The inequivalence of the two CH protons and all four methyls suggests that in solution the R group is not rotating (i.e. it is fixed in solution) and both C<sup>N</sup> ligands are chemically inequivalent. Similarly, in complex **2.24b-Dipp**, the  $^1\text{H}$  NMR spectrum shows two septets at  $\delta$  3.48 and at  $\delta$  2.68 and four 3H doublet at  $\delta$  1.18, 1.03, 0.87 and 0.62, also suggesting that the R group is fixed in solution. The mass spectrum (HR-ESI) for complex **2.24a-Dipp** shows a molecular ion at  $m/z$  782 and  $m/z$  760 for complex **2.24b-**

**Dipp**. The IR spectra for complex **2.24a-Dipp** and **2.24b-Dipp** shows a  $\nu(\text{C}=\text{N})_{\text{imine}}$  stretch at  $1581\text{ cm}^{-1}$  and  $1582\text{ cm}^{-1}$ , respectively, in comparison to the free ligand at  $1635\text{ cm}^{-1}$ . Complexes **2.24a-Dipp** and **2.24b-Dipp** with the most sterically bulky complexes have evidently shown that the R group does not rotate in solution. It was important to achieve this feature when designing the complexes as Park's theory suggests that in solution the N-aryl bond is free to rotate whilst in the solid there is restricted rotation around the N-aryl bond. Therefore, the bulky R groups that are fixed in solution should not lead to non-radiative decay.

Crystals suitable for X-Ray crystallography were obtained of **2.24a-<sup>i</sup>Pr** (from DCM/hexane), **2.24a-Dipp** (from  $\text{CHCl}_3 / \text{CH}_3\text{OH}$ ) and **2.21b-Dipp** (from  $\text{CHCl}_3$ ). The X-Ray structures are shown in Figures 2.25 and 2.26 with selected bond lengths and bond angles Tables 2.1 and 2.2. All three complexes show the same general features with *cis* metallated carbons and *trans* nitrogen atoms of the C<sup>^</sup>N ligands, as expected for similar complexes.<sup>21, 29</sup> In complexes **2.24a-<sup>i</sup>Pr** and **2.24a-Dipp** the angle N(ppy)—Ir—N(ppy) is  $173.2^\circ$  and  $170.2^\circ$ , respectively. In the ppz complex (**2.24b-Dipp**), the angle between N(1)—Ir(1)—N(3) is  $171.0^\circ$ . This shows that the Ir centre has a distorted octahedral geometry. In **2.24a-<sup>i</sup>Pr**, the Ir(1)—N(1) bond length to the imine (2.157(10) Å) is more than 0.1 Å longer than the Ir—N(ppy) bonds Ir(1)—N(3) 2.060(10) Å and Ir(1)—N(2) 2.087(10) Å due to the *trans* influence of the C atom of the cyclometallating ligand. The same is true in complexes **2.24a-Dipp** and **2.24b-Dipp** (See Table 2.1 and 2.2 for bond lengths). The packing diagrams of complexes **2.24a-<sup>i</sup>Pr**, **2.24a-Dipp** and **2.24b-Dipp** did not show any  $\pi$ -stacking in the crystal form, therefore any emission observed in the solid state is not due to  $\pi$ - $\pi$  stacking.

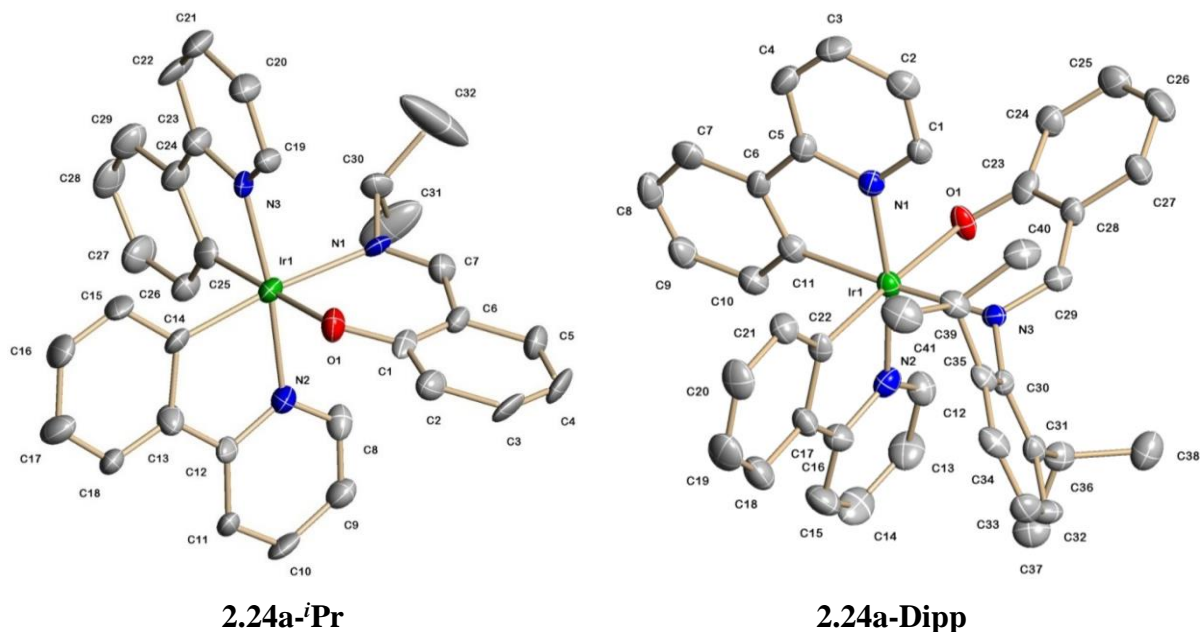


**Figure 2.25:** X-Ray structures of **2.24a-*i*Pr** **2.21a** with 50% displacement ellipsoids; solvent molecules and hydrogen atoms have been omitted for clarity.

<b>Table 2.1:</b> Selected bond length (Å) and bond angles (°) for complexes <b>2.24a-<i>i</i>Pr</b> and <b>2.24a-Dipp</b> .			
<b>2.24a-<i>i</i>Pr</b>	(Å)	<b>2.24a-Dipp</b>	(Å)
Ir(1)—N <sub>py</sub> (3)	2.060(10)	Ir(1)—N <sub>py</sub> (1)	2.044(5)
Ir(1)—N <sub>py</sub> (2)	2.087(10)	Ir(1)—N <sub>py</sub> (2)	2.023(5)
Ir(1)—N <sub>im</sub> (1)	2.157(10)	Ir(1)—N <sub>im</sub> (3)	2.159(5)
Ir(1)—C(14)	2.010(12)	Ir(1)—C(11)	1.989(6)
Ir(1)—C(25)	2.006(13)	Ir(1)—C(22)	1.977(6)
Ir(1)—O(1)	2.161(8)	Ir(1)—O(1)	2.160(4)
<b>2.24a-<i>i</i>Pr</b>	(°)	<b>2.24a-Dipp</b>	(°)
N <sub>py</sub> (3)—Ir(1)—N <sub>py</sub> (2)	173.2(4)	N <sub>py</sub> (2)—Ir(1)—N <sub>py</sub> (1)	170.2(2)
N <sub>py</sub> (3)—Ir(1)—C(25)	82.6(5)	N <sub>py</sub> (2)—Ir(1)—C(22)	80.2(2)
N <sub>py</sub> (2)—Ir(1)—C(14)	80.3(4)	N <sub>py</sub> (1)—Ir(1)—C(11)	80.1(2)
N <sub>im</sub> (1)—Ir(1)—O(1)	86.5(4)	N <sub>im</sub> (3)—Ir(1)—O(1)	85.63(16)

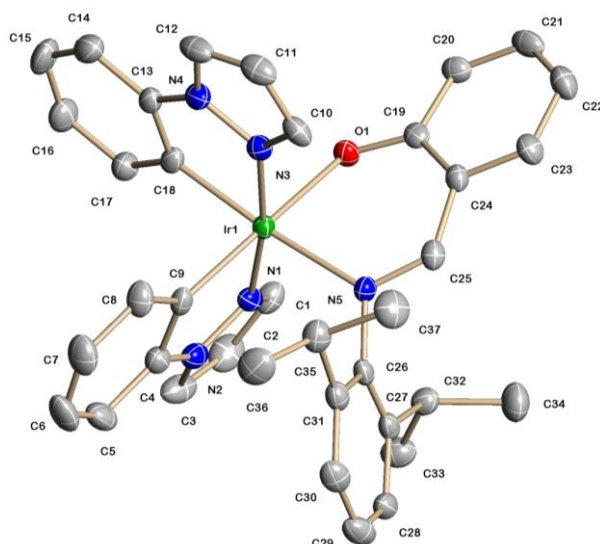


**Figure 2.26:** X-Ray structure of complex **2.24b-Dipp** with 50% displacement ellipsoids; solvent molecule and hydrogen atoms have been omitted for clarity.

<b>Table 2.2:</b> Selected bond lengths (Å) and angles (°) for complex <b>2.24b-Dipp</b> .			
<b>2.24b-Dipp</b>	(Å)	<b>2.24b-Dipp</b>	(°)
Ir(1)—N <sub>pz</sub> (1)	1.993(4)	N <sub>pz</sub> (1)—Ir(1)—N <sub>pz</sub> (3)	171.01(14)
Ir(1)—N <sub>pz</sub> (3)	2.018(4)	N <sub>pz</sub> (1)—Ir(1)—C(9)	79.95(17)
Ir(1)—N <sub>im</sub> (5)	2.138(4)	N <sub>pz</sub> (3)—Ir(1)—C(18)	80.05(17)
Ir(1)—C(9)	1.997(4)	N <sub>im</sub> (5)—Ir(1)—O(1)	86.38(12)
Ir(1)—C(18)	1.989(4)		
Ir(1)—O(1)	2.131(3)		

## 2.2.2 Photophysical Investigation of [Ir(C<sup>^</sup>N)<sub>2</sub>(N<sup>^</sup>O)] (N<sup>^</sup>O = salicylimine)

### Absorption Spectroscopy

There are three bands observed in the absorption spectra of complexes [Ir(C<sup>^</sup>N)<sub>2</sub>(N<sup>^</sup>O)] (N<sup>^</sup>O = salicylimine) ( $\pi - \pi^*$ , <sup>1</sup>MLCT, <sup>3</sup>MLCT). The most intense absorption is below 300 nm and it is assigned as intraligand ( $\pi - \pi^*$ ) transitions. The moderately intense absorption between 300 – 400 nm are attributed to spin allowed metal to ligand charge transfer (<sup>1</sup>MLCT). Weak bands  $\lambda > 400$  nm are due to the spin forbidden transition (<sup>3</sup>MLCT). Figures 2.27 and 2.28 shows the absorption spectra of ppy complexes (**2.24a-R**) and ppz complexes (**2.24b-R**), respectively. Table 2.3 shows the electronic absorption data for all the complexes, except **2.24a-Ph** and **2.24b-Ph**.

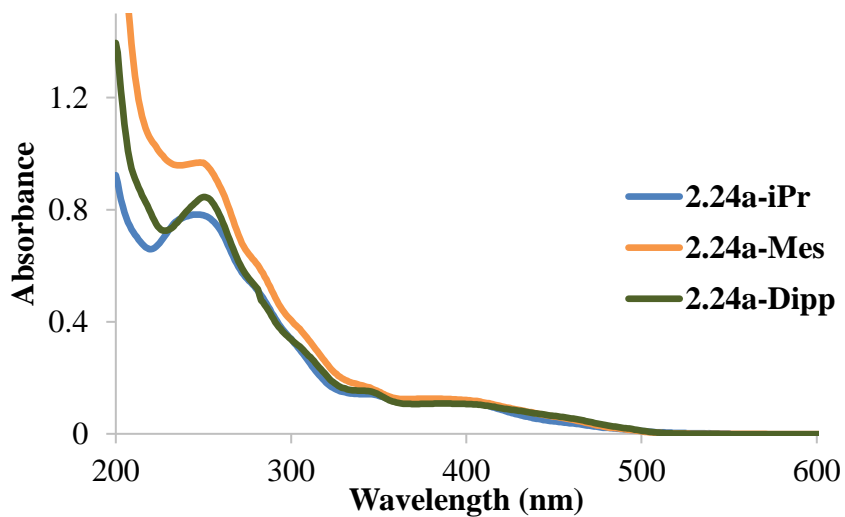


**Figure 2.27:** Absorption spectra of ppy complexes **2.24a-R** in MeCN at 0.02 mM concentration.

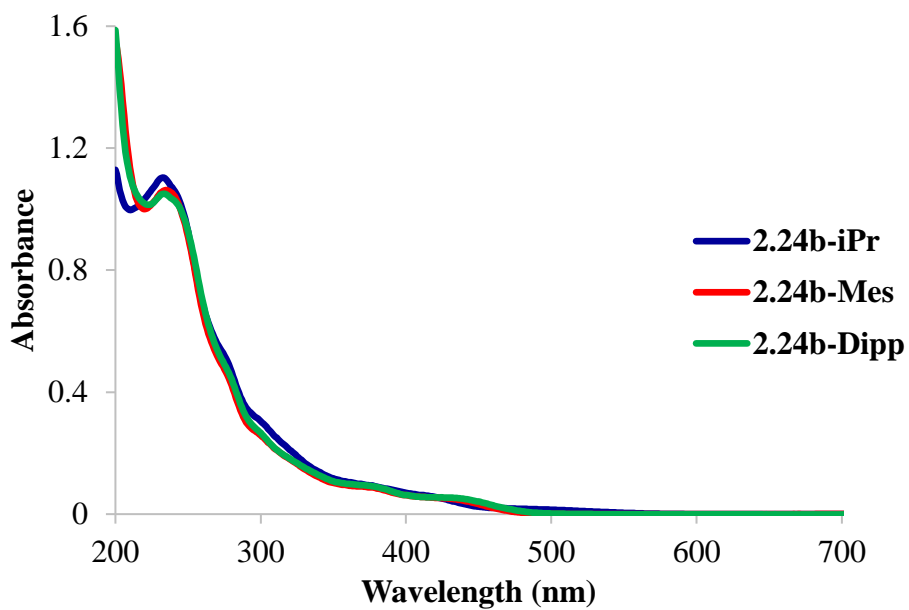


**Figure 2.28:** Absorption spectra of ppz complexes **2.24b-R** in MeCN at 0.02 mM concentration.

<b>Table 2.3:</b> Electronic absorption spectral data of [Ir(C <sup>^</sup> N) <sub>2</sub> (N <sup>^</sup> O)] complexes ( <b>2.24a,b-<sup>i</sup>Pr</b> , <b>2.20a,b-Mes</b> and <b>2.21a,b-Dipp</b> ) in HPLC grade MeCN.	
<b>Complex</b>	<b><math>\lambda_{\text{abs}}</math> [nm] (<math>\epsilon_{\text{max}}</math>[dm<sup>3</sup>mol<sup>-1</sup>cm<sup>-1</sup>])</b>
<b>2.24a-<sup>i</sup>Pr</b>	246 (39100), 349 (6900), 382 (5950)
<b>2.24b-<sup>i</sup>Pr</b>	233 (55200), 304 sh (14300), 381 (4450), 426 sh (2500)
<b>2.24a-Mes</b>	249 (48400), 346 sh (7950), 378 (6250)
<b>2.24b-Mes</b>	235 (53150), 281 sh (20450), 376 (4400), 437 sh (2350)
<b>2.24a-Dipp</b>	251 (42250), 344 (7600), 386 (5400)
<b>2.24b-Dipp</b>	234 (52500), 280 sh (22100), 381 (4450), 429 (2700)

### Emission Spectroscopy

Emission studies were carried out in solution (100% MeCN) and in the solid state by a method of precipitation using MeCN:H<sub>2</sub>O mixtures (1:9). As mentioned previously, upon addition of a *poor* solvent (i.e. H<sub>2</sub>O), small particles are formed. This is a method that has been discussed in Section 2.1. Figures 2.29 and 2.30 shows the emission spectra of ppy (**2.24a-R**) and ppz complexes (**2.24b-R**) (R = <sup>i</sup>Pr, Mes and Dipp), respectively. All complexes show enhanced emission (dashed line) in comparison to in solution (solid line). Ppy complexes are also EPESS active.

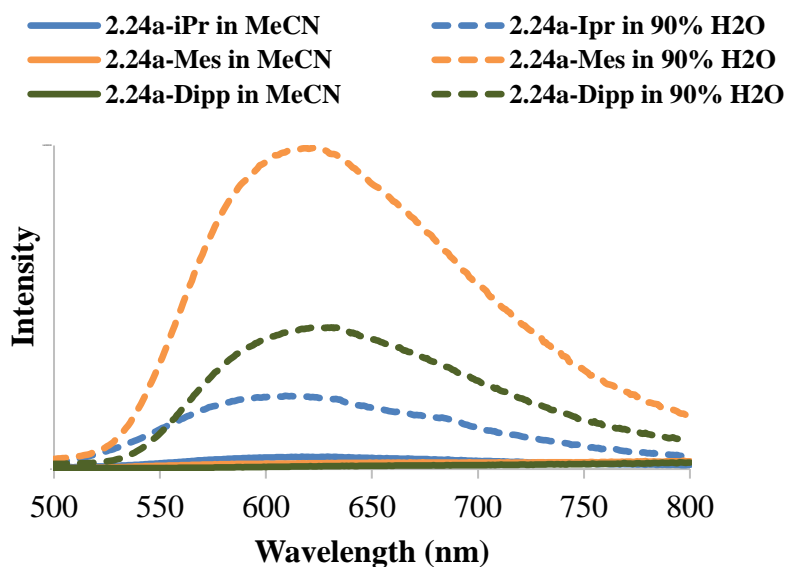


**Figure 2.29:** Emission spectra of ppy complexes (**2.24a-R**) at 0.02 mM concentration in MeCN and H<sub>2</sub>O:MeCN (9:1) mixtures in air.

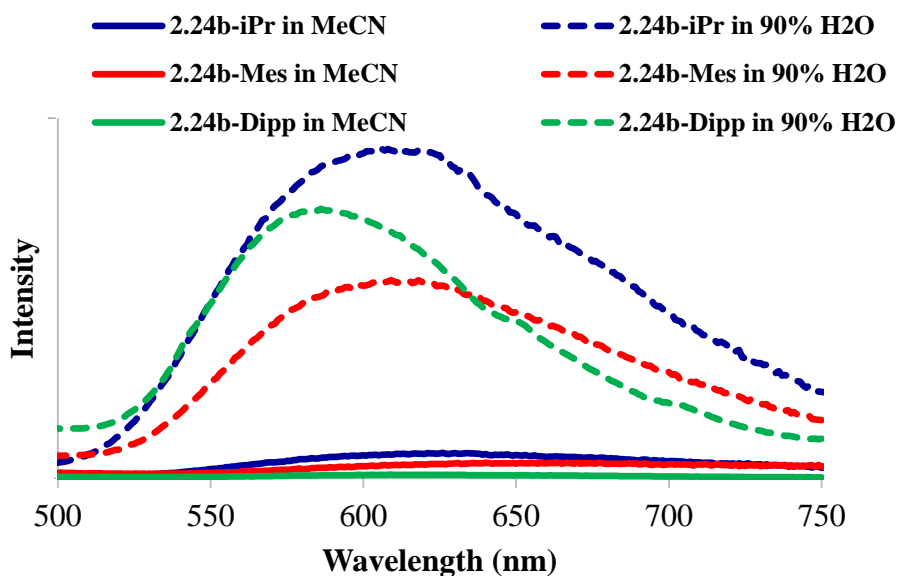


**Figure 2.30:** Emission spectra of ppz complexes (**2.24b-R**) at 0.02 mM concentration in HPLC grade MeCN and H<sub>2</sub>O:MeCN (9:1) in air.

<b>Table 2.4:</b> Solid-state emission wavelengths and quantum yields of neat solids and solids in a PMMA matrix. Measurements taken in air.						
	<b>Solid</b>	$\lambda_{\text{max}}$	<b>Solid QY</b>	<b>PMMA</b>	$\lambda_{\text{max}}$	<b>PMMA</b>
	<b>(nm)</b>			<b>(nm)</b>		<b>QY</b>
<b>2.24a-<sup>i</sup>Pr</b>	581		0.036	534		0.117
<b>2.24a-Ph</b>	609		0.058	570		0.134
<b>2.24a-Mes</b>	622		-	-		-
<b>2.24a-Dipp</b>	607		0.028	570		0.109
<b>2.24b-<sup>i</sup>Pr</b>	580		0.028	559		0.047
<b>2.24b-Ph</b>	602		0.080	578		0.086
<b>2.24b-Mes</b>	609		-	-		-
<b>2.24b-Dipp</b>	592		0.049	569		0.099

The emission spectra show that complexes **2.24a,b-R** (R = <sup>i</sup>Pr, Ph, Mes, Dipp) display enhanced emission in the solid state with  $\lambda_{\text{max}}$  between 581–622 nm. Park and co-workers<sup>21</sup> suggested that restricted intramolecular rotation around the N-aryl bond of the salicylimine ligand in the solid state suppressed a non-radiative decay pathway giving rise to EPESS. If rotation around the N-aryl bond was giving rise to a non-

radiative pathway, then complexes in which rotation is fixed **2.24a,b-Mes** and **2.24a,b-Dipp** would be expected to be emissive in solution and hence not show significant EPESS. This is clearly not the case. Our results show that even when the R group is not able to rotate in solution (complexes **2.24a,b-Mes** and **2.24a,b-Dipp**), emission is not observed in solution. These results, as well as others reported in the literature showing complexes with fixed substituents that display EPESS,<sup>20</sup> confirm that restricted rotation around the N-aryl bond is not the cause of EPESS in these complexes.  $\pi$ -stacking has also been suggested as the cause of EPESS but it always involved ppy as the cyclometallating ligand.<sup>20, 22</sup> Here, we replaced the cyclometalated ppy ligand with ppz which typically does not show  $\pi$ -stacking in the solid state.<sup>36-41</sup> Complexes **2.24b-<sup>i</sup>Pr**, **2.24b-Mes** and **2.24b-Dipp** containing ppz as the cyclometallating ligand show EPESS. Also, as described previously the crystal structures of complexes **2.24a-<sup>i</sup>Pr**, **2.24a-Dipp** and **2.24b-Dipp** did not show  $\pi$ -stacking. Furthermore, our collaborators carried out further solid state studies<sup>29</sup> to test the possibility of  $\pi$ -stacking or aggregation using a PMMA matrix (see Experimental). Using PMMA matrix allows isolation of neighbouring molecules therefore aggregation is not likely to occur. In the complexes studied, the solid-state emission maxima in PMMA are blue shifted by 21–47 nm compared to the corresponding complexes in the undiluted solid state (Table 2.4). Red shifts in solid-state absorption and emission spectra are typically observed due to intermolecular interactions,<sup>42</sup> and the blue shifts observed here confirm that intermolecular solid-state interactions are less prevalent when the complexes are placed in the polymer matrix (i.e. the molecules are more isolated). In addition, in each case, the emission quantum yield of the complex in PMMA is higher than that of the solid demonstrating that the solid-state emission is partially quenched in the aggregated form. These results are consistent with the more common aggregation caused quenching (ACQ) effect<sup>1</sup> and demonstrate that  $\pi$ -stacking or aggregation of these complexes in the solid state is not giving rise to EPESS. In fact,  $\pi$ -stacking or aggregation is actually detrimental to the enhancement of the emission observed. In addition, the  $\pi$ -stacking that has been previously reported<sup>20, 22</sup> always involved phenylpyridine cyclometallating ligands. We also observe EPESS behaviour in complexes bearing phenylpyrazole ligands which typically do not show long-range  $\pi$ -stacking in the solid state.<sup>37</sup> This suggests that  $\pi$ -stacking is not the cause of EPESS in these complexes, instead another factor may be playing a part in diminishing the emission in solution.

By designing complexes that would test both theories we have showed that neither agrees with the facts, therefore computational studies were carried out to study the origin of EPESS in these complexes.

### 2.2.3 Computational Studies

As shown in the photophysical studies, neither  $\pi$ - $\pi$  stacking nor restricted rotation are the cause for EPESS in complexes  $[\text{Ir}(\text{C}^{\wedge}\text{N})_2(\text{N}^{\wedge}\text{O})]$ . To help identify the underlying cause of EPESS in these type of complexes, DFT calculations were performed by Professor F. Lelj (University della Basilicata Potenza, Italy) for all complexes except **2.24a,b-Mes**. TD-DFT calculations on complexes **2.24a,b-Dipp** show that the lowest lying triplet consists mainly of LUMO-HOMO transition. Unrestricted DFT (UDFT) calculations of the lowest energy triplet state of complexes **2.24a,b-Dipp** shows that the HSOMO (Highest Singly Occupied Molecular Orbital) and HSOMO-1 contain Ir metal character and contributions from the two cyclometallated ligands and the ancillary ligand (Figure 2.31). This is consistent with emission arising from a  $^3\text{MLLCT}$  state. This suggests that the nature of both the cyclometallating ligands as well as the ancillary  $\text{N}^{\wedge}\text{O}$  ligand is important for the observed emission. (For complexes **2.24a,b-<sup>i</sup>Pr** and **2.24a,b-Ph** see Appendix).

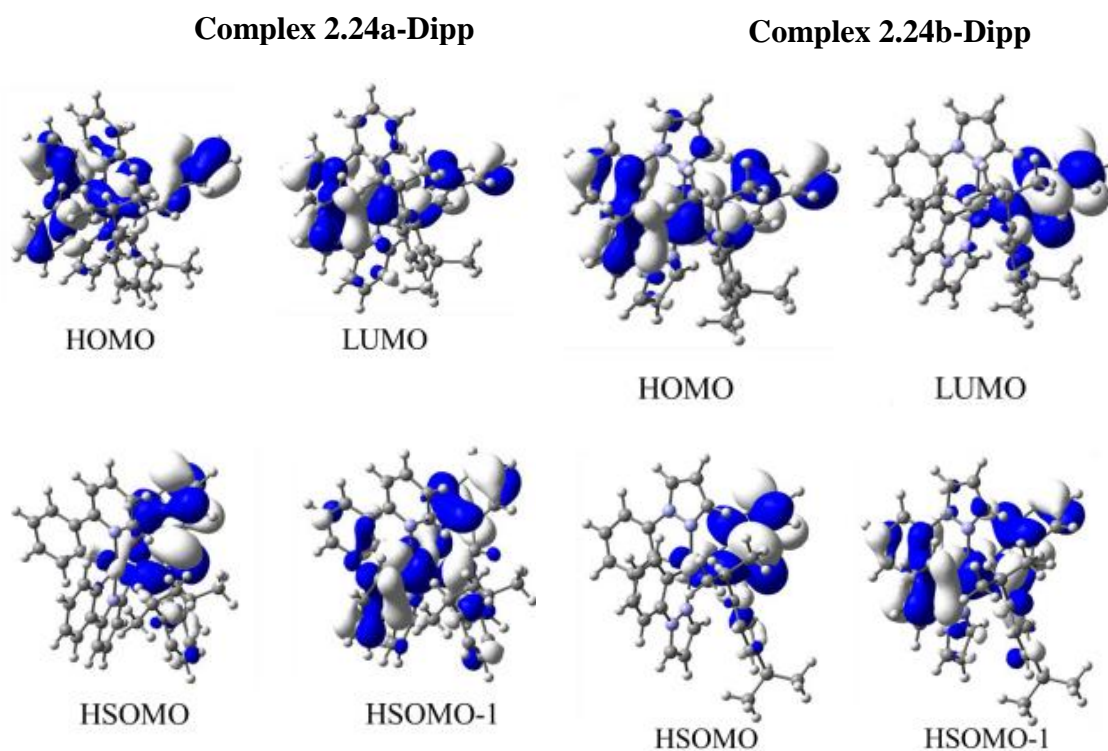


**Figure 2.31:** Ground state frontier molecular orbital images of the ground state (top) and HSOMO<sup>-1</sup> and HSOMO images of the triplet state (bottom) for complexes **2.24a-Dipp** and **2.24b-Dipp**, respectively.

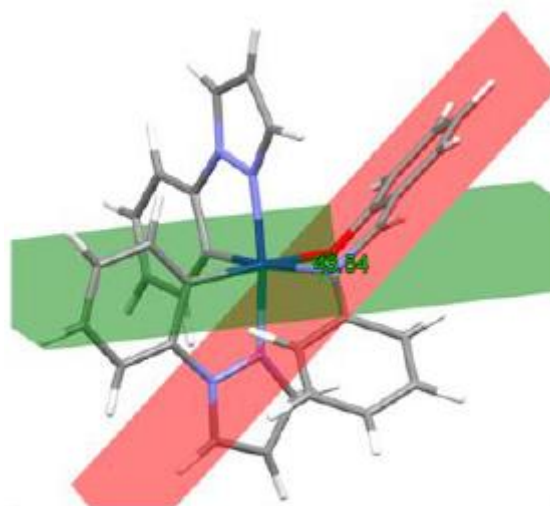


**Figure 2.32:** Molecular distortion of the salicylimine ligand in the excited state of complex **2.24b-Ph** (red: phenol imine plane; green: equatorial plane)

For complex **2.24b-Ph**, the ground state calculations show that in the most stable structure the plane of the phenol imine ligand and the equatorial plane are almost coplanar, with the angle between the planes to be  $5.94^\circ$ . In this case, the equatorial plane refers to the plane of the cyclometallated phenyl carbons, Ir and the nitrogen and oxygen atoms of the salicylimine ligand. However, in the triplet excited state the phenol imine (red) tilts with respect to the equatorial plane (green) leading to two stable conformations of this state: tilted up ( $43.54^\circ$ ) (Figure 2.32) or down ( $-25.65^\circ$ ). The cause of this distortion is because the LUMO has antibonding character between Ir and the phenol imine ligand. Therefore, the plane of the phenol imine (red) tilts with respect to the equatorial plane (green) to reduce the antibonding interaction to allow population of this orbital in the triplet excited state ( $T_1$ ). Therefore, a rotatable imine substituent is not required for EPES to be observed. In complex **2.24b-Ph**, the largest barrier separating the two conformers is  $15.7 \text{ kJ mol}^{-1}$  (Figure 2.33) resulting in a rapid interconversion between the conformers in solution at room temperature. This geometrical change in the excited state gives rise to a non-radiative decay pathway which deactivates the  $^3\text{MLLCT}$  state in solution at room temperature. Similar distortions were observed in complexes **2.24a,b-<sup>i</sup>Pr**, **2.24a-Ph** and **2.24a,b-Dipp** (see Appendix) suggesting that the non-radiative decay pathway has the same origin in all cases. Calculations that simulate a solid state matrix, show that the triplet state is much less distorted than in solution. This leads to an enhancement in the contribution of the Franck Condon factor for the  $^3\text{MLLCT}$  emission and hence makes this transition more probable in the solid state, hence emission is observed.

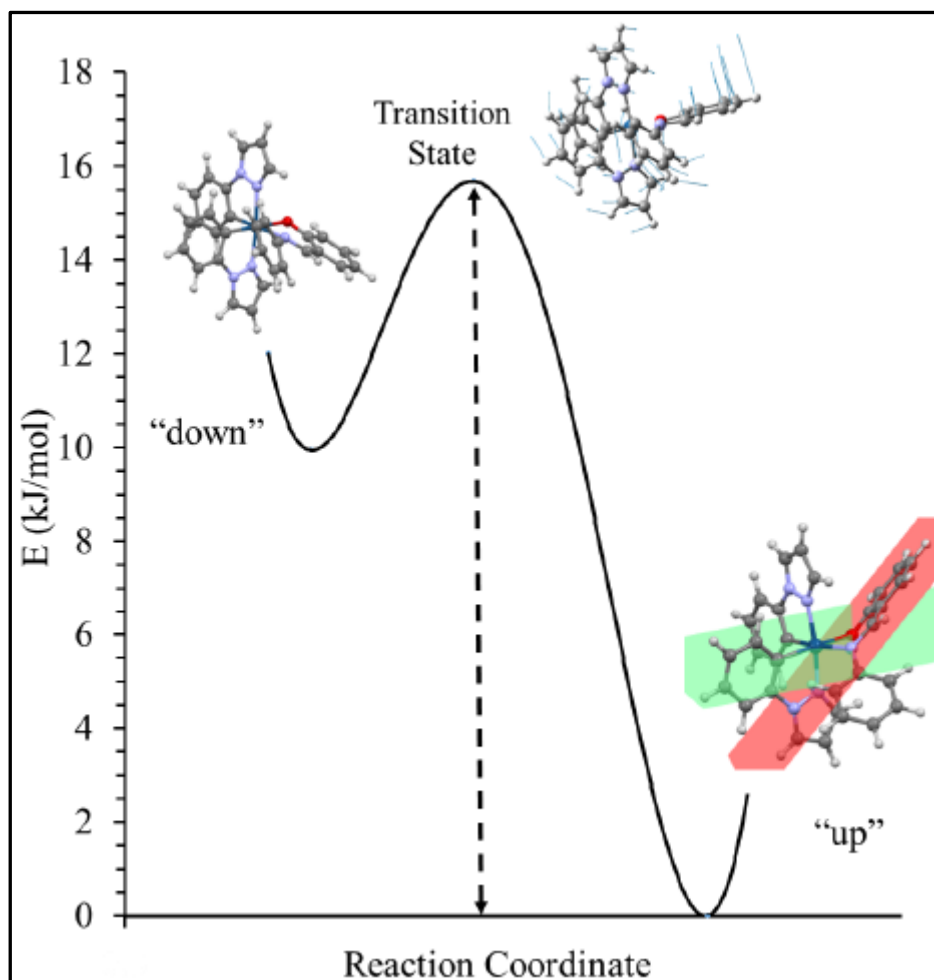


**Figure 2.33:** Computed energy profile for the excited triplet state geometry of complex **2.24b-Ph** in solution. The green plane is the equatorial plane and the red plane is the phenol imine ligand plane. Blue arrows show the transition vectors related to the interconversion between minima.

Computational studies were also performed on known cyclometallated Ir (III) complexes  $[\text{Ir}(\text{C}^{\wedge}\text{N})_2(\text{O}^{\wedge}\text{O})]$ , **2.25a,b-R** ( $\text{R} = \text{CH}_3, \text{Ph}$ ) (Figure 2.34). For complexes that are EPESS active, the ground state HOMO and/or LUMO must contain a significant contribution from the  $\text{N}^{\wedge}\text{O}$  or  $\text{O}^{\wedge}\text{O}$  ancillary ligand. In complex **2.25b-CH<sub>3</sub>**, the triplet excited state shows ligand distortions that lead to non-radiative decay in solution and therefore emission is not observed, but emission is enhanced in the solid state and therefore showing EPESS.<sup>22, 43</sup> This evidence demonstrates that excited state ligand distortions weaken the emission in solution as observed similarly to complexes with  $\text{N}^{\wedge}\text{O}$  ligands. Similarly, complexes **2.25a-Ph** and **2.25b-Ph** also show excited state ligand distortions and therefore both demonstrate EPESS.<sup>22, 43, 44</sup> On the other hand, complex **2.25a-CH<sub>3</sub>** is emissive in solution and the solid state. In this case, in the triplet

state the acac remains planar with respect to the equatorial plane. Therefore, in complex **2.25a-CH<sub>3</sub>** emission is observed in solution and in the solid state and does not demonstrate EPESS. In complex **2.25a-CH<sub>3</sub>**, the HOMO and LUMO do not show any contribution from the acac ancillary ligand. While the origin of the excited state ligand distortions is very complex, these results suggest that involvement of the ancillary ligand is essential for distortion to occur.

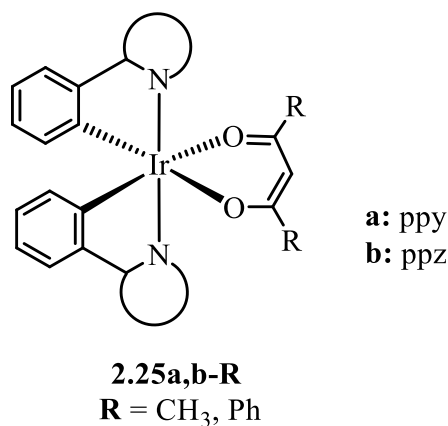


**Figure 2.34:** [Ir(C<sup>^</sup>N)<sub>2</sub>(O<sup>^</sup>O)] complexes that also show EPESS (except **2.25a-CH<sub>3</sub>**).

#### 2.2.4 Conclusion

The complexes studied in this chapter as well as complexes synthesised by Li and Park contain an ancillary ligand forming a six-membered chelate ring. Our study helped elucidate the origin of EPESS in complexes with general formula [Ir(C<sup>^</sup>N)<sub>2</sub>(N<sup>^</sup>O)]. We were able to disprove Li's theory of  $\pi$ - $\pi$  interactions by designing the complexes where the C<sup>^</sup>N ligand is ppz which does not show  $\pi$ - $\pi$  interactions but does show EPESS. We were also able to disprove Park's theory of restricted intramolecular rotation of the N-aryl bond in the solid state by designing complexes where rotation is impeded in the solid and in the solution. We therefore elucidated the theory of ligand distortion of the excited state in solution as the cause of non-radiative decay in solution. These distortions are very weak in the solid state and therefore emission is observed. DFT calculations played a key role in elucidating the cause of EPESS in these types of complexes. This work has been published.<sup>29</sup>

## 2.3 Bibliography

1. J. B. Birks, *Photophysics of Aromatic Molecules*, Wiley, London, 1970.
2. J. Mei, Y. N. Hong, J. W. Y. Lam, A. J. Qin, Y. H. Tang and B. Z. Tang, *Adv. Mater.*, 2014, **26**, 5429-5479.
3. J. D. Luo, Z. L. Xie, J. W. Y. Lam, L. Cheng, H. Y. Chen, C. F. Qiu, H. S. Kwok, X. W. Zhan, Y. Q. Liu, D. B. Zhu and B. Z. Tang, *Chem. Commun.*, 2001, 1740-1741.
4. B. Z. Tang, X. W. Zhan, G. Yu, P. P. S. Lee, Y. Q. Liu and D. B. Zhu, *J. Mater. Chem.*, 2001, **11**, 2974-2978.
5. Y. N. Hong, J. W. Y. Lam and B. Z. Tang, *Chem. Commun.*, 2009, 4332-4353.
6. J. Feng, X. Chen, Q. Han, H. Wang, P. Lu and Y. Wang, *J. Lumin.*, 2011, **131**, 2775-2783.
7. N. L. C. Leung, N. Xie, W. Yuan, Y. Liu, Q. Wu, Q. Peng, Q. Miao, J. W. Y. Lam and B. Z. Tang, *Chem. Eur. J.*, 2014, **20**, 15349-15353.
8. J. Mei, N. L. C. Leung, R. T. K. Kwok, J. W. Y. Lam and B. Z. Tang, *Chem. Rev.*, 2015, **115**, 11718-11940.
9. K. Sharma nee Kamaldeep, S. Kaur, V. Bhalla, M. Kumar and A. Gupta, *J. Mater. Chem. A*, 2014, **2**, 8369-8375.
10. J. Liu, Q. Meng, X. Zhang, X. Lu, P. He, L. Jiang, H. Dong and W. Hu, *Chem. Commun.*, 2013, **49**, 1199-1201.
11. Y. Hong, J. W. Y. Lam and B. Z. Tang, *Chem. Soc. Rev.*, 2011, **40**, 5361-5388.
12. Y. Chen, W.-C. Xu, J.-F. Kou, B.-L. Yu, X.-H. Wei, H. Chao and L.-N. Ji, *Inorg. Chem. Commun.*, 2010, **13**, 1140-1143.
13. X.-L. Xin, M. Chen, Y.-b. Ai, F.-l. Yang, X.-L. Li and F. Li, *Inorg. Chem.*, 2014, **53**, 2922-2931.
14. H. Honda, Y. Ogawa, J. Kuwabara and T. Kanbara, *Eur. J. Inorg. Chem.*, 2014, **2014**, 1865-1869.
15. Y. Li, D. P.-K. Tsang, C. K.-M. Chan, K. M.-C. Wong, M.-Y. Chan and V. W.-W. Yam, *Chem. Eur. J.*, 2014, **20**, 13710-13715.

16. Z. Chen, K. M.-C. Wong, E. C.-H. Kwok, N. Zhu, Y. Zu and V. W.-W. Yam, *Inorg. Chem.*, 2011, **50**, 2125-2132.
17. T. J. Wadas, Q.-M. Wang, Y.-j. Kim, C. Flaschenreim, T. N. Blanton and R. Eisenberg, *J. Am. Chem. Soc.*, 2004, **126**, 16841-16849.
18. S. Liu, H. Sun, Y. Ma, S. Ye, X. Liu, X. Zhou, X. Mou, L. Wang, Q. Zhao and W. Huang, *J. Mater. Chem.*, 2012, **22**, 22167-22173.
19. M. Ghedini, A. Golemme, I. Aiello, N. Godbert, R. Termine, A. Crispini, M. La Deda, F. Lelj, M. Amati and S. Belviso, *J. Mater. Chem.*, 2011, **21**, 13434-13444.
20. K. W. Huang, H. Z. Wu, M. Shi, F. Y. Li, T. Yi and C. H. Huang, *Chem. Commun.*, 2009, 1243-1245.
21. Y. You, H. S. Huh, K. S. Kim, S. W. Lee, D. Kim and S. Y. Park, *Chem. Commun.*, 2008, 3998-4000.
22. Q. Zhao, L. Li, F. Y. Li, M. X. Yu, Z. P. Liu, T. Yi and C. H. Huang, *Chem. Commun.*, 2008, 685-687.
23. H. Wu, T. Yang, Q. Zhao, J. Zhou, C. Li and F. Li, *Dalton Trans.*, 2011, **40**, 1969-1976.
24. G. G. Shan, D. X. Zhu, H. B. Li, P. Li, Z. M. Su and Y. Liao, *Dalton Trans.*, 2011, **40**, 2947-2953.
25. Y. Wu, H.-Z. Sun, H.-T. Cao, H.-B. Li, G.-G. Shan, Y.-A. Duan, Y. Geng, Z.-M. Su and Y. Liao, *Chem. Commun.*, 2014, **50**, 10986-10989.
26. P. Alam, P. Das, C. Climent, M. Karanam, D. Casanova, A. R. Choudhury, P. Alemany, N. R. Jana and I. R. Laskar, *J. Mater. Chem. C*, 2014, **2**, 5615-5628.
27. P. Alam, C. Climent, G. Kaur, D. Casanova, A. Roy Choudhury, A. Gupta, P. Alemany and I. R. Laskar, *Cryst. Growth Des.*, 2016, **16**, 5738-5752.
28. P. A. Scattergood, U. Khushnood, A. Tariq, D. J. Cooke, C. R. Rice and P. I. P. Elliott, *Inorg. Chem.*, 2016, **55**, 7787-7796.
29. A. J. Howarth, R. Patia, D. L. Davies, F. Lelj, M. O. Wolf and K. Singh, *Eur. J. Inorg. Chem.*, 2014, **2014**, 3657-3664.

30. D. L. Davies, M. P. Lowe, K. S. Ryder, K. Singh and S. Singh, *Dalton Trans.*, 2011, **40**, 1028-1030.
31. R. Herscovitch, J. J. Charette and E. De Hoffmann, *J. Am. Chem. Soc.*, 1973, **95**, 5135-5140.
32. S. Chang, L. Jones, C. Wang, L. M. Henling and R. H. Grubbs, *Organometallics*, 1998, **17**, 3460-3465.
33. M. D. Jones, M. G. Davidson, C. G. Keir, L. M. Hughes, M. F. Mahon and D. C. Apperley, *Eur. J. Inorg. Chem.*, 2009, **2009**, 635-642.
34. S. Singh, *Thesis: Luminescent Cyclometallated Ir(III) complexes: Synthesis, characterisation and Applications*, 2010.
35. P. J. Spellane, R. J. Watts and C. J. Curtis, *Inorg. Chem.*, 1983, **22**, 4060-4062.
36. L.-L. Wu, I. W. Sun and C.-H. Yang, *Polyhedron*, 2007, **26**, 2679-2685.
37. T.-H. Kwon, H. S. Cho, M. K. Kim, J.-W. Kim, J.-J. Kim, K. H. Lee, S. J. Park, I.-S. Shin, H. Kim, D. M. Shin, Y. K. Chung and J.-I. Hong, *Organometallics*, 2005, **24**, 1578-1585.
38. A. B. Tamayo, S. Garon, T. Sajoto, P. I. Djurovich, I. M. Tsyba, R. Bau and M. E. Thompson, *Inorg. Chem.*, 2005, **44**, 8723-8732.
39. K. Hanson, A. Tamayo, V. V. Diev, M. T. Whited, P. I. Djurovich and M. E. Thompson, *Inorg. Chem.*, 2010, **49**, 6077-6084.
40. S. Kammer, I. Starke, A. Pietrucha, A. Kelling, W. Mickler, U. Schilde, C. Dosche, E. Kleinpeter and H.-J. Holdt, *Dalton Trans.*, 2012, **41**, 10219-10227.
41. G.-G. Shan, H.-B. Li, H.-T. Cao, D.-X. Zhu, Z.-M. Su and Y. Liao, *J. Organomet. Chem.*, 2012, **713**, 20-26.
42. S.-Y. Chang, J. Kavitha, S.-W. Li, C.-S. Hsu, Y. Chi, Y.-S. Yeh, P.-T. Chou, G.-H. Lee, A. J. Carty, Y.-T. Tao and C.-H. Chien, *Inorg. Chem.*, 2006, **45**, 137-146.
43. S. Lamansky, P. Djurovich, D. Murphy, F. Abdel-Razzaq, H.-E. Lee, C. Adachi, P. E. Burrows, S. R. Forrest and M. E. Thompson, *J. Am. Chem. Soc.*, 2001, **123**, 4304-4312.

44. T. Fei, X. Gu, M. Zhang, C. Wang, M. Hanif, H. Zhang and Y. Ma, *Synth. Met.*, 2009, **159**, 113-118.

## 2.4 Appendix

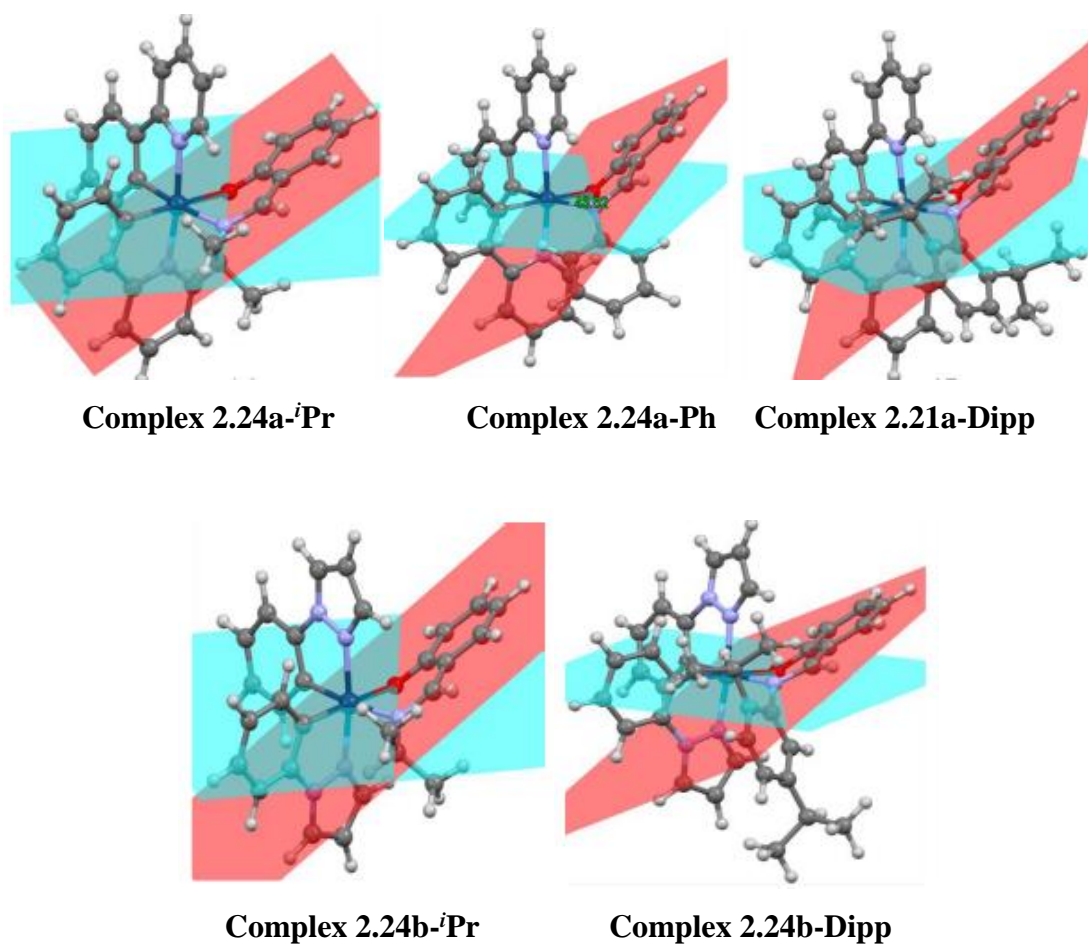


**Figure A2.1:** Excited triplet state geometry of complexes **2.18a,b-*i*Pr**, **2.24a-Ph** and **2.24a,b-Dipp** showing ligand distortions. In each case the ‘titled up’ version is shown. The green plane is the equatorial plane and the red plane is the phenol imine ligand plane.

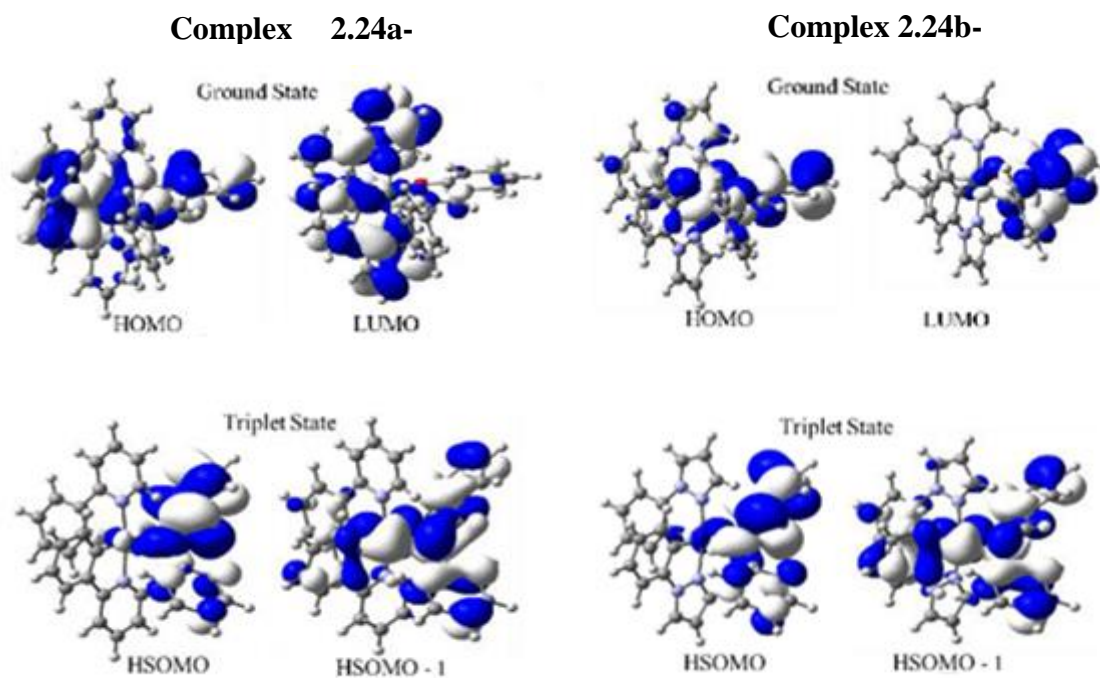


**Figure A2.2:** Ground state frontier molecular orbital images of the ground state (top) and HSOMO<sup>-1</sup> and HSOMO images of the triplet state (bottom) for complexes **2.24a-Ph** and **2.24b-Ph**, respectively.

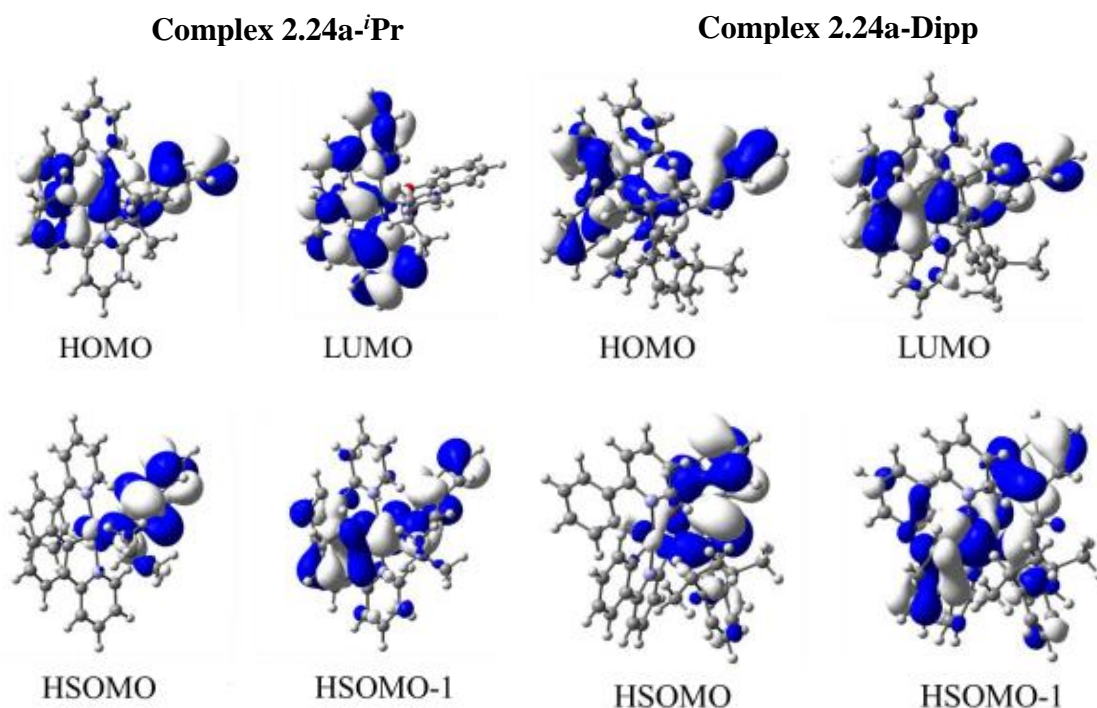


**Figure A2.3:** Ground state frontier molecular orbital images of the ground state (top) and HSOMO-1 and HSOMO images of the triplet state (bottom) for complexes for complexes **2.24a-<sup>i</sup>Pr** and **2.24a-Dipp**, respectively.

## Chapter 3: Bis-Cyclometallated Ir(III) Complexes with *exocyclic* Imine Bonds

### 3.1 Introduction

Chapter 2 contained a discussion of the mechanism of EPESS in  $[\text{Ir}(\text{C}^{\wedge}\text{N})_2(\text{N}^{\wedge}\text{O})]$  complexes, where  $\text{N}^{\wedge}\text{O}$  is a 6-membered salicylimine (**I**) (Figure 3.1). This chapter describes complexes with the same general formula  $[\text{Ir}(\text{C}^{\wedge}\text{N})_2(\text{N}^{\wedge}\text{O})]$  but with isomeric  $\text{N}^{\wedge}\text{O}$  ligands that form a 5-membered ring (**II**) to study the effect of ring size on EPESS. In **II**, the imine bond is *exocyclic* which creates the possibility of *cis* and *trans* isomers of the C=N bond. These systems could potentially be used in molecular switches.

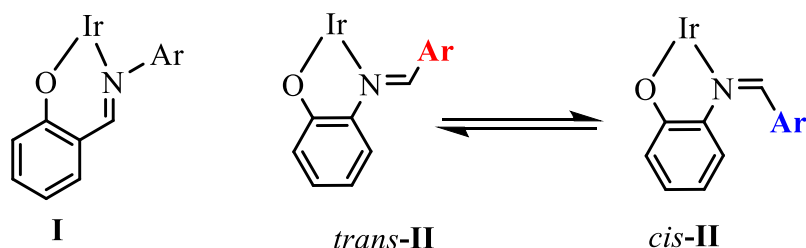
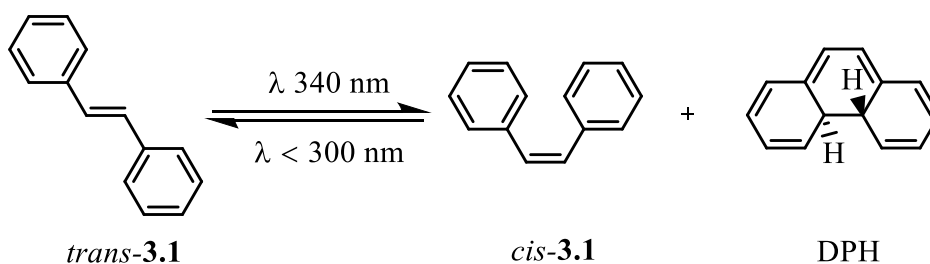


**Figure 3.1:** Ir metal bound to  $\text{N}^{\wedge}\text{O}$  ligand forming a 6-membered ring (**I**) and a 5-membered ring (**II**) with isomeric ligand.

Molecular switches and rotors are able to interconvert from one structural state to another by an external stimulus such as light or heat.<sup>1-3</sup> This section will describe three types of molecular switches with C=C, N=N and C=N bonds.

#### 3.1.1 Photoisomerisation of C=C bonds

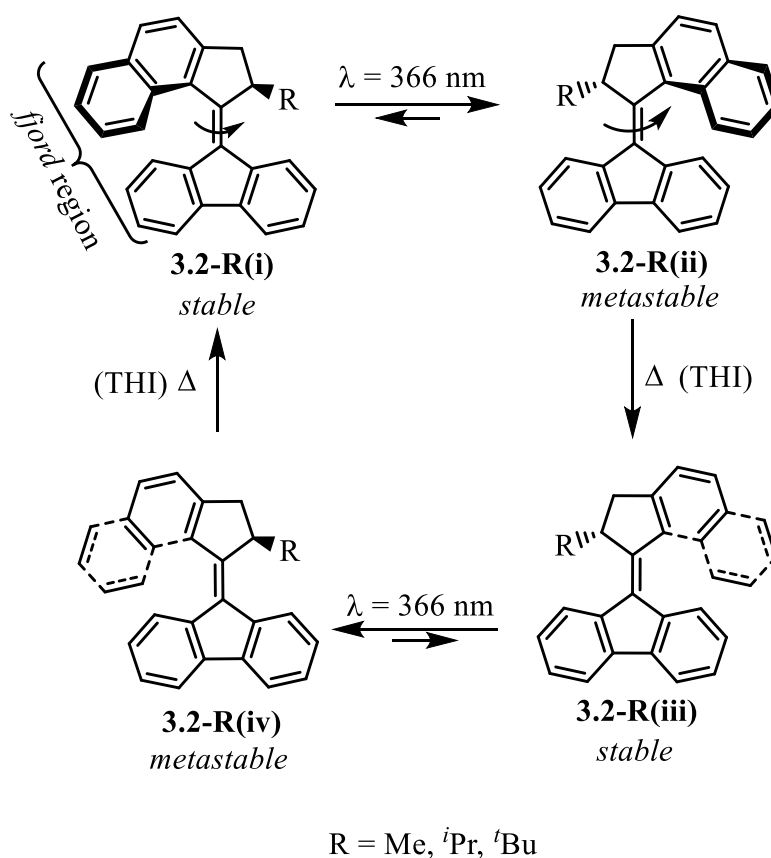
Stilbene (**3.1**) is an example of a simple molecular switch with a C=C bond that allows a change in geometrical structure (*trans* and *cis*) that is necessary for a functioning switch. The photoisomerisation of **3.1** has been extensively investigated showing that *trans-3.1* isomerises to *cis-3.1* when irradiated at 340 nm, whilst the reverse reaction occurs at shorter wavelength ( $< \lambda$  300 nm) (Scheme 3.1).<sup>4,5</sup> In this example, thermal isomerisation does not occur at room temperature as the barrier for thermal *cis-trans* isomerisation is 41-46 kcal mol<sup>-1</sup>.<sup>5</sup> In addition to forming the *trans* isomer, photoexcitation of *cis-3.1* generates the cyclic product 4,4-dihydrophenanthrene (DPH) in 10% yield.<sup>6-8</sup> The yields of the three processes add up to approximately 1, suggesting that only one pathway may be available for the deactivation of the excited stilbene.<sup>9</sup> Studies have shown that isomerisation of stilbene occurs via a rotation mechanism.<sup>10-12</sup>



**Scheme 3.1:** Photoisomerisation of stilbene (**3.1**).

Saltiel and co-workers proposed the most commonly accepted mechanism of isomerisation of **3.1** to be the 90° twisting (or rotation) about the C=C bond in the first excited singlet state which is very short lived.<sup>13-17</sup> This observation is consistent with a study done by Minoru and co-workers<sup>18</sup> that found after exciting *trans*-**3.1** to the first excited singlet state, *cis*-**3.1** was observed and detected while the decay of the *trans*-**3.1** population matches the rise of the *cis*-**3.1**. The major relaxation channel for excited *cis*-**3.1** is the decay to the ground-state to *trans* and *cis* forms whilst the minor channel is the formation of DPH.<sup>7</sup> The *cis-trans* isomerisation requires UV light ( $\lambda < 300 \text{ nm}$ ), which may cause undesired photoreactions of biomolecules, such as formation of thymine dimers which can be unfavourable in DNA photo-responsive switches leading to a non-functioning switch.<sup>19</sup>

Feringa is internationally recognised as a pioneer in the field of molecular switches and rotors based on overcrowded alkenes. Overcrowded alkenes (**3.2-R**) consist of an upper part (rotor) connected by the C=C bond to a lower part (stator). They are forced to adopt a helical shape to avoid unfavourable steric interactions around the central C=C bond.<sup>20</sup> In overcrowded alkenes, unidirectional rotation around the central C=C bond is achieved by four steps: two endergonic photo induced steps and two exergonic thermal steps.<sup>21</sup> The two light induced isomerisations are each associated with a 180° rotation around the C=C bond and each is followed by a thermal helix inversion (THI) step, which effectively blocks the reverse rotation and thus ensures that the four individual steps add up to one full 360° rotation (Scheme 3.2).



**Scheme 3.2:** Unidirectional motion of overcrowded alkene **3.2-R**.

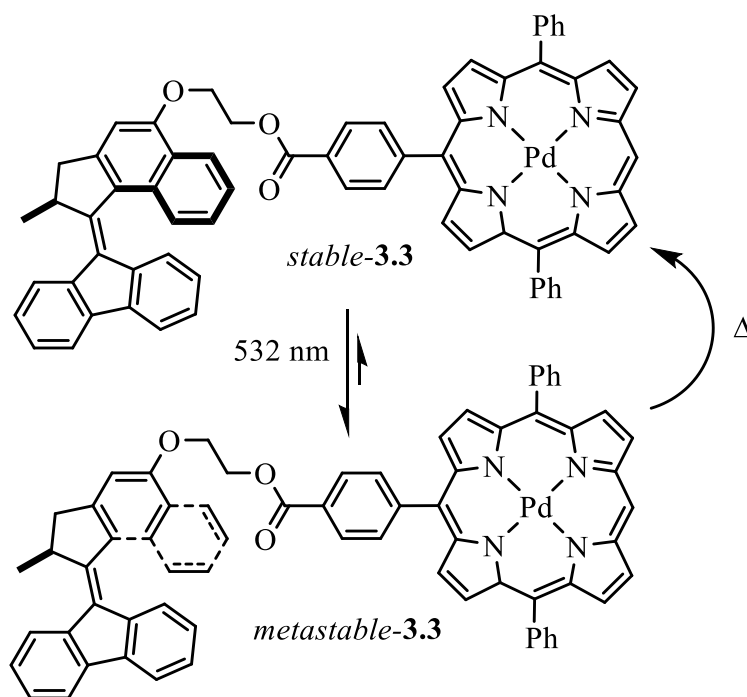
<b>Table 3.1:</b> Key data for rotation of overcrowded alkenes <b>3.2-R</b> .				
	<b>DFT Studies</b>		<b>Experimental Data (metastable)</b>	
	C=C Bond length (Å)	Torsion angle (°)	$\Delta G^\ddagger$ (kcal mol <sup>-1</sup> )	$t_{1/2}$ (s)
<b>3.2-Me</b>	1.3775	30.5	20.3	587
<b>3.2-<sup>i</sup>Pr</b>	1.3800	31.6	20.1	95
<b>3.2-<sup>t</sup>Bu</b>	1.3859	38.2	14.3	$5.74 \times 10^{-3}$

*Torsion angle refers to angle between the naphthalene upper half and fluorene;  $\Delta G^\ddagger$  = activation barrier to rotation,  $t_{1/2}$  = half-life of metastable forms*

The rate of the thermal steps is heavily dependent on the steric hindrance in the *fjord* region. Overcrowded alkenes **3.2-R** (R = Me, <sup>i</sup>Pr and <sup>t</sup>Bu) were used to tune the speed of rotation by varying the size of the substituents (Table 3.1).<sup>22</sup> The  $t_{1/2}$  of the *metastable* forms decreases as the size of R increases (R = -**Me**  $t_{1/2}$  = 587 s; R = -**<sup>i</sup>Pr**  $t_{1/2}$  = 95 s; R = -**<sup>t</sup>Bu**  $t_{1/2}$  =  $5.74 \times 10^{-3}$  s;). DFT studies predict a large torsion angle between the naphthalene upper half and fluorene lower half of 38.2° for **3.2-<sup>t</sup>Bu**. The large <sup>t</sup>Bu group

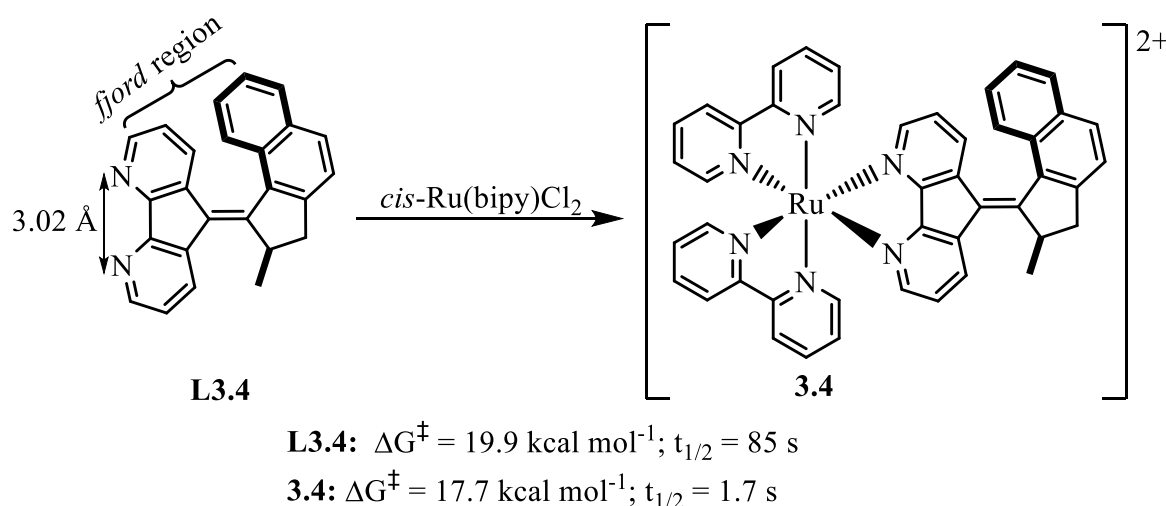
pushes the upper half out of the plane of the lower half during the thermal steps of the *metastable* forms, resulting in reduced “double bond character” and increasing the C=C distance. This allows the naphthalene upper half to slip past the lower half more easily during the thermal steps (*metastable* form to *stable* form).<sup>22</sup> Hence, the increase in the size of the substituents lowers the energy barrier resulting in an acceleration of the THI step.<sup>22</sup>

Feringa attached overcrowded alkene **3.2-Me** to a Pd-porphyrin to give triplet sensitiser **3.3** (Scheme 3.3).<sup>23</sup> The incorporation of a Pd-porphyrin unit allows irradiation in the visible region at 532 nm in comparison to irradiation of free **3.2-Me** at 365 nm. Photoisomerisation of **3.3** occurs via energy transfer from the porphyrin unit to the overcrowded alkene to give the unidirectional motion. The energy of activation for the *metastable* form has not been reported but by introducing a metalloporphyrin, shows a slight change in the photostationary state (PSS) ratio of *stable:metastable* forms in complex **3.3** to be 67:33 in comparison to the free alkene at 75:25. It was also noted that phosphorescence emission of the Pd-porphyrin fragment in **3.3** is quenched due to the presence of the overcrowded alkene. Shifting the irradiation wavelength to the visible region is an important step for the potential use of molecular switches in biological systems.



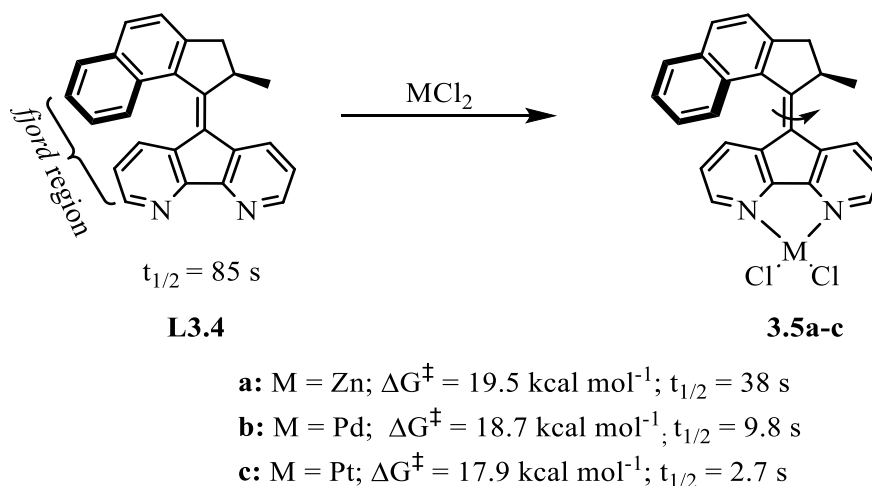
**Scheme 3.3:** Photoisomerisation of complex **3.3**.

Feringa and co-workers designed the first molecular motor to act as a ligand by replacing the fluorene stator part of **3.2** with 4,5-diazafluorenyl moiety (**L3.4**) (Scheme 3.4).<sup>24</sup> In **L3.4**, the photoisomerisation process occurs using UV light (390 nm), but when bound to Ru in complex **3.4**, the photoisomerisation process can be initiated with visible light ( $\lambda_{\text{max}} = 450$  nm) via intramolecular energy transfer. The N-N distance in **L3.4** is 3.02 Å but after coordination to the Ru centre, it decreases to 2.80 Å. This leads to a contraction of the lower half of the rotor upon coordination to Ru centre resulting in a decrease in steric hindrance in the *ffjord* region. The  $\Delta G^\ddagger$  and the  $t_{1/2}$  of *metastable-3.4* are lower than in **L3.4** leading to a faster unidirectional rotation of the C=C bond. The mechanism for complex **3.4** is very similar to **3.2-R** (Scheme 3.2). Furthermore, emission of **3.4** was quenched in comparison to the moderately emissive  $[\text{Ru}(\text{bipy})_3]^{2+}$ .



**Scheme 3.4:** The first molecular motor to act as a ligand in complex **3.4**.

**L3.4** can also coordinate to other metal centres (**3.5a-c**, Scheme 3.5) to tune the rotational speed of the rotor.<sup>25</sup> Similar to complex **3.4**, upon coordination to the metal centre, a decrease in steric hindrance in the *ffjord* region was observed, resulting in an increase in the rotational speed. In addition, as with complex **3.4**, complexes **3.5a-c** have the benefit of shifting the wavelength of irradiation towards the visible region ( $\lambda_{\text{max}}$  for **3.5a** and **3.5b** is 405 nm and 422 nm for **3.5c**) in comparison to **L3.4** at 390 nm. This becomes particularly important in biological systems where high energy light can cause damage to living cells.

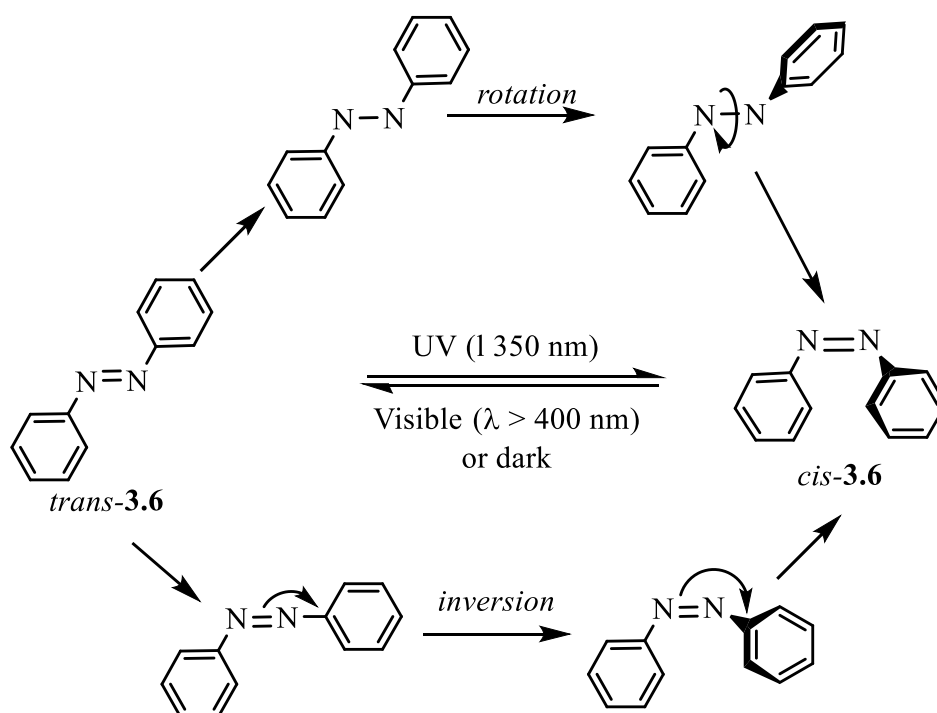


**Scheme 3.5:** Molecular rotor with tuneable rotational speed for complexes **3.5a-c**.

( $t_{1/2}$  is the half-life of the *metastable* isomer at 20° C)

### 3.1.2 Photoisomerisation of N=N bonds

The N=N analogue of stilbene is azobenzene (**3.6**) with an N=N bond that gives the possibility of *trans-cis* photoisomerisation. *Trans-3.6* undergoes isomerisation via irradiation at 340 nm to form *cis-3.6* which adopts a bent conformation with the phenyl twisted out of plane from the azo group<sup>26</sup> whilst the reverse isomerisation is induced by light or is thermally accessible in the dark.<sup>27</sup> The thermal *cis-trans* isomerisation takes place with an activation barrier of 22-25 kcal mol<sup>-1</sup> and with a  $t_{1/2}$  of the *cis*-isomer of 2 days,<sup>28</sup> whilst in stilbenes the barrier to thermal isomerisation is larger (41.8 kcal mol<sup>-1</sup>). Two different mechanisms have been proposed for the isomerisation of azobenzenes (i) a rotation around the N=N bond<sup>29</sup> and (ii) an in-plane inversion through a linear transition state<sup>30</sup> (Scheme 3.6). However, recent advances suggest that concerted inversion or inversion assisted rotation could also be possible pathways for the isomerisation in azobenzenes, which are a combination of rotation and inversion pathways.<sup>9</sup> The rotation pathway involves the disruption of the N=N  $\pi$ -bond to allow rotation of the N—N  $\sigma$ -bond. According to Eyring, the rotation changes the C—N—N—C dihedral angle while keeping the N—N—C at approximately 120°.<sup>29</sup> In the inversion mechanism, one of the N=N—C angles increases to 180° which results in a transition state with one *sp* hybridised azo-nitrogen atom.<sup>30</sup> In the concerted inversion mechanism, both N=N—C bond angles increase to 180° generating a linear transition state, whilst in the inversion-assisted rotation, large changes in the C—N=N—C dihedral angle and small changes in the N=N—C angles are important for isomerisation to take place.<sup>9</sup>



**Scheme 3.6:** Proposed mechanisms for isomerisation of azobenzene **3.6**.

Azobenzenes can act as donor ligands as shown in complex **3.7** where the N=N bond becomes part of a chelate ring and isomerisation cannot take place (Figure 3.2).<sup>31</sup> Alternatively, to maintain the isomerisation properties, azobenzene groups have been attached to metal complexes as a pendant unit at the back of a ligand giving the possibility of photoisomerisation around the N=N double bond.

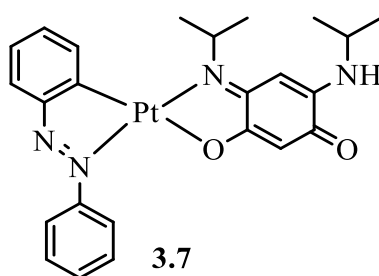


**Figure 3.2:** Complex **3.7** where N=N is part of the chelate ring.

Nishihara and co-workers designed mononuclear and dinuclear complexes (**3.8a-b** and **3.9a-b**) with azobenzene moiety bound to terpyridine ligands (**L3.8** and **L3.9**) (Figure 3.3).<sup>32</sup> The *trans-cis* isomerisation in **L3.8** and **L3.9** are photochemically induced with 366 nm light whilst *cis-trans* photoisomerisation proceeds in the dark or upon irradiation with 450 nm light. Upon complexation, **3.8a** shows *trans-cis* photoisomerisation at 366 nm with a PSS of 80:20 favouring *trans-3.8a*. Reverse *cis-*

*trans* isomerisation of **3.8a** occurs in the dark or with 440 nm light, whilst dinuclear complex **3.9a** did not show any photoisomerisation. Rh(III) complexes **3.8b** and **3.9b** undergo *trans-cis* photoisomerisation with 366 nm light with almost full conversion to the *cis* isomer and thermal *cis-trans* isomerisation at 120 °C in the dark returning to 100% *trans*. This study shows that the isomerisation behaviour of pendant N=N bonds in metal complexes is dependent on the metal fragment.

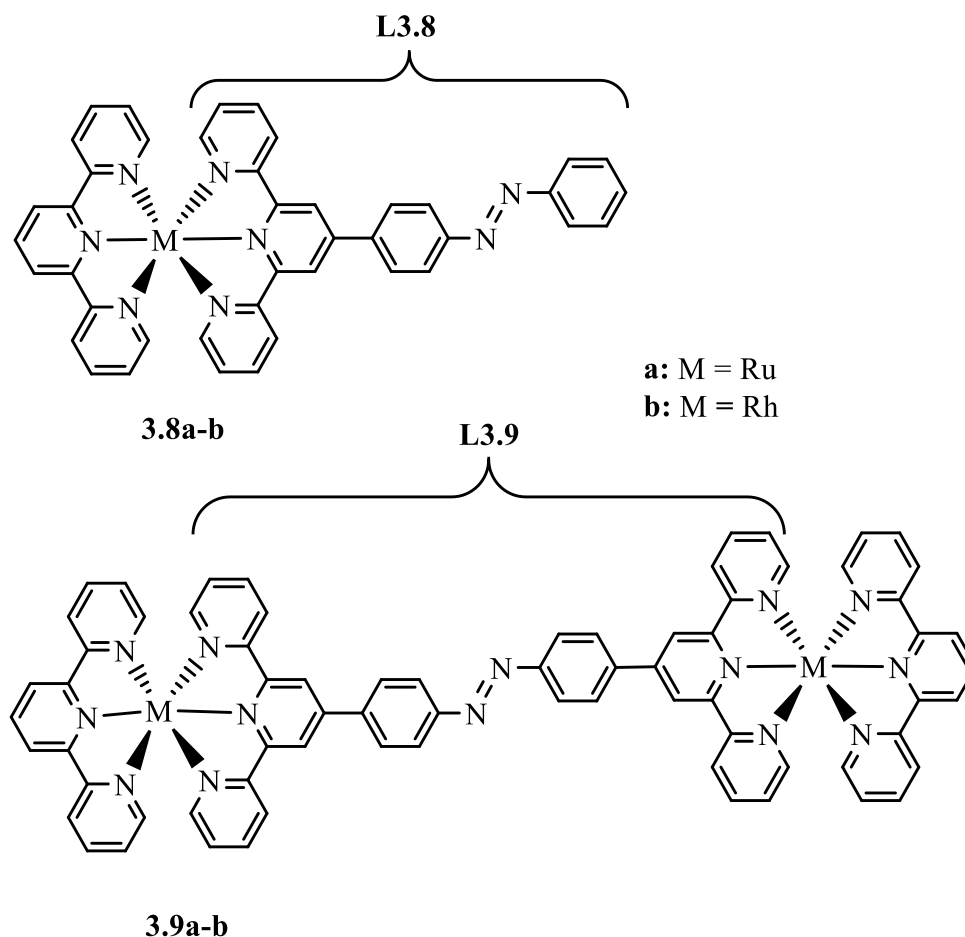


**Figure 3.3:** Complexes **3.8a-b** and **3.9a-b**.

The following examples show the effect of position of the azobenzene unit and the effect of linkers on photoisomerisation. Previous studies suggest that photoisomerisation in azobenzene-containing polypyridine metal complexes can be suppressed due to of the energy transfer from the  $\pi\text{-}\pi^*$  excited state of the azobenzene unit to the MLCT state.<sup>32-34</sup> It was reported that complex **3.10** (Figure 3.4) did not show any photo or thermal isomerisation due to the efficient communication along the backbone.<sup>35</sup> On the other hand, complex *mer*-**3.11** with an aliphatic linker shows *trans-cis* photoisomerisation at 349 nm and reverse *cis-trans* isomerisation in the dark.<sup>36</sup> The

authors reported that the aliphatic group disrupted the good communication along the backbone of the ligand, hence isomerisation was observed.<sup>36</sup>

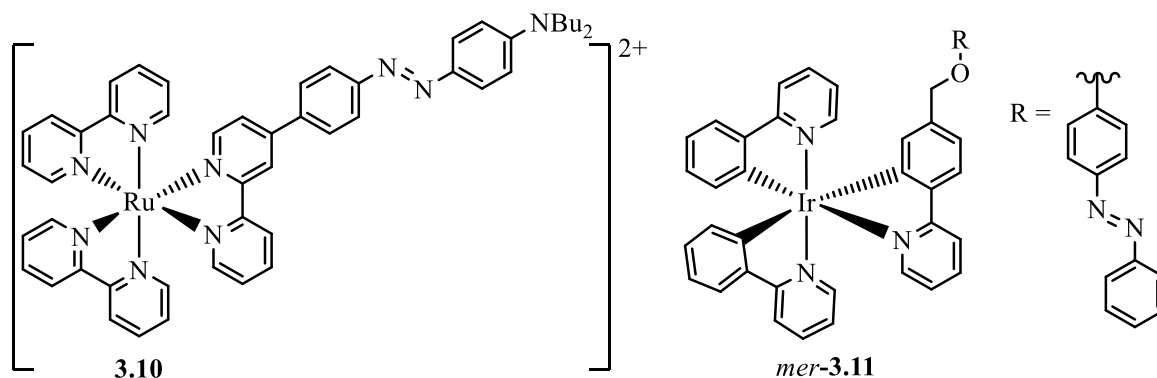


**Figure 3.4:** Ru(II) complex **3.10** and Ir(III) complex *mer*-**3.11** with azobenzene as a pendant unit.

Figure 3.5 shows complexes **3.12** and **3.13** that display *trans-cis* isomerisation at 366 and 359 nm respectively, and *cis-trans* isomerisation in the dark at room temperature.<sup>36</sup> The position of the N=N unit (phenyl vs pyridyl) gave virtually the same PSS ratio (*trans:cis* 15:85 and 14:86, respectively) and the  $t_{1/2}$  of the *cis* isomer was also very similar at 5900 s and 6500 s, respectively. In this case, changing the position of the N=N unit in the cyclometallated ligand did not show a significant change in the PSS ratio or the  $t_{1/2}$  of the *cis* isomer. Furthermore, the <sup>1</sup>H NMR spectra of complexes **3.12** and **3.13** showed that they can exist as *trans-trans* (C<sub>2</sub> symmetric) and *trans-cis* (C<sub>1</sub>-symmetric) isomers resulting from the isomerisation of just one of the azobenzene unit.

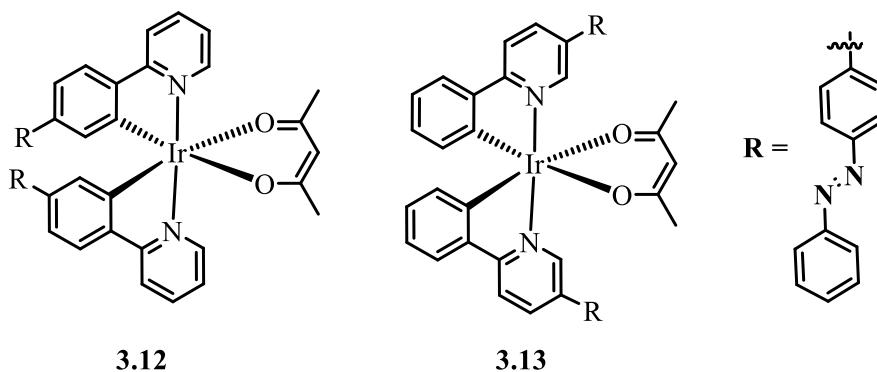


**Figure 3.5:** Ir(III) complexes with azobenzene unit attached to the phenyl ring (**3.12**) and pyridyl ring (**3.13**).

Complexes **3.14** and **3.15** (Figure 3.6) with ethynyl and triazolyl linkers, respectively, show *trans-cis* photoisomerisation at 436 nm and *cis-trans* thermal isomerisation at room temperature in the dark.<sup>35</sup> Although, changing the linker did not show a significant

difference on the *trans:cis* PSS of **3.14** and **3.15**, the  $t_{1/2}$  of *cis*-**3.14** is short lived ( $t_{1/2} = 315$  s) in comparison to *cis*-**3.15** ( $t_{1/2} = 1390$  s).

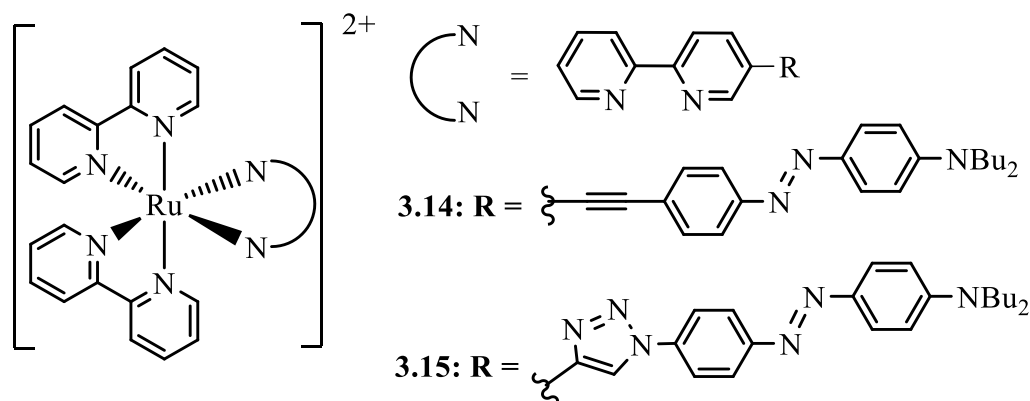
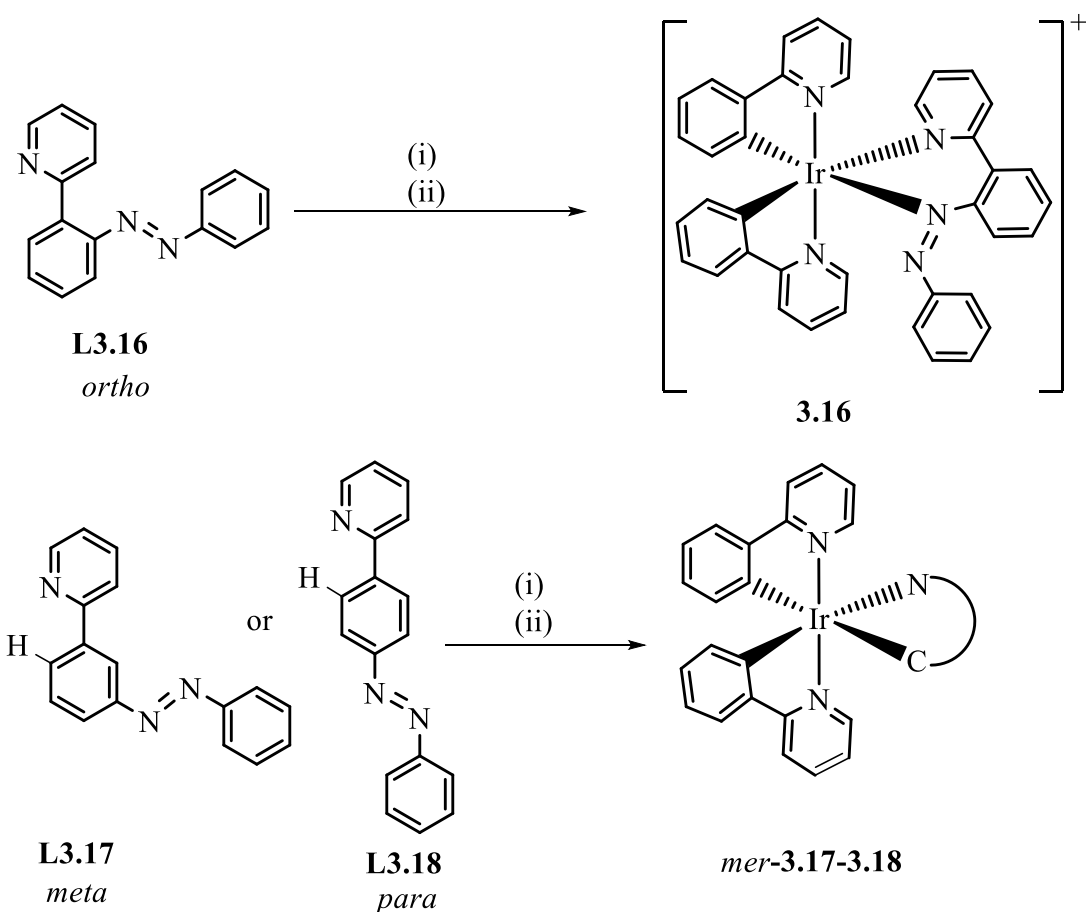


**Figure 3.6:** Ru(II) complexes **3.14-3.15** with different linkers.

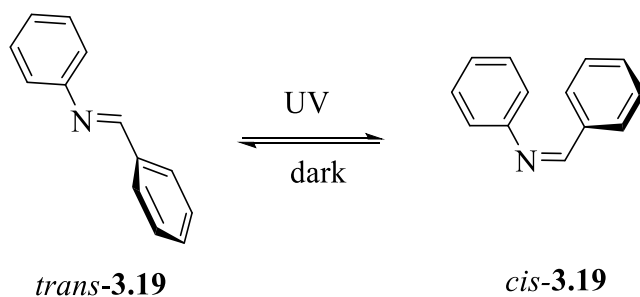
Freixa and co-workers synthesised complexes with isomeric azobenzene ligands (**L3.16-L3.18**) and found that cyclometallation took place with the *meta* (**L3.17**) and *para* (**L3.18**) isomers but not with the *ortho* isomer (**L3.16**) (Scheme 3.7).<sup>37</sup> Instead, the *ortho* isomer acted as a neutral N<sup>^</sup>N ligand forming a 6-membered chelate complex **3.16**. The position of the azobenzene (**3.17** vs **3.18**) has an effect on photoisomerisation. Hence, complex **3.17** displayed a low degree of photoisomerisation when irradiated at 409 nm, whilst irradiation of complex **3.18**, at 351 nm gave *trans-cis* photoisomerisation and the reverse *cis-trans* isomerisation was thermally induced at 55 °C. The group proposed that photoisomerisation in **3.17** is not observed due to sterically hindered azo group in the *meta* position. Complex **3.16** with an *exocyclic* N=N bond does not show photoisomerisation. However, photoisomerisation is observed for *exocyclic* N=N half-sandwich complexes (see Chapter 4).



**Scheme 3.7:** Complexes **3.16-3.18** with isomeric N=N unit. (i) AgOTf, acetone (55 °C, 2 h); (ii) [Ir(ppy)<sub>2</sub>Cl], NEt<sub>3</sub>, acetone, (55 °C, 15 hrs)

### 3.1.3 Photoisomerisation of C=N bonds

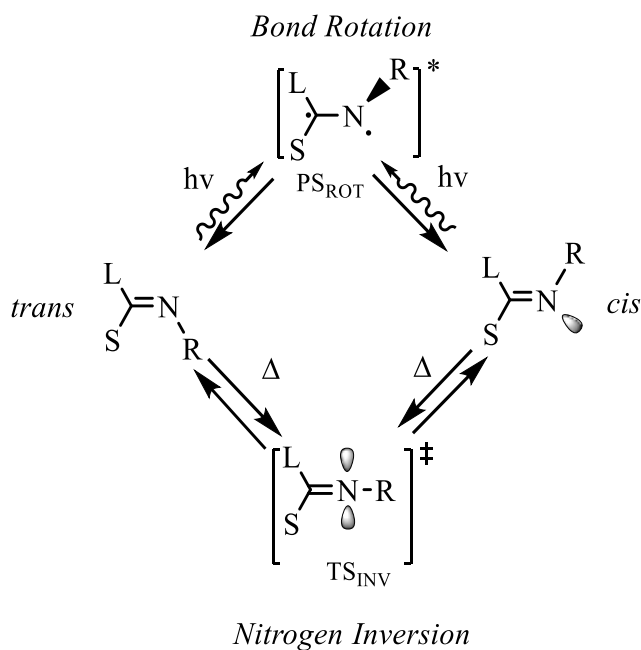
Benzylidene aniline (**3.19**) is the C=N analogue of stilbene and azobenzene where the C=N bond can be regarded as the fusion of C=C and N=N halves. *Trans*-**3.19** is non-planar with torsion angle (Ph—C=N) at 55° (Scheme 3.8).<sup>38, 39</sup> In contrast, *trans*-stilbene and *trans*-azobenzene are planar.



**Scheme 3.8:** Isomerisation of benzylidene aniline (**3.19**).

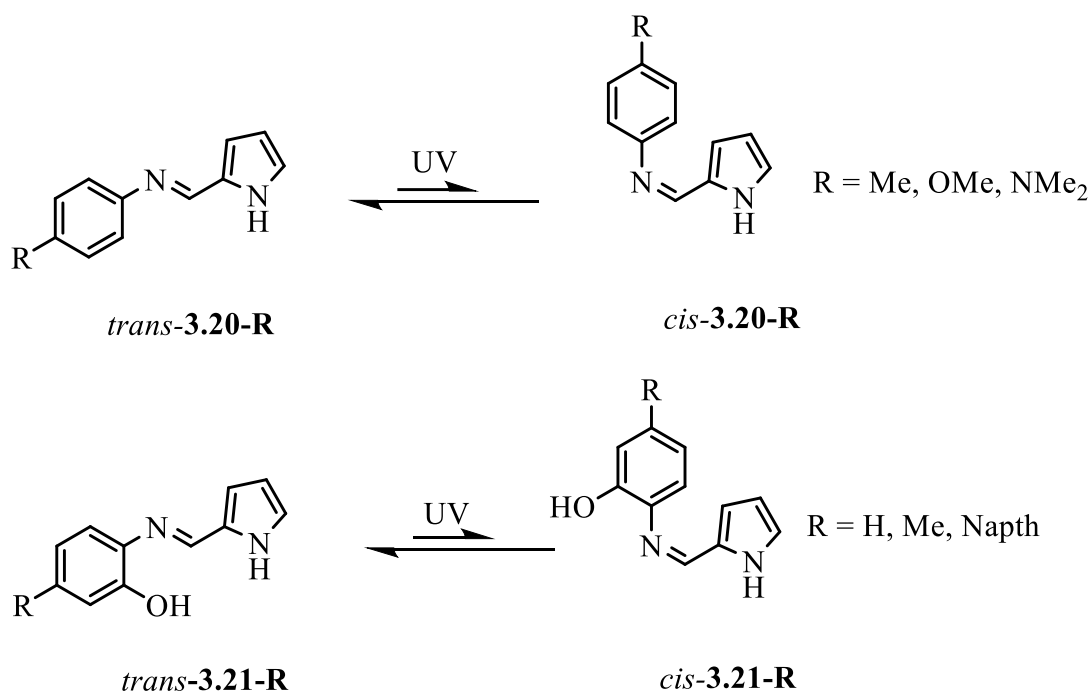
The activation energy for thermal *cis-trans* isomerisation in **3.19**<sup>40</sup> is 16.7 kcal mol<sup>-1</sup> which is lower than in azobenzene<sup>41</sup> (22.7 kcal mol<sup>-1</sup>) and stilbene<sup>42</sup> (41.8 kcal mol<sup>-1</sup>). Therefore, the backward reaction from *cis-trans* is very fast with a short  $t_{1/2}$  of *cis-3.19* of 1 s at 25 °C.<sup>43, 44</sup> Experimental and computational findings show that thermal isomerisation of *cis-3.19* goes through an inversion mechanism rather than rotation about the C=N bond.<sup>45</sup>

Lehn proposed that imines can undergo configurational isomerisation thermally and photochemically.<sup>46</sup> Scheme 3.9 shows two mechanisms for configurational isomerisation of imines which interconvert the more thermodynamically stable *trans* isomers to the less stable *cis* isomers. The out-of-plane rotation mechanism around the C=N bond (PS<sub>ROT</sub>) is photoactivated whilst the in-plane nitrogen inversion, via linear transition state (TS<sub>INV</sub>), is a thermal process. This mechanism is similar in azobenzene whilst stilbene isomerises only by internal rotation about the C=C bond.



**Scheme 3.9:** Mechanisms of isomerisation in imines. L = large substituent; S = small substituent.

Coelho and co-workers studied the photoisomerisation properties of a series of pyrrolidene imines **3.20-R** and **3.21-R** (Scheme 3.10).<sup>47</sup> The studies show that upon UV irradiation at room temperature *trans-cis* photoisomerisation of the C=N double bond was observed with the reverse reaction thermally accessible in the dark. The relevant data are shown in Table 3.2.



**Scheme 3.10:** Isomerisation of **3.20-R** and **3.21-R**.

<b>Table 3.2:</b> PSS, activation energy for <i>cis-trans</i> isomerisation and $t_{1/2}$ of <i>cis</i> isomer for <b>3.20-R</b> and <b>3.21-R</b> .			
	PSS ( <i>trans:cis</i> )	$\Delta G^\ddagger$ of <i>cis-to-trans</i> (kcal mol <sup>-1</sup> )	$t_{1/2}$ of the <i>cis</i> isomer (s)
<b>3.20-Me</b>	94:6	16.25	14
<b>3.20-OMe</b>	76:24	19.60	36
<b>3.20-NMe<sub>2</sub></b>	60:40	16.49	48
<b>3.21-H</b>	92:8	15.77	7.5
<b>3.21-Me</b>	88:12	14.81	10
<b>3.21-Naph</b>	97:3	15.30	3.1

The  $\Delta G^\ddagger$  of *cis-trans* isomerisation in **3.20-R** and **3.21-R** is between 14.81 and 19.60 kcal mol<sup>-1</sup> which is similar to previous studies in other imine compounds.<sup>45</sup> The  $t_{1/2}$  of *cis-3.21-R* are shorter ( $t_{1/2}$  = 3.1 to 10 s) than *cis-3.20-R* ( $t_{1/2}$  = 14 to 48 s). **3.20-OMe** and **3.20-NMe<sub>2</sub>** with more electron donating substituents have a higher percentage of the *cis* isomer (24% and 40%, respectively) in comparison to the less donating substituent **3.20-Me** (6%). The data show that the isomerisation in **3.20-R** and **3.21-R** can be controlled by changing the nature of the aniline ring (phenyl vs phenol) and the other substituents on this ring. In general, the thermal *cis-trans* isomerisation of **3.20-**

**R** and **3.21-R** is much slower than other imines which can only be detected at low temperatures.<sup>43</sup>

Similar to azobenzenes, imines can coordinate to metals as part of a chelate ring; though, this then prevents photoisomerisation. There are some examples of *exocyclic* imine complexes **2.22**<sup>48</sup> and **2.23**<sup>49</sup> with reported *cis* and *trans* isomers around the C=N bond (Figure 3.7), but in neither case was isomerisation investigated.<sup>48 49</sup>

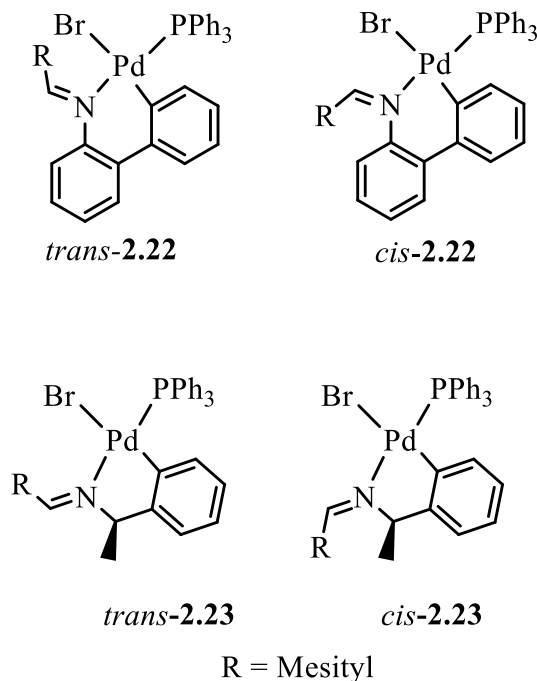


**Figure 3.7:** Pd(II) complexes with *exocyclic* C=N bond.

There are very few examples of bis-cyclometallated Ir(III) complexes with *exocyclic* C=N bonds and these are described below. Complex **3.24** with a nitron unit (Figure 3.8) has been reported to show no emission. The authors suggested that the isomerisation of the C=N unit was the cause for the absence of emission.<sup>50</sup>

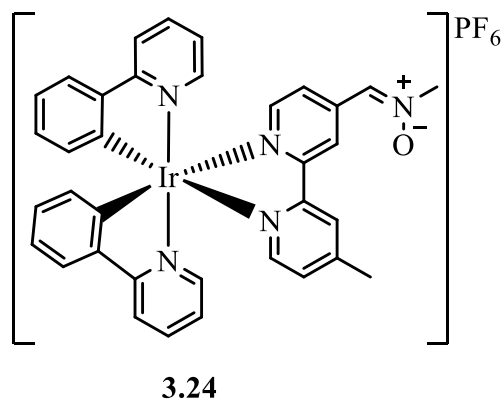
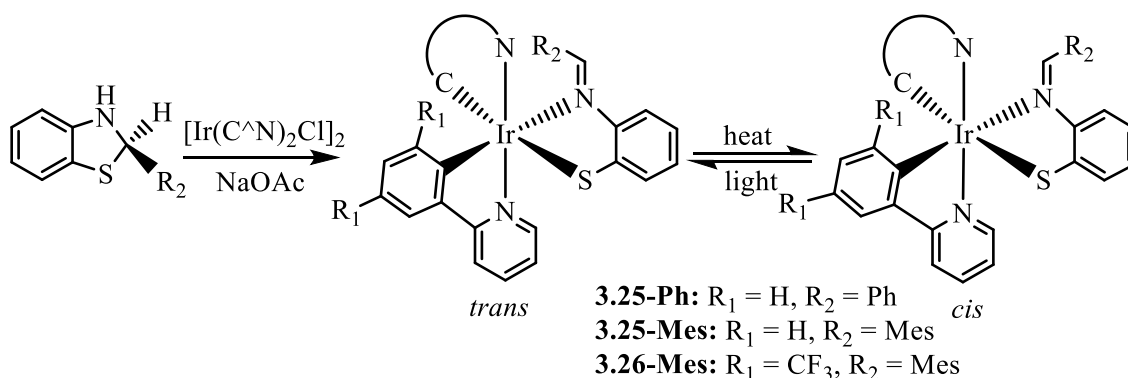


**Figure 3.8:** Bis-cyclometallated Ir(III) complex **3.24** with a nitronium unit.

Kawamoto and co-workers reported Ir(III) complexes with an *exocyclic* C=N bond with general formula  $[\text{Ir}(\text{C}^{\wedge}\text{N})_2(\text{N}^{\wedge}\text{S})]$  (**3.25-R** and **3.26-Mes**) made by ring opening of a benzothiazoline ligand (Scheme 3.11).<sup>51</sup> After purification, the initial *trans*:*cis* ratios for the complexes are: 1:1.6 (**3.25-Ph**), 100:0 (**3.25-Mes**) and 100:0 (**3.26-Mes**). The authors did not report the ratios for the crude products.



**Scheme 3.11:** Bis-cyclometallated Ir(III) complexes with *exocyclic* C=N bond.

After dissolution of the crystals of complex **3.25-Mes**, only the *trans* isomer was present but after 6 h a *trans*:*cis* ratio of 3:1 was observed. Heating *trans*-**3.25-Mes** in the solid state to 280 °C gave pure *cis*-**3.25-Mes**. Irradiation of pure *cis*-**3.25-Mes** with a mercury lamp for 5 h gave a *trans*:*cis* ratio of 3:1 though it was not determined if this was the PSS ratio. Similarly, when a sample of *trans*-**3.26-Mes**, containing CF<sub>3</sub>-functionalised cyclometallated ligand, was heated at 190 °C, 100% of *cis*-**3.26-Mes** was formed. Irradiation of *cis*-**3.26-Mes** with a mercury lamp for 5 h gave full conversion to *trans*-**3.26-Mes**. Hence, in complexes **3.25-Mes** and **3.26-Mes**, the *cis* isomer is the thermodynamically favoured isomer i.e. coordination to the metal has swapped the

stability of the two isomers compared to free imines. In addition, the barrier to reverse thermal isomerisation is very high in the complexes judging by the temperatures used. Photophysical studies for **3.25-Ph** were not carried out. However, immediately after dissolution of crystals of the *cis*-isomer in DMSO-*d*<sub>6</sub> at room temperature, the <sup>1</sup>H NMR spectrum showed the presence of both isomers suggesting a rather faster isomerisation than for **3.25-Mes** described above. The mechanism for these isomerisations has not been discussed, however since in these cases the nitrogen atom is attached to the Ir centre it is unlikely that the nitrogen inversion process is occurring, instead rotation around the C=N bond is more likely, consistent with the high temperature.

In summary, *cis-trans* isomerisation of C=C, N=N and C=N bonds can be used as molecular switches. The activation energy for thermal *cis-trans* isomerisation in stilbene<sup>42</sup> is 41.8 kcal mol<sup>-1</sup> which is higher than azobenzene<sup>41</sup> (22.7 kcal mol<sup>-1</sup>) and benzylidene aniline<sup>40</sup> (16.7 kcal mol<sup>-1</sup>). Feringa has shown that by increased steric hindrance the barrier to rotation can be reduced (Scheme 3.2 and Table 3.1).<sup>22</sup> In addition using overcrowded alkenes as ligands also reduces the barrier to isomerisation in comparison to the non-complexed alkene (Scheme 3.4 and 3.5). The incorporation of a metal fragment can also change the irradiation wavelength from the UV to the visible region making it more suitable for use in biological systems.

For azobenzene, the barrier to thermal isomerisation is lower than in stilbene, however the *t*<sub>1/2</sub> of the *cis*-azobenzene is still around two days. An azobenzene can be attached to a metal complex as a pendant unit at the back of a ligand. However, the effect of this on the isomerisation is hard to predict and depends on the position of the azobenzene in the ligand, the presence and type of linker and the identity of the metal fragment (Figures 3.4-3.6). If the azobenzene is insulated from the metal fragment through an aliphatic chain then the isomerisation is less perturbed than if the N=N unit is conjugated with the metal centre. Azobenzenes can also act as donor ligands in which an N atom is directly bound to the metal either forming an *endocyclic* N=N bond which prevents photoisomerisation or an *exocyclic* N=N bond which in principle can isomerise. An example of an exocyclic N=N complex is **3.16** but this does not photoisomerise.

## Aims and Objectives

As mentioned above benzylidene aniline has a lower barrier to *cis-trans* isomerisation than either stilbene or azobenzene. As a result, it is impossible to isolate separate *cis* and *trans* isomers. The lower barrier to isomerisation for N=N and C=N bonds compared to C=C is almost certainly because the first two can isomerise by nitrogen inversion whereas for C=C there must be rotation about the double bond which involves more bond breaking and hence a higher barrier. Very little work has been done on *trans-cis* isomerisation of *exocyclic* C=N bonds in metal complexes. However, upon complexation of the N atom it cannot isomerise via nitrogen inversion unless the N atom dissociates from the metal, instead rotation around the C=N bond is more likely which leads to a higher barrier to isomerisation compared to free imines. This is consistent with the complexes studied by Kawamoto (Scheme 3.11) which show very high barriers to *cis-trans* isomerisation. Consequently, metal ligand interactions have been shown to play an important role in changing the photostability and rate of isomerisation of C=C, N=N and C=N bonds.

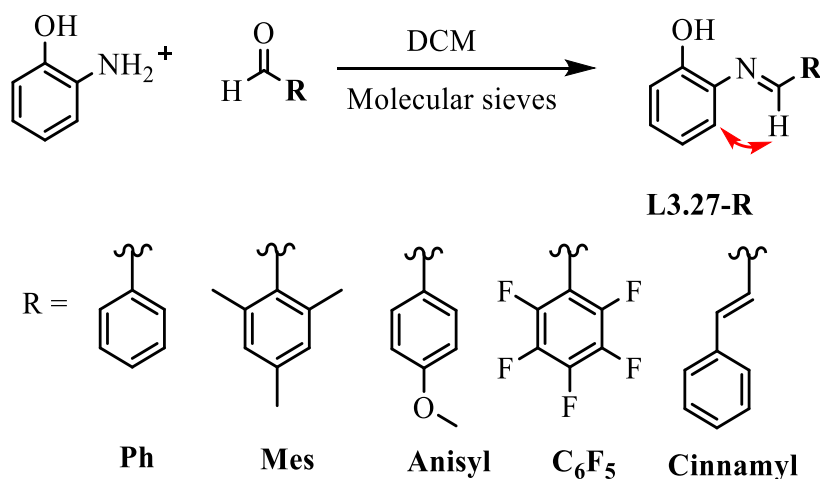
This chapter will describe the synthesis and characterisation of bis-cyclometallated Ir(III) complexes with general formula  $[\text{Ir}(\text{C}^{\wedge}\text{N})_2(\text{N}^{\wedge}\text{O})]$  where the  $\text{N}^{\wedge}\text{O}$  ligand forms a 5-membered *exocyclic* chelate ring after complexation. The photophysical properties are described and comparisons made with the isomeric complexes studied in Chapter 2.

## 3.2 Results and Discussion

### 3.2.1 Synthesis and Characterisation of *Exocyclic* Imine Complexes

#### $[\text{Ir}(\text{C}^{\wedge}\text{N})_2(\text{N}^{\wedge}\text{O})]$

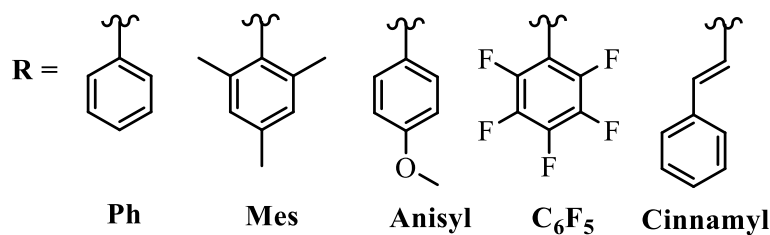
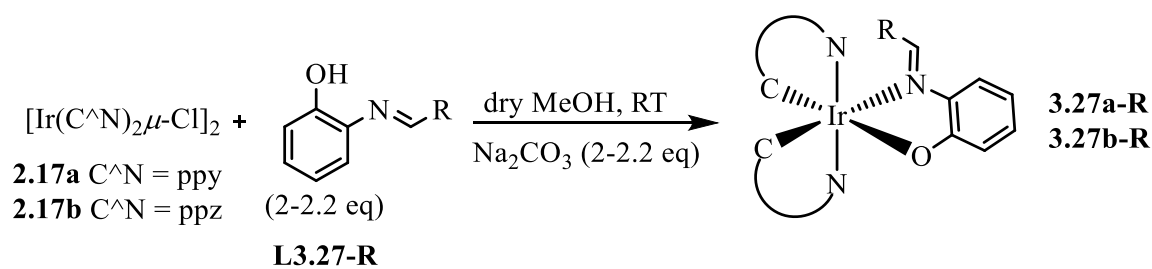
The imine ligands (**L3.27-R**) are all known<sup>52-55</sup> and were synthesised using a typical condensation reaction between 2-aminophenol and the respective aldehyde in the presence of molecular sieves in DCM (Scheme 3.12).



**Scheme 3.12:** Synthesis of imine ligands **L3.27R**.

The  $^1\text{H}$  NMR spectra of the ligands show only the *trans* isomer and the spectroscopic data agree with the literature.<sup>52-55</sup> The imine protons for **L3.27-R** are observed between  $\delta$  8.48 and 9.04. The presence of the *trans* isomer was confirmed by the NOESY spectrum showing a NOE between the imine proton and the *ortho* proton of the phenol ring in all cases (red arrow). The  $^1\text{H}$  NMR spectra of **L3.27-Mes**, **L3.27-Anisyl** and **L3.27-C<sub>6</sub>F<sub>5</sub>** are consistent with the aryl group rotating fast in solution however it is also possible that the R group is fixed and is perpendicular to the plane of the imine bond.

Dichloro-bridged  $[\text{Ir}(\text{C}^{\wedge}\text{N})_2\mu\text{-Cl}]_2$  dimers (**2.17a-b**) and the respective N<sup>^</sup>OH ligand (**L3.27-R**) were reacted in the presence of  $\text{Na}_2\text{CO}_3$  to give *exocyclic* imine complexes **3.27a-R** and **3.27b-R** in good to excellent yields (72-91%) (Scheme 3.13). Occasionally, small amounts of **3.28a** was formed due to the hydrolysis of the ligand (Figure 3.9) and this was removed via column chromatography. During monitoring, the  $^1\text{H}$  NMR spectrum of **3.27b-Ph** showed the presence of a second species that integrated to the same number of protons as the desired complex, with similar proton splitting and a second imine peak. This was presumed to be due to the *cis* isomer. Similar observations have been reported in bis-cyclometallated Ir(III) complexes **3.25-3.26**.<sup>51</sup> On close examination, a second species was observed in all cases and attempts to separate the isomers and analysis of the second species will be described later.



**Scheme 3.13:** Synthesis of complexes **3.27a-R** and **3.27b-R** with an *exocyclic* imine bond.

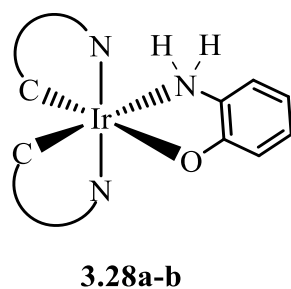


**Figure 3.9:** Complex **3.28a-b** is an occasional side product in the reaction.

Firstly, the  $^1\text{H}$  NMR spectra of the *trans*-isomers will be described. The spectra of complexes **3.27a-R** and **3.27b-R** show double the number of protons for the  $\text{C}^{\wedge}\text{N}$  ligand in comparison to the dichloro-bridged dimers **2.23a-b**. This is due to the chelation of the unsymmetrical  $\text{N}^{\wedge}\text{O}$  ligand and loss of  $\text{C}_2$ -symmetry as seen in Chapter 2. The proton assignment of complex **3.27b-Mes** is described first as the Mes group helps identify key correlations that aid the assignment of the two  $\text{C}^{\wedge}\text{N}$  ligands. A similar approach was described in Chapter 2.

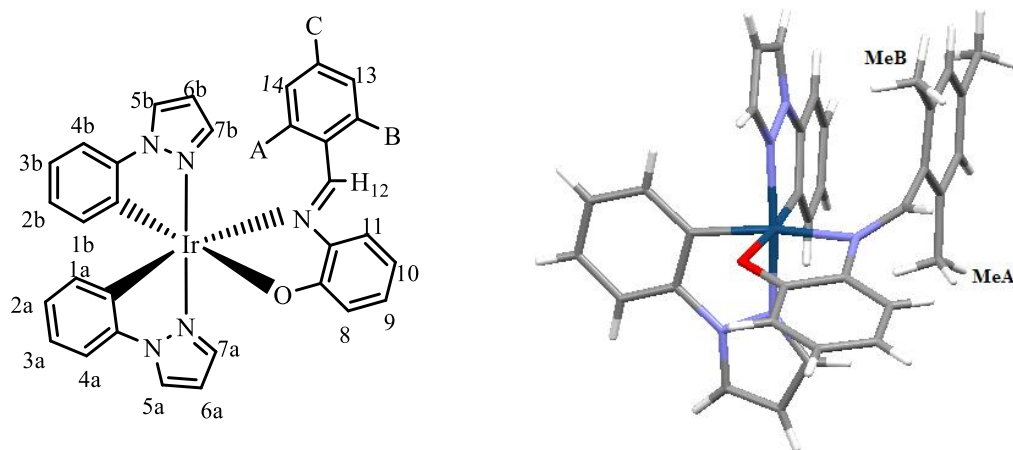


**Figure 3.10:** Numbering system and 3D representation of complex **3.27b-Mes**.

Figure 3.10 shows the numbering system used for the assignment of each proton and the X-Ray structure of **3.27b-Mes** to illustrate the  $^1\text{H}$ - $^1\text{H}$  correlations.

In complex **3.27b-Mes**, the mesityl group appears as a 3H singlet at  $\delta$  1.39, a 6H singlet at  $\delta$  1.96 and two inequivalent 1H aromatic protons at  $\delta$  5.82 and 6.35. The 3H singlet at  $\delta$  1.39 shows a NOE with only one mesityl proton, that at  $\delta$  6.35, suggesting that it is an *ortho*-Me and therefore both *ortho*-Me groups are inequivalent and the mesityl is not rotating in solution. Therefore, the 6H singlet is due to accidental overlap of the other *ortho*-Me and the *para*-Me. This is confirmed by two cross peaks from the 6H singlet in the  $^{13}\text{C}$ - $^1\text{H}$  HMQC spectrum. The TOCSY and the NOE spectra allowed identification of the linkage between pyrazole and phenyl rings. The identification of C $\wedge$ N ligand *a* and *b* was established by using the NOE spectrum of the alkyl area. The 6H singlet at  $\delta$  1.96 shows a NOE with a pyrazole proton H $^{7a}$  at  $\delta$  7.34, and with a phenyl proton H $^{1b}$  at  $\delta$  5.95. This must arise from the *ortho*-Me as the *para*-Me is too far away to correlate with H $^{7a}$  and H $^{1b}$ . From the 3D representation in Figure 3.10, the *ortho*-Me pointing towards H $^{7a}$  and H $^{1b}$  is therefore *ortho*-Me<sub>A</sub> and the 3H singlet at  $\delta$  1.39 corresponds to *ortho*-Me<sub>B</sub> which shows a weak NOE with H $^{7b}$ . Proton H $^{1a}$  and H $^{1b}$  were observed as 1H doublet of doublets at  $\delta$  5.75 and 5.95, respectively which are typically upfield due to ring current effects as seen in Chapter 2. The remaining protons of C $\wedge$ N ligands *a* and *b* were identified using the COSY spectrum. Imine proton H $^{12}$  is assigned as the most downfield singlet at  $\delta$  8.81 and shows an NOE to *ortho* phenol proton H $^{11}$  at  $\delta$  7.21, indicating that it is the *trans*-isomer. The remaining phenol protons were assigned using the COSY spectrum. The ASAP mass spectrum for complex **3.27b-Mes** shows a molecular ion at  $m/z$  718 whilst the IR spectrum shows a

$\nu(\text{C}=\text{N})_{\text{imine}}$  stretch at  $1576\text{ cm}^{-1}$  in comparison to the free ligand at  $1623\text{ cm}^{-1}$ . This is due to backbonding effect.

The  $^1\text{H}$  NMR spectrum of ppy-complex **3.27a-Mes** shows three 3H singlets two *ortho*-Me groups at  $\delta$  2.04 and 1.24 and the *para*-Me at  $\delta$  2.06 that shows an NOE with two 1H singlets at  $\delta$  5.86 and 6.34. The inequivalence of the mesityl group is evidence that it is not rotating in solution. The most downfield singlet is assigned as the imine proton at  $\delta$  8.93 which shows an NOE with *ortho*-Me at  $\delta$  1.24 and with the adjacent *ortho* phenol proton at  $\delta$  7.24 indicating that it is the *trans* form. Similarly to **3.27b-Mes**, the two aromatic upfield doublets correspond to  $\text{H}^{1a}$  and  $\text{H}^{1b}$  at  $\delta$  6.17 and 5.75. The ASAP mass spectrum of complex **3.27a-Mes** shows a molecular ion at  $m/z$  740 whilst the IR spectrum shows a  $\nu(\text{C}=\text{N})_{\text{imine}}$  stretch at  $1579\text{ cm}^{-1}$  in comparison to the free ligand at  $1623\text{ cm}^{-1}$  due to backbonding.

For complexes **3.27a-Ph** and **3.27b-Ph**, the imine peaks appear as singlets at  $\delta$  8.77 and 8.92 respectively. The characteristic upfield aromatic signals that correspond to  $\text{H}^{1a}$  and  $\text{H}^{1b}$  appear at  $\delta$  6.25 and 6.38 for **3.27a-Ph** and at  $\delta$  6.28 and 6.32 for **3.27b-Ph**. In both complexes the imine signal shows an NOE with the adjacent phenol proton identifying the *trans* isomer. The ASAP mass spectra for complexes **3.27a-Ph** and **3.27b-Ph** each show a molecular ion at  $m/z$  698 and  $m/z$  676 respectively. The IR spectra show a  $\nu(\text{C}=\text{N})$  stretch at  $1579\text{ cm}^{-1}$  for **3.27a-Ph** and  $1574\text{ cm}^{-1}$  for **3.27b-Ph** in comparison to the free ligand at  $1629\text{ cm}^{-1}$ .

In complex **3.27a-Anisyl**, the imine proton appears at  $\delta$  8.58 whilst in **3.27b-Anisyl**, it appears at  $\delta$  8.73. The  $^1\text{H}$  NMR spectra of complexes **3.27a-Anisyl** and **3.27b-Anisyl** each show a 3H singlet at  $\delta$  3.63 and  $\delta$  3.71, respectively, corresponding to the OMe group. Each complex shows two 2H doublets at  $\delta$  6.10 and  $\delta$  6.66 for **3.27a-Anisyl** and at  $\delta$  6.26 and  $\delta$  6.81 for **3.27b-Anisyl**, that correspond to the  $\text{A}_2\text{B}_2$  system, indicating that the anisyl ring is rotating in solution. The  $\text{C}^{\wedge}\text{N}$  protons for both complexes **3.27a-Anisyl** and **3.27b-Anisyl** shows similar characteristics with upfield aromatic protons corresponding to  $\text{H}^{1a}$  and  $\text{H}^{1b}$  (See Experimental). The ASAP mass spectra for complexes **3.27a-Anisyl** and **3.27b-Anisyl** show molecular ions at  $m/z$  728 and  $m/z$  706 respectively and the IR spectra show a  $\nu(\text{C}=\text{N})_{\text{imine}}$  stretch at  $1577\text{ cm}^{-1}$  for both complexes in comparison to the free ligand at  $1627\text{ cm}^{-1}$ .

The  $^1\text{H}$  NMR spectrum of complex **3.27a-C<sub>6</sub>F<sub>5</sub>** shows the imine proton at  $\delta$  8.48, whilst that for **3.27b-C<sub>6</sub>F<sub>5</sub>** appears at  $\delta$  8.54. The  $^{19}\text{F}$  NMR spectrum of each complex show

five different fluorine resonances (see Experimental) indicating that the C<sub>6</sub>F<sub>5</sub> group is fixed in solution for both complexes. The ASAP mass spectra show a molecular ion at  $m/z$  788 for complex **3.27a-C<sub>6</sub>F<sub>5</sub>** and at  $m/z$  766 for complex **3.27b-C<sub>6</sub>F<sub>5</sub>**. The IR spectra show a  $\nu(\text{C}=\text{N})_{\text{imine}}$  stretch at 1582 cm<sup>-1</sup> for complex **3.27a-C<sub>6</sub>F<sub>5</sub>** and 1575 cm<sup>-1</sup> for complex **3.27b-C<sub>6</sub>F<sub>5</sub>** in comparison to the free ligand at 1619 cm<sup>-1</sup>. The <sup>1</sup>H NMR spectra of complexes **3.27a-Cinnamyl** and **3.27b-Cinnamyl** show similar features but the imine peaks are doublets rather than singlets, at  $\delta$  8.55 and  $\delta$  8.50, respectively. The ASAP mass spectra show a molecular ion at  $m/z$  724 for **3.27a-Cinnamyl** and at  $m/z$  702 for **3.27b-Cinnamyl**, whilst the IR spectra show a  $\nu(\text{C}=\text{N})_{\text{imine}}$  stretch at 1581 cm<sup>-1</sup> for **3.27a-Cinnamyl** and 1574 cm<sup>-1</sup> for **3.27b-Cinnamyl** in comparison to the free ligand at 1629 cm<sup>-1</sup>.

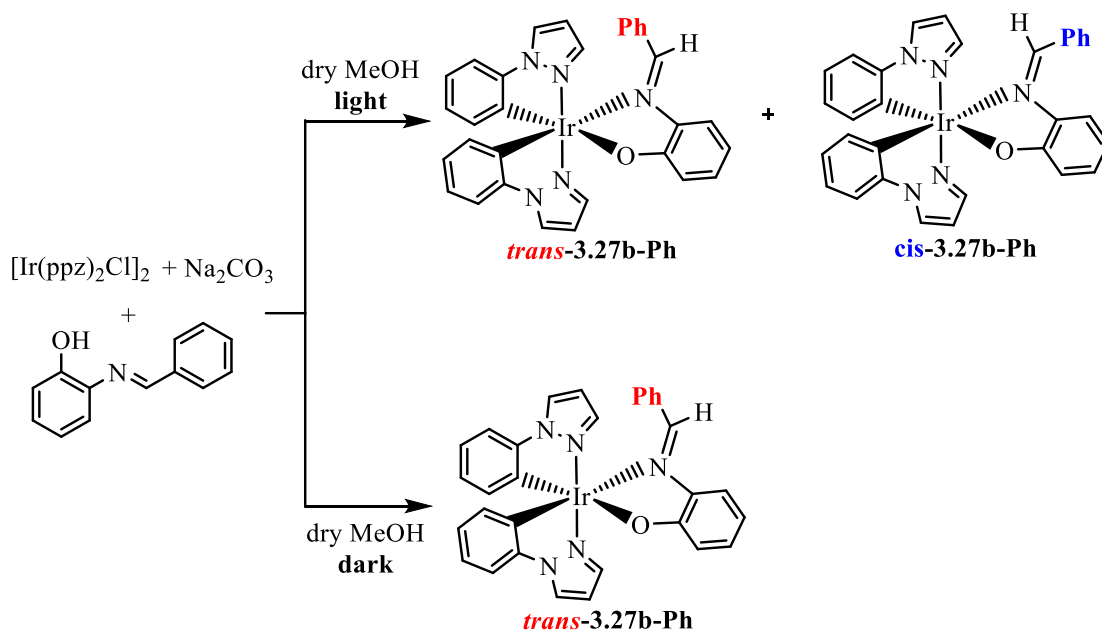
As mentioned above in some cases a small amount of another isomer was observed in the NMR spectra. Unfortunately, the mixture of isomers could not be separated via column chromatography. Since the pure *trans* isomers have been characterised (see above) it was possible to assign some of the *cis* isomer when present in a mixture. The <sup>1</sup>H NMR spectra of all the *cis* isomers showed two 1H doublets at high field ( $\delta$  6.24 to 6.39) corresponding to the H<sup>1a</sup> and H<sup>1b</sup> protons showing the presence of a bis-cyclometallated fragment. These signals are observed more downfield in comparison to their respective *trans* isomer. The imine protons are observed between  $\delta$  7.34 and 7.77 which is between 1 and 1.5 ppm more upfield in comparison to the *trans* isomer. This is consistent with the imine proton in the *cis* isomers lying above one of the cyclometallated rings and so being shifted upfield by a ring current effect. In addition, the <sup>1</sup>H NMR spectra showed extra signals that corresponded to the R group. For example, in *cis*-**3.27a-Mes** the mesityl group appears as three 3H singlets at  $\delta$  2.25, 2.16 and 1.23 and the two 1H singlets at  $\delta$  6.67 and 6.84 indicating that it is fixed in solution. For *cis*-**3.27b-Mes**, the mesityl group is also fixed with three 3H singlets at  $\delta$  2.17, 2.09 and 1.35 but the mesityl protons were not identified due to the overlap with the *trans* isomer. For the anisyl complexes, the OMe signal is observed at  $\delta$  3.70 for *cis*-**3.27a-Anisyl** and  $\delta$  3.81 for *cis*-**3.27b-Anisyl** whilst the aromatic protons give an A<sub>2</sub>B<sub>2</sub> pattern in each case (for *cis*-**3.27b-Anisyl** one 2H signal was overlapping with the *trans* isomer) showing that in both cases the anisyl group is rotating in solution.

The <sup>19</sup>F NMR spectra for *cis*-**3.27a-C<sub>6</sub>F<sub>5</sub>** and *cis*-**3.27b-C<sub>6</sub>F<sub>5</sub>** each showed three 1F signals and a 2F broad singlet.

In *cis*-**3.27a-Cinnamyl** and *cis*-**3.27b-Cinnamyl**, it was not possible to identify the signals related to the R group due to the highly conjugated group and overlap of the *trans* isomer.

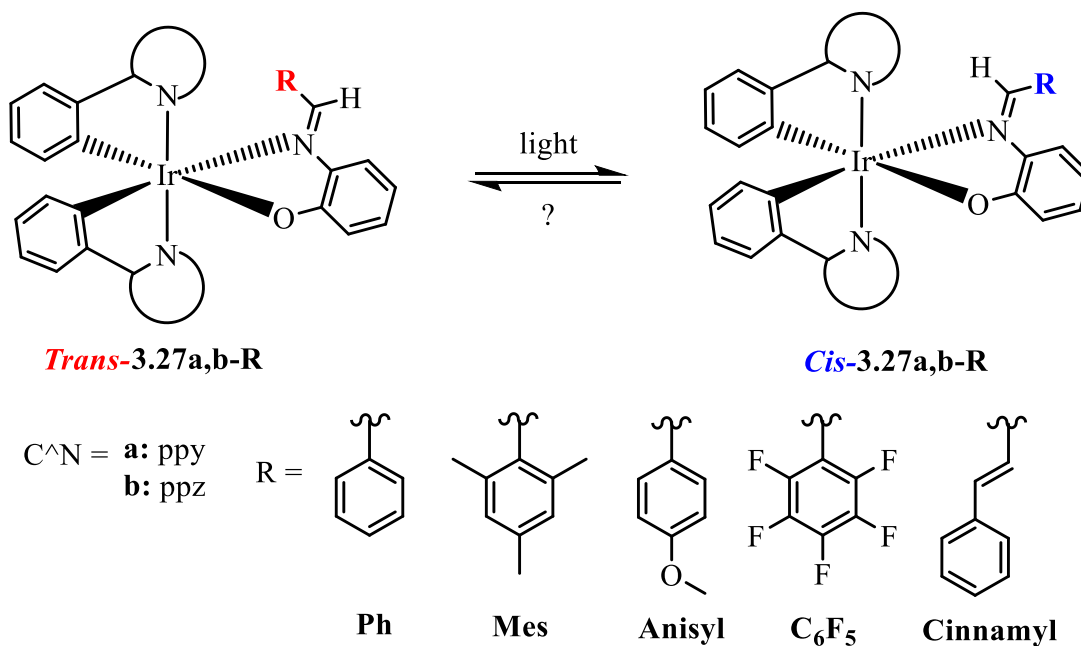
Crystallisation was successful in providing the *trans* isomer for complexes **3.27a,b-Ph**, **3.27a,b-Mes** and **3.27b-Anisyl**, however, no sample of a pure *cis*-isomer was obtained. The <sup>1</sup>H NMR spectrum of crystals of *trans*-**3.27b-Ph** only showed one species (*trans*-**3.27b-Ph**) but after 30 mins under ambient light, signals due to *cis*-**3.27b-Ph** started to appear. This confirms that the second species formed during the reaction is the *cis* isomer and that the *trans* form isomerises to the *cis* form.

The effect of light on isomerisation was tested and found that when crystals of complex *trans*-**3.27b** were dissolved in CDCl<sub>3</sub> and protected from light, the <sup>1</sup>H NMR spectrum showed only *trans*-**3.27b** present, even after several days at room temperature. However, when the same sample was exposed to ambient light for 15 min signals due to *cis*-**3.27b** started to appear. After 3 hrs, a 1:1 ratio was obtained with no further change with additional irradiation with a halogen lamp hence this ratio corresponds to the PSS. When the 1:1 mixture was left in the dark for several days, the ratio did not change. Therefore, the *trans-to-cis* isomerisation is initiated by light. To confirm this, complex **3.27b** was synthesised in the presence and absence of light and monitored until the reaction reached completion. It was found that when the reaction was done under ambient light a mixture of *trans* and *cis* isomers was formed, but when carried out in the dark, only *trans*-**3.27b** was formed (Scheme 3.14). This observation was true for all the complexes **3.27a,b-R** in this chapter. Although, only the *trans* isomer is formed in the dark, if the aminophenolate product (**2.28a-b**) is present in the crude mixture, purification by column chromatography was necessary. This was not easy to be carried out as the column needed to be protected from light to prevent the formation of *cis* isomer; hence some *cis* isomer was sometimes present after purification.



**Scheme 3.14:** Synthesis of **3.27b-Ph** in the presence and absence of light.

After establishing that the isomerisation was photochemically induced, the complexes were irradiated using a halogen lamp until the *trans*:*cis* ratio did not change (Table 3.3). Where feasible (**3.27a,b-Ph**, **3.27a,b-Mes** and **3.27b-Anisyl**), the photoisomerisation was initiated with the pure *trans* isomer, otherwise a mixture with mostly *trans* was irradiated with a halogen lamp at room temperature in  $\text{CDCl}_3$ .



<b>Table 3.3:</b> PSS Ratios obtained for complexes <b>3.27a-R</b> and <b>3.27b-R</b> after irradiation under halogen lamp at room temperature.			
<b>Ppy Complex</b>	<b>Ratio <i>trans:cis</i></b>	<b>Ppz complex</b>	<b>Ratio <i>trans:cis</i></b>
<b>3.27a-Ph</b>	37:63	<b>3.27b-Ph</b>	48:52
<b>3.27a-Mes</b>	52:48	<b>3.27b-Mes</b>	57:43
<b>3.27a-Anisyl</b>	50:50	<b>3.27b-Anisyl</b>	56:44
<b>3.27a-C<sub>6</sub>F<sub>5</sub></b>	62:38	<b>3.27b-C<sub>6</sub>F<sub>5</sub></b>	61:39
<b>3.27a-Cinnamyl</b>	45:55	<b>3.27b-Cinnamyl</b>	50:50

Unfortunately, none of the systems completely converted to the *cis* isomer upon irradiation for 10 hours; complex **3.27a-Ph** showed the greatest proportion of *cis* isomer at 63%. Complexes with ppy ligands (**3.27a-R**) show a slightly greater preference for the *cis* isomer in comparison to the respective ppz complexes (**3.27b-R**). Changing the R group did not shift the ratios dramatically hence there is no clear relationship between electronic and steric effects of the R group and the isomer ratio. Solid-state isomerisation studies were also carried out and showed that *trans-cis* photoisomerisation takes place in a thin film although, it is slower than in solution (see Section 6.1 for experimental details). For complex **3.27b-Mes**, the ratio in the thin film after 6 hours of irradiation was 86:14 *trans:cis*, whilst in solution a *trans:cis* ratio of 57:43 was reached after 3 hours of irradiation. Furthermore, when crystals of only *trans*-**3.27b-Mes** are exposed to ambient light no *cis* isomer could be detected when the crystals were dissolved. As mentioned above (See Section 3.1.3), when pure *cis*-**3.26-Mes** was irradiated it converted fully to the *trans* form in the solid state. This isomerisation is in the opposite direction to the complexes studies in this thesis. The reason for this apparent difference is not clear.

To establish if the *cis-trans* reverse isomerisation is thermally accessible, samples with a mixture of both isomers were heated in the dark at 60 °C for 6 hrs (Table 3.4). All complexes show *cis-trans* thermal isomerisation except for **3.27a-Mes** that showed no change in the ratio and **3.27b-Mes** that shows a slight increase of the amount of *cis* isomer after heating. The latter observation may be because the sample was exposed to light and the initial sample was not at the PSS. Complexes **3.27a-Cinnamyl** and **3.27b-Cinnamyl** show 100% conversion back to the *trans* isomer after 6 hrs in the dark at 60 °C. The complexes in Table 3.4 have been categorised as A where no there is no

isomerisation in the dark at 60 °C hence indicating a large energy barrier for thermal isomerisation; category B is where some *cis-trans* isomerisation is observed but it does not convert to *trans* completely in 6 hrs at 60 °C; and category C where 100% *cis-trans* isomerisation is observed in this period, suggesting a lower barrier for thermal isomerisation in comparison to categories A and B. The initial data show that complexes with the bulkier substituent R = Mes appear to have a higher energy barrier. There is some evidence that changing the C<sup>N</sup> may also have an effect on the energy barrier; isomerisation of **3.27b-Ph** is slower than **3.27a-Ph** and the same appears to be the case for **3.27b-Anisyl** and **3.27a-Anisyl**, however further investigations are required to establish this. It is consistent with the observations of Kawamoto who showed that a changing the C<sup>N</sup> ligand altered the ease of thermal isomerisation (complexes **3.25-Mes** and **3.26-Mes**, Scheme 3.11).

<b>Table 3.4: Thermal isomerisation studies for complexes 3.27a-R and 3.27b-R.</b>			
	<b>Before heating</b>	<b>After heating (dark 60 °C, 6h)</b>	<b>Category</b>
	<i>trans:cis</i>	<i>trans:cis</i>	
<b>3.27a-Ph</b>	39:61	51:49	B
<b>3.27b-Ph</b>	48:52	55:45	A/B
<b>3.27a-Mes</b>	51:49	51:49	A
<b>3.27b-Mes</b>	64:36	60:40	-
<b>3.27a-Anisyl</b>	50:50	78:22	B
<b>3.27b-Anisyl</b>	56:44	61:39	A/B
<b>3.27a-C<sub>6</sub>F<sub>5</sub></b>	61:39	81:19	B
<b>3.27a-Cinnamyl</b>	47:57	100:0	C
<b>3.27b-Cinnamyl</b>	50:50	100:0	C
Category A = large barrier (no isomerisation at 60 °C dark), B = modest barrier (isomerisation over hours/days at 60 °C in dark), C = low barrier (full conversion to the <i>trans</i> isomer).			

### X-Ray Crystallography

Complexes **3.27a,b-Ph**, **3.27a,b-Mes** and **3.27b-Anisyl** afforded crystals from DCM/MeOH suitable for X-Ray crystallography. All the X-ray structures show the same features with *cis* metallated carbons and *trans* nitrogen (ppy/ppz) atoms as also

seen in Chapter 2 and in similar complexes.<sup>56, 57</sup> The five structures (Figure 3.11 and Appendix) show a distorted octahedral geometry at the Ir centre with bond angles [*trans* N—Ir—N angle] between 173.3° and 175.7°. The Ir—N(imine) bond is longer than the Ir—N(ppy/ppz) bonds because it is *trans* to a C atom. Table 3.5 shows selected bond lengths and bond angles for the five complexes. After complexation, the C=N bond length ranges between 1.27 Å and 1.30 Å which are longer, due to backbonding, in comparison to free imines that range between 1.24 Å and 1.26 Å<sup>54, 58</sup>

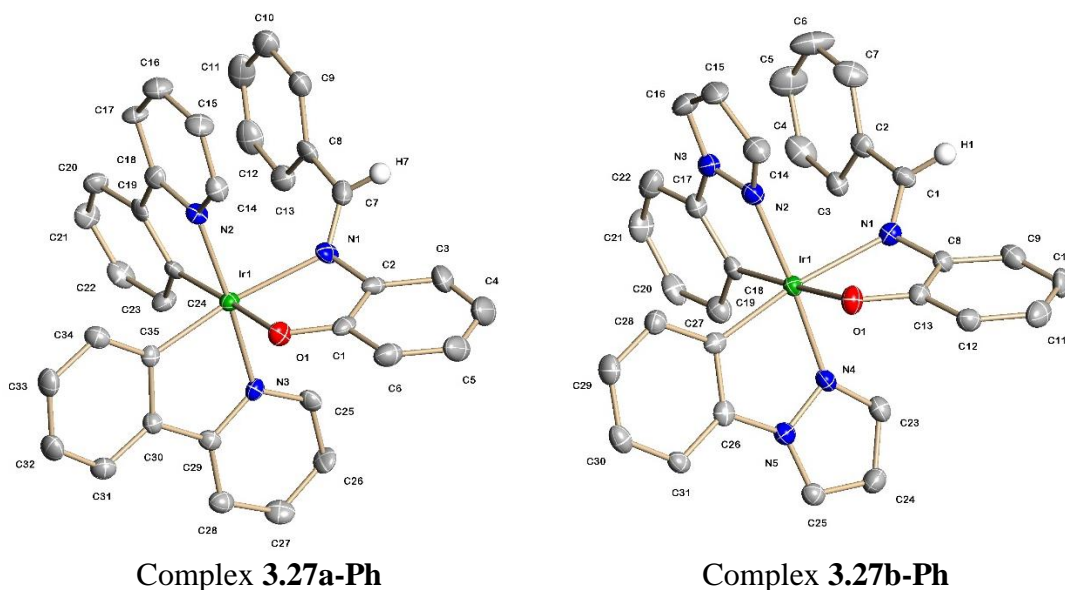


**Figure 3.11:** X-ray structures of complexes **3.27a-Ph** and **3.27b-Ph** showing 50% ellipsoids with hydrogen atoms omitted for clarity (except for the imine proton).

<b>3.27a-Ph</b>	(Å)	<b>3.27b-Ph</b>	(Å)
Ir(1)—N(2)	2.023(5)	Ir(1)—N(2)	2.014(5)
Ir(1)—N(3)	2.030(5)	Ir(1)—N(4)	2.012(4)
Ir(1)—N(1)	2.191(5)	Ir(1)—N(1)	2.185(4)
Ir(1)—C(35)	2.002(6)	Ir(1)—C(27)	2.020(5)
Ir(1)—C(24)	2.004(6)	Ir(1)—C(18)	1.995(5)
Ir(1)—O(1)	2.145(4)	Ir(1)—O(1)	2.144(4)
N(1)—C(7)	1.295(8)	N(1)—C(1)	1.271(7)
centroid—centroid	3.917	centroid—centroid	3.779

<b>3.27a-Ph</b>	(°)	<b>3.27b-Ph</b>	(°)
N(2)—Ir(1)—N(3)	174.9(2)	N(4)—Ir(1)—N(2)	175.71(17)
C(24)—Ir(1)—N(2)	80.4(2)	C(18)—Ir(1)—N(2)	79.8(2)
C(35)—Ir(1)—N(3)	80.8(2)	N(4)—Ir(1)—C(27)	80.33(19)
O(1)—Ir(1)—N(1)	77.31(18)	O(1)—Ir(1)—N(1)	77.28(15)

Figure 3.12 shows parallel views of complexes **3.27a,b-Ph** which illustrate that intramolecular  $\pi$ - $\pi$  interactions are present between the aryl group of the N<sup>^</sup>O ligand and the adjacent phenyl ring of the C<sup>^</sup>N ligand [centroid—centroid distance between 3.56 Å and 3.92 Å]. Complex **3.25-Mes** (see Section 3.1.3) also observed intramolecular  $\pi$ - $\pi$  interactions with a centroid—centroid distance of 3.24 Å.<sup>51</sup> These interactions could be helping to stabilise the *trans* isomer. In complexes **3.27a,b-Ph**, **3.27a,b-Mes** and **3.27b-Anisyl**, the R group is almost perpendicular to the phenol plane with dihedral angles between 78.7° and 85.1° as illustrated in Figure 3.13 for complex **3.27b-Ph**.

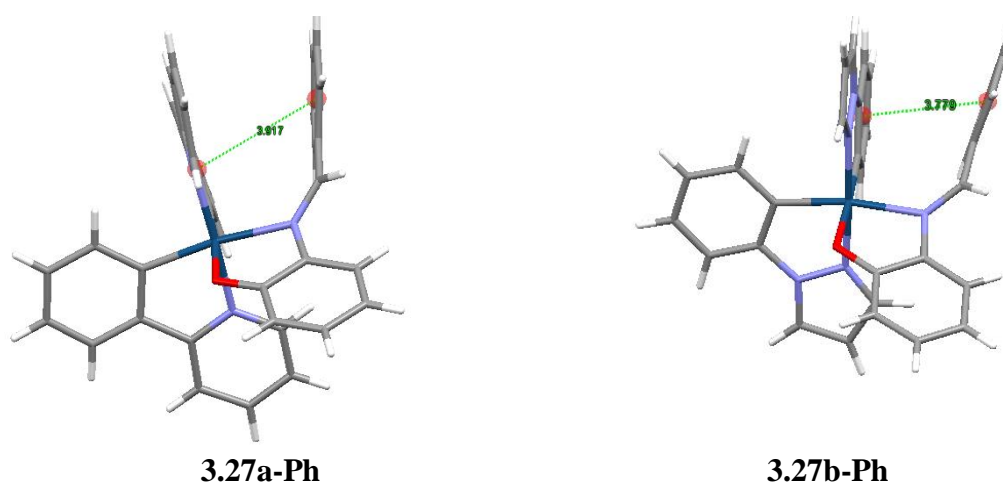


**Figure 3.12:** Parallel views of the X-Ray structure of complex **3.27a,b-Ph**.

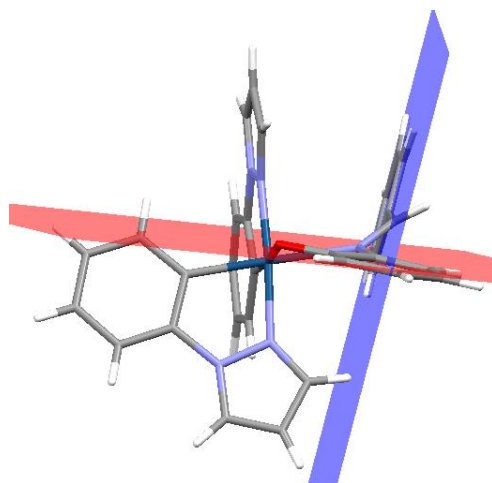


**Figure 3.13:** Dihedral angle ( $82.5^\circ$ ) between the aryl substituent and the phenol plane in **3.27b-Ph**.

### 3.2.3 Photophysical Properties of $[\text{Ir}(\text{C}^{\wedge}\text{N})_2(\text{N}^{\wedge}\text{O})]$ Complexes

#### Absorption Spectroscopy

The absorption spectrum of complex **3.27b-Ph** shows three bands (Figure 3.14). The most intense absorption is below 300 nm and it is assigned as intraligand ( $\pi - \pi^*$ ) transitions, the moderately intense absorption between 300 – 400 nm is attributed to spin allowed metal to ligand charge transfer ( $^1\text{MLCT}$ ) and the weak absorption band greater than 400 nm (Table 3.6). The UV-Vis spectra of *trans*-**3.27b-Ph** and as a mixture is shown in Figure 3.14 the major difference in absorbance between the *trans* and *cis* isomer is in the  $\pi$ - $\pi^*$  band.

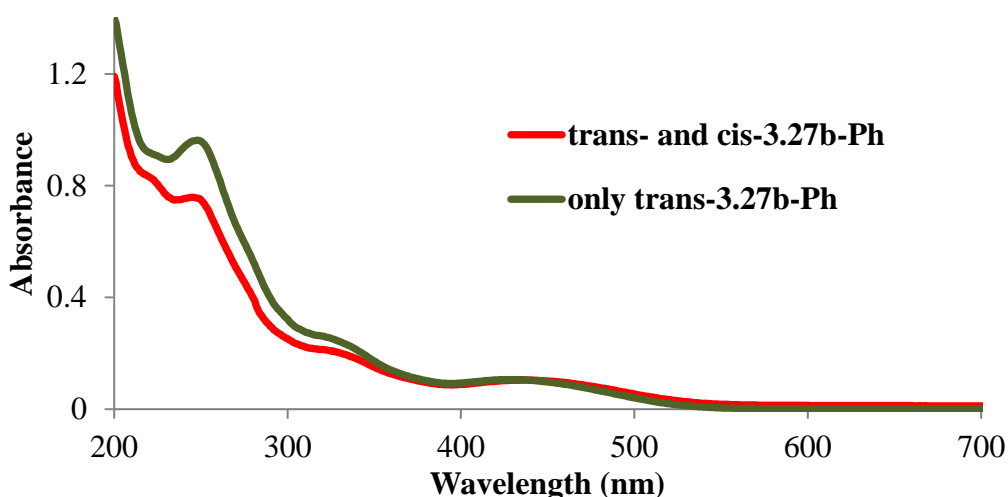


**Figure 3.14:** Electronic absorption spectrum of complex **3.27b-Ph** at 0.02 mM in MeCN.

<b>Table 3.6:</b> Electronic absorption spectral data of complex <b>3.27b-Ph</b> in HPLC grade MeCN.	
<b>Complex</b>	$\lambda_{\text{abs}}$ [nm] ( $\epsilon_{\text{max}}$ [ $\text{dm}^3\text{mol}^{-1}\text{cm}^{-1}$ ])
<b>3.27b-Ph (only trans)</b>	248 (37803), 318 (1318), 430 (532)
<b>3.27b-Ph (both isomers)</b>	245 (37944), 321 (1067), 438 (523)

### Emission Spectroscopy

To study the effect of ring size (5-membered vs 6-membered) on EPES emission studies were carried out in solution (100% MeCN) and in the solid state by precipitation using MeCN:H<sub>2</sub>O mixtures (1:9)<sup>59</sup> as described in Chapter 2. Complex **3.27b-Ph** did not show emission in aerated solution but gave weak emission in deaerated solution (purged with argon) (Figure 3.15). In addition, no enhancement in emission was observed in the solid state. The same was observed for the remaining complexes.

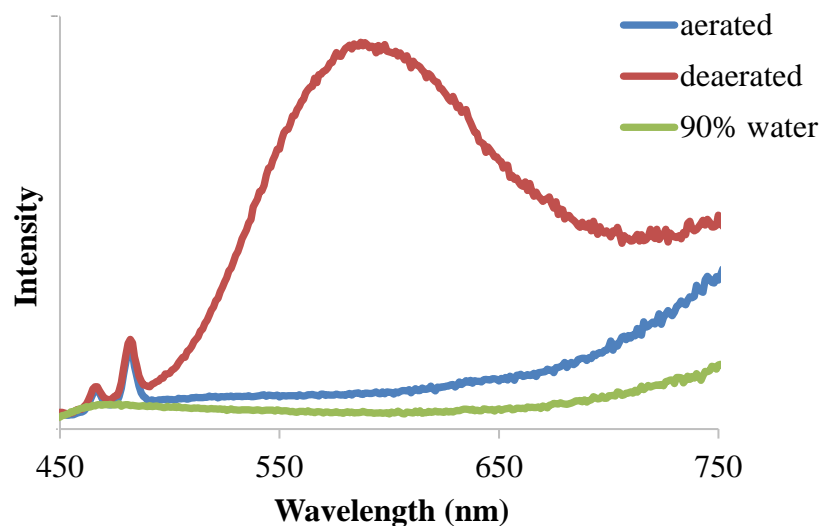


**Figure 3.15:** Emission spectra of **3.27b-Ph** in aerated and deaerated solutions in HPLC grade MeCN at  $\lambda_{\text{ex}} = 397$  nm.

Changing the ring size from 6-membered to 5-membered chelate ring has had an effect on EPESS. Whilst the 6-membered complexes **2.24a,b-R** (Chapter 2) show EPESS, the 5-membered complexes **3.27a-R** and **3.27b-R** do not. Instead, *trans-cis* photoisomerisation is observed. Although further studies would need to be carried out, the photoisomerisation process could be a quenching pathway hence only weak emission is observed.

### 3.2.4 Computational Studies

As shown above complex **3.27b-Ph** is not EPESS active, instead photoisomerisation is observed. To help identify the cause of this phenomenon, DFT calculations were performed by Professor F. Lelj (University della Basilicata Potenza, Italy). DFT studies show that *trans-3.27b-Ph* exists as two stable conformations: a) CHPh below plane of phenol as in the solid state and b) CHPh above plane of phenol as the less stable conformation, with the energy difference between both conformations being  $0.81 \text{ kcal mol}^{-1}$  (Figure 3.16). The energy barrier between these conformers is very small ( $4.03 \text{ kcal mol}^{-1}$  with reference to the most stable conformer) suggesting that this motion is very easy at RT and the average is seen by NMR spectroscopy.

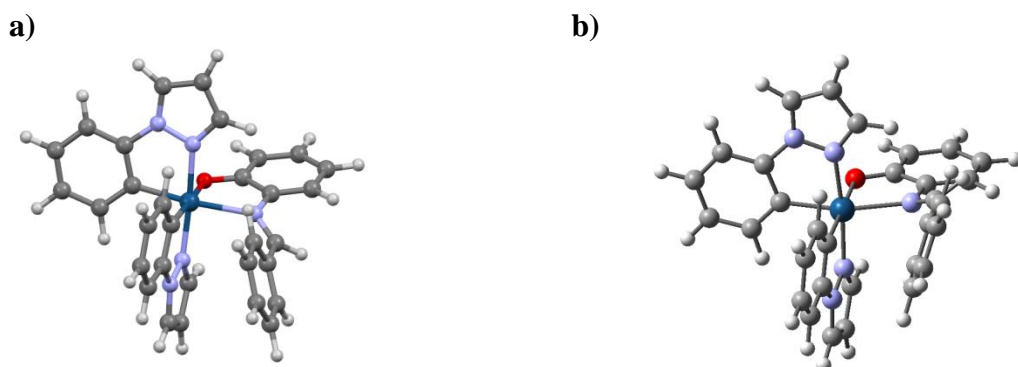


**Figure 3.16:** Two most stable conformations around the C-NCHPh bond in **3.27b-Ph**: a) “down” conformation as in solid state ( $0.0 \text{ kcal mol}^{-1}$ ); b) “up” conformation ( $0.81 \text{ kcal mol}^{-1}$ )

The energy difference between *trans* and *cis* isomers of **3.27b-Ph** was computed to be  $3.73 \text{ kcal mol}^{-1}$ . Figure 3.17 shows the *trans* and *cis* isomers in their best overall conformation for complex **3.27b-Ph**. In all **3.27a,b-R** complexes the *trans* isomer is computed to be more stable than the *cis* and the relative energies for the *cis* isomer for the remaining complexes was between  $3.65$  and  $6.78 \text{ kcal mol}^{-1}$  (See Appendix).

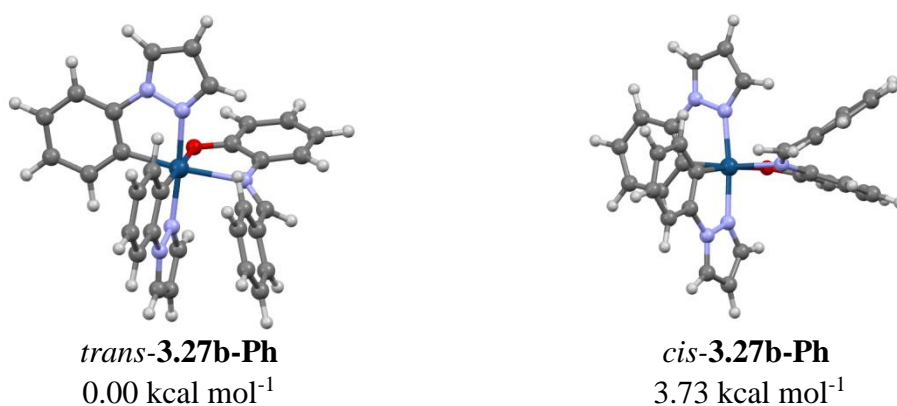


**Figure 3.17:** Energies of the *trans*-**3.27a-Ph** and *cis*-**3.27b-Ph** in their best overall conformation using the *trans* isomer as the reference.

In **3.27b-Ph**, the *cis-trans* isomerisation has been located starting from the two different stable isomers “down” and “up” (Figure 3.18). Their structures and energies are reported below.

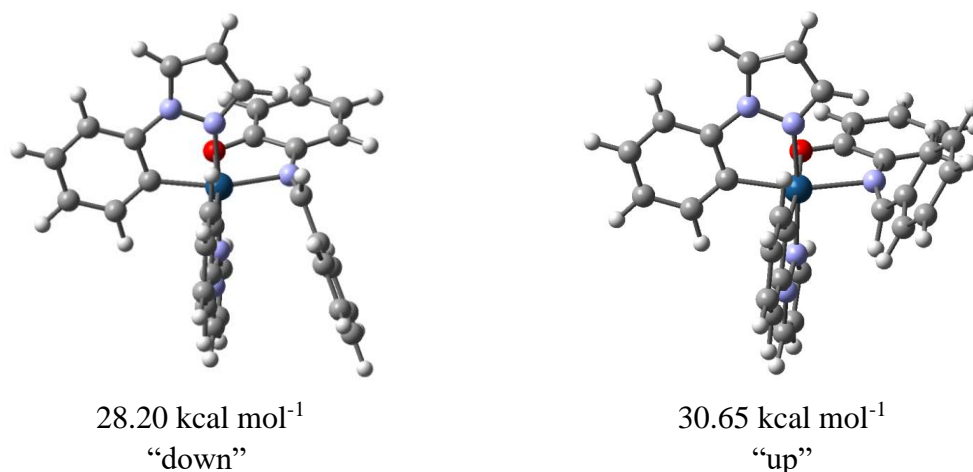


**Figure 3.18:** Transition states for the *cis-trans* isomerisation of **3.27b-Ph**.

This barrier is consistent with no isomerisation taking place in the dark at room temperature. Complexes **3.27a-Cinnamyl** and **3.27b-Cinnamyl** show complete *cis-trans* isomerisation at 60 °C (Table 3.4) whilst in the remaining complexes *cis-trans* isomerisation is just accessible at 60 °C. Analysis of the triplet state in case of the **3.27b-Ph** reveals that CHPh of the imine is almost perpendicular to the phenol plane and is very close to the conformation of the transition state for the *cis-trans* isomerisation (Figure 3.19). Therefore, it is not unreasonable that population of the triplet state can give rise to both isomers. Further computations will need to be carried out to verify this hypothesis and whether it applies to the other complexes.

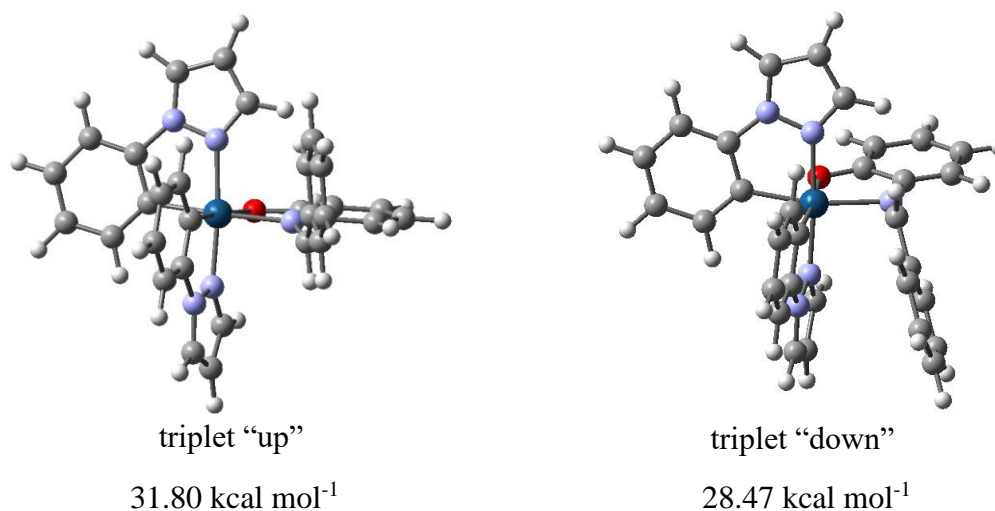


**Figure 3.19:** Triplet geometries of **3.27b-Ph**.

Figure 3.20 shows the energy profile of *trans-cis* and *cis-trans* isomerisation. The *trans* isomer is computed to be more stable than the *cis* isomer. Step A is the barrier to rotation starting from the most stable *trans* isomer, B is the energy difference between the two

*trans* forms (up and down), Step C is the energy for thermal *cis-trans* isomerisation, and D is the energy difference between the *trans* and the *cis* isomer.

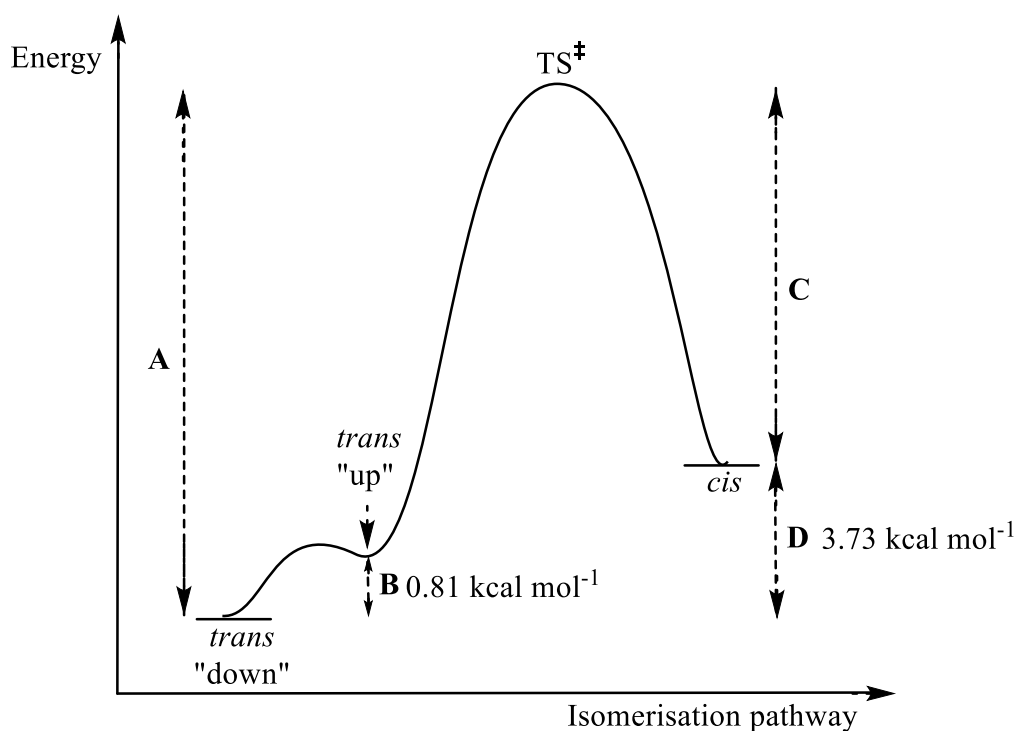


**Figure 3.20:** Energy profile of complex **3.27b-Ph**.

### 3.2.4 Conclusion

The *exocyclic* imine complexes (**3.27a-R** and **3.27b-R**) studied in this chapter do not show EPSS, instead *trans-cis* photoisomerisation is observed upon irradiation. When the synthesis of the complexes is carried out in the dark, only the *trans* isomer is formed, but in the presence of light, both isomers are formed. This shows that the *trans-cis* isomerisation is photoinduced. The reverse thermal isomerisation for most complexes is thermally accessible in the dark at 60 °C (Table 3.4) though complete conversion to the *trans* isomer was only observed for complexes **3.27a,b-Cinnamyl**. To date, only one group<sup>51</sup> has reported a similar *cis-trans* isomerisation in related complexes **3.25-R** and **3.26-Mes**. In **3.27a-R** and **3.27b-R**, the *trans-cis* isomerisation occurs under halogen lamp and computation suggests that the *trans* isomers are thermodynamically more stable. However for **3.25-Mes** and **3.26-Mes**<sup>51</sup> the situation is reversed, *cis-trans* isomerisation is photochemically induced whilst *trans-cis* isomerisation was achieved thermally though at high temperatures (> 190 °C). It should be noted that both

isomerisations in those cases were done in the solid state whereas in this thesis the isomerisations are mostly done in solution.

In imine ligands, the thermodynamically stable isomer is the *trans* form, with the *cis* form being very short lived and having a very low barrier of *cis-trans* isomerisation. After complexation, the *trans* form in **3.27a,b-R** is still the most stable isomer but the energy barrier to *cis-trans* isomerisation is considerably higher than for the free imines. These results show that *exo* imine complexes provide a good framework to synthesise molecular switches with control of the barrier to thermal switching. This concept is pursued further in Chapter 4.

### 3.3 Bibliography

1. B. L. Feringa, R. A. van Delden, N. Koumura and E. M. Geertsema, *Chem. Rev.*, 2000, **100**, 1789-1816.
2. B. L. Feringa, W. F. Jager, B. De Lange and E. W. Meijer, *J. Am. Chem. Soc.*, 1991, **113**, 5468-5470.
3. B. L. Feringa, *Acc. Chem. Res.*, 2001, **34**, 504-513.
4. D. H. Waldeck, *Chem. Rev.*, 1991, **91**, 415-436.
5. W.-G. Han, T. Lovell, T. Liu and L. Noodleman, *Chem. Phys. Chem.*, 2002, **3**, 167-178.
6. J. M. Rodier and A. B. Myers, *J. Am. Chem. Soc.*, 1993, **115**, 10791-10795.
7. H. Petek, K. Yoshihara, Y. Fujiwara, Z. Lin, J. H. Penn and J. H. Frederick, *J. Phys. Chem.*, 1990, **94**, 7539-7543.
8. F. Negri and G. Orlandi, *Chem. Phys. Lett.*, 1992, **195**, 523-530.
9. H. M. D. Bandara and S. C. Burdette, *Chem. Soc. Rev.*, 2012, **41**, 1809-1825.
10. Y. Dou, W. Wu, H. Tang and R. E. Allen, *Chem. Phys.*, 2008, **353**, 104-108.
11. C. Jiang, R. Xie, F. Li and R. E. Allen, *Chem. Phys. Lett.*, 2009, **474**, 263-267.
12. J. Quenneville and T. J. Martínez, *J. Phys. Chem. A*, 2003, **107**, 829-837.
13. J. Saltiel, G. R. Marchand, E. Kirkor-Kaminska, W. K. Smothers, W. B. Mueller and J. L. Charlton, *J. Am. Chem. Soc.*, 1984, **106**, 3144-3151.
14. J. Saltiel, A. D. Rousseau and B. Thomas, *J. Am. Chem. Soc.*, 1983, **105**, 7631-7637.
15. J. Saltiel, *J. Am. Chem. Soc.*, 1968, **90**, 6394-6400.
16. G. S. Hammond, J. Saltiel, A. A. Lamola, N. J. Turro, J. S. Bradshaw, D. O. Cowan, R. C. Counsell, V. Vogt and C. Dalton, *J. Am. Chem. Soc.*, 1964, **86**, 3197-3217.
17. J. Saltiel, *J. Am. Chem. Soc.*, 1967, **89**, 1036-1037.
18. S. Minoru and Y. Keitaro, *Bull. Chem. Soc. Jpn.*, 1982, **55**, 85-89.
19. Y. Kamiya and H. Asanuma, *Acc. Chem. Res.*, 2014, **47**, 1663-1672.

20. B. Feringa and H. Wynberg, *J. Am. Chem. Soc.*, 1977, **99**, 602-603.
21. N. Koumura, R. W. J. Zijlstra, R. A. van Delden, N. Harada and B. L. Feringa, *Nature*, 1999, **401**, 152-155.
22. J. Vicario, M. Walko, A. Meetsma and B. L. Feringa, *J. Am. Chem. Soc.*, 2006, **128**, 5127-5135.
23. A. Cnossen, L. Hou, M. M. Pollard, P. V. Wesenhagen, W. R. Browne and B. L. Feringa, *J. Am. Chem. Soc.*, 2012, **134**, 17613-17619.
24. S. J. Wezenberg, K.-Y. Chen and B. L. Feringa, *Angew. Chem., Int. Ed.*, 2015, **54**, 11457-11461.
25. A. Faulkner, T. van Leeuwen, B. L. Feringa and S. J. Wezenberg, *J. Am. Chem. Soc.*, 2016, **138**, 13597-13603.
26. H. Fliegl, A. Köhn, C. Hättig and R. Ahlrichs, *J. Am. Chem. Soc.*, 2003, **125**, 9821-9827.
27. H. Rau and E. Lueddecke, *J. Am. Chem. Soc.*, 1982, **104**, 1616-1620.
28. R. J. W. Le Fevre and J. Northcott, *J. Chem. Soc. (Resumed)*, 1953, 867-870.
29. J. L. Magee, W. Shand and H. Eyring, *J. Am. Chem. Soc.*, 1941, **63**, 677-688.
30. D. Y. Curtin, E. J. Grubbs and C. G. McCarty, *J. Am. Chem. Soc.*, 1966, **88**, 2775-2786.
31. N. Deibel, S. Hohloch, M. G. Sommer, D. Schweinfurth, F. Ehret, P. Braunstein and B. Sarkar, *Organometallics*, 2013, **32**, 7366-7375.
32. T. Yutaka, I. Mori, M. Kurihara, J. Mizutani, K. Kubo, S. Furusho, K. Matsumura, N. Tamai and H. Nishihara, *Inorg. Chem.*, 2001, **40**, 4986-4995.
33. S. Kume and H. Nishihara, *Dalton Trans.*, 2008, 3260-3271.
34. T. Yutaka, M. Kurihara, K. Kubo and H. Nishihara, *Inorg. Chem.*, 2000, **39**, 3438-3439.
35. A. Amar, P. Savel, H. Akdas-Kilig, C. Katan, H. Meghezzi, A. Boucekkine, J.-P. Malval and J.-L. Fillaut, *Chem. Eur. J.*, 2015, **21**, 8262-8270.
36. J. Perez-Miqueo, A. Altube, E. Garcia-Lecina, A. Tron, N. D. McClenaghan and Z. Freixa, *Dalton Trans.*, 2016, **45**, 13726-13741.

37. J. Perez-Miqueo, A. Telleria, M. Munoz-Olasagasti, A. Altube, E. Garcia-Lecina, A. de Cozar and Z. Freixa, *Dalton Trans.*, 2015, **44**, 2075-2091.
38. J. Bernstein and I. Izak, *J. Chem. Soc., Perkin Trans. 2*, 1976, 429-434.
39. A. V. Gaenko, A. Devarajan, L. Gagliardi, R. Lindh and G. Orlandi, *Theor. Chem. Acc.*, 2007, **118**, 271-279.
40. K. Geibel, B. Staudinger, K. H. Grellmann and H. Wendt, *Ber. der Bunsenges. Phys. Chem.*, 1972, **76**, 1246-1251.
41. E. V. Brown and G. R. Granneman, *J. Am. Chem. Soc.*, 1975, **97**, 621-627.
42. G. B. Kistiakowsky and W. R. Smith, *J. Am. Chem. Soc.*, 1934, **56**, 638-642.
43. E. Fischer and Y. Frei, *J. Chem. Phys.*, 1957, **27**, 808-809.
44. G. Wettermark, J. Weinstein, J. Sousa and L. Dogliotti, *J. Phys. Chem.*, 1965, **69**, 1584-1587.
45. Y. Luo, M. Utecht, J. Dokić, S. Korchak, H.-M. Vieth, R. Haag and P. Saalfrank, *Chem. Phys. Chem.*, 2011, **12**, 2311-2321.
46. J.-M. Lehn, *Chem. Eur. J.*, 2006, **12**, 5910-5915.
47. P. J. Coelho, M. C. R. Castro and M. M. M. Raposo, *J. Photochem. Photobiol., A*, 2013, **259**, 59-65.
48. J. Albert, J. Granell, J. A. Durán, A. Lozano, A. Luque, A. Mate, J. Quirante, M. K. Khosa, C. Calvis, R. Messeguer, L. Baldomà and J. Badia, *J. Organomet. Chem.*, 2017, **839**, 116-125.
49. J. Albert, J. Granell, J. Sales, M. Font-Bardia and X. Solans, *Organometallics*, 1995, **14**, 1393-1404.
50. L. C.-C. Lee, J. C.-W. Lau, H.-W. Liu and K. K.-W. Lo, *Angew. Chem., Int. Ed.*, 2016, **55**, 1046-1049.
51. T. Kawamoto, Y. Takino, K. Sakoda and T. Konno, *Chem. Lett.*, 2010, **39**, 1264-1266.
52. Y.-H. Cho, C.-Y. Lee and C.-H. Cheon, *Tetrahedron*, 2013, **69**, 6565-6573.
53. C.-L. Chen, Y.-H. Liu, S.-M. Peng and S.-T. Liu, *J. Organomet. Chem.*, 2004, **689**, 1806-1815.

54. C. L. Allaway, M. Daly, M. Nieuwenhuyzen and G. C. Saunders, *J. Fluorine Chem.*, 2002, **115**, 91-99.
55. A. M. Nassar, A. M. Hassan and S. S. Alabd, *Synth. React. Inorg. Metal-Org. Nano-Met. Chem.*, 2015, **45**, 256-270.
56. Y. You, H. S. Huh, K. S. Kim, S. W. Lee, D. Kim and S. Y. Park, *Chem. Commun.*, 2008, 3998-4000.
57. A. J. Howarth, R. Patia, D. L. Davies, F. Leij, M. O. Wolf and K. Singh, *Eur. J. Inorg. Chem.*, 2014, **2014**, 3657-3664.
58. X. Qin, G. Ding, Z. Wang, S. Zhang, H. Li, Z. Luo and F. Gao, *J. Photochem. Photobiol., A*, 2017, **339**, 25-35.
59. G. Li, W. Guan, S. Du, D. Zhu, G. Shan, X. Zhu, L. Yan, Z. Su, M. R. Bryce and A. P. Monkman, *Chem. Commun.*, 2015, **51**, 16924-16927.

### 3.4 Appendix

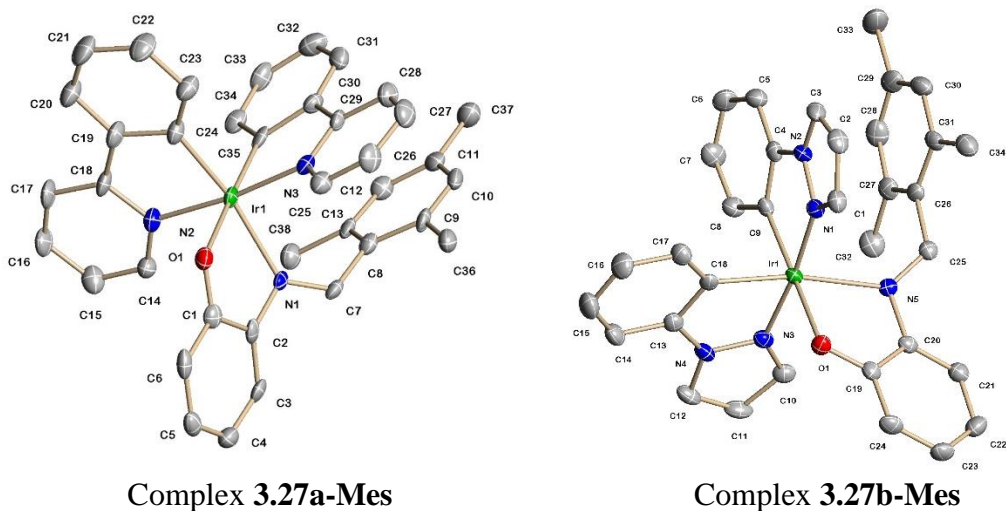


**Figure A3.1:** X-ray structures of complexes **3.27a-Mes** and **3.27b-Mes**.

<b>Table A3.1:</b> Selected bond length (Å) and bond angles (°) for complexes <b>3.27a-Mes</b> and <b>3.27b-Mes</b> . <i>Centroid-centroid distance refers to the distance between the phenyl ring of the adjacent cyclometallated ligand and the R = Mes of the imine ligand.</i>			
<b>3.27a-Mes</b>	(Å)	<b>3.27b-Mes</b>	(Å)
Ir(1)—N(3)	2.044(6)	Ir(1)—N(1)	2.010(3)
Ir(1)—N(2)	2.060(6)	Ir(1)—N(3)	2.020(3)
Ir(1)—N(1)	2.187(5)	Ir(1)—N(5)	2.182(3)
Ir(1)—C(24)	2.012(7)	Ir(1)—C(18)	2.015(3)
Ir(1)—C(35)	1.977(8)	Ir(1)—C(9)	2.013(3)
Ir(1)—O(1)	2.151(5)	Ir(1)—O(1)	2.149(2)
N(1)—C(7)	1.303(8)	N(5)—C(25)	1.284(4)
centroid—centroid	3.562	centroid—centroid	3.624
<b>3.27a-Mes</b>	(°)	<b>3.27b-Mes</b>	(°)
N(3)—Ir(1)—N(2)	173.5(2)	N(1)—Ir(1)—N(3)	173.57(11)
C(35)—Ir(1)—N(3)	80.8(3)	N(1)—Ir(1)—C(9)	79.85(12)
C(24)—Ir(1)—N(2)	80.8(3)	C(18)—Ir(1)—N(3)	80.17(13)
O(1)—Ir(1)—N(1)	76.88(19)	O(1)—Ir(1)—N(5)	77.51(9)

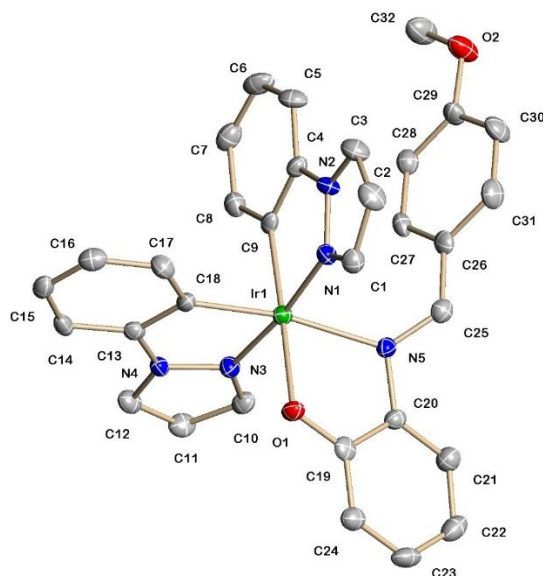


**Figure A3.2:** X- Ray structure of complex **3.27b-Anisyl**.

<b>Table A3.2:</b> Selected bond length (Å) and bond angles (°) for complex <b>3.27b-Anisyl</b> . <i>Centroid-centroid distance refers to the distance between the phenyl ring of the adjacent cyclometallated ligand and the R = Anisyl of the imine ligand.</i>			
<b>3.27b-Anisyl</b>	(Å)	<b>3.27b-Anisyl</b>	(°)
Ir(1)—N(1)	2.014(4)	N(3)—Ir(1)—N(1)	173.30(15)
Ir(1)—N(3)	1.999(4)	C(9)—Ir(1)—N(1)	80.47(17)
Ir(1)—N(5)	2.174(4)	C(18)—Ir(1)—N(3)	79.89(17)
Ir(1)—C(18)	1.994(4)	O(1)—Ir(1)—N(5)	77.82(13)
Ir(1)—C(9)	2.005(4)		
Ir(1)—O(1)	2.136(3)		
N(5)—C(25)	1.297(5)		
centroid—centroid	3.678		

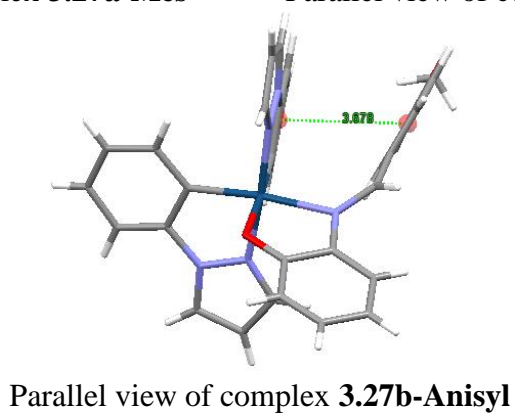
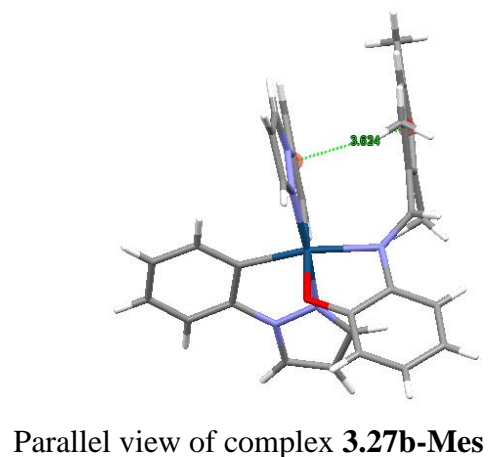
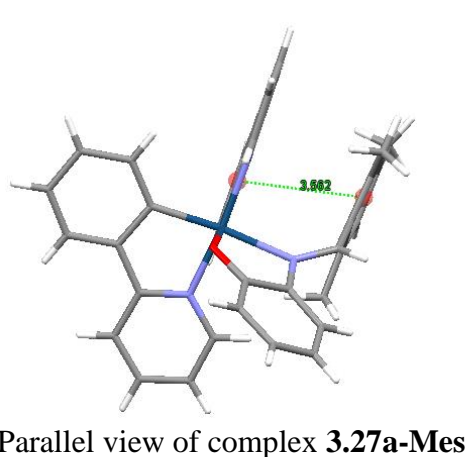


**Figure A3.3:** Parallel views of the X-Ray structures of complexes **3.27a,b-Mes** and **3.27b-Anisyl**.

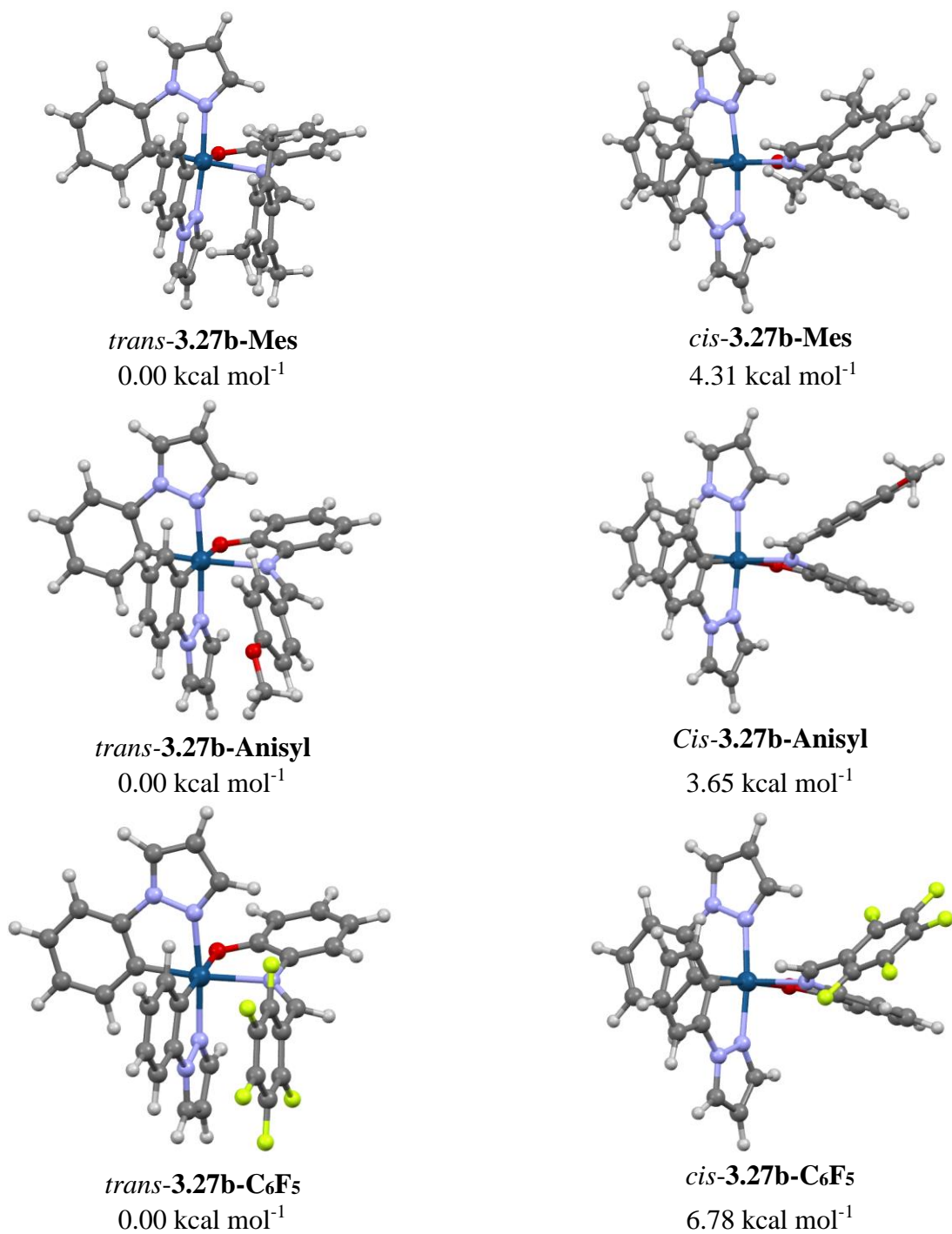
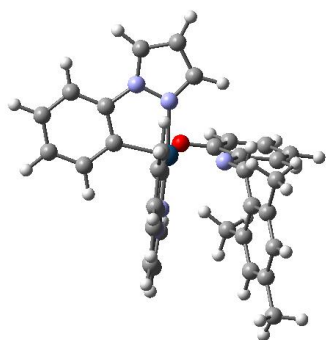


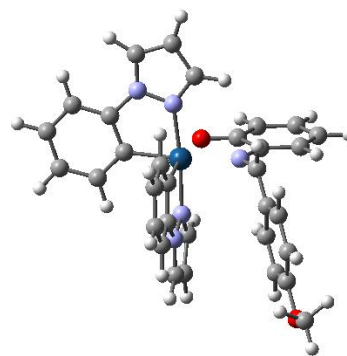
**Figure A3.4:** Energies\* of the *cis* and *trans* isomers in their best overall conformation

\* energy of *trans* conformation has been used as reference.



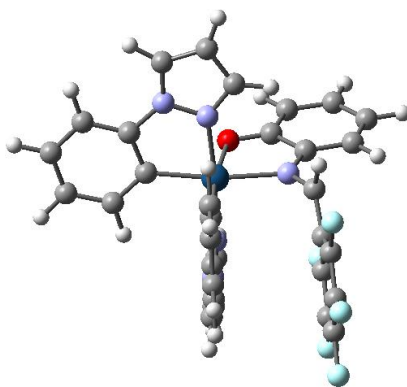
**3.27b-Mes** triplet “down”

71.3 kcal mol<sup>-1</sup>



**3.27b-Anisyl** triplet “down”

29.8 kcal mol<sup>-1</sup>



**3.27b-C<sub>6</sub>F<sub>5</sub>** triplet “down”

31.1 kcal mol<sup>-1</sup>

**Figure A3.5:** Triplet geometries of complexes **3.27b-R**. (R = Mes, Anisyl and C<sub>6</sub>F<sub>5</sub>)

## Chapter 4: Photoisomerisation in Half-Sandwich Complexes

### 4.1 Introduction

Chapter 3 contained a discussion of complexes with the general formula  $[\text{Ir}(\text{C}^{\wedge}\text{N})_2(\text{N}^{\wedge}\text{O})]$  where the  $\text{N}^{\wedge}\text{O}$  ligand forms a 5-membered chelate ring with an *exocyclic*  $\text{C}=\text{N}$  bond which created the possibility of *cis* and *trans* isomers. This chapter will describe a similar photoisomerisation process in half-sandwich complexes and look at the effect of changing the metal fragment on the photoswitching properties of imines. To date, there are no examples of half-sandwich complexes with  $\text{C}=\text{C}$  bonds that can photoisomerise to form *cis* isomers, therefore only examples of half-sandwich complexes with  $\text{N}=\text{N}$  and  $\text{C}=\text{N}$  bonds will be discussed.

#### 4.1.1 Photoisomerisation of $\text{N}=\text{N}$ Bonds in Half-Sandwich Complexes

As explained in Chapter 3, if the  $\text{N}=\text{N}$  bond is *endocyclic* no photoisomerisation can occur. There are several examples of functionalised azobenzenes acting as chelating ligands in Ru(II) half-sandwich complexes forming *endocyclic* 5- and 6-membered chelate rings e.g. complexes **4.1** and **4.2**, respectively (Figure 4.1).<sup>1-3</sup> In both cases, the Ru centre binds to the *alpha*-N atom, incorporating the  $\text{N}=\text{N}$  unit into the chelate ring and preventing any possible photoisomerisation of the  $\text{N}=\text{N}$  bond.

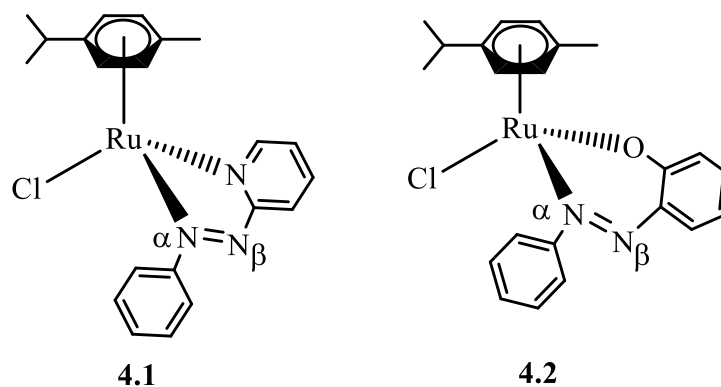


**Figure 4.1:** Half-sandwich complexes **4.1** and **4.2** with *endocyclic*  $\text{N}=\text{N}$  bond.

As discussed in Chapter 3 the first strategy used to create photoisomerisable complexes involved putting the  $\text{N}=\text{N}$  unit at the periphery of the chelate ligand and half-sandwich examples of this type are described below. When describing a group of half-sandwich complexes, Ir(III), Rh(III) and Ru(II) fragments will be referred as **a**, **b** and **c**, respectively. Early studies by Yamamoto reported half-sandwich complexes (**4.3a-c**) in the *trans* conformation with azobenzene unit on to the periphery of the monodentate ligand (Figure 4.2).<sup>4</sup> Complexes **4.3a** and **4.3b** undergo *trans-cis* photoisomerisation

under irradiation with a mercury lamp to give *trans*:*cis* mixtures, 81:19 and 83:17, respectively. In comparison, the free ligand gives a *trans*:*cis* ratio of 76:24 under the same conditions. The reverse *cis*-*trans* isomerisation was accessible at room temperature in the dark for **4.3a** and **4.3b** though no kinetic studies were reported. In contrast, **4.3c** is photochemically unstable and decomposes upon irradiation.

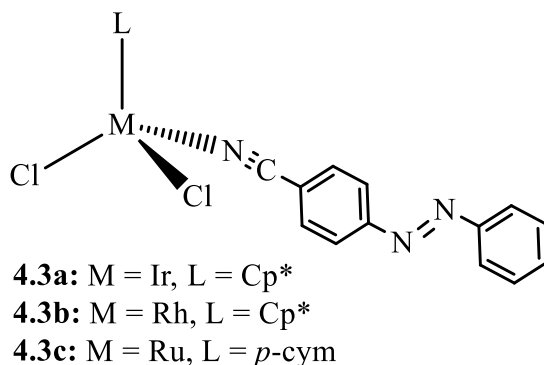


**Figure 4.2:** Half-sandwich complexes (**4.3a-c**) with N=N unit at the periphery.

Freixa and co-workers synthesised Ru(II) half-sandwich complexes (**4.4i** and **4.4ii**) as *trans* isomers with the N=N unit attached to a pyridine ligand **L4.4** (Figure 4.3).<sup>5</sup> According to the UV-Vis spectra, **4.4i** did not show significant photochemical *trans*-*cis* isomerisation. On the other hand, complex **4.4ii** showed significant *trans*-*cis* photoisomerisation with reverse *cis*-*trans* thermal isomerisation in the dark at 65 °C. Both complexes show a significantly longer  $t_{1/2}$  of the *cis* isomer of 231 min in comparison to free ligand **L4.4** at 29 min. This shows that upon complexation, the *cis* isomer is long lived and the energy barrier of thermal isomerisation is higher in comparison to the **L4.4**.

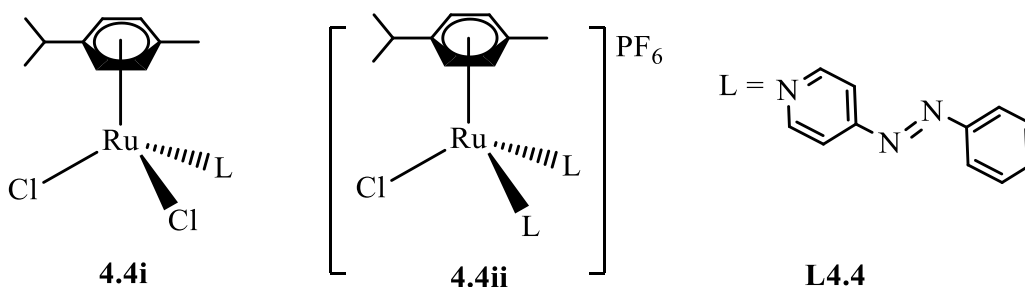


**Figure 4.3:** Ru(II) complexes (**4.4i** and **4.4ii**) with N=N unit at the periphery.

Additionally, Freixa and co-workers also synthesised complexes **4.5-4.7** with an N=N unit at the periphery of a bipy ligand (Figure 4.4).<sup>5</sup> Complex **4.5** did not show any photoisomerisation. However, complexes, **4.6** and **4.7** undergo photoisomerisation when irradiated at 350 nm and 322 nm, respectively with reverse thermal *cis*-*trans*

isomerisation in the dark at 65 °C. Complex **4.7** shows slower *cis-trans* isomerisation ( $t_{1/2} = 165$  min) than complex **4.6** ( $t_{1/2} = 58$  min), which shows that the position of the photoswitching N=N unit has an effect on the barrier of the thermal *cis-trans* isomerisation. The  $t_{1/2}$  (165 min) of *cis* **4.7** is faster than that of the free ligand **L4.7** (231 min), showing that complexation has reduced the barrier to *cis-trans* isomerisation in this case. This is the opposite observation for the  $t_{1/2}$  of *cis* isomer in monodentate complexes **4.4i** and **4.4ii** as described above. The authors proposed that in complex **4.5** there is better delocalisation between the azo group and the Ru centre than with complexes **4.6** and **4.7** hence, *trans-cis* isomerisation is quenched in **4.5**.

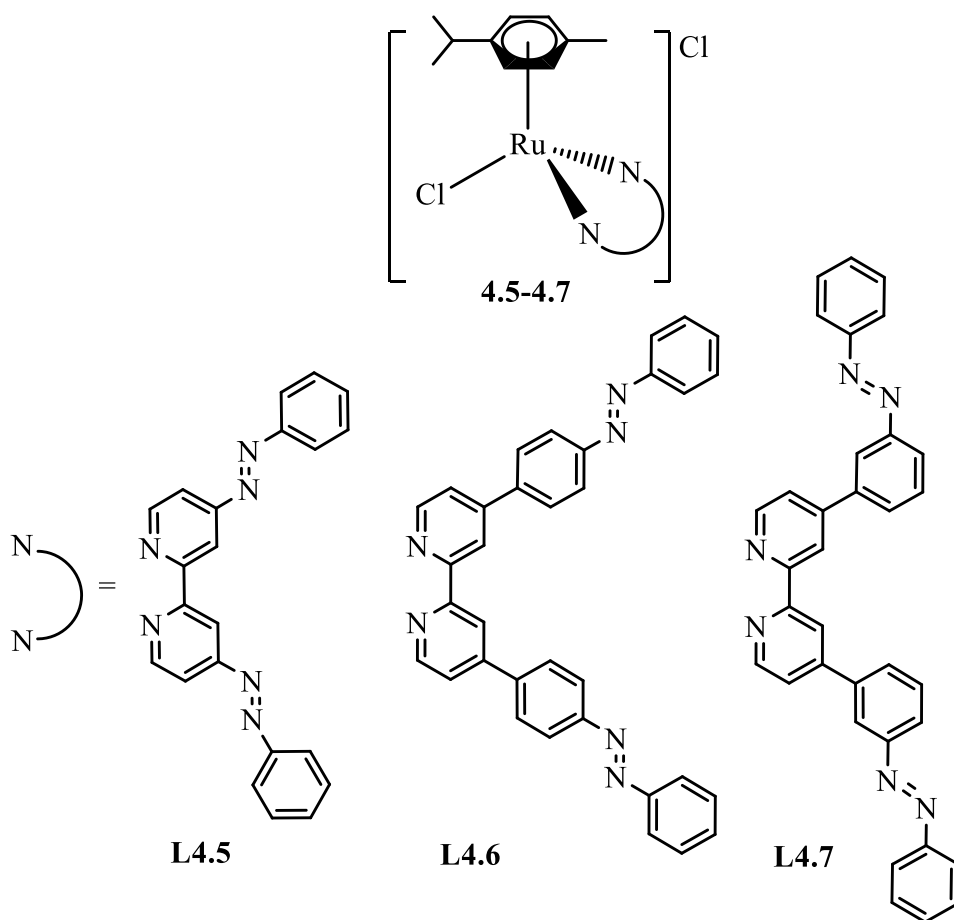
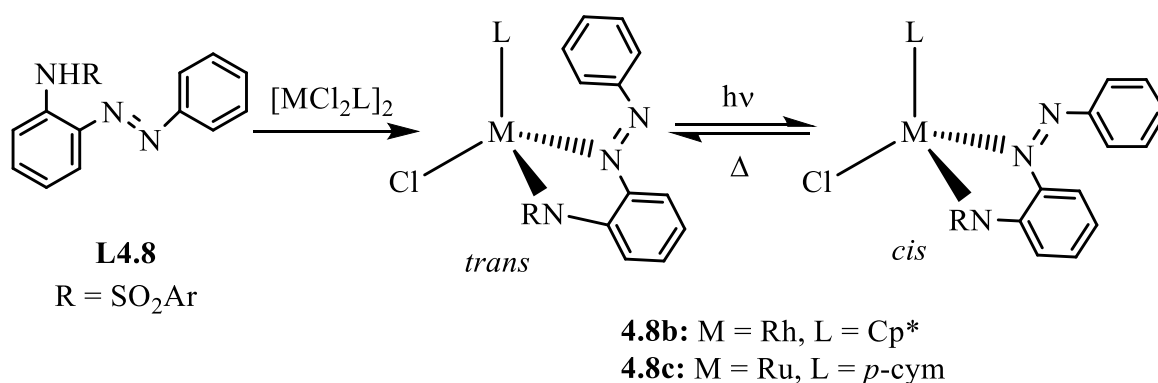


**Figure 4.4:** Half-sandwich Ru(II) complexes (**4.5-4.7**) with N=N unit on the periphery of a bidentate ligand.

Another potential method to achieve photoswitching N=N complexes is to have an *exocyclic* N=N group. As mentioned in Chapter 3, this strategy was tried for bis-cyclometallated Ir(III) complex **3.16** however, this was still not photoactive. Recently, Bogliotti and Xie synthesised half-sandwich *exocyclic* N=N complexes *trans*-**4.8b** and *trans*-**4.8c** by complexation of **L4.8** (Scheme 4.1).<sup>6, 7</sup> **L4.8** itself undergoes *trans-cis*

photoisomerisation at 315 nm and reverse isomerisation in the dark at room temperature. Complexes *trans*-**4.8b** and *trans*-**4.8c** convert to their respective *cis* forms when irradiated at 406 nm with the reverse thermal isomerisation being accessible in the dark at room temperature.<sup>6, 7</sup> The  $t_{1/2}$  for *cis*-**4.8b** (17.9 min) is longer than that of *cis*-**4.8c** ( $t_{1/2}$  = 6.5 min) hence the energy barrier of the reverse *cis-trans* isomerisation is higher when M = Rh in comparison to when M = Ru. The introduction of a metal centre Rh(III) or Ru(II) has also red-shifted the irradiation wavelength by 91 nm to the visible region which is beneficial for the potential use in biological systems.



**Scheme 4.1:** Half-sandwich complexes **4.8b** and **4.8c** with exocyclic N=N unit.

#### 4.1.2 Photoisomerisation in C=N Bonds in Half-Sandwich Complexes

Several half-sandwich complexes with imine-based ligands are used in catalysis and anti-cancer treatment and some examples are shown in Figure 4.5.<sup>8-13</sup> Complexes **4.9a-c**, **4.10a-c** and **4.11a-c** have an *endocyclic* chelate ring preventing any possible photoisomerisation around the C=N bond.

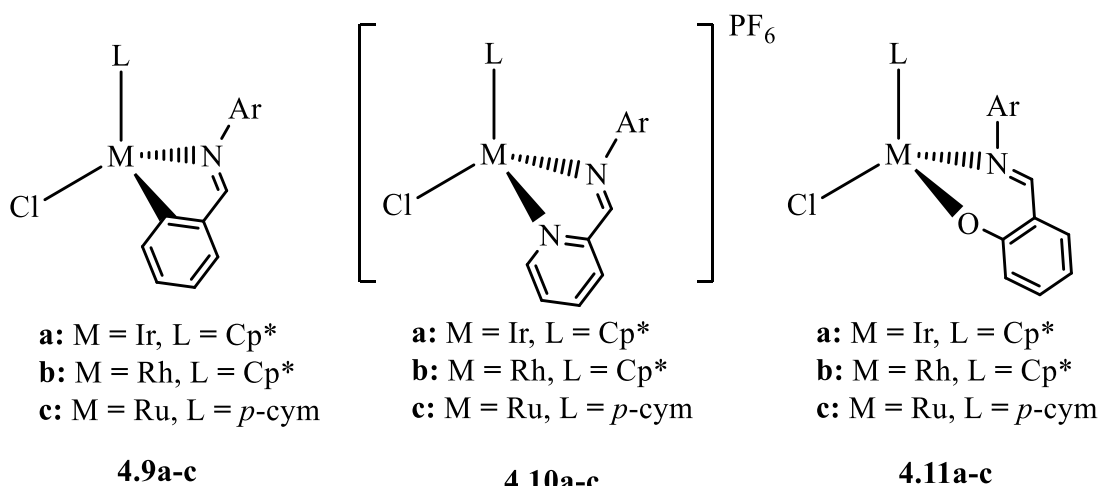
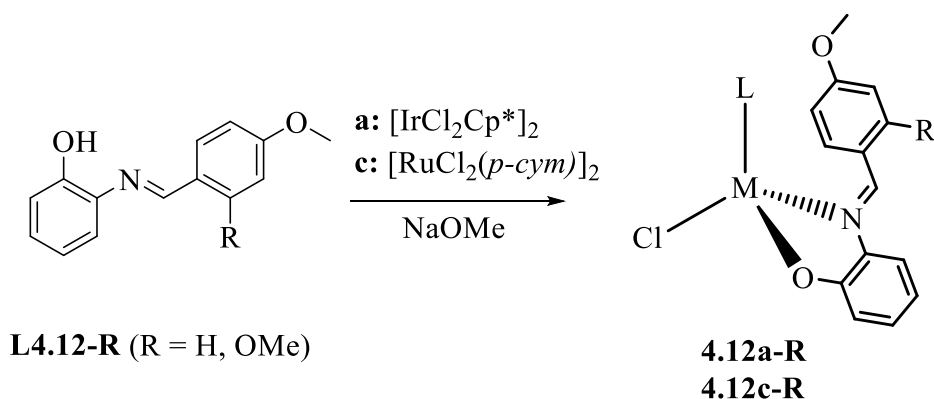


**Figure 4.5:** Examples of half-sandwich complexes **4.9a-c**, **4.10a-c** and **4.11a-c** with bidentate imines; the aryl substituent may vary for the different complexes.

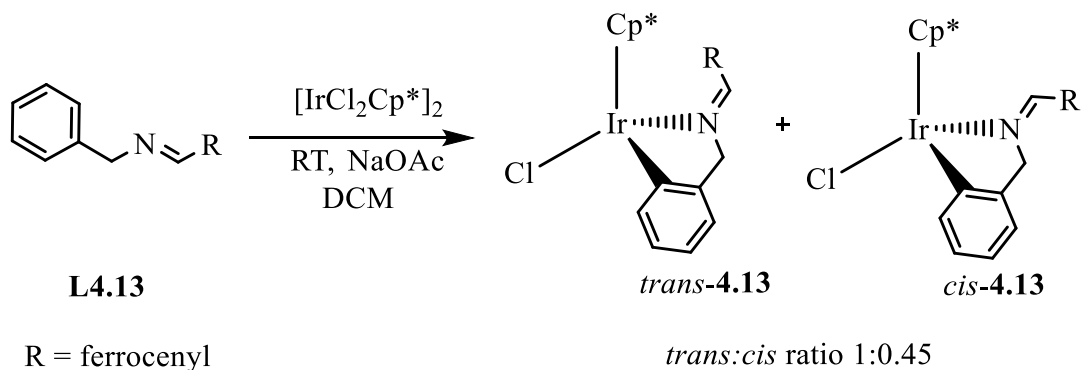
As described in Chapter 3 (for C=N) and above for N=N, to be able to observe any photoswitching properties the X=N bond (X = C, N) needs to be *exocyclic* upon coordination to the metal centre. Beck and co-workers<sup>14</sup> reported Ir(III) and Ru(II) half-sandwich complexes (**4.12a-R** and **4.12c-R**) with a 5-membered chelate N<sup>^</sup>O ring where the C=N bond is *exocyclic* as shown in Scheme 4.2. Although there was a potential occurrence for photoisomerisation around the C=N bond, only the *trans* isomer was reported with no evidence of a *cis* isomer, though no photochemical studies were carried out on these complexes.



**Scheme 4.2:** Half-sandwich complexes **4.12a,c-R** with exocyclic C=N bond (L = Cp\* or *p*-cymene).

More recently, Richards and co-workers reported the formation of *cis* and *trans* **4.13** (Scheme 4.3).<sup>15</sup> After complexation, the crude mixture showed a *trans*:*cis* ratio of 1:0.45 and after isolation, no change was observed in the ratio over 24 hrs suggesting that following isolation imine isomerisation does not occur. No attempts were carried

out to isolate *cis*-**4.13** but its presence shows that both isomers are stable at room temperature and that the barrier for reverse isomerisation is higher than **L4.13** for which only one isomer (presumably *trans*) is observed. No photochemical studies were reported.



**Scheme 4.3:** Ir(III) half-sandwich complex with exocyclic C=N bond.

### Aims and Objectives

In summary, to design photoactive metal complexes with N=N or C=N bonds requires these bonds to be at the periphery of the complex or in an *exocyclic* position. Yamamoto's work shows that changing the metal centre has an effect on photochemical properties of an N=N bond e.g. complexes **4.3a** and **4.3b** show photoisomerisation of the *exocyclic* N=N bond whilst **4.3c** with the same azobenzene ligand did not.<sup>4</sup> Bogliotti showed that for complexes **4.8b-c** with an *exocyclic* N=N bond, the *cis* isomer is formed under visible light (406 nm) whilst the free ligand UV irradiation (315 nm) is used, and the reverse reaction is accessible at room temperature in the dark.<sup>7</sup> This shows that metal complexes can shift the irradiation wavelength to the visible region as also shown with the work done by Feringa for C=C bonds<sup>16</sup> (see Chapter 3). Although very little has been done to explore the photoswitching properties of C=N bonds in half-sandwich complexes, Bogliotti's work and the precedents described in Chapter 3 suggest that similar half-sandwich complexes with an *exocyclic* C=N bond may also show photoisomerisation despite no such properties being reported by Beck.<sup>14</sup> Chapter 4 will include the synthesis of Ir(III), Rh(III) and Ru(II) half-sandwich complexes with anionic N<sup>-</sup>OH and neutral N<sup>-</sup>N ligands designed to have an *exocyclic* C=N bond and to study their photoisomerisation properties upon irradiation using ambient light or halogen lamp.

## 4.2 Results and Discussion

Ligands **L3.27-R** (Figure 4.6) were synthesised using the same method as mentioned in Chapter 3. Dichloro-bridged dimers  $[\text{MCl}_2\text{Cp}^*]_2$  (**4.14**) ( $\text{M} = \text{Ir, a, Rh, b}$ )<sup>17</sup> and  $[\text{RuCl}_2(p\text{-cym})]_2$  (**4.14c**)<sup>18</sup> were prepared using literature methods.

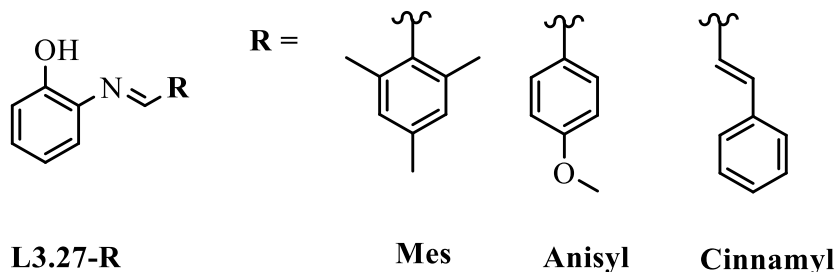
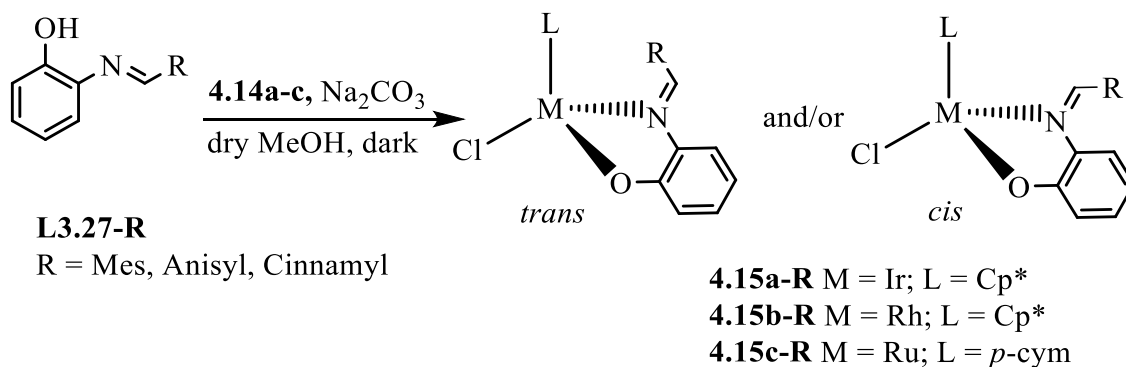


**Figure 4.6:** Structures of ligands **L3.27-R**.

### 4.2.1 Synthesis, Characterisation and Photoisomerisation Studies of $\text{N}^{\wedge}\text{O}$

#### Complexes

Dichloro-bridged dimers (**4.14a-c**) and the respective  $\text{N}^{\wedge}\text{OH}$  ligand (**L3.27-R**) were reacted in the dark in the presence of  $\text{Na}_2\text{CO}_3$  to give *exocyclic* imine complexes **4.15a,c-R** in good yields (Scheme 4.4). Figures 4.7-4.8 and 4.10-4.12 show the numbering scheme used to assign the NMR spectra of the complexes.



**Scheme 4.4:** Synthesis of half-sandwich complexes **4.15a-c-R** with *exocyclic*  $\text{N}^{\wedge}\text{O}$  ligand.

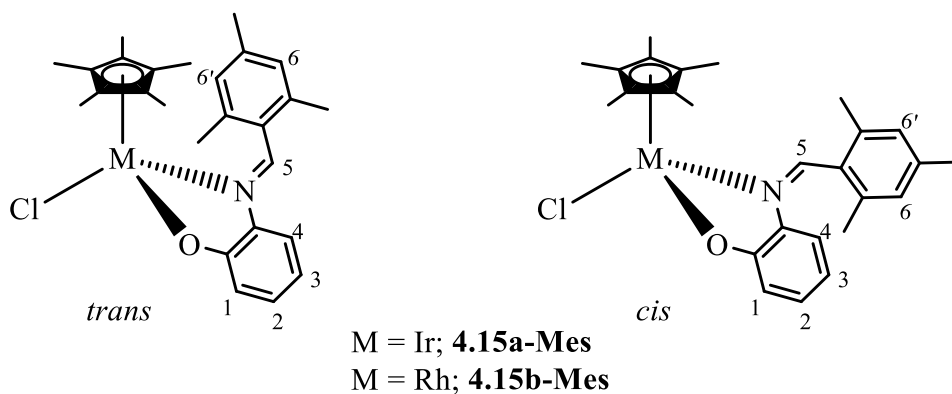


**Figure 4.7:** Numbering scheme for *trans* and *cis* isomer for **4.15a,b-Mes**.

The  $^1\text{H}$  NMR spectrum of **4.15a-Mes** shows only one isomer in the crude product after precipitation. The  $^1\text{H}$  NMR spectrum of the single isomer in **4.15a-Mes** shows an imine proton ( $\text{H}^5$ ) at  $\delta$  8.70. The mesityl gives rise to three 3H singlets at  $\delta$  2.42, 2.31 and 2.01 and  $\text{H}^6$  and  $\text{H}^{6'}$  appear as two 1H singlets at  $\delta$  6.95 and 6.82 indicating that it is fixed in solution. Proton  $\text{H}^5$  shows an NOE with the  $\text{Cp}^*$  ring at  $\delta$  1.67 and not with proton  $\text{H}^4$  at  $\delta$  6.42 from the phenol group, instead  $\text{H}^4$  shows a NOE with the *ortho*-Me at  $\delta$  2.01. These NOEs show that the complex is the *cis* isomer. The ES mass spectrum shows a molecular ion peak  $[\text{M}-\text{Cl}]^+$  at  $m/z$  567 and the IR spectrum shows a  $\nu(\text{C}=\text{N})_{\text{imine}}$  stretch at  $1583\text{ cm}^{-1}$  in comparison to the free ligand at  $1623\text{ cm}^{-1}$ . This is due to backbonding effect.

*Cis*-**4.15a-Mes** was irradiated under a halogen lamp for 3 h showing a second species (4%). The ratio did not change with further irradiation for 2 days. The  $^1\text{H}$  NMR spectrum of the 4:96 mixture showed a signal at  $\delta$  1.35 with integration of 15H corresponding to the  $\text{Cp}^*$  and a 3H peak at  $\delta$  2.17 that correspond to one of the methyl peaks of the mesityl group and a 1H imine peak at  $\delta$  9.22. The imine peak is more downfield in comparison to the *cis* isomer due to absence of shielding by the  $\text{Cp}^*$ . This data agrees with the presence of the *trans* isomer, with the remaining peaks overlapping with the major *cis* isomer. When the *trans*:*cis* 4:96 mixture was left in the dark at room temperature, the signals for the *trans* isomer disappeared after 3 hrs. Therefore, the most stable isomer of **4.15a-Mes** is the *cis* isomer.

Complex **4.15b-Mes** was prepared using the same method as **4.15a-Mes** and the  $^1\text{H}$  NMR spectra of the crude product and after precipitation again only showed one isomer. The imine peak is observed at  $\delta$  8.67 compared to  $\delta$  8.70 in the Ir complex. All the signals of the mesityl are inequivalent (see experimental section for details) indicating

that the mesityl group is fixed in solution. As for *cis*-**4.15a-Mes**, imine proton H<sup>5</sup> shows a NOE with the Cp\* at  $\delta$  1.68 but not with H<sup>4</sup> at  $\delta$  6.33 from the phenol ring, instead, H<sup>4</sup> shows an NOE with the *ortho*-Me at  $\delta$  2.43. This identifies the product as the *cis* isomer. The ES mass spectrum shows a molecular ion peak [M-Cl]<sup>+</sup> at  $m/z$  476 and the IR spectrum shows a  $\nu(\text{C}=\text{N})_{\text{imine}}$  stretch at 1581 cm<sup>-1</sup> in comparison to the free ligand at 1623 cm<sup>-1</sup>

A solution of *cis*-**4.15b-Mes** was irradiated under halogen lamp and monitored using <sup>1</sup>H NMR spectroscopy. After 1 h, a second species was observed with a ratio of 9:91 in favour of the *cis* isomer with no significant change in ratio after 4 hrs. The mixture showed a new imine peak at  $\delta$  9.11 (*cf*  $\delta$  8.67 for the *cis* isomer) a singlet at  $\delta$  1.35 for the Cp\* and a 3H singlet at  $\delta$  2.35 for one of the methyl groups of the mesityl. Two 1H doublet of doublet of doublets at  $\delta$  6.38 and 7.00 and a 1H doublet at  $\delta$  7.18 from the phenol group were also observed. When this mixture was kept in the dark, the minor species converted back to the *cis* isomer providing convincing evidence that the minor species is the *trans* isomer and that the *cis* isomer is the thermodynamically preferred isomer. This could be due to the steric bulk of the mesityl group being too close to the Cp\* in the *trans* conformation, in comparison to the *cis*. Even in the *cis* isomer the mesityl group is unable to rotate freely in solution.

Complex **4.15c-Mes** was prepared as shown in Scheme 4.4, and the numbering scheme for the NMR assignment is shown in Figure 4.8. The crude <sup>1</sup>H NMR spectrum of complex **4.15c-Mes** showed a mixture of two Ru species in a 78:22 ratio favouring the *trans* isomer. The two species were separated by recrystallisation. Each set of crystals were analysed by 1D and 2D NMR spectroscopy and X-Ray crystallography (see later). The two species were identified as *trans*-**4.15c-Mes** and *cis*-**4.15c-Mes**.

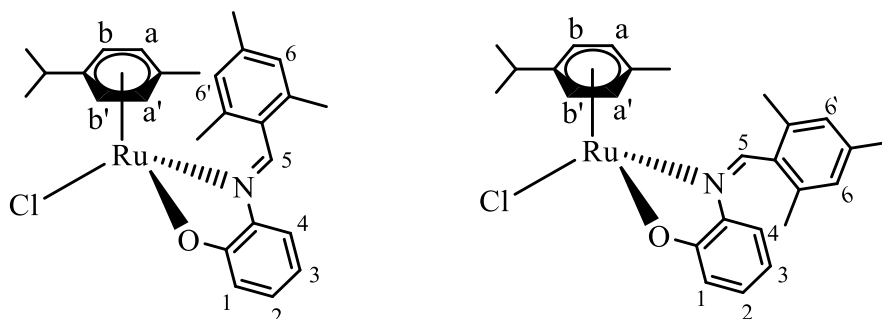


**Figure 4.8:** Numbering of complexes *trans*-**4.15c-Mes** and *cis*-**4.15c-Mes**.

The <sup>1</sup>H NMR spectrum of *trans*-**4.15c-Mes** shows an imine peak (H<sup>5</sup>) at  $\delta$  9.01. The mesityl group, gives rise to two 1H singlets at  $\delta$  7.06 and 7.04 and three 3H singlets at

$\delta$  2.50, 2.43 and 2.41 suggesting it is not rotating in solution. The methyl of the *p*-cymene was identified at  $\delta$  2.00 as it shows NOEs to signals between  $\delta$  3.50 and 5.18 that correspond to H<sup>a</sup> and H<sup>a'</sup>, whilst the isopropyl gives a 1H septet at  $\delta$  2.75 and two 3H doublets at  $\delta$  1.21 and 1.07. To confirm the *trans* configuration, H<sup>5</sup> shows an NOE with phenol proton H<sup>4</sup> at  $\delta$  7.31 whilst H<sup>b</sup> or H<sup>b'</sup> at  $\delta$  4.99 shows an NOE with the methyl at  $\delta$  2.41 of the mesityl. Therefore, it is evident that the R = Mes is pointing towards the *p*-cymene ring, and the imine proton H<sup>5</sup> is pointing towards the phenol, as expected for the *trans* isomer. The <sup>1</sup>H NMR spectrum of *cis*-**4.15c-Mes** shows the imine peak at  $\delta$  9.02 which is virtually identical to *trans*-**4.15c-Mes**. The mesityl gives rise to three 3H singlets at  $\delta$  2.47, 2.32 and 1.96 and two 1H singlets at  $\delta$  6.95 and 6.81 indicating a fixed mesityl group in solution. The *p*-cymene ring shows the expected signals (see Experimental). The *cis* conformation was confirmed by a NOESY cross peak between proton H<sup>5</sup> and the *p*-cymene protons at  $\delta$  5.48 and 5.18 and the absence of an NOE between H<sup>5</sup> and phenol proton H<sup>4</sup> at  $\delta$  6.42. The ES mass spectrum shows a molecular ion peak [M-Cl]<sup>+</sup> at *m/z* 476 and the IR spectrum shows a  $\nu(\text{C}=\text{N})_{\text{imine}}$  stretch at 1597 cm<sup>-1</sup> in comparison to the free ligand at 1623 cm<sup>-1</sup>.

The stability of both isomers in the dark were tested and found that *trans*-**4.15c-Mes** does not convert to *cis*-**4.15c-Mes** in the dark nor *vice versa* for two days at room temperature. When pure *trans*-**4.15c-Mes** was irradiated under ambient light after several days, some converted to *cis*-**4.15c-Mes** giving a *trans*:*cis* ratio of 70:30 (Table 4.1); the ratio did not change after irradiation with a halogen lamp. When a sample with majority *cis*-**4.15c-Mes** (*trans*:*cis* 17:83) was irradiated under ambient light for several days the *trans*:*cis* ratio changed to 59:41 favouring the *trans* isomer with no further change after irradiating with the halogen lamp (Table 4.1). In both cases, the ratio obtained favoured the *trans* isomer, although the final *trans*:*cis* ratios are not the same possibly due to some decomposition occurring during the photoisomerisation as judged by the appearance of mesitaldehyde and free *p*-cymene in the <sup>1</sup>H NMR spectrum. This type of decomposition was not observed with the Ir(III) and Rh(III) half sandwich complexes with the same ligand (**4.15a-Mes** and **4.15b-Mes**).

<b>Table 4.1:</b> Photoisomerisation studies of complexes <i>trans</i> - <b>4.15c-Mes</b> and <i>cis</i> - <b>4.15c-Mes</b> under ambient light in CDCl <sub>3</sub> .		
<b>Time</b>	<b>Starting from <i>trans</i> (<i>trans</i>:<i>cis</i>)</b>	<b>Starting from <i>cis</i> (<i>trans</i>:<i>cis</i>)</b>
After dissolution	0:100	17:83
After 1h	0:100	20:80
After 24 h	93:7	27:73
7 days	73:27	55:45
11 days	70:30	59:41
11+ days	70:30	59:41

For Ru complex **4.15c-Mes** each isomer could be isolated separately hence the UV-Vis spectra could be measured separately (Figure 4.9). The UV-Vis spectra of both complexes are very similar with absorption being below 300 nm and assigned as intraligand ( $\pi - \pi^*$ ) transitions and the moderately intense absorption between 300 – 500 nm are attributed as MLCT bands (Table 4.2).

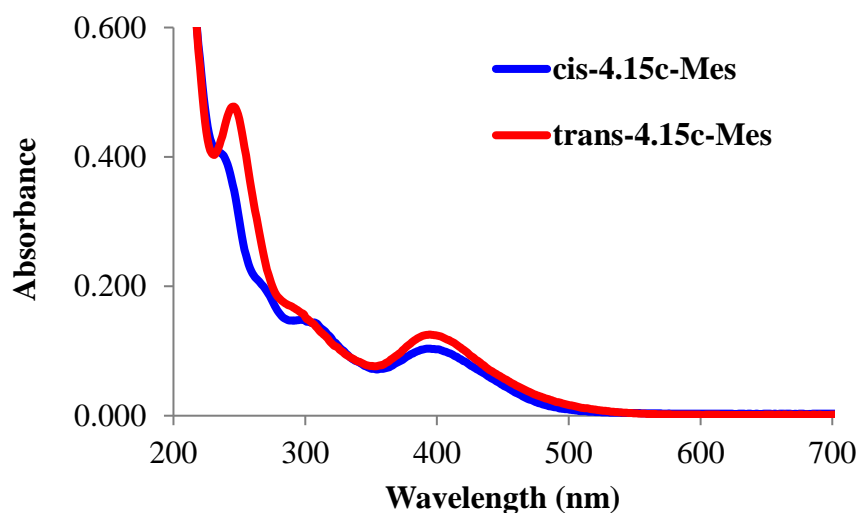


**Figure 4.9:** UV-Vis of complexes *trans*-**4.15c-Mes** (red) and *cis*-**4.15c-Mes** (blue) in HPLC grade MeCN at 0.02 mM.

<b>Table 4.2:</b> Electronic absorption spectral data of complexes <i>trans</i> - <b>4.15c-Mes</b> and <i>cis</i> - <b>4.15c-Mes</b> at 0.02 mM in MeCN.	
<b>Complex</b>	<b><math>\lambda_{\text{abs}}</math> [nm] (<math>\epsilon_{\text{max}}</math>[<math>\text{dm}^3\text{mol}^{-1}\text{cm}^{-1}</math>])</b>
<i>Trans</i> - <b>4.15c-Mes</b>	245 (23900), 295 (8100), 395 (6250)
<i>Cis</i> - <b>4.15c-Mes</b>	234 (20400), 268 sh (10000), 307 (7200), 398 (5150)

Known complex **4.15a-Anisyl**<sup>14</sup> and Rh analogue **4.15b-Anisyl** were prepared using the method shown in Scheme 4.4 and the NMR numbering scheme is shown in Figure 4.10. The crude <sup>1</sup>H NMR spectrum of **4.15a-Anisyl** showed only one isomer but after precipitation, two isomers with a 96:4 ratio were observed. After recrystallisation, the major isomer was isolated. The <sup>1</sup>H NMR spectrum of the major isomer shows H<sup>5</sup> at δ 8.90, an OMe peak at δ 3.89 and two 2H doublets at δ 7.00 and 8.42, indicative of a rotating anisyl group in solution. H<sup>7</sup> and H<sup>7'</sup> were assigned as they show a NOE with the OMe group, whilst H<sup>5</sup> shows a NOE with H<sup>6</sup> and H<sup>6'</sup> at δ 8.42. Although no NOE correlations between Cp\* at δ 1.41 and the anisyl ring were observed, H<sup>5</sup> shows a NOE with H<sup>4</sup> at δ 7.38 indicative of the *trans* isomer. The ES mass spectrum shows a molecular ion peak [M-Cl+MeCN]<sup>+</sup> at *m/z* 595 and the IR spectrum shows a ν(C=N)<sub>imine</sub> stretch at 1577 cm<sup>-1</sup> in comparison to the free ligand at 1627 cm<sup>-1</sup>.

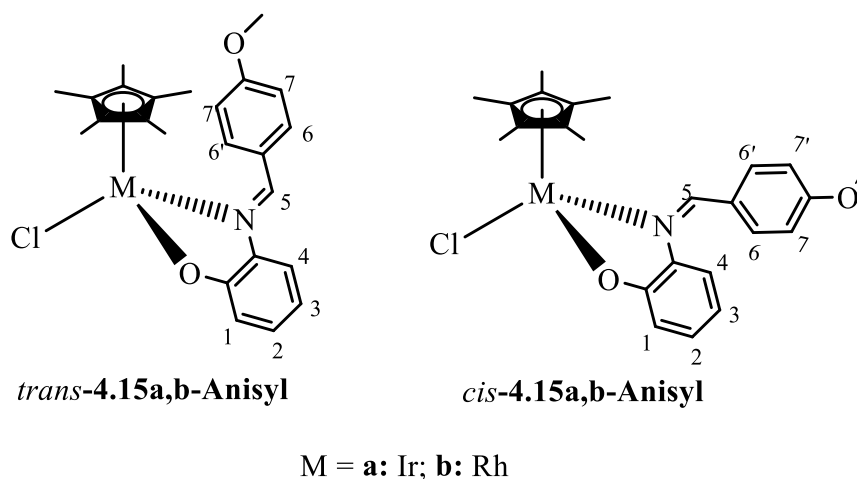


**Figure 4.10:** Numbering of complexes *trans*-**4.15a,b-Anisyl** and *cis*-**4.15a,b-Anisyl**.

When pure *trans*-**4.15a-Anisyl** was irradiated under a halogen lamp for 2 hrs, a ratio of 60:40 was observed favouring the *trans* isomer. After further irradiation the ratio did not change. The <sup>1</sup>H NMR spectrum of this mixture showed some signals that overlap with the *trans* isomer but enough are present to identify the *cis* isomer. In the *cis* isomer, the imine proton (H<sup>5</sup>) appears at δ 8.39 and the anisyl groups appears as a 3H singlet at δ 3.83 and two 2H doublets at δ 6.85 and δ 7.49 indicating that the anisyl group is also rotating in solution. Additionally, H<sup>2</sup> or H<sup>3</sup> of the phenol ring appears at δ 6.08 and the Cp\* for the *cis* isomer appears at δ 1.66 as a 15H singlet. This data agrees with the second species observed after precipitation.

When pure *trans*-**4.15a-Anisyl** was kept in the dark, no isomerisation took place but when a *trans*:*cis* 60:40 mixture was kept in the dark overnight, it was found that *cis*-*trans* isomerisation was thermally accessible showing 100% conversion to *trans*-**4.15a-Anisyl**. Given the small amount of *cis*-isomer formed in the initial reaction and that the *cis* isomer converts to the *trans* at room temperature it is perhaps not surprising that the literature preparation of **4.15a-Anisyl**<sup>14</sup> only reported the *trans* isomer.

The crude <sup>1</sup>H NMR spectrum of **4.15b-Anisyl** showed only one isomer, but after precipitation a second species was present in a 91:9 ratio. The major isomer was isolated via recrystallisation. The <sup>1</sup>H NMR spectrum of the major isomer was identified as the *trans* isomer and showed very similar features to *trans*-**4.15a-Anisyl** with the imine proton (H<sup>5</sup>) at δ 8.88 and a rotating anisyl group (see Chapter 5 for details). The ES mass spectrum shows a molecular ion peak [M-Cl]<sup>+</sup> at *m/z* 464 and the IR spectrum shows a ν(C=N)<sub>imine</sub> stretch at 1570 cm<sup>-1</sup> in comparison to the free ligand at 1627 cm<sup>-1</sup>. A sample of pure *trans*-**4.15b-Anisyl** was kept in the dark for several days and no isomerisation took place. After irradiation of *trans*-**4.15b-Anisyl** under a halogen lamp for 3 hrs, a 70:30 *trans*:*cis* mixture was observed with no change in the ratio after further irradiation. The presence of the *cis* isomer was confirmed though some signals overlap with the major *trans* isomer. Proton H<sup>5</sup> appears at δ 8.31 and two 2H doublets at δ 6.82 and 7.49 with an OMe signal at δ 3.82 indicating that the anisyl ring is rotating in solution with the Cp\* signal at δ 1.64. When the *trans*:*cis* mixture was kept in the dark overnight, the peaks corresponding to the *cis* isomer disappeared. Hence, for **4.15a-Anisyl** and **4.15b-Anisyl**, the *trans*-*cis* isomerisation is photochemically induced and *cis*-*trans* occurs thermally in the dark at room temperature.

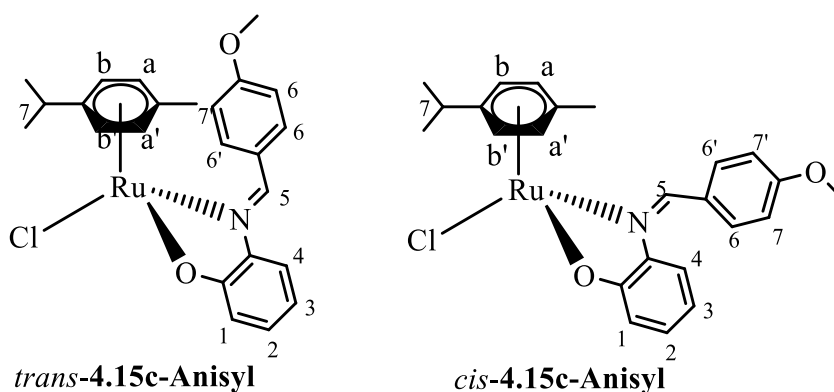


**Figure 4.11:** Numbering of complexes *trans*-**4.15c-Anisyl** and *cis*-**4.15c-Anisyl**.

Complex **4.15c-Anisyl** was prepared as shown in Scheme 4.4 and the  $^1\text{H}$  NMR of the crude product showed the presence of only one isomer. For complex **4.15c-Anisyl**, the  $\text{H}^5$  signal appears at  $\delta$  9.04 and the anisyl group appears as a 3H singlet at  $\delta$  3.93 and two 2H doublets at  $\delta$  7.07 ( $\text{H}^7, \text{H}^{7'}$ ) and 8.29 ( $\text{H}^6, \text{H}^{6'}$ ) which show that the anisyl ring is rotating in solution. The imine proton ( $\text{H}^5$ ) shows an NOE with  $\text{H}^4$  from the phenol ring and the anisyl protons  $\text{H}^6$  and  $\text{H}^{6'}$  show an NOE with *p*-cymene protons at  $\delta$  4.72 ( $\text{H}^b/\text{H}^{b'}$ ) and  $\delta$  4.58 ( $\text{H}^a/\text{H}^{a'}$ ). This is evidence that the *trans* isomer is formed exclusively in this reaction unlike in **4.15c-Mes** where a mixture of 78:22 was formed favouring the *trans* isomer. The ES mass spectrum shows a molecular ion peak  $[\text{M}-\text{Cl}]^+$  at  $m/z$  462 and the IR spectrum shows a  $\nu(\text{C}=\text{N})_{\text{imine}}$  stretch at  $1577\text{ cm}^{-1}$  in comparison to the free ligand at  $1627\text{ cm}^{-1}$ .

When *trans*-**4.15c-Anisyl** was kept in the dark for 2 days no isomerisation took place at room temperature. When the same sample was exposed to a halogen lamp, after 5 hrs a 70:30 *trans*:*cis* ratio was observed. The ratio did not change after further irradiation, but some slow hydrolysis of the imine was observed as for **4.15c-Mes**. When the mixture of 70:30 was left in the dark at room temperature the ratio changed after 2 days to 86:14 favouring the *trans* isomer with no change after that. This shows that back thermal isomerisation to the *trans* isomer did occur at room temperature but did not go completely. The  $^1\text{H}$  NMR spectrum of the *cis*-**4.15c-Anisyl** could be extracted from that of the *trans*-*cis* mixture. It showed an imine peak at  $\delta$  8.72, a 3H singlet at  $\delta$  3.87 and the two 2H doublets at  $\delta$  7.46 ( $\text{H}^6, \text{H}^{6'}$ ) and  $\delta$  6.82 ( $\text{H}^7, \text{H}^{7'}$ ) due to the anisyl which is rotating in solution.  $\text{H}^5$  shows an NOE with the *p*-cymene protons  $\text{H}^a, \text{H}^{a'}$ , whilst  $\text{H}^6, \text{H}^{6'}$  show an NOE with  $\text{H}^4$  from the phenol ring indicating that it is the *cis* isomer.

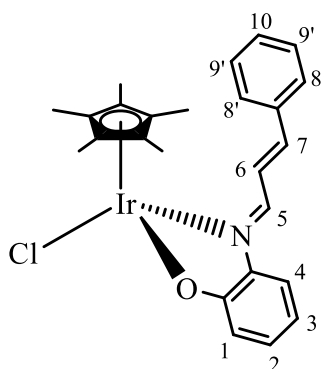


**Figure 4.12:** Numbering of complex *trans*-**4.15a-Cinnamyl**.

The  $^1\text{H}$  NMR spectrum **4.15a-Cinnamyl** showed only one isomer for the crude sample. The imine proton  $\text{H}^5$  appears as a doublet at  $\delta$  8.36 showing an NOE with phenol proton  $\text{H}^4$  at  $\delta$  7.24 whilst the  $\text{Cp}^*$  signal at  $\delta$  1.64 shows an NOE with phenyl protons from the cinnamyl group that appear as a multiplet between  $\delta$  7.40 and 7.55 consistent with the *trans* isomer which was confirmed by the X-Ray structure (see later). The ES mass spectrum shows a molecular ion peak  $[\text{M}-\text{Cl}]^+$  at  $m/z$  550 and the IR spectrum shows a  $\nu(\text{C}=\text{N})_{\text{imine}}$  stretch at  $1575\text{ cm}^{-1}$ .

Interestingly, complex *trans*-**4.15a-Cinnamyl** did not undergo any isomerisation under irradiation (halogen lamp for 2 hrs and ambient light for 18 hrs) or when left in the dark for two days. From all the half-sandwich complexes with *exocyclic*  $\text{N}^{\wedge}\text{O}$  ligand that have been synthesised, complex **4.15a-Cinnamyl** is the first example where isomerisation is not observed. It is possible that isomerisation does occur but that the reverse isomerisation is fast even at room temperature. Further experiments would need to be done to investigate this possibility.

#### **X-Ray crystallography of $\text{N}^{\wedge}\text{O}$ complexes**

Complexes *trans*-**4.15a-Cinnamyl**, *trans*-**4.15c-Mes**, *cis*-**4.15c-Mes**, *trans*-**4.15c-Anisyl**, *cis*-**4.15c-Anisyl** afforded crystals from DCM/hexane suitable for X-Ray crystallography. The X-Ray structures for the five complexes are shown in Figure 4.13-4.15 and the selected bond length and angles are shown in Table 4.3 and 4.4. All complexes are pseudo-octahedral with the  $\eta^6$ -*p*-cymene ligand that is  $\pi$ -bonded to the Ru centre and  $\eta^5$ - $\text{Cp}^*$  ligand for Ir centre, occupying one face of the octahedron. The other three sites are occupied by the anionic donor  $\text{N}^{\wedge}\text{O}$  ligand creating a 5-membered chelate ring with an *exocyclic*  $\text{C}=\text{N}$  bond and the chloride ligand. The  $\text{O}(1)\text{---M}(1)\text{---N}(1)$  ( $\text{M} = \text{Ir}$  or  $\text{Ru}$ ) angle is between  $78.2^\circ$  and  $79.2^\circ$  typical of a 5-membered ring. In complex **4.15c-Mes**, the coordination environment around the Ru is very similar in both isomers (see Table 4.3) as is the case for complex **4.15c-Anisyl** (Table 4.4).

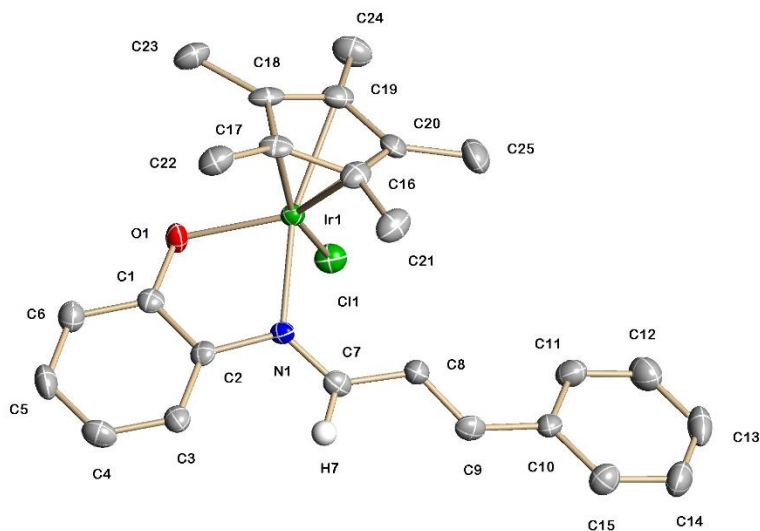


**Figure 4.13:** X-Ray structure of complex *trans*-**4.15a-Cinnamyl** showing 50% ellipsoids. The hydrogen atoms (with exception of imine proton) have been omitted from the diagrams for clarity. Selected bond lengths (Å) and angle (°) for *trans*-**4.15a-Cinnamyl**: Ir(1)—O(1), 2.089(4); Ir(1)—N(1), 2.098(4); Ir(1)—Cl(1), 2.3990(15); N(1)—C(7), 1.288(6) ,O(1)—Ir(1)—N(1), 78.21(15).

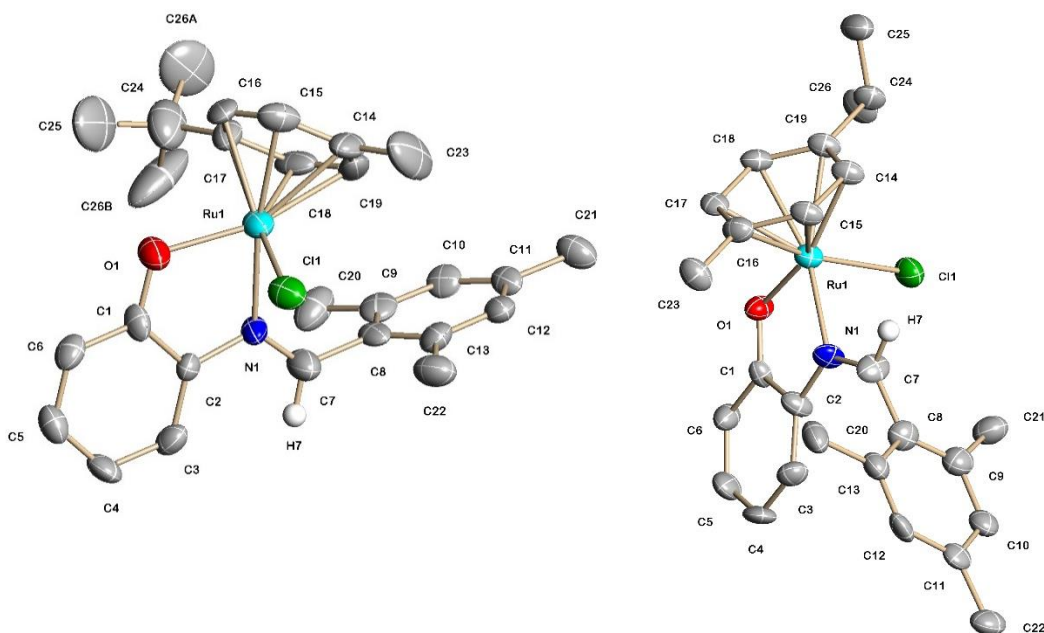


**Figure 4.14:** X-Ray Structures of *trans*-**4.15c-Mes** and *cis*-**4.15c-Mes** respectively showing 50% ellipsoids. The hydrogen atoms (with exception of imine proton) have been omitted from the diagrams for clarity.

**Table 4.3:** Selected bond lengths (Å) and angles (°) for *trans*-4.15c-Mes and *cis*-4.15c-Mes.

	<i>trans</i> -4.15c-Mes	<i>cis</i> -4.15c-Mes
O(1)—Ru(1)—N(1)	78.6(2)	79.7(4)
Ru(1)—O(1)	2.026(5)	2.018(10)
Ru(1)—N(1)	2.133(6)	2.122(11)
Ru(1)—Cl(1)	2.411(2)	2.417(4)
N(1)—C(7)	1.286(8)	1.288(17)
Ru(1)— <i>p</i> -cymene (centroid)	1.668	1.677

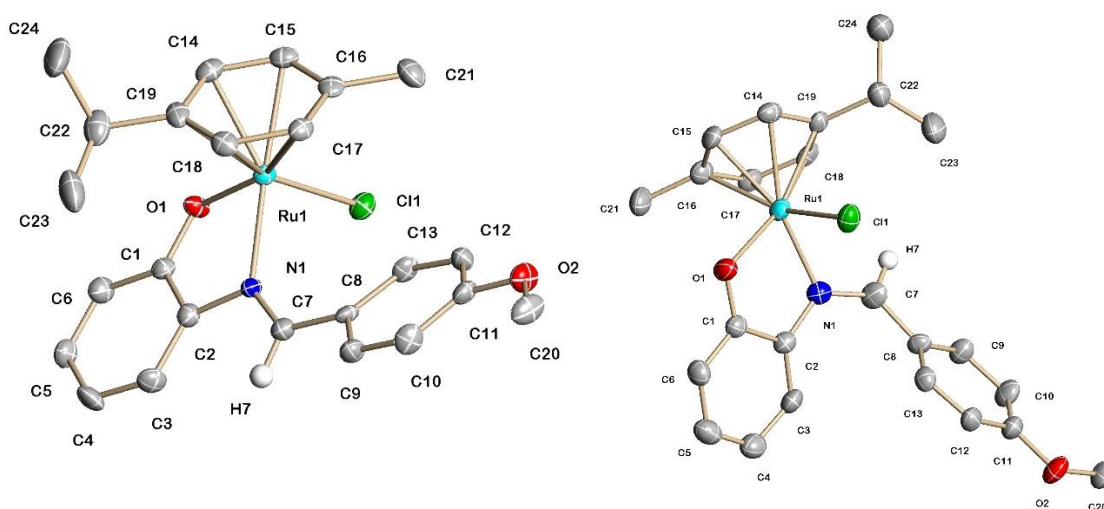


**Figure 4.15:** X-Ray Structures of *trans*-4.15c-Anisyl and *cis*-4.15c-Anisyl respectively showing 50% ellipsoids. The hydrogen atoms (exception H7) have been omitted from the diagrams for clarity.

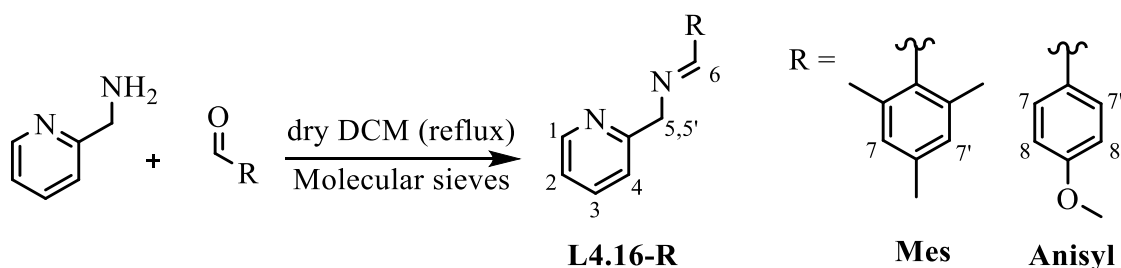
**Table 4.4:** Selected bond lengths (Å) and angle (°) for *trans*-4.15c-Anisyl and *cis*-4.15c-Anisyl.

	<i>trans</i> -4.15c-Anisyl	<i>cis</i> -4.15c-Anisyl
O(1)—Ru(1)—N(1)	79.16(11)	78.76(19)
Ru(1)—O(1)	2.046(3)	2.062(4)
Ru(1)—N(1)	2.129(3)	2.118(5)
Ru(1)—Cl(1)	2.4254(11)	2.4180(19)
N(1)—C(7)	1.293(5)	1.288(7)
Ru(1)— <i>p</i> -cymene (centroid)	1.673	1.667

In *cis*-**4.15c-Mes** and *trans*-**4.15c-Mes**, the mesityl group is not conjugated as it is approximately perpendicular (81.2° and 86.5° respectively) to the phenol plane. On the other hand, in *trans*-**4.15c-Anisyl**, the anisyl ring is less tilted (34.6°) in relation to the plane of the phenol ring in comparison to *cis*-**4.15c-Anisyl** (52.2°), showing that *trans*-**4.15c-Anisyl** is slightly more conjugated than the *cis* form.

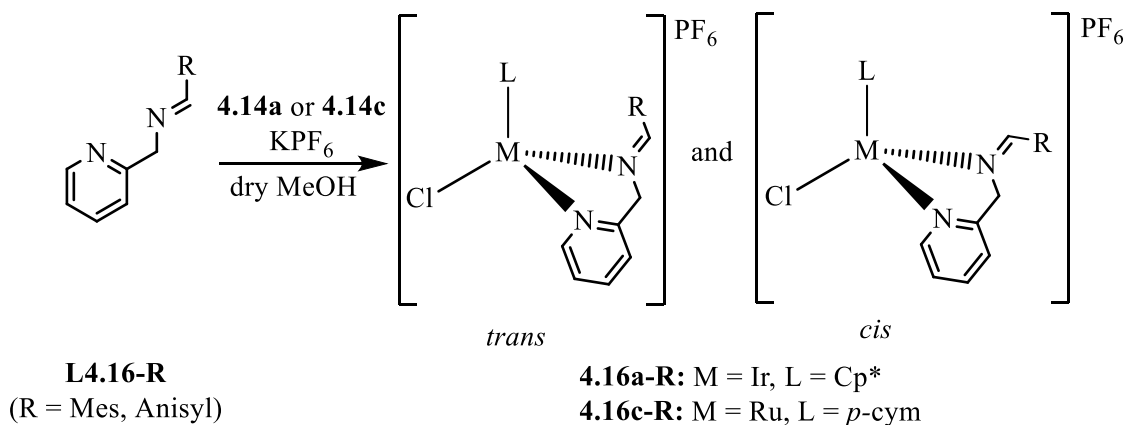
#### 4.2.2 Synthesis, Characterisation and Photoisomerisation Studies of N<sup>N</sup> Complexes

Ligands **L4.16-R** (R = Mes, Anisyl) were synthesised in very high yields by refluxing 2-picolylamine and the respective aldehyde in the presence of molecular sieves and dry DCM (Scheme 4.5). **L4.16-R** were stored under nitrogen to prevent hydrolysis. Ligand **L4.16-Anisyl** is known<sup>19</sup> whilst ligand **L4.16-Mes** is not. Some of the experimental work was carried out under my guidance by Abdirashid Obsiye, MChem project 2017. The <sup>1</sup>H NMR spectrum of **L4.16-Mes** shows an imine peak at δ 8.80 and a mesityl group with a 6H singlet at δ 2.43 and a 3H singlet at δ 2.28 with the aromatic protons appearing as 2H singlet at δ 6.87, in addition the CH<sub>2</sub> gives a 2H singlet at δ 4.97. Therefore, either the mesityl group is rotating fast in solution or it is fixed perpendicular to the imine plane. The <sup>1</sup>H NMR spectrum of **L4.16-Anisyl** shows an imine peak at δ 8.41 and a CH<sub>2</sub> group at δ 4.93 with the anisyl giving rise to a 3H singlet at δ 3.84 and an A<sub>2</sub>B<sub>2</sub> system at δ 7.72 and 6.99 which suggests that it is rotating fast in solution or it is fixed perpendicular to the imine plane. Similarly to the N<sup>O</sup>H ligands, the N<sup>N</sup> ligands adopt the *trans* conformation which was determined by the NOESY spectra where the imine peak shows a NOE with the CH<sub>2</sub> group in both ligands. The ESI mass spectra for **L4.16-Mes** and **L4.16-Anisyl** each show a molecular ion peak [M+H]<sup>+</sup> at *m/z* 239 and 227, respectively. Scheme 4.5 shows the numbering scheme used in this section for complexes **4.16a,c-R**.



**Scheme 4.5:** Synthesis of ligands **L4.16-R**.

$[\text{IrCl}_2\text{Cp}^*]_2$  (**4.14a**) and  $[\text{RuCl}_2(p\text{-cym})]_2$  (**4.14c**) were reacted with the respective neutral N^N ligand (**L4.16-R**) in the presence of  $\text{KPF}_6$  in dry MeOH at room temperature for 2 hrs to give *exocyclic* complexes **4.16a-R** and **4.16c-R** (R = Mes and Anisyl) in high yields (Scheme 4.6).



**Scheme 4.6:** Synthesis of half-sandwich complexes **4.16a,c-R** with *exocyclic* N^N ligand.

The  $^1\text{H}$  NMR spectrum of complex **4.16a-Mes** before isolation showed only one isomer but after precipitation a 90:10 ratio was observed. The  $^1\text{H}$  NMR spectrum of the major isomer shows the imine proton ( $\text{H}^6$ ) as the most downfield singlet at  $\delta$  9.31. After complexation, protons  $\text{H}^5$  and  $\text{H}^{5'}$  become chemically inequivalent (diastereotopic) appearing as two 1H doublets at  $\delta$  5.64 and 5.55. Mesityl protons  $\text{H}^7$  and  $\text{H}^{7'}$  appear as a 2H singlet at  $\delta$  6.90 and the methyl groups appear as a 6H singlet at  $\delta$  2.34 and a 3H singlet at  $\delta$  2.31, hence, the mesityl group is rotating freely in solution. Proton  $\text{H}^6$  shows a NOE with  $\text{H}^5$  and  $\text{H}^{5'}$  and the  $\text{Cp}^*$  signal at  $\delta$  1.39 shows an NOE with the 6H singlet at  $\delta$  2.34 which are indicative of the *trans* isomer. The ES mass spectrum shows a molecular ion peak  $[\text{M}]^+$  at  $m/z$  601 and the IR spectrum shows a  $\nu(\text{C}=\text{N})_{\text{imine}}$  stretch at  $1607\text{ cm}^{-1}$ .

A sample of **4.16a-Mes** (90:10) favouring the *trans* was left in the dark showing no change in the ratio at room temperature. The same mixture was irradiated using a halogen lamp and after 4 hrs a 4:96 ratio favouring the *cis* isomer was observed with no change in the ratio after further irradiation. The  $^1\text{H}$  NMR spectrum showed that the imine peak  $\text{H}^6$  for *cis*-**4.16a-Mes** appears at  $\delta$  8.96 and diastereotopic protons  $\text{H}^5$  and  $\text{H}^{5'}$  appear as two doublets at  $\delta$  5.09 and 4.95 and the methyl groups appear as three 3H singlets at  $\delta$  2.37, 2.33 and 2.12. Hence, it is evident that in *cis*-**4.16a-Mes**, the mesityl

group is fixed but in *trans*-**4.16a-Mes** it is rotating. The mixture with 4:96 *trans:cis* ratio was kept in the dark at room temperature for 5 days and no isomerisation occurred consistent with the observation on the 90:10 mixture mentioned above.

Complex **4.16c-Mes** was prepared using the same method as in Scheme 4.6. The  $^1\text{H}$  NMR spectrum of the crude product showed a ratio of 82:18 and after purification the ratio did not change. When the mixture was kept in the dark for 3 days no isomerisation occurred at room temperature. In the major isomer,  $\text{H}^6$  appears at  $\delta$  9.05 and the mesityl shows three 3H singlets and two 1H singlets which indicate that the mesityl is fixed in solution. The imine proton ( $\text{H}^6$ ) shows an NOE with  $\text{H}^5$  and  $\text{H}^{5'}$  and the *ortho* methyl peaks show an NOE with a *p*-cymene proton at  $\delta$  5.08 ( $\text{H}^b/\text{H}^{b'}$ ). Therefore, the major isomer is the *trans* isomer. In the minor isomer some signals overlap with the *trans* isomer, but some were identified notably an imine proton at  $\delta$  9.13 and four aromatic signals for a *p*-cymene. The ES mass spectrum shows a molecular ion peak  $[\text{M}]^+$  at  $m/z$  509 and the IR spectrum shows a  $\nu(\text{C}=\text{N})_{\text{imine}}$  stretch at  $1576\text{ cm}^{-1}$ .

The  $^1\text{H}$  NMR spectrum of **4.16a-Anisyl** only showed one isomer with an imine peak  $\text{H}^6$  at  $\delta$  8.83, two diastereotopic protons  $\text{H}^5$  and  $\text{H}^{5'}$  at  $\delta$  5.37 and 5.22 and a rotating anisyl group (see Chapter 5 for details). Proton  $\text{H}^6$  shows an NOE with signal at  $\delta$  5.37 ( $\text{H}^5/\text{H}^{5'}$ ) and the  $\text{Cp}^*$  signal at  $\delta$  1.52 shows an NOE with  $\text{H}^7/\text{H}^{7'}$  and not with  $\text{H}^6$ . These data are consistent with the presence of the *trans* isomer. The ES mass spectrum shows a molecular ion peak  $[\text{M}]^+$  at  $m/z$  589 and the IR spectrum shows a  $\nu(\text{C}=\text{N})_{\text{imine}}$  stretch at  $1603\text{ cm}^{-1}$ .

When *trans*-**4.16a-Anisyl** was left in the dark for 5 days it did not show any isomerisation at room temperature. Irradiation of the sample for 5 hrs gave a *trans:cis* ratio of 34:66; further irradiation resulted in some hydrolysis of the ligand. This sample was kept in the dark at room temperature and the ratio did not change therefore no thermal back isomerisation took place. Some signals of *cis*-**4.16a-Anisyl**, are clear in the spectrum of the mixture. Hence,  $\text{H}^6$  appears at  $\delta$  8.66 and a 3H singlet and two 2H doublets at  $\delta$  7.22 and 7.93 indicate that the anisyl ring is rotating in solution with a  $\text{Cp}^*$  signal at  $\delta$  1.64.

The  $^1\text{H}$  NMR spectrum of complex **4.16c-Anisyl** only showed one isomer. Proton  $\text{H}^6$  appears at  $\delta$  8.85 and the anisyl group is rotating in solution.  $\text{H}^6$  shows a weak NOE with the signal at  $\delta$  5.12 ( $\text{H}^5/\text{H}^{5'}$ ) whilst anisyl protons ( $\text{H}^7/\text{H}^{7'}$ ) show an NOE with *p*-cymene protons at  $\text{H}^b$  and  $\text{H}^{b'}$  which are evidence of the *trans* isomer. The ES mass

spectrum shows a molecular ion peak  $[M]^+$  at  $m/z$  497 and the IR spectrum shows a  $\nu(\text{C}=\text{N})_{\text{imine}}$  stretch at  $1598\text{ cm}^{-1}$ .

When *trans*-**4.16c-Anisyl** was left in the dark for 24 hours no isomerisation took place at room temperature. When exposed to a halogen lamp for 6 hrs no photoisomerisation was noticeable. This situation is the same as that for N<sup>^</sup>O complex **4.15a-Cinnamyl** discussed above; isomerisation may occur but the reverse isomerisation may be fast even at room temperature so the *cis* isomer is not observed. Further experiments would need to be done to investigate this possibility.

### 4.2.3 Computational Studies

DFT calculations performed by Professor F. Lelj (University della Basilicata Potenza, Italy) showed that in **4.15a-Mes**, the *cis* isomer is more stable than the *trans* form. On the other hand, in **4.15a-Anisyl** the *trans* isomer is more stable than the *cis* form. This is consistent with experimental data. Although, the energies shown in Figure 4.16 are preliminary, the studies show that the *cis* isomer is preferred when R = Mes and the *trans* isomer is preferred when R = Anisyl. Hence the size of the R group can control the stability of the preferred isomer in half-sandwich complexes where M = Ir.

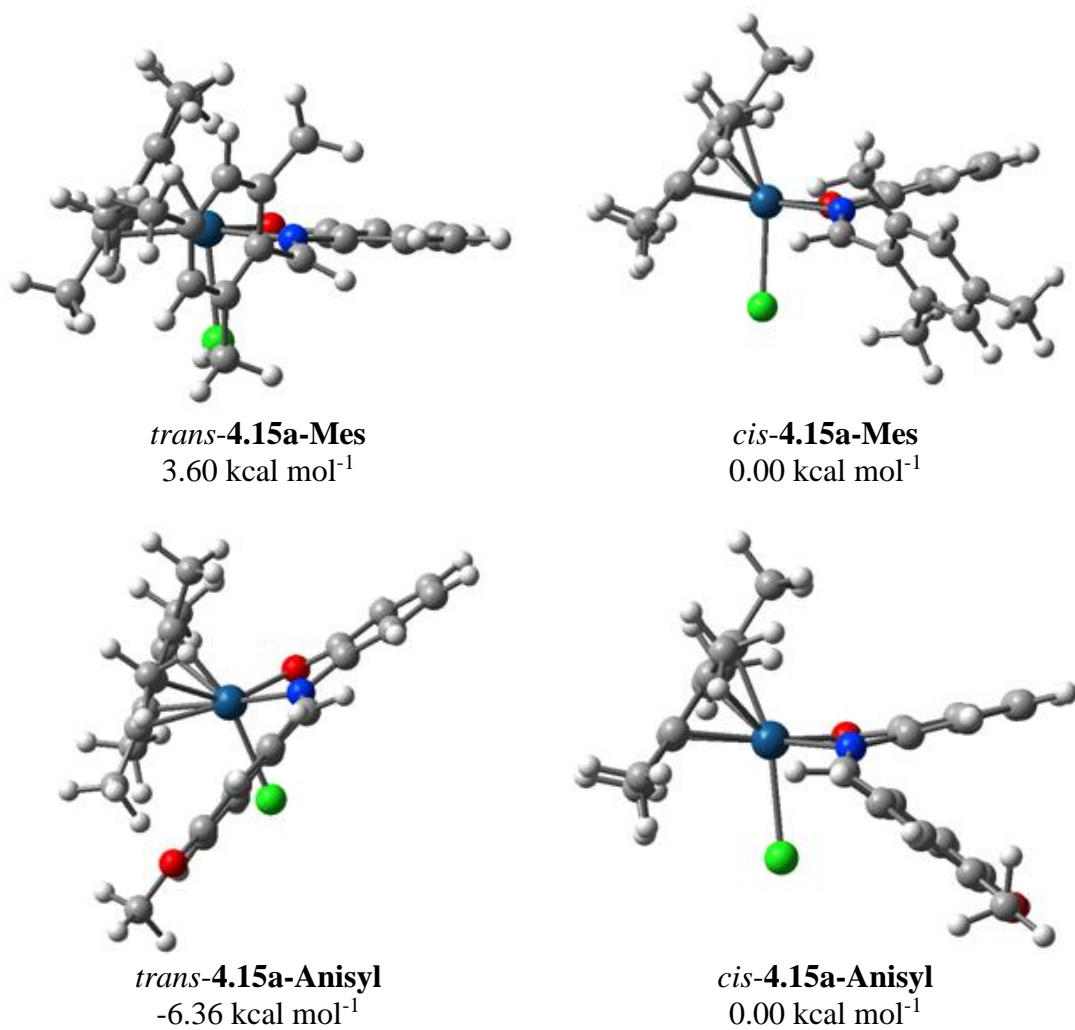


**Figure 4.16:** Energies of the *trans*-4.15a-R and *cis*-4.15a-R using the *cis* isomer as the reference. (R = Mes, Anisyl).

DFT calculations on complex *trans*-4.15c-Mes shows that in the ground state the *p*-cymene has two possible conformations relative to the Mes group (Figure 4.17), with a difference in energy of approximately 1.8 kcal mol<sup>-1</sup> where the most stable conformer has the <sup>i</sup>Pr group pointing away from the Mes group.

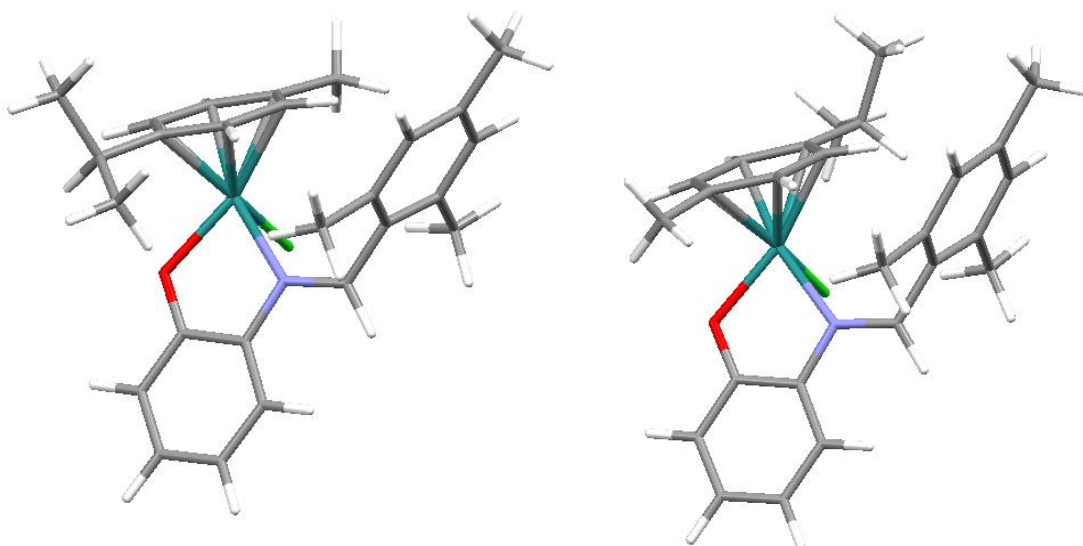


**Figure 4.17:** Conformers of *trans*-4.15c-Mes in the ground state.

#### 4.2.4 Conclusion

The results in this Chapter have shown that complexation of N<sup>O</sup> ligands (**L4.15-R**, R = Mes, Anisyl) and N<sup>N</sup> ligands (**L4.16-R** R = Mes, Anisyl) to Cp<sup>\*</sup>M (M = Ir, Rh) or (*p*-cymene)Ru fragments can have a considerable effect on the configuration of the imine and the ease of isomerisation. Both free ligands only show the *trans* isomer and this agrees with the 2D NMR. The results after complexation for N<sup>O</sup> ligands and N<sup>N</sup> ligands are summarised in Tables 4.5 and 4.6.

<b>Table 4.5:</b> Summary of isomerisation results for complexes <b>4.15a-c-R</b> .				
	<b>Irradiation<sup>a</sup></b>		<b>Thermal (dark, RT)</b>	<b>Type<sup>b</sup></b>
	before	after		
	<i>trans:cis</i>	<i>trans:cis</i>	<i>trans:cis</i>	
<b>4.15a-Mes</b>	0:100	4:96	4:96 converts to 100% <i>cis</i>	B
<b>4.15b-Mes</b>	0:100	9:91	9:91 converts to 100% <i>cis</i>	B
<b>4.15c-Mes</b>	100:0	70:30	<i>Trans</i> stable in the dark; <i>Cis</i> stable in the dark	A
	0:100	59:41		
<b>4.15a-Anisyl</b>	100:0	60:40	<i>Trans</i> stable in the dark; 60:40 gave 100% <i>trans</i>	B
<b>4.15b-Anisyl</b>	100:0	70:30	<i>Trans</i> stable in the dark; 70:30 gave 100% <i>trans</i>	B
<b>4.15c-Anisyl</b>	100:0	70:30	<i>Trans</i> stable in the dark. 70:30 gave 86:14 (2 days)	B
<b>4.15c-Cinnamyl</b>	100:0	no change	<i>Trans</i> stable in the dark	C

*a* Irradiation using halogen lamp.  
*b* Type A = large barrier (no isomerisation at RT in dark), B = modest barrier (isomerisation over hours/days at RT in dark), C = no evidence for isomerisation (could be due to low barrier).

After complexation, **4.15a-Mes** and **4.15b-Mes** only show the *cis* isomer after work up but a small amount of *trans* isomer was formed after irradiation. However, the *trans* isomer is not stable and the reverse isomerisation (*trans-cis*) occurs at room temperature in the dark. In contrast, the corresponding Ru complex **4.15c-Mes** is formed as a 78:22 (*trans-cis*) mixture and in this case the isomers can be separated. Both isomers are stable in the dark so, in this case, it is not yet known which is the most thermodynamically stable isomer. For anisyl complexes **4.15a,b,c-Anisyl** the major isomer formed is the *trans* isomer in each case, consistent with Anisyl being less bulky than Mes. In all three complexes upon irradiation some of the *cis* isomer was formed (30-40%). For all three complexes the *cis* isomer is unstable and the reverse *cis-trans* isomerisation was accessible in the dark at room temperature. The isomerisation of the Ru complex **4.15c-Anisyl** is slower than the Ir or Rh complex **4.15a,b-Anisyl**.

Complex **4.15c-Cinnamyl** is formed as just the *trans* isomer and did not show any isomerisation under the halogen lamp or in the dark. It is possible that isomerisation

does occur but that the reverse isomerisation is fast at room temperature. Further experiments would need to be done to investigate this possibility.

<b>Table 4.6:</b> Summary of isomerisation results for complexes <b>4.16a,c-R</b> .				
	<b>Irradiation<sup>a</sup></b>		<b>Thermal (dark, RT)</b>	<b>Type<sup>b</sup></b>
	before	after		
	<i>Trans:cis</i>	<i>Trans:cis</i>	<i>Trans:cis</i>	
<b>4.16a-Mes</b>	90:10	4:96	90:10 no isomerisation in dark 4:96 no isomerisation in dark	A
<b>4.16c-Mes</b>	82:18	no change	82:18 no isomerisation in dark	A
<b>4.16a-Anisyl</b>	100:0	100% <i>trans</i> gave 34:66	100% <i>trans</i> stable in the dark 34:66 no isomerisation in dark	A
<b>4.16c-Anisyl</b>	100:0	no change	100% <i>trans</i> stable in the dark	C
<i>a</i> Irradiation using halogen lamp.				
<i>b</i> Type A = large barrier (no isomerisation at RT in dark), B = modest barrier (isomerisation over hours/days at RT in dark), C = no evidence for isomerisation (could be due to low barrier).				

For all the N<sup>N</sup> complexes, even **4.16a-Mes**, which is sterically the most crowded, the *trans* isomer is favoured. The Ir complexes **4.16a-Mes** and **4.16a-Anisyl** both undergo photoisomerisation and in the case of **4.16a-Mes** the isomerisation is almost complete from 90:10 to 4:96, hence this is the most efficient complex studied in terms of the extent of photoisomerisation. For both complexes the *cis* isomers are stable at room temperature and so the reverse isomerisation is not yet proven. Surprisingly, neither **4.16c-Mes** nor **4.16c-Anisyl** show evidence for photoisomerisation. In the former case it may be that the starting ratio is close to the photostationary state so there is no net change, whilst for **4.16c-Anisyl** it may be that isomerisation occurs but the reverse isomerisation is fast. In both cases further study is needed to clarify these issues.

Changing the chelating ligand from N<sup>O</sup> to N<sup>N</sup> clearly influences which isomer is preferred. For example, for N<sup>O</sup> complex **4.15a-Mes** the *cis* isomer is the preferred isomer whilst for the N<sup>N</sup> cationic complex **4.16a-Mes** the *trans* isomer is formed preferentially. Although in both complexes the chelating ligand forms a 5-membered

ring, the N<sup>^</sup>O chelate is aromatic whilst the N<sup>^</sup>N chelate is saturated making the N<sup>^</sup>N chelate ring slightly more flexible. Similarly, for both N<sup>^</sup>O (**4.15a-Anisyl**) and N<sup>^</sup>N (**4.16a-Anisyl**) the *trans* isomer is the major isomer formed and in both cases the *cis* isomer is formed upon irradiation, but the reverse thermal isomerisation is accessible at room temperature in the dark for the neutral N<sup>^</sup>O complex (**4.15a-Anisyl**) but is not for cationic complex **4.16a-Anisyl**. In this case, the nature of the ligand or the charge on the metal may influence the reverse thermal step. Ru(II) complexes, **4.15c-Anisyl** and **4.16c-Anisyl** both formed exclusively the *trans* isomer. When **4.15c-Anisyl** was irradiated *trans:cis* isomerisation took place with slow reverse thermal isomerisation in the dark, however with **4.16c-Anisyl** the *trans* form did not convert to the *cis* upon irradiation or thermally at room temperature. Thus, the work in this Chapter (and that in Chapter 3) demonstrates that the nature of the R group on the imine, the nature of the chelating attaching group and of the other ML fragment can all have an effect on the photoisomerisation and the thermal stability of the isomers. Clearly some more work is needed to establish the reverse process in some cases and to see how robust the complexes are after repeated switching between *cis* and *trans* isomers. However, overall imine chelating ligands which can provide an *exo* imine when coordinated offers an excellent platform for further investigation of molecular switches.

### 4.3 Bibliography

1. S. J. Dougan, M. Melchart, A. Habtemariam, S. Parsons and P. J. Sadler, *Inorg. Chem.*, 2006, **45**, 10882-10894.
2. F. Ding, Y. Sun and F. Verpoort, *Eur. J. Inorg. Chem.*, 2010, **2010**, 1536-1543.
3. R. K. Rath, M. Nethaji and A. R. Chakravarty, *J. Organomet. Chem.*, 2001, **633**, 79-84.
4. Y. Yamamoto, H. Nakamura and J.-F. Ma, *J. Organomet. Chem.*, 2001, **640**, 10-20.
5. A. Telleria, P. W. N. M. van Leeuwen and Z. Freixa, *Dalton Trans.*, 2017, **46**, 3569-3578.
6. C. Deo, N. Bogliotti, R. Métivier, P. Retailleau and J. Xie, *Organometallics*, 2015, **34**, 5775-5784.
7. C. Deo, H. Wang, N. Bogliotti, Y. Zang, P. Retailleau, X.-P. He, J. Li and J. Xie, *J. Organomet. Chem.*, 2016, **820**, 111-119.
8. Z.-J. Yao, K. Li, P. Li and W. Deng, *J. Organomet. Chem.*, 2017, **846**, 208-216.
9. S. Thangavel, M. Paulpandi, H. B. Friedrich, K. Murugan, S. Kalva and A. A. Skelton, *J. Inorg. Biochem.*, 2016, **159**, 50-61.
10. B. Li, C. Darcel, T. Roisnel and P. H. Dixneuf, *J. Organomet. Chem.*, 2015, **793**, 200-209.
11. P. Govindaswamy, Y. A. Mozharivskyj and M. R. Kollipara, *Polyhedron*, 2005, **24**, 1710-1716.
12. J. M. Gichumbi, H. B. Friedrich and B. Omondi, *Inorg. Chim. Acta*, 2017, **456**, 55-63.
13. A. R. Burgoyne, B. C. E. Makhubela, M. Meyer and G. S. Smith, *Eur. J. Inorg. Chem.*, 2015, **2015**, 1433-1444.
14. O. Briel, A. Fehn, K. Polborn and W. Beck, *Polyhedron*, 1998, **18**, 225-242.
15. R. A. Arthurs, P. N. Horton, S. J. Coles and C. J. Richards, *Eur. J. Inorg. Chem.*, 2017, **2017**, 229-232.

16. A. Cnossen, L. Hou, M. M. Pollard, P. V. Wesenhagen, W. R. Browne and B. L. Feringa, *J. Am. Chem. Soc.*, 2012, **134**, 17613-17619.
17. R. G. Ball, W. A. G. Graham, D. M. Heinekey, J. K. Hoyano, A. D. McMaster, B. M. Mattson and S. T. Michel, *Inorg. Chem.*, 1990, **29**, 2023-2025.
18. J. Tönnemann, J. Risse, Z. Grote, R. Scopelliti and K. Severin, *Eur. J. Inorg. Chem.*, 2013, **2013**, 4558-4562.
19. S. Padilla, R. Tejero, J. Adrio and J. C. Carretero, *Org. Lett.*, 2010, **12**, 5608-5611.

## Chapter 5: Conclusions and Future Work

This thesis describes the synthesis of a series of bis-cyclometallated Ir(III) complexes with general formula  $[\text{Ir}(\text{C}^{\wedge}\text{N})_2(\text{X}^{\wedge}\text{Y})]$  and the final results chapter describes the synthesis half-sandwich complexes.

Chapter 1 describes the general properties and synthesis of cyclometallated Ir(III) complexes with general formula  $[\text{Ir}(\text{C}^{\wedge}\text{N})_2(\text{X}^{\wedge}\text{Y})]^{n+}$  ( $n = 0, 1$ ). Different approaches to tuning the emission in cyclometallated  $[\text{Ir}(\text{C}^{\wedge}\text{N})_2(\text{X}^{\wedge}\text{Y})]^{n+}$  ( $n = 0, 1$ ) complexes and their applications were also described. Cyclometallated  $[\text{Ir}(\text{C}^{\wedge}\text{N})_2(\text{X}^{\wedge}\text{Y})]^{n+}$  ( $n = 0, 1$ ) complexes can be tuned through the visible region and to near infrared by varying the cyclometallated  $\text{C}^{\wedge}\text{N}$  ligand and/or the  $\text{X}^{\wedge}\text{Y}$  ligand. The emission could also be tuned by varying the degree of conjugation, presence and location of heteroatoms and addition of substituents on either of the ligands. Owing to their rich photophysical and electrochemical properties, these complexes will continue to be used in diverse applications.

A series of bis-cyclometallated Ir(III) complexes with general formula  $[\text{Ir}(\text{C}^{\wedge}\text{N})_2(\text{N}^{\wedge}\text{O})]$  with different cyclometallated  $\text{C}^{\wedge}\text{N}$  ligands (ppz or ppy) bearing 6-membered  $\text{N}^{\wedge}\text{O}$  ancillary ligand ( $\text{N}^{\wedge}\text{O} = \text{salicylimine}$ ) were studied in Chapter 2. The EPESS effect was studied by using different cyclometallated ligands (ppy and ppz) and varying the R group on the  $\text{N}^{\wedge}\text{O}$  ancillary ligand. The theory of  $\pi$ - $\pi$  interaction on the ppy ligands was challenged and it was shown that changing the cyclometallated ligand did not have a significant effect on the emission properties. The restricted intramolecular rotation of the N-aryl was also tested and showed that complexes with fixed R group on the  $\text{N}^{\wedge}\text{O}$  ligand in also showed the EPESS phenomenon. With the aid of DFT calculation, it was found that ligand distortion of the excited state in solution caused of non-radiative decay in solution whilst these distortions were weak in the solid state, giving rise to a new theory of EPESS in these types of complexes.

Further studies on this topic lead to the work carried out in Chapter 3. To test if ring size on the  $\text{N}^{\wedge}\text{O}$  ligand would have an effect on EPESS, synthesis of new Ir(III) complexes with general formula  $[\text{Ir}(\text{C}^{\wedge}\text{N})_2(\text{N}^{\wedge}\text{O})]$  was carried out. In these complexes, the  $\text{N}^{\wedge}\text{O}$  ligand formed an isomeric 5-membered chelate ring with an *exocyclic* imine bond (instead of 6-membered ring as seen in Chapter 2). The study showed that changing the ring size had a negative effect on EPESS but instead a *trans-cis* photoisomerisation was observed upon irradiation. During the synthesis of these

complexes, the results showed that in the dark only the *trans* isomer was formed but in the presence of light both *trans* and *cis* are present, therefore *trans-cis* isomerisation was photoinduced. The reverse (*cis-trans*) thermal isomerisation was accessible for most complexes in the dark at 60 °C. DFT calculations were carried out for some of the complexes showed that thermodynamically most stable isomer is the *trans* form, but the energy barrier to *cis-trans* isomerisation is higher in comparison to free imines. This work has shown that *exo*-imine complexes provide a good framework for the synthesis of molecular switches whilst having the control of the barrier of thermal switching.

The isomerisation of complexes imines was pursued further by synthesising half-sandwich complexes as shown in Chapter 4. The work in Chapter 4 demonstrated that the nature of the R group in *exocyclic* imine ligands, the nature of the chelating attaching group and ML fragment can all have an effect in the photoisomerisation and the thermal stability of the isomers. In both N<sup>^</sup>O and N<sup>^</sup>N ligands, a 5-membered *exocyclic* chelate ring is formed, but the N<sup>^</sup>O chelate is aromatic whilst the N<sup>^</sup>N is saturated making the N<sup>^</sup>N chelate ring slightly more flexible. It was noted that changing the chelating ligand from N<sup>^</sup>O to N<sup>^</sup>N influences which isomer is preferred.

In the future, kinetic studies using UV-Vis spectrometer would need to be carried out in the complexes in Chapter 3, where the isomerisation is reversible. Some complexes with higher energy barrier would need to be exposed to higher temperature to be able to overcome the energy barrier of isomerisation. However, decomposition or ligand dissociation would need to be taken into consideration while carrying out these studies. Furthermore, different solvent mixtures could be used to try to physically separate the *cis* form as this was unsuccessful in this study.

In Chapter 4, additional studies would need to be carried out in establishing the reverse process and to see how robust the complexes are after repeating switching processes between *cis* and *trans* isomers. Using different wavelengths of light could also be used to establish which isomer is preferred at different wavelengths. When carrying out these studies it is important to keep in mind the stability of these complexes, as any decomposition or ligand dissociation could affect the results.

## Chapter 6: Experimental

### 6.1 General information and materials

All reactions for the syntheses of all complexes were carried out at room temperature and under inert atmosphere of nitrogen. On some occasions, reactions were carried out in the absence of light by wrapping the flask in aluminium foil (Chapter 3 and 4). After work up, all the complexes were air stable but were sensitive to light in solution (Chapter 3 and 4).

All starting materials were obtained from Precious Metal Online ( $\text{IrCl}_3 \cdot 3\text{H}_2\text{O}$ ), Aldrich (2-aminophenol, 2-picolyamine, mesityldehyde), Alfa Aesar (2-phenylpyridine, 1-phenylpyrazole, anisaldehyde), Fluorochem (pentafluorobenzaldehyde), Lancaster (*trans*-cinnamaldehyde, benzaldehyde) or Fisher Scientific ( $\text{Na}_2\text{CO}_3$ ,  $\text{KPF}_6$ ).

1D and 2D NMR spectra were obtained using a Bruker DRX 400 and DRX 500 MHz spectrometer. Chemical shifts were recorded in ppm (on  $\delta$  scale with tetramethylsilane as internal reference), and coupling constants are reported in Hz.

The compounds were analysed by LC-MS using a Xevo QToF mass spectrometer (Waters) coupled to an Acquity LC system (Waters) using ASAP (Atmospheric Solids Analysis Probe), the corona discharge pin current was 5  $\mu\text{A}$ , cone voltage 30 V and collision energy 4 eV.

The MS acquisition rate was 5 spectra per second and  $m/z$  data ranging from 50 to 1000 Da was collected. Mass accuracy was carried out by Mr Mick Lee by using a reference lock mass scan, once every 10 seconds in ESI mode. The electrospray (ES) mass spectra were recorded using a micromass Quattro LC mass spectrometer in HPLC grade acetonitrile.

X-Ray Crystallography was carried out by Mr Kuldip Singh on a Bruker APEX 2000 CCD diffractometer at 150 K using graphite-monochromated  $\text{Mo-K}_\alpha$  radiation ( $\lambda = 0.71073 \text{ \AA}$ ). The data was corrected for Lorentz and polarization effects, and empirical absorption corrections were applied. Structure solution by direct methods and structure refinement based on full-matrix least-squares on  $F^2$  employed SHELXTL, version 6.10. Hydrogen atoms were included in calculated positions ( $\text{C-H} = 0.95\text{--}1.00 \text{ \AA}$ ) riding on the bonded atom with isotropic displacement parameters set to  $1.5 U_{\text{eq}}(\text{C})$  for methyl H atoms and  $1.2 U_{\text{eq}}(\text{C})$  for all other H atoms. All non-H atoms were refined with anisotropic displacement parameters.

UV–Vis absorption measurements were carried out on a Shimadzu UV–1600 series spectrometer in HPLC grade acetonitrile unless stated otherwise. Luminescence studies were performed using a Jobin Yvon Horiba Fluoromax–P spectrofluorimeter in HPLC grade acetonitrile and deionised water at 0.02 mM concentration. Samples were carried out in air unless stated otherwise. The experimental data obtained for Table 2.4 (Chapter 2) are the following: the solid-state emission spectra were obtained at 298 K by drop-casting a DCM solution of each complex onto a glass slide; the absolute quantum yields were determined with an integrating sphere coupled to the PTI fluorimeter; the neat solid quantum yields were obtained from drop-casting of a DCM/hexane (1:1) solution of each complex and the PMMA matrix quantum yields were drop-cast from DCM.

Photoisomerisation studies were carried out using 3–5 mg of complex in  $\text{CDCl}_3$  in an NMR tube and exposed to a halogen lamp and/or ambient light. Samples kept in the dark were wrapped in foil. Solid state isomerisation studies (Chapter 3) was carried out using samples of 100% *trans* isomer. For the control, a sample of *trans* isomer crystals were dissolved in minimum amount of DCM in the dark then placed on a glass plate to create a thin film. The same was repeated for the test sample. When the DCM evaporated, only the control was wrapped in foil and both (control and test) samples were exposed to the halogen lamp. After exposure, the ratio for both samples were obtained by  $^1\text{H}$  NMR spectroscopy in  $\text{CDCl}_3$ .

In Chapter 2, all complexes except **2.24a-Mes** and **2.24b-Mes** were studied by *ab initio* DFT and TD-DFT calculations performed by Professor Francesco Lej using Gaussian09, version C01. Preliminary calculations were performed using the hybrid xc functional B3LYP<sup>1</sup>; this has been shown to have some drawbacks because of the wrong asymptotic behavior; therefore the 1 parameter xc functionals mPW1PW91<sup>2</sup> and the PB1PBE<sup>3</sup> and the more recent M06<sup>4</sup> meta-hybrid functional were also used. For all second period atoms the Dunning<sup>5</sup> all electron basis set augmented by a set of d polarization functions (D95(d)) was used. Hydrogen atoms not involved in any hydrogen bond, were described by the same Dunning basis set that does not include p polarization functions. For Ir the new double  $\zeta$  Stuttgart<sup>6</sup> basis set including f polarization functions and relativistic effects by a fully relativistic small core pseudopotential<sup>3</sup> (SDD09) were used and not the default SDD as included in Gaussian09c01. The ultrafine option with 99590 grid points was used thoroughly for the integral calculations for all atoms except Ir where a total of 1566228 grid points

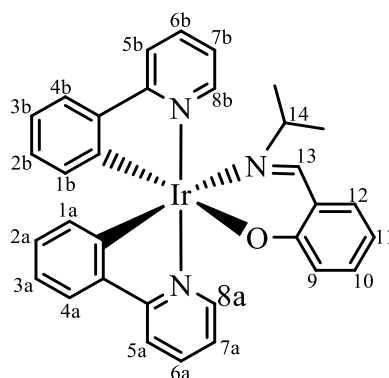
were used. The first triplet state structure was computed using the unrestricted approach. All energy minimized structures were characterized by the calculation of the Hessian matrix in order to check that they were minima and not simple stationary points on the molecular Born-Oppenheimer energy surface. Wavefunctions were checked against possible internal instability.<sup>7, 8</sup> TD-DFT calculations were performed by increasing the initial configuration space for the Davidson<sup>9</sup> diagonalization, unlike the default option in the program. A dichloromethane solvent environment was simulated by the self-consistent reaction field.<sup>10</sup> Vibrational band structure was evaluated by computing the Frank-Condon contribution<sup>11, 12</sup> between the ground state  $S_0$  structure and  $T_1$  structures and their harmonic vibrational properties. Further  $T_1$  structures were computed constraining the O<sup>^</sup>N-Ph ligand conformation of the N-Ir-O-C and C-N-Ir-O dihedral angle as in the ground state while optimizing all the remaining geometrical parameters to simulate the effect of the solid state constraining those internal degrees of freedom. DFT calculations were performed by Professor Francesco Lelej. The reported computations in Chapter 3 and 4 were performed by using the Gaussian09 rev. D.01 software.<sup>13</sup> All studies were performed by applying the Density Functional Theory (DFT).<sup>14, 15</sup> SCF and structure optimization convergence criteria are the default ones using the D95(d,p)<sup>5</sup> basis sets as in case of geometry optimization For Ir and Ru the new double  $\zeta$  Stuttgart<sup>6</sup> basis set including f polarization functions and relativistic effects by a fully relativistic small core pseudopotential (SDD09) were used and not the default SDD as included in Gaussian09 rev. D.01. Solvation effects were included by the means of the IEFPCM method<sup>10, 16, 17</sup> implemented in the standard software without any change with respect to the default parameters. Different xc functionals, hybrid PBE1PBE,<sup>18</sup> double hybrid B2PLYPD3,<sup>19</sup> and meta-hybrid M06 xc functional<sup>4</sup> were used in some computations. In all the computations, the integration grid was augmented in comparison to the default one (“int=ultrafine” key), as suggested for limiting errors originated by small integration-grids in energy computations with meta-GGA xc functionals.<sup>20</sup> Triplet states were computed using the unrestricted approach within DFT.

## 6.2 Experimental procedures for Chapter 2

### General procedure for synthesis of $[\text{Ir}(\text{C}^{\wedge}\text{N})_2\text{N}^{\wedge}\text{O}]$ ( $\text{N}^{\wedge}\text{O}$ = salicylimine)

The appropriate dimer  $[\text{Ir}(\text{C}^{\wedge}\text{N})_2\mu\text{-Cl}]_2$ , the relevant imine (2.2 equiv) and  $\text{Na}_2\text{CO}_3$  or  $\text{NaOMe}$  (2.2 equiv) were placed in an evacuated Schlenk tube and allowed to stir at room temperature under nitrogen atmosphere in dry  $\text{MeOH}$  (6-10 ml). The reaction was monitored by  $^1\text{H}$  NMR spectroscopy until completion and the solvent was removed *in vacuo* leaving behind the crude product which was dissolved in  $\text{DCM}$  (8-12 ml) and passed through celite to remove  $\text{NaCl}$ . The filtrate was reduced in volume and hexane was added slowly to induce precipitation. The precipitate was isolated, washed with hexane and dried *in vacuo*. In certain reactions, column chromatography was used to purify the product.

### Complex **2.24a-*i*Pr**



Complex **2.24a-*i*Pr** was prepared using dimer **2.23a** (60 mg, 0.056 mmol),  $\text{N}^{\wedge}\text{OH}$  ligand **L2.24-*i*Pr** (20 mg, 0.123 mmol) and  $\text{NaOMe}$  (7 mg, 0.123 mmol) and was left to stir at room temperature for 3 h in dry  $\text{MeOH}$  (7 ml). After passing through celite, the crude product was purified using column chromatography (silica) and eluted with  $\text{DCM}:\text{MeOH}$  (9:1) to give a yellow solid (53 mg, 72%). Complex **2.24a-*i*Pr** was crystallised from  $\text{DCM}/\text{hexane}$ .

$^1\text{H}$  NMR (400 MHz,  $\text{CDCl}_3$ )  $\delta$  8.92 (1H, d,  $J = 5.1$  Hz,  $\text{H}^{8\text{b}}$ ), 8.49 (1H, d,  $J = 5.1$  Hz,  $\text{H}^{8\text{a}}$ ), 8.15 (1H, s,  $\text{H}^{13}$ ), 7.83 (1H, d,  $J = 8.3$  Hz,  $\text{H}^{5\text{b}}$ ), 7.80 (1H, d,  $J = 8.0$  Hz,  $\text{H}^{5\text{a}}$ ), 7.73 (1H, td,  $J = 1.2$  Hz, 7.5 Hz,  $\text{H}^{6\text{b}}$ ), 7.62 (1H, t,  $J = 7.8$  Hz,  $\text{H}^{6\text{a}}$ ), 7.58 (1H, d,  $J = 7.7$  Hz,  $\text{H}^{4\text{b}}$ ), 7.52 (1H, d,  $J = 7.1$  Hz,  $\text{H}^{4\text{a}}$ ), 7.16-7.06 (3H, m,  $\text{H}^{7\text{b}}$ ,  $\text{H}^{10}$ ,  $\text{H}^{12}$ ), 6.93 (1H, t,  $J = 6.3$  Hz,  $\text{H}^{7\text{a}}$ ), 6.80 (2H, m,  $\text{H}^{3\text{a}}$ ,  $\text{H}^{3\text{b}}$ ), 6.71 (1H, td,  $J = 0.9, 7.4$  Hz,  $\text{H}^{2\text{a}}$  or  $\text{H}^{2\text{b}}$ ), 6.65 (1H, td,  $J = 1.1, 8.4$  Hz,  $\text{H}^{2\text{a}}$  or  $\text{H}^{2\text{b}}$ ), 6.62 (1H, d,  $J = 8.6$  Hz,  $\text{H}^9$ ), 6.37 – 6.35 (2H, m,  $\text{H}^{11}$ ,  $\text{H}^{1\text{a}}$

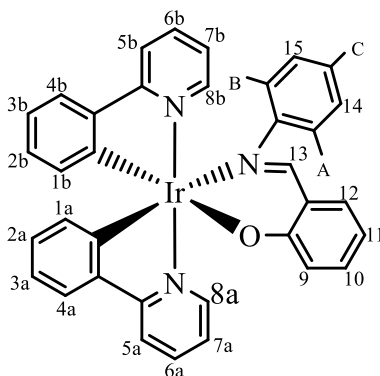
or H<sup>1b</sup>), 6.15 (1H, d,  $J = 7.4$  Hz, H<sup>1a</sup> or H<sup>1b</sup>), 3.54 (1H, sept,  $J = 6.7$  Hz, H<sup>14</sup>), 1.12 (3H, d,  $J = 6.7$  Hz, CH(CH<sub>3</sub>)<sub>2</sub>), 0.53 (3H, d,  $J = 6.6$  Hz, CH(CH<sub>3</sub>)<sub>2</sub>).

<sup>13</sup>C{<sup>1</sup>H} NMR (100 MHz, CDCl<sub>3</sub>)  $\delta$  168.5, 158.8 (C<sup>13</sup>), 152.8, 151.2, 149.2 (C<sup>8b</sup>), 148.9 (C<sup>8a</sup>), 144.4, 136.8 (C<sup>5b</sup>), 136.5 (C<sup>6a</sup>), 134.6 (C<sup>6b</sup>), 133.5, 133.1 (C<sup>1a</sup> or C<sup>1b</sup>), 131.9 (C<sup>1a</sup> or C<sup>1b</sup>), 129.4 (C<sup>2a</sup> or C<sup>2b</sup>), 129.2 (C<sup>2a</sup> or C<sup>2b</sup>), 124.2, 123.8 (C<sup>4b</sup>), 123.7 (C<sup>4a</sup>), 121.9, 121.6, 121.3, 121.2 (C<sup>7a</sup>), 120.1, 118.9 (C<sup>5a</sup>), 118.0 (C<sup>5b</sup>), 113.1 (C<sup>11</sup>), 57.2 (C<sup>14</sup>), 23.3 (CH(CH<sub>3</sub>)<sub>2</sub>), 23.2 (CH(CH<sub>3</sub>)<sub>2</sub>).

**HR ESI-MS:** Calcd for C<sub>32</sub>H<sub>29</sub>N<sub>3</sub>OIr: 664.1940; Found: 664.1935 [M+H]<sup>+</sup>.

**IR (solid state):**  $\nu$ (C=N)<sub>imine</sub> 1581 cm<sup>-1</sup>

### Complex 2.24a-Mes



Complex **2.24a-Mes** was prepared using dimer **2.23a** (100 mg, 0.093 mmol), N<sup>^</sup>OH ligand **L2.24-Mes** (49 mg, 0.205 mmol) and Na<sub>2</sub>CO<sub>3</sub> (22 mg, 0.205 mmol) in dry MeOH (6 ml) and allowed to stir overnight at room temperature. After passing through celite, the crude product was precipitated with hexane and washed several times to remove the excess ligand to give an orange solid (104 mg, 76%).

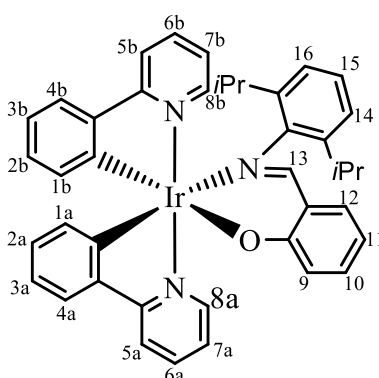
<sup>1</sup>H NMR (500 MHz, CDCl<sub>3</sub>)  $\delta$  9.16 (1H, dd,  $J = 5.7, 0.8$  Hz, H<sup>8b</sup>), 8.85 (1H, d,  $J = 5.4$  Hz, H<sup>8a</sup>), 7.92 (1H, s, H<sup>13</sup>), 7.81 (1H, d,  $J = 7.9$  Hz, H<sup>5a</sup>), 7.67 – 7.61 (2H, m, H<sup>6a</sup>, H<sup>6b</sup>), 7.54 (1H, dd,  $J = 7.8, 0.7$  Hz, H<sup>4a</sup>), 7.51 (1H, d,  $J = 8.0$  Hz, H<sup>5b</sup>), 7.16 (1H, ddd,  $J = 8.7, 6.8, 1.9$  Hz, H<sup>10</sup>), 7.10 – 7.06 (2H, m, H<sup>7b</sup>, H<sup>12</sup>), 6.94 (1H, dd,  $J = 7.8, 0.9$  Hz, H<sup>4b</sup>), 6.91 (1H, ddd,  $J = 7.4, 6.0, 1.4$  Hz, H<sup>7a</sup>), 6.77 (1H, t,  $J = 7.5$  Hz, H<sup>3a</sup>), 6.65 – 6.62 (2H, m, H<sup>2a</sup>, H<sup>9</sup>), 6.51 (1H, t,  $J = 7.4$  Hz, H<sup>3b</sup>), 6.43 (1H, td,  $J = 7.4, 1.2$  Hz, H<sup>2b</sup>), 6.41 – 6.37 (2H, m, H<sup>11</sup>, H<sup>15</sup>), 6.27 (1H, dd,  $J = 7.5, 0.8$  Hz, H<sup>1b</sup>), 6.14 (1H, s, H<sup>14</sup>), 5.98 (1H, d,  $J = 7.8$  Hz, H<sup>1a</sup>), 2.05 (3H, s, Me<sup>C</sup>), 1.93 (3H, s, Me<sup>A</sup>), 1.21 (3H, s, Me<sup>B</sup>).

$^{13}\text{C}\{^1\text{H}\}$  NMR (125 MHz,  $\text{CDCl}_3$ )  $\delta$  169.3, 169.1, 167.9, 164.0, 151.2, 150.6, 149.5, 148.2, 147.5, 144.6, 144.3, 136.8, 136.6, 135.1, 134.3, 134.2 (2 x C), 131.7, 129.6, 129.4 (2 x C), 129.0, 128.4, 127.8, 127.3, 126.4, 124.7, 123.8, 122.4, 122.1, 121.0, 120.2, 119.6, 118.3, 118.2, 113.2, 31.0, 21.7, 20.4, 16.9.

**HR-MS (ASAP):**  $\text{C}_{38}\text{H}_{32}\text{Ir}^{193}\text{N}_3\text{O}$  calculated:  $m/z$  740.2253; Found:  $m/z$  740.2260  $[\text{M}+\text{H}]^+$ .

**IR (solid state):**  $\nu(\text{C}=\text{N})_{\text{imine}}$  1581  $\text{cm}^{-1}$

### Complex 2.24a-Dipp



Complex **2.24a-Dipp** was prepared using dimer **2.23a** (80 mg, 0.075 mmol),  $\text{N}^{\text{OH}}$  ligand **L2.24-Dipp** (46 mg, 0.165 mmol) and NaOMe (9 mg, 0.165 mmol) in dry MeOH (7 ml) and was left to reflux overnight. After passing through celite, the crude product was purified using column chromatography (alumina) and eluted with Petroleum ether:diethyl ether (100:0 to 80:20) to give an orange solid (72 mg, 61%). Complex **2.24a-Dipp** was crystallised from  $\text{CHCl}_3/\text{MeOH}$ .

$^1\text{H}$  NMR (400 MHz,  $\text{CDCl}_3$ )  $\delta$  9.25 (1H, d,  $J = 5.1$  Hz,  $\text{H}^{8\text{a}}$ ), 8.82 (1H, d,  $J = 5.4$  Hz,  $\text{H}^{8\text{b}}$ ), 8.01 (1H, s,  $\text{H}^{13}$ ), 7.80 (1H, d,  $J = 7.6$  Hz,  $\text{H}^{5\text{a}}$ ), 7.66-7.61 (2H, m,  $\text{H}^{6\text{a}}$ ,  $\text{H}^{6\text{b}}$ ), 7.57 (1H, d,  $J = 7.6$  Hz,  $\text{H}^{5\text{b}}$ ), 7.50 (1H, d,  $J = 7.9$  Hz,  $\text{H}^{4\text{a}}$ ), 7.19-7.14 (2H, m,  $\text{H}^{7\text{a}}$ ,  $\text{H}^9$  or  $\text{H}^{10}$  or  $\text{H}^{11}$ ), 7.05 (2H, m,  $\text{H}^{4\text{b}}$ ,  $\text{H}^{12}$ ), 6.93 (1H, td,  $J = 1.3$  Hz, 6.6 Hz,  $\text{H}^{7\text{b}}$ ), 6.86 (1H, t,  $J = 7.6$  Hz,  $\text{H}^{15}$ ), 6.80 (1H, dd,  $J = 0.9$ , 7.6 Hz,  $\text{H}^{14}$  or  $\text{H}^{16}$ ), 6.75 (1H, t,  $J = 7.1$  Hz,  $\text{H}^{3\text{a}}$ ), 6.64-6.59 (3H, m,  $\text{H}^{2\text{a}}$ ,  $\text{H}^{10}$  or  $\text{H}^{11}$ ,  $\text{H}^{14}$  or  $\text{H}^{16}$ ), 6.50 (2H, m,  $\text{H}^{2\text{b}}$ ,  $\text{H}^{3\text{b}}$ ), 6.40 (1H, t,  $J = 7.1$  Hz,  $\text{H}^{10}$  or  $\text{H}^{11}$ ), 6.17 (1H, d,  $J = 7.6$  Hz,  $\text{H}^{1\text{b}}$ ), 5.59 (1H, d,  $J = 7.6$  Hz,  $\text{H}^{1\text{a}}$ ), 3.33 (1H, sept,  $J = 6.7$  Hz,  $\text{CH}(\text{CH}_3)_2$ ), 2.48 (1H, sept,  $J = 6.4$  Hz,  $\text{CH}(\text{CH}_3)_2$ ), 1.14 (3H, d,

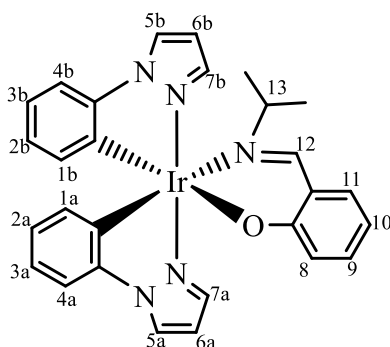
$J = 7.0$  Hz,  $\text{CH}(\text{CH}_3)_2$ ), 0.89 (3H, d,  $J = 6.7$  Hz,  $\text{CH}(\text{CH}_3)_2$ ), 0.88 (3H, d,  $J = 6.9$  Hz,  $\text{CH}(\text{CH}_3)_2$ ), 0.39 (3H, d,  $J = 6.7$  Hz,  $\text{CH}(\text{CH}_3)_2$ ).

$^{13}\text{C}\{^1\text{H}\}$  NMR (100 MHz,  $\text{CDCl}_3$ )  $\delta$  168.4, 168.1, 167.3, 164.8 ( $\text{C}^{13}$ ), 149.7 ( $\text{C}^{8b}$ ), 149.4, 148.1 ( $\text{C}^{8a}$ ), 147.9, 146.2, 143.3, 143.1, 140.6, 139.0, 135.9 ( $\text{C}^{6a}$  or  $\text{C}^{6b}$ ), 135.7 ( $\text{C}^{6a}$  or  $\text{C}^{6b}$ ), 134.1, 133.5 ( $\text{C}^{1b}$ ), 129.9 ( $\text{C}^{1a}$ ), 128.3, 127.8, 124.7, 123.3 ( $\text{C}^{4b}$ ), 122.7, 121.9, 121.7, 121.0, 120.9, 120.7, 120.1 ( $\text{C}^{7b}$ ), 118.7 ( $\text{C}^{5b}$ ), 118.5 ( $\text{C}^{5a}$ ), 117.7, 117.3, 112.6, 26.9 ( $\text{CH}(\text{CH}_3)_2$ ), 26.7( $\text{CH}(\text{CH}_3)_2$ ), 26.6( $\text{CH}(\text{CH}_3)_2$ ) , 24.5 ( $\text{CH}(\text{CH}_3)_2$ ), 21.6 ( $\text{CH}(\text{CH}_3)_2$ ), 20.6 ( $\text{CH}(\text{CH}_3)_2$ ).

**HR ESI-MS:** Calcd for  $\text{C}_{41}\text{H}_{39}\text{N}_3\text{OIr}$ : 782.2723; Found: 782.2726  $[\text{M}+\text{H}]^+$ .

**IR (solid state):**  $\nu(\text{C}=\text{N})_{\text{imine}}$  1581  $\text{cm}^{-1}$

### Complex **2.24b-*i*Pr**



Complex **2.24b-*i*Pr** was prepared using dimer **2.23b** (90 mg, 0.088 mmol),  $\text{N}^{\wedge}\text{OH}$  ligand **L2.24-*i*Pr** (32 mg, 0.194 mmol) and NaOMe (10 mg, 0.194 mmol) and was left to stir for 6 hrs in dry MeOH (10 ml). After passing through celite, the crude product was purified using column chromatography (silica) and eluted with DCM:MeOH (20:0.5) to give a yellow solid (84 mg, 74%).

$^1\text{H}$  NMR (500 MHz,  $\text{CDCl}_3$ )  $\delta$  8.06 (1H, s,  $\text{H}^{12}$ ), 8.04 (1H, d,  $J = 2.6$  Hz,  $\text{H}^{7a}$ ), 7.95 (1H, d,  $J = 2.6$  Hz,  $\text{H}^{7b}$ ), 7.66 (1H, d,  $J = 1.9$  Hz,  $\text{H}^{5a}$ ), 7.47 (1H, d,  $J = 1.9$  Hz,  $\text{H}^{5b}$ ), 7.17 (1H, ddd,  $J = 1.9, 6.8, 8.6$  Hz,  $\text{H}^9$  or  $\text{H}^{10}$ ), 7.13 (1H, dd,  $J = 0.8, 7.9$  Hz,  $\text{H}^{4a}$  or  $\text{H}^{4b}$ ), 7.08 (2H, m,  $\text{H}^{4a}$  or  $\text{H}^{4b}$ ,  $\text{H}^{11}$ ), 6.82 – 6.78 (2H, m,  $\text{H}^{3a}$ ,  $\text{H}^{3b}$ ), 6.68 – 6.65 (2H, m,  $\text{H}^{2b}$ ,  $\text{H}^8$ ), 6.61 (1H, td,  $J = 1.1, 7.3$  Hz,  $\text{H}^{2a}$ ), 6.58 (1H, t,  $J = 2.6$  Hz,  $\text{H}^{6a}$ ), 6.46 (1H, t,  $J = 2.6$  Hz,  $\text{H}^{6b}$ ), 6.38 (1H, t,  $J = 7.3$  Hz,  $\text{H}^9$  or  $\text{H}^{10}$ ), 6.25 (1H, dd,  $J = 0.9, 7.5$  Hz,  $\text{H}^{1a}$ ), 6.18

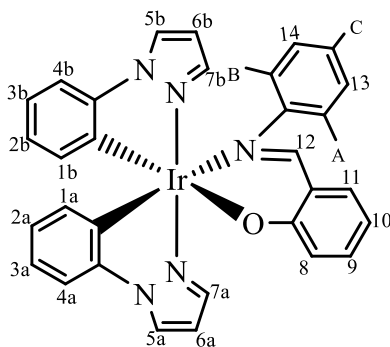
(1H, d,  $J = 0.9, 7.6$  Hz,  $H^{1b}$ ), 3.72 (1H, sept,  $J = 6.6$  Hz,  $H^{13}$ ), 1.18 (3H, d,  $J = 6.7$  Hz,  $CH(CH_3)_2$ ), 0.55 (3H, d,  $J = 6.7$  Hz,  $CH(CH_3)_2$ ).

$^{13}C\{^1H\}$  NMR (125 MHz,  $CDCl_3$ )  $\delta$  166.5 ( $C^{12}$ ), 159.2, 144.2 ( $C^{5a}$ ), 143.9 ( $C^{5b}$ ), 138.5 ( $C^{11}$ ), 138.2, 134.9, 134.8 ( $C^9$  or  $C^{10}$ ), 134.2, 133.5, 131.5, 125.9 ( $C^{7b}$ ), 125.6 ( $C^{2a}$  or  $C^{2b}$ ), 125.6 ( $C^{2a}$  or  $C^{2b}$ ), 125.2 ( $C^{7a}$ ), 123.5 ( $C^8$ ), 122.1, 121.7 ( $C^{3a}$  or  $C^{3b}$ ), 120.8 ( $C^{3a}$  or  $C^{3b}$ ), 112.9 ( $C^9$  or  $C^{10}$ ), 110.5 ( $C^{4a}$  or  $C^{4b}$ ), 110.4 ( $C^{4a}$  or  $C^{4b}$ ), 107.0 ( $C^{6a}$ ), 106.8 ( $C^{6b}$ ), 58.3 ( $C^{13}$ ), 23.0 ( $CH(CH_3)_2$ ), 22.8 ( $CH(CH_3)_2$ ).

**HR ESI-MS:** Calcd for  $C_{28}H_{27}N_5OIr$ : 642.1845; Found: 642.1849  $[M+H]^+$ .

**IR (solid state):**  $\nu(C=N)_{imine}$  1598  $cm^{-1}$

### Complex 2.24b-Mes



Complex **2.24b-Mes** was prepared using dimer **2.24b** (70 mg, 0.068 mmol),  $N^A OH$  ligand **L2.24-Mes** (36 mg, 0.150 mmol) and  $Na_2CO_3$  (16 mg, 0.150 mmol) and was left to stir for 4 h at room temperature in dry MeOH (6 ml). After passing through celite, the crude product was precipitated with hexane and washed several times to remove the excess ligand to give a yellow solid (74 mg, 76%).

$^1H$  NMR (500 MHz,  $CDCl_3$ )  $\delta$  8.00 (1H, d,  $J = 1.5$  Hz,  $H^{5b}$ ), 7.96 (1H, d,  $J = 2.5$  Hz,  $H^{7a}$ ), 7.83 (1H, s,  $H^{12}$ ), 7.80 (1H, d,  $J = 2.5$  Hz,  $H^{7b}$ ), 7.68 (1H, d,  $J = 1.6$  Hz,  $H^{5a}$ ), 7.16 (1H, t,  $J = 7.8$  Hz,  $H^9$  or  $H^{10}$ ), 7.10 (1H, d,  $J = 7.9$  Hz,  $H^{4a}$ ), 7.07 (1H, d,  $J = 7.6$  Hz,  $H^{11}$ ), 6.79 (1H, t,  $J = 7.5$  Hz,  $H^{2a}$  or  $H^{3a}$ ), 6.62 – 6.59 (4H, m,  $H^9$  or  $H^{10}$ ,  $H^{2a}$  or  $H^{3a}$ ,  $H^{4b}$ ,  $H^{6b}$ ), 6.52 (1H, t,  $J = 7.5$  Hz,  $H^{2b}$  or  $H^{3b}$ ), 6.43 – 6.38 (4H, m,  $H^{2b}$  or  $H^{3b}$ ,  $H^{6a}$ ,  $H^8$ ,  $H^{14}$ ), 6.27 (1H, d,  $J = 7.3$  Hz,  $H^{1b}$ ), 6.21 (1H, s,  $H^{13}$ ), 5.97 (1H, d,  $J = 7.5$  Hz,  $H^{1a}$ ), 2.04 (6H, s, *ortho*-Me<sub>A</sub>, *para*-Me<sub>C</sub>), 1.43 (3H, s, *ortho*-Me<sub>B</sub>).



$^{13}\text{C}\{^1\text{H}\}$  NMR (125 MHz,  $\text{CDCl}_3$ )  $\delta$  168.6, 166.0 ( $\text{C}^{12}$ ), 149.2, 143.7, 141.4, 139.9, 139.8 ( $\text{C}^{7a}$ ), 138.2 ( $\text{C}^{7b}$ ), 134.5, 136.4 ( $\text{C}^{1b}$ ), 135.0 ( $\text{C}^{11}$ ), 134.5 ( $\text{C}^9$ ), 133.5 ( $\text{C}^{1a}$ ), 132.5, 127.7, 126.0, 125.8 ( $\text{C}^{5b}$ ), 125.7 ( $\text{C}^{5a}$ ), 125.6, 124.9 ( $\text{C}^{2b}$ ), 123.9, 123.0, 122.0, 121.9 ( $\text{C}^{3a}$ ), 121.7, 120.3 ( $\text{C}^{3b}$ ), 113.6 ( $\text{C}^{10}$ ), 110.4 ( $\text{C}^{4a}$ ), 109.3, 108.1, 106.2 ( $\text{C}^{6a}$ ), 27.7 ( $\text{CH}(\text{CH}_3)_2$ ), 27.2 ( $\text{CH}(\text{CH}_3)_2$ ), 27.4 ( $\text{CH}(\text{CH}_3)_2$ ), 25.7 ( $\text{CH}(\text{CH}_3)_2$ ), 23.3 ( $\text{CH}(\text{CH}_3)_2$ ), 21.8 ( $\text{CH}(\text{CH}_3)_2$ ).

**HR ESI-MS:** Calcd for  $\text{C}_{37}\text{H}_{37}\text{N}_5\text{OIr}$ : 760.2628; Found: 760.2626  $[\text{M}+\text{H}]^+$ .

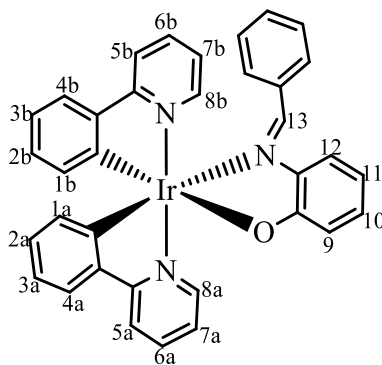
**IR (solid state):**  $\nu(\text{C}=\text{N})_{\text{imine}}$  1582  $\text{cm}^{-1}$

### 6.3 Experimental procedures for Chapter 3

#### General procedure for synthesis of $[\text{Ir}(\text{C}^{\wedge}\text{N})_2(\text{N}^{\wedge}\text{O})]$ ( $\text{N}^{\wedge}\text{O}$ = *exocyclic imine*)

The appropriate dimer  $[\text{Ir}(\text{C}^{\wedge}\text{N})_2\mu\text{-Cl}]_2$  (**2.23a-b**) (0.088 – 0.097 mmol, 90 – 100 mg), the relevant ligand **3.27-R** (2.1 – 2.2 equiv) and  $\text{Na}_2\text{CO}_3$  (2.1 – 2.2 equiv) were placed in an evacuated Schlenk tube which was wrapped in aluminium foil to protect it from light (unless stated otherwise) and allowed to stir at room temperature under nitrogen atmosphere in dry MeOH (10 ml). The reaction was monitored by  $^1\text{H}$  NMR spectroscopy until completion and the solvent was removed *in vacuo* leaving behind the crude product which was dissolved in DCM (8-12 ml) and passed through celite to remove NaCl. The crude filtrate was purified using column chromatography with silica as the stationary phase and DCM:MeOH as the mobile phase. In this section, the  $^1\text{H}$  NMR data of the *cis* isomers have not been fully assigned due to the overlap of the *trans* isomers in the mixtures. However, some key data has been described in the results and discussion of Chapter 3.

#### Complex 3.27a-Ph



Complex **3.27a-Ph** was prepared using dimer **2.23a** (100 mg, 0.093 mmol), ligand **L3.27-Ph** (39 mg, 0.196 mmol) and Na<sub>2</sub>CO<sub>3</sub> (21 mg, 0.196 mmol) and was left to stir for 4 h in dry MeOH (10 ml). After passing through celite, the crude product was purified using column chromatography (silica) and eluted with DCM:MeOH (20:0.5) to give an orange-red solid (96 mg, 74%). Product was recrystallized using DCM:MeOH to give red crystals on *trans*-**3.27a-Ph**.

#### *Trans*-**3.27a-Ph**

<sup>1</sup>H NMR (400 MHz, CDCl<sub>3</sub>) δ 8.77 (1H, s, H<sup>13</sup>), 8.69 (1H, ddd, *J* = 5.7, 1.6, 0.7 Hz, H<sup>8a</sup>), 8.58 (1H, ddd, *J* = 5.8, 1.7, 0.8 Hz, H<sup>8b</sup>), 7.84 (1H, d, *J* = 7.9 Hz, H<sup>5b</sup>), 7.67 (1H, ddd, *J* = 8.2, 7.4, 1.5 Hz, H<sup>6b</sup>), 7.54 (1H, ddd, *J* = 8.2, 7.4, 1.6 Hz, H<sup>6a</sup>), 7.50 (1H, dd, *J* = 7.8, 1.2 Hz, H<sup>aryl</sup>), 7.30 (1H, d, *J* = 8.0 Hz, H<sup>5a</sup>), 7.10 – 7.05 (2H, m, H<sup>12</sup>, H<sup>9</sup> or H<sup>10</sup> or H<sup>11</sup>), 7.03 – 6.88 (5H, m, H<sup>7a</sup>, H<sup>7b</sup>, H<sup>3a</sup> or H<sup>4a</sup>, H<sup>3b</sup> or H<sup>4b</sup>, H<sup>9</sup> or H<sup>10</sup> or H<sup>11</sup>), 6.80 – 6.74 (3H, m, H<sup>3a</sup> or H<sup>4a</sup>, H<sup>3b</sup> or H<sup>4b</sup>, H<sup>aryl</sup>), 6.67 – 6.56 (5H, m, H<sup>2a</sup>, H<sup>2b</sup>, 3 x H<sup>aryl</sup>), 6.43 (1H, *J* = 8.0, 6.8, 1.3 Hz, H<sup>10</sup> or H<sup>11</sup>), 6.19 (1H, m, H<sup>1a</sup>), 5.98 (1H, dd, *J* = 7.7, 1.0 Hz, H<sup>1b</sup>).

<sup>13</sup>C{<sup>1</sup>H} NMR (100 MHz, CDCl<sub>3</sub>) δ 168.6, 168.4, 168.2, 162.8, 155.0, 150.5, 148.8, 147.0, 144.0, 143.9, 143.5, 136.5, 136.2, 132.9, 132.6, 131.7, 130.6, 129.4, 129.3, 129.2, 127.8, 126.7, 124.0, 123.8, 122.1, 121.4, 121.1, 121.0, 120.1, 119.8, 119.0, 117.4, 113.2.

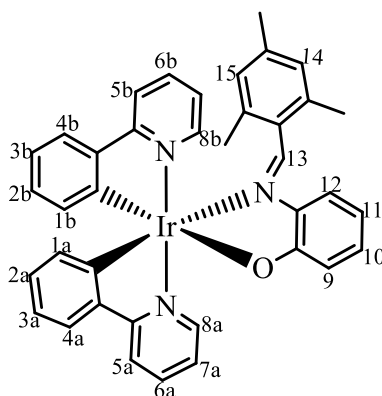
#### *Cis*-**3.27a-Ph**

<sup>1</sup>H NMR (400 MHz, CDCl<sub>3</sub>) δ 8.91 (1H, dd, *J* = 5.8, 0.9 Hz, H<sup>8a</sup> or H<sup>8b</sup>), 8.40 (1H, dd, *J* = 5.9, 0.8 Hz, H<sup>8a</sup> or H<sup>8b</sup>), 7.81 (1H, d, *J* = 8.0 Hz), 7.65 – 7.63 (1H, m), 7.34 (1H, s, H<sup>13</sup>), 7.25 – 6.69 (18H, m), 6.38 (1H, dd, *J* = 7.6, 0.8 Hz, H<sup>1a</sup> or H<sup>1b</sup>), 6.24 (1H, dd, *J* = 7.5, 0.9 Hz, H<sup>1a</sup> or H<sup>1b</sup>), 6.04 – 6.00 (1H, m).

**MS (ASAP):** Calcd for C<sub>35</sub>H<sub>26</sub>Ir<sup>193</sup>N<sub>3</sub>O 698.1784; Found *m/z* 698.1764 [M+H]<sup>+</sup>.

**IR (solid state):** ν(C=N)<sub>imine</sub> 1579 cm<sup>-1</sup>

### Complex 3.27a-Mes



Complex **3.27a-Mes** was prepared using dimer **2.23a** (100 mg, 0.093 mmol), ligand **L3.27-Mes** (47 mg, 0.196 mmol) and  $\text{Na}_2\text{CO}_3$  (21 mg, 0.196 mmol) was left to stir for 3 hrs in dry MeOH (10 ml). After passing through celite, the crude product was purified using column chromatography (silica) and eluted with DCM:MeOH (20:0.5). After evaporation of the solvent, a yellow solid was obtained. (112 mg, 81%).

#### *Trans*-3.27a-Mes

$^1\text{H}$  NMR (400 MHz,  $\text{CDCl}_3$ )  $\delta$  8.93 (1H, s,  $\text{H}^{13}$ ), 8.86 (1H, dd,  $J = 5.7, 1.0$  Hz,  $\text{H}^{8a}$  or  $\text{H}^{8b}$ ), 8.46 (1H, dd,  $J = 5.8, 0.8$  Hz,  $\text{H}^{8a}$  or  $\text{H}^{8b}$ ), 7.79 (1H, d,  $J = 7.8$  Hz) 7.67 – 7.62 (2H, m), 7.48 – 7.45 (2H, m), 7.24 (1H, dd,  $J = 8.0, 1.6$  Hz,  $\text{H}^{12}$ ), 7.11 – 7.06 (2H, m), 6.90 (1 H, m), 6.87 – 6.85 (2 H, m), 6.74 – 6.70 (1H, m), 6.57 – 6.43 (4H, m), 6.34 (1H, s,  $\text{H}^{14}$  or  $\text{H}^{15}$ ), 6.17 (1H, dd,  $J = 7.5, 0.9$  Hz,  $\text{H}^{1a}$  or  $\text{H}^{1b}$ ), 5.86 (1H, s,  $\text{H}^{14}$  or  $\text{H}^{15}$ ), 5.75 (1H, dd,  $J = 7.7, 0.8$  Hz,  $\text{H}^{1a}$  or  $\text{H}^{1b}$ ), 2.06 (3H, *ortho*-Me), 2.04 (3H, *para*-Me), 1.24 (3H, *ortho*-Me).

$^{13}\text{C}\{^1\text{H}\}$  NMR (100 MHz,  $\text{CDCl}_3$ )  $\delta$  169.5, 168.48, 168.3, 164.1( $\text{C}^{13}$ ), 150.6, 149.3, 148.4, 143.4, 138.9, 136.5, 136.0, 132.3( $\text{C}^{1a}$  or  $\text{C}^{1b}$ ), 131.1( $\text{C}^{1a}$  or  $\text{C}^{1b}$ ), 130.7, 129.4, 128.5 ( $\text{C}^{14}$  or  $\text{C}^{15}$ ), 128.2, 126.5 ( $\text{C}^{14}$  or  $\text{C}^{15}$ ), 123.9, 123.1, 121.4, 121.2, 121.3, 121.2, 119.3, 118.7, 118.6, 118.0, 113.2, 21.5 (*ortho*-Me), 21.1(*para*-Me), 18.6 (*ortho*-Me)

#### *Cis*-3.27a-Mes

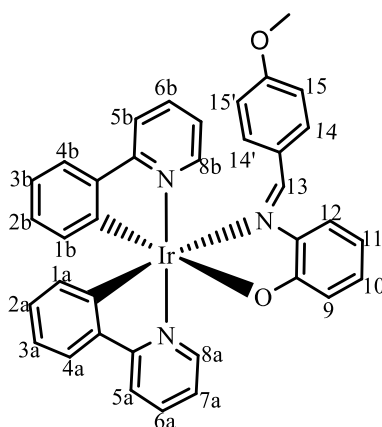
$^1\text{H}$  NMR (400 MHz,  $\text{CDCl}_3$ ):  $\delta$  8.92 (1H, d,  $J = 5.9$  Hz,  $\text{H}^{8a}$  or  $\text{H}^{8b}$ ), 8.42 (1H, d,  $J = 6.5$  Hz,  $\text{H}^{8a}$  or  $\text{H}^{8b}$ ), 7.87 – 7.82 (2H, m), 7.72 – 7.68 (1H, m), 7.57 (1H, dd,  $J = 7.7, 1.1$

Hz), 7.53 (1H, dd,  $J = 7.8, 1.2$  Hz), 7.12 – 7.06 (2H, m), 6.98 – 6.79 (6H, m), 6.67 (1H, s,  $H^{14}$  or  $H^{15}$ ), 6.58 – 6.44 (5H, m), 6.39 (1H, dd,  $J = 7.5, 0.9$  Hz,  $H^{1a}$  or  $H^{1b}$ ), 6.31 (1H, dd,  $J = 7.4, 0.8$  Hz,  $H^{1a}$  or  $H^{1b}$ ), 5.97 (1H, ddd,  $J = 8.4, 6.0, 2.3$  Hz), 2.24 (3H, s, Me), 2.16 (3H, s, Me), 1.23 (3H, s, Me).

**MS (ASAP):** Calcd for  $C_{38}H_{32}Ir^{193}N_3O$  740.2253; Found  $m/z$  740.2258  $[M+H]^+$ .

**IR (solid state):**  $\nu(C=N)_{imine}$  1579  $cm^{-1}$

### Complex 3.27a-Anisyl



Complex **3.27a-Anisyl** was prepared using dimer **2.23a** (100 mg, 0.093 mmol), ligand **L3.27-Anisyl** (44 mg, 0.196 mmol) and  $Na_2CO_3$  (21 mg, 0.196 mmol) was left to stir for 3 hrs in dry MeOH (10 ml). After passing through celite, the crude product was purified using column chromatography (silica) and eluted with DCM:MeOH (20:0.5) to give an orange solid (117 mg, 87%).

### *Trans*-3.27a-Anisyl

$^1H$  NMR (400 MHz,  $CDCl_3$ )  $\delta$  8.63 (1H, d,  $J = 5.6$  Hz,  $H^{8a}$  or  $H^{8b}$ ), 8.58 (1H, s,  $H^{13}$ ), 8.52 (1H, d,  $J = 5.7$  Hz,  $H^{8a}$  or  $H^{8b}$ ), 7.77 (1H, d,  $J = 8.0$  Hz), 7.60 (1H, t,  $J = 7.8$  Hz), 7.47 (1H, t,  $J = 7.8$  Hz), 7.43 (1H, dd,  $J = 7.7, 0.8$  Hz,  $H^{5a}$  or  $H^{5b}$ ), 7.27 (1H, d,  $J = 8.0$  Hz,  $H^{4a}$  or  $H^{4b}$ ), 7.01 – 6.87 (5H, m,  $H^{2a}$  or  $H^{2b}$ ), 6.80 (1H, dd,  $J = 8.3, 1.2$  Hz), 6.71 (1H, m), 6.66 (2H, d,  $J = 11.2$  Hz,  $H^{14}, H^{14'}$ ), 6.57 – 6.52 (3H, m), 6.35 (1H, t,  $J = 7.7$  Hz,  $H^{10}$  or  $H^{11}$ ), 6.16 – 6.12 (1H, m), 6.10 (2H, d,  $J = 8.8$  Hz,  $H^{15}, H^{15'}$ ), 5.93 (1H, dd,  $J = 7.6, 0.8$  Hz), 3.63 (3H, s,  $OCH_3$ ).



1.1), 7.24 (2H, m), 7.12 (2H, m), 6.98 (1H, m), 6.95 (1H, dd,  $J = 8.4, 1.2$ ), 6.78 (1H, td,  $J = 7.5, 1.1$ ), 6.62 (3H, m), 6.48 (1H, td,  $J = 7.5, 1.2$ ), 6.22 (1H, d,  $J = 7.1$ , H<sup>1a</sup> or H<sup>1b</sup>), 5.90 (1H, dd,  $J = 7.7, 1.0$ , H<sup>1a</sup> or H<sup>1b</sup>).

<sup>19</sup>F{<sup>1</sup>H} (376 MHz, CDCl<sub>3</sub>)  $\delta$  -137.88 (1F, d,  $J = 24.7$ ), -143.51 (1F, dd,  $J = 23.8, 6.74$ ), -152.10 (1F, t,  $J = 21.4$ ), -156.84 (1F, td,  $J = 24.1, 7.4$ ), -163.23 (1F, td,  $J = 21.7, 8.8$ ).

<sup>13</sup>C{<sup>1</sup>H} NMR (100 MHz, CDCl<sub>3</sub>)  $\delta$  179.1, 168.1, 147.6, 145.9, 143.8, 142.6, 142.5, 141.9, 140.5, 139.1, 135.6, 134.7, 134.4, 131.9, 129.9, 128.9, 126.8, 125.7, 125.3, 123.7, 123.3, 122.4, 120.7, 115.3, 112.9, 110.8, 106.9, 105.3.

### *Cis*-**3.27a**-C<sub>6</sub>F<sub>5</sub>

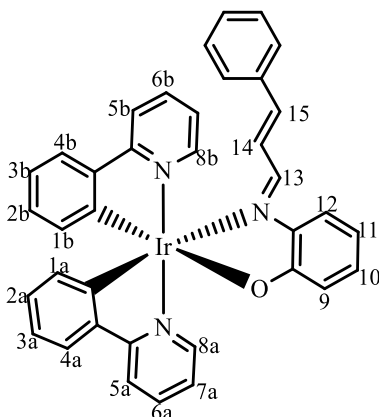
<sup>1</sup>H NMR (400 MHz, CDCl<sub>3</sub>)  $\delta$  8.05 (1H, d,  $J = 2.0$  Hz, H<sup>8a</sup> or H<sup>8b</sup>), 7.65 – 6.63 (1H, m), 7.49 – 7.47 (1H, m), 7.39 (1H, s, H<sup>13</sup>), 7.19 – 6.55 (14H, m), 6.32 (1H, dd,  $J = 7.4, 0.8$  Hz, H<sup>1a</sup> or H<sup>1b</sup>), 6.25 (1H, dd,  $J = 7.5, 0.8$  Hz, H<sup>1a</sup> or H<sup>1b</sup>), 6.13 (1H, ddd,  $J = 8.3, 6.2, 2.1$  Hz).

<sup>19</sup>F{<sup>1</sup>H} NMR (376 MHz, CDCl<sub>3</sub>)  $\delta$  -159.80 (bs, 2F), -150.96 (t,  $J = 20.7$  Hz, 1F), -138.44 (bs, 1F), -135.83 (bs, 1F).

MS (ASAP): Calcd for C<sub>35</sub>H<sub>21</sub>F<sub>5</sub>Ir<sup>193</sup>N<sub>3</sub>O 788.1312; Found  $m/z$  788.1326 [M+H]<sup>+</sup>

IR (solid state):  $\nu(\text{C}=\text{N})_{\text{imine}}$  1582 cm<sup>-1</sup>

### Complex **3.27a**-Cinnamyl



Complex **3.27a**-Cinnamyl was prepared using dimer **2.23a** (100 mg, 0.093 mmol), ligand **L3.27**-Cinnamyl (44 mg, 0.196 mmol) and Na<sub>2</sub>CO<sub>3</sub> (21 mg, 0.196 mmol) was

left to stir for 1.5 hrs in dry MeOH (10 ml). After passing through celite, the crude product was purified using column chromatography (silica) and eluted with DCM:MeOH (20:0.5) to give a red solid after evaporation of the solvent. (97 mg, 72%).

### *Trans*-3.27-Cinnamyl

$^1\text{H NMR}$  (500 MHz,  $\text{CDCl}_3$ )  $\delta$  8.70 (1H, d,  $J = 5.5$  Hz,  $\text{H}^{8a}$  or  $\text{H}^{8b}$ ), 8.55 (1H, d,  $J = 9.5$  Hz,  $\text{H}^{13}$ ), 8.34 (1H, d,  $J = 5.9$  Hz,  $\text{H}^{8a}$  or  $\text{H}^{8b}$ ), 7.84 (1H, d,  $J = 8.3$  Hz,  $\text{H}^{5a}$  or  $\text{H}^{5b}$ ), 7.79 (1H, d,  $J = 7.7$  Hz,  $\text{H}^{5a}$  or  $\text{H}^{5b}$ ), 7.66 – 7.63 (3H, m), 7.53 (1H, d,  $J = 7.7$  Hz,  $\text{H}^{4a}$  or  $\text{H}^{4b}$ ), 7.35 (1H, d,  $J = 8.3$  Hz,  $\text{H}^{12}$ ), 7.23 – 7.18 (3H, m), 7.08 – 7.03 (2H, m), 6.98 – 6.90 (4H, m,  $\text{H}^{14}$ ), 6.86 – 6.76 (5H, m,  $\text{H}^{15}$ ), 6.69 (1H, t,  $J = 7.5$  Hz,  $\text{H}^{2a}$  or  $\text{H}^{2b}$ ), 6.48 – 6.44 (2H, m,  $\text{H}^{1a}$  or  $\text{H}^{1b}$ ,  $\text{H}^{11}$ ), 6.05 (1H, d,  $J = 7.5$  Hz,  $\text{H}^{1a}$  or  $\text{H}^{1b}$ ).

$^{13}\text{C}\{^1\text{H}\}$  NMR (125 MHz,  $\text{CDCl}_3$ )  $\delta$  166.1, 157.8, 149.4, 149.3, 148.9, 147.1, 146.8, 145.3, 145.1, 142.7, 140.0, 136.7, 136.5, 133.1, 131.4, 130.6, 130.1, 129.7, 129.6, 128.9, 128.4, 128.2, 127.7, 127.2, 124.6, 123.9, 122.4, 122.0, 121.6, 121.5, 120.2, 119.0, 118.3, 117.1, 113.6

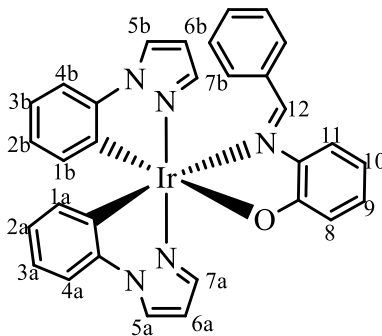
### *Cis*-3.27-Cinnamyl

$^1\text{H NMR}$  (400 MHz,  $\text{CDCl}_3$ )  $\delta$  8.82 (1H, dd,  $J = 5.7, 0.8$  Hz,  $\text{H}^{8a}$  or  $\text{H}^{8b}$ ), 8.29 (1H, dd,  $J = 5.9, 0.8$  Hz,  $\text{H}^{8a}$  or  $\text{H}^{8b}$ ), 7.85 – 6.37 (25H, m), 6.21 (1H, d,  $J = 6.7$  Hz,  $\text{H}^{1a}$  or  $\text{H}^{1b}$ ).

**MS (ASAP):** Calcd for  $\text{C}_{37}\text{H}_{28}\text{Ir}^{193}\text{N}_3\text{O}$  724.1940; Found  $m/z$  724.1963.

**IR (solid state):**  $\nu(\text{C}=\text{N})_{\text{imine}}$  1581  $\text{cm}^{-1}$

### Complex 3.27b-Ph



Complex **3.27b-Ph** was prepared using dimer **2.23b** (100 mg, 0.097 mmol), ligand **L3.27-Ph** (42 mg, 0.213 mmol) and  $\text{Na}_2\text{CO}_3$  (23 mg, 0.213 mmol) was left to stir for 3

h in dry MeOH (10 ml). After passing through celite, the crude product was purified using column chromatography (silica) and eluted with DCM:MeOH (10:0.5) to give a red solid after evaporation of the solvent. (118 mg, 90%). Recrystallisation took place with DCM:MeOH to give red crystals of *trans*-**3.27b-Ph**.

#### *Trans*-**3.27b-Ph**

**<sup>1</sup>H NMR** (400 MHz, CD<sub>2</sub>Cl<sub>2</sub>) δ 8.92 (1H, s, H<sup>12</sup>), 8.10 (1H, dd, *J* = 2.9, 0.6 Hz, H<sup>5b</sup>), 7.84 (1H, dd, *J* = 2.9, 0.7 Hz, H<sup>5a</sup>), 7.61 (1H, dd, *J* = 2.3, 0.6 Hz, H<sup>7a</sup>), 7.57 (1H, dd, *J* = 2.2, 0.6 Hz, H<sup>7b</sup>), 7.20 (1H, dd, *J* = 7.9, 1.1 Hz, H<sup>4a</sup>), 7.17 (1H, dd, *J* = 8.0, 1.6 Hz, H<sup>11</sup>), 7.11 – 7.05 (2H, m, H<sup>phenol</sup>, H<sup>aryl</sup>), 6.91 (1H, td, *J* = 7.6, 1.3 Hz, H<sup>3a</sup>), 6.88 – 6.76 (1H, m, H<sup>4b</sup>, H<sup>phenol</sup>, 4 x H<sup>aryl</sup>), 6.72 – 6.66 (2H, m, H<sup>2a</sup>, H<sup>3b</sup>), 6.60 – 6.58 (2H, m, H<sup>6a</sup>, H<sup>6b</sup>), 6.50 – 6.42 (2H, m, H<sup>2b</sup>, H<sup>10</sup>), 6.10 (1H, dd, *J* = 7.6, 1.3 Hz, H<sup>1a</sup>), 5.87 (1H, dd, *J* = 7.5, 1.3 Hz, H<sup>1b</sup>).

**<sup>13</sup>C{<sup>1</sup>H} NMR** (100 MHz, CD<sub>2</sub>Cl<sub>2</sub>) δ 169.4, 163.2, 144.6, 143.5, 143.3, 138.6, 137.4, 135.1, 134.5, 133.6, 133.4, 130.5, 130.0, 129.4, 127.8 (2 x C), 126.9 (2 x C), 126.1, 125.5, 125.4, 125.3, 121.9, 120.5, 120.1, 119.5, 113.0, 110.8, 110.4, 107.2, 106.7.

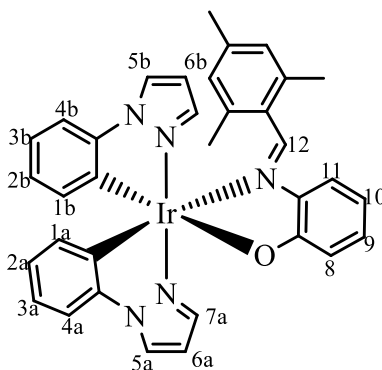
#### *Cis*-**3.27b-Ph**

**<sup>1</sup>H NMR** (400 MHz, CDCl<sub>3</sub>) δ 8.05 (1H, dd, *J* = 2.8 Hz, H<sup>5a</sup> or H<sup>5b</sup> or H<sup>7a</sup> or H<sup>7b</sup>), 8.03 (1H, dd, *J* = 2.9 Hz, H<sup>5a</sup> or H<sup>5b</sup> or H<sup>7a</sup> or H<sup>7b</sup>), 7.77 (1H, s, H<sup>12</sup>), 7.65 – 7.64 (1H, m, H<sup>5a</sup> or H<sup>5b</sup> or H<sup>7a</sup> or H<sup>7b</sup>), 7.48 (1H, d, *J* = 2.3 Hz, H<sup>5a</sup> or H<sup>5b</sup> or H<sup>7a</sup> or H<sup>7b</sup>), 7.41 – 7.39 (2H, m), 7.33 – 7.31 (3H, m), 7.19 – 7.14 (2H, m), 6.98 – 6.69 (7H, m), 6.55 – 6.52 (2H, m), 6.31 (1H, dd, *J* = 7.4, 1.2 Hz, H<sup>1a</sup> or H<sup>1b</sup>), 6.27 (1H, dd, *J* = 7.4, 1.2 Hz, H<sup>1a</sup> or H<sup>1b</sup>), 6.04 – 6.01 (1H, m).

**MS (ASAP):** Calcd for C<sub>31</sub>H<sub>24</sub>Ir<sup>193</sup>N<sub>5</sub>O 676.1689; Found *m/z* 676.1711

**IR (solid state):** ν(C=N)<sub>imine</sub> 1574 cm<sup>-1</sup>

### Complex 3.27b-Mes



Complex **3.27b-Mes** was prepared using dimer **2.23b** (100 mg, 0.097 mmol), ligand **L3.27-Mes** (51 mg, 0.213 mmol) and  $\text{Na}_2\text{CO}_3$  (23 mg, 0.213 mmol) was left to stir for overnight in dry MeOH (10 ml). After passing through celite, the crude product was purified using column chromatography (silica) and eluted with DCM:MeOH (100:1) to give a yellow solid after evaporation of the solvent. Recrystallisation took place with DCM:MeOH to give yellow crystals. (102 mg, 73%).

#### *Trans*-3.27b-Mes

$^1\text{H}$  NMR (500 MHz,  $\text{CD}_2\text{Cl}_2$ )  $\delta$  8.81 (1H, s,  $\text{H}^{12}$ ), 7.95 (1H, d,  $J = 3.0$  Hz,  $\text{H}^{5a}$ ), 7.73 (1H, d,  $J = 2.7$  Hz,  $\text{H}^{5b}$ ), 7.63 (1H, d,  $J = 2.1$  Hz,  $\text{H}^{7b}$ ), 7.34 (1H, d,  $J = 2.1$  Hz,  $\text{H}^{7a}$ ), 7.21 (1H, dd,  $J = 8.0, 1.4$  Hz,  $\text{H}^{11}$ ), 7.05 (1H, dd,  $J = 7.9, 0.7$  Hz,  $\text{H}^{4a}$ ), 6.94 (1H, t,  $J = 7.7$  Hz,  $\text{H}^9$ ), 6.74 (1H, td,  $J = 7.7, 1.6$  Hz,  $\text{H}^{3a}$ ), 6.57 (1H, dd,  $J = 8.3, 1.2$  Hz,  $\text{H}^8$ ), 6.55 (1H, t,  $J = 2.5$  Hz,  $\text{H}^{6b}$ ), 6.52 – 6.46 (2H, m,  $\text{H}^{2a}$ ,  $\text{H}^{3b}$ ), 6.44 – 6.42 (2H, m,  $\text{H}^{4b}$ ,  $\text{H}^{6a}$ ), 6.38 – 6.32 (3H, m,  $\text{H}^{2b}$ ,  $\text{H}^{10}$ ,  $\text{H}^{13}$ ), 5.95 (1H, dd,  $J = 7.6, 1.0$  Hz,  $\text{H}^{1b}$ ), 5.82 (1H, s,  $\text{H}^{14}$ ), 5.75 (1H, dd,  $J = 7.5, 1.2$  Hz,  $\text{H}^{1a}$ ), 1.96 (6H, s, *ortho*-Me, *para*-Me), 1.39 (3H, s, *ortho*-Me).

$^{13}\text{C}\{^1\text{H}\}$  NMR (125 MHz,  $\text{CD}_2\text{Cl}_2$ )  $\delta$  169.6, 164.9, 144.3, 143.6, 143.4, 139.8, 139.1, 137.9, 135.5, 134.2, 134.0, 133.5, 132.5, 131.9, 131.0, 130.9, 127.7, 126.9, 126.4, 125.7, 125.6, 125.1, 122.2, 120.7, 119.8, 118.9, 113.2, 111.2, 110.1, 107.6, 107.4, 21.2, 21.1, 18.9.

#### *Cis*-3.27b-Mes

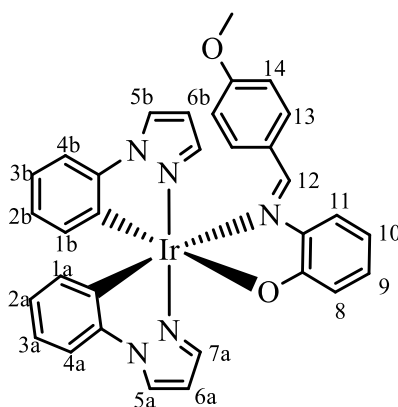
$^1\text{H}$  NMR (500 MHz,  $\text{CDCl}_3$ )  $\delta$  8.03 (1H, bd,  $J = 2.6$  Hz,  $\text{H}^{5a}$  or  $\text{H}^{5b}$  or  $\text{H}^{7a}$  or  $\text{H}^{7b}$ ), 7.99 (1H, bd,  $J = 2.6$  Hz,  $\text{H}^{5a}$  or  $\text{H}^{5b}$  or  $\text{H}^{7a}$  or  $\text{H}^{7b}$ ), 7.77 – 7.76 (1H, m), 7.67 (1H, s,  $\text{H}^{12}$ ),

7.45 (1H, bd,  $J = 1.5$  Hz,  $H^{5a}$  or  $H^{5b}$  or  $H^{7a}$  or  $H^{7b}$ ), 7.08 (2H, t,  $J = 7.2$  Hz), 6.94 – 6.92 (2H, m), 6.85 (2H, d,  $J = 9.2$  Hz), 6.73 – 6.72 (2H, m), 6.58 – 6.56 (2H, m), 6.53 – 6.49 (2H, m), 6.47 – 6.37 (4H, m), 6.33 (1H, d,  $J = 7.4$  Hz,  $H^{1a}$  or  $H^{1b}$ ), 2.17 (3H, s, Me), 2.09 (3H, s, Me), 1.35 (3H, s, Me).

**MS (ASAP):** Calcd for  $C_{34}H_{30}Ir^{193}N_5O$  718.2158; Found  $m/z$  718.2189

**IR (solid state):**  $\nu(C=N)_{imine}$  1576  $cm^{-1}$

### Complex 3.27b-Anisyl



Complex **3.27b-Anisyl** was prepared using dimer **2.23b** (100 mg, 0.097 mmol), ligand **L3.27-Anisyl** (46 mg, 0.204 mmol) and  $Na_2CO_3$  (22 mg, 0.204 mmol) was left to stir for 3 hrs in dry MeOH (10 ml). After passing through celite, the crude product was purified using column chromatography (silica) and eluted with DCM:MeOH (100:1) to give an orange-red solid after evaporation of the solvent (102 mg, 75%).

### *Trans*-3.27b-Anisyl

**$^1H$  NMR** (400 MHz,  $CDCl_3$ )  $\delta$  8.73 (1H, s,  $H^{12}$ ), 7.99 (1H, d,  $J = 2.8$  Hz,  $H^{5a}$  or  $H^{5b}$ ), 7.73 (1H, d,  $J = 2.8$  Hz,  $H^{5a}$  or  $H^{5b}$ ), 7.62 (1H, d,  $J = 2.2$  Hz,  $H^{7a}$  or  $H^{7b}$ ), 7.46 (1H, d,  $J = 2.0$  Hz,  $H^{7a}$  or  $H^{7b}$ ), 7.08 – 7.02 (3H, m), 6.88 (1H, dd,  $J = 8.2, 1.1$  Hz), 6.81 (2H, d,  $J = 8.7$  Hz), 6.79 (1H, d,  $J = 8.7$  Hz,  $H^{13}$ ,  $H^{13'}$ ), 6.73 (1H, d,  $J = 7.8$  Hz,  $H^{4a}$  or  $H^{4b}$ ), 6.65 (1H, td,  $J = 7.6, 1.1$  Hz), 6.58 (1H, td,  $J = 7.5, 1.0$  Hz,  $H^{2a}$  or  $H^{2b}$ ), 6.50 – 6.47 (3H, m,  $H^{2a}$  or  $H^{2b}$ ), 6.41 (1H, t,  $J = 7.6$  Hz), 6.26 (2H, d,  $J = 8.7$  Hz,  $H^{14}$  or  $H^{14'}$ ), 6.06 (1H, dd,  $J = 7.6, 1.0$  Hz,  $H^{1a}$  or  $H^{1b}$ ), 5.89 (1H, dd,  $J = 7.5, 1.0$  Hz,  $H^{1a}$  or  $H^{1b}$ ), 3.71 (1H, s,  $OCH_3$ ).

$^{13}\text{C}\{^1\text{H}\}$  NMR (100 MHz,  $\text{CDCl}_3$ )  $\delta$  168.9, 162.8, 156.7, 145.1, 143.6, 143.2, 138.6, 137.5, 136.7, 135.3, 135.0, 134.5, 134.4, 133.8, 130.6, 130.2, 129.9, 129.2, 126.5, 125.7, 125.4, 125.0, 121.9, 121.4, 120.3, 119.6, 114.0, 113.1, 112.3, 110.7, 110.1, 107.1, 107.0, 106.6, 55.1 ( $\text{OCH}_3$ ).

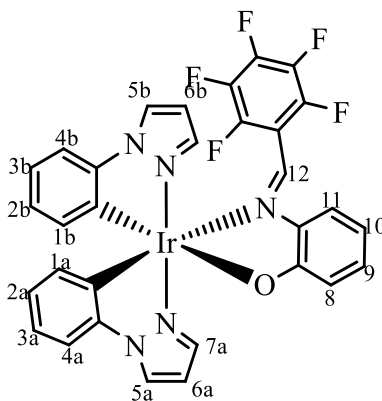
#### *Cis*-**3.27b**-Anisyl

$^1\text{H}$  NMR (400 MHz,  $\text{CDCl}_3$ )  $\delta$  8.04 (1H, d,  $J = 2.4$  Hz,  $\text{H}^{5a}$  or  $\text{H}^{5b}$ ), 8.02 (1H, d,  $J = 2.2$  Hz,  $\text{H}^{5a}$  or  $\text{H}^{5b}$ ), 7.71 (1H, s,  $\text{H}^{12}$ ), 7.63 – 7.62 (1H, m), 7.46 – 7.45 (1H, m), 7.42 (2H, d,  $J = 8.8$  Hz), 7.18 – 6.30 (16H, m), 3.83 (3H, s,  $\text{OCH}_3$ ).

MS (ASAP): Calcd for  $\text{C}_{32}\text{H}_{26}\text{Ir}^{193}\text{N}_5\text{O}_2$  706.1794; Found  $m/z$  706.1805

IR (solid state):  $\nu(\text{C}=\text{N})_{\text{imine}}$  1577  $\text{cm}^{-1}$

#### Complex **3.27b**- $\text{C}_6\text{F}_5$



Complex **3.27b**- $\text{C}_6\text{F}_5$  was prepared using dimer **2.23b** (100 mg, 0.097 mmol), ligand **L3.27**- $\text{C}_6\text{F}_5$  (46 mg, 0.204 mmol) and  $\text{Na}_2\text{CO}_3$  (22 mg, 0.204 mmol) was left to stir for 3 hrs in dry MeOH (10 ml). After passing through celite, the crude product was purified using column chromatography (silica) and eluted with DCM:MeOH (100:1) to give a red solid after evaporation of the solvent. (124 mg, 84%).

#### *Trans*-**3.27a**- $\text{C}_6\text{F}_5$

$^1\text{H}$  NMR (400 MHz,  $\text{CDCl}_3$ )  $\delta$  8.54 (1H, s,  $\text{H}^{12}$ ), 7.98 (2H, t,  $J = 3.1$  Hz,  $\text{H}^{5a}$ ,  $\text{H}^{5b}$ ), 7.63 (1H, d,  $J = 2.2$  Hz,  $\text{H}^{7a}$  or  $\text{H}^{7b}$ ), 7.49 (1H, s,  $\text{H}^{7a}$  or  $\text{H}^{7b}$ ), 7.29 (1H, dd,  $J = 8.2, 1.3$  Hz,  $\text{H}^{11}$ ), 7.14 (1H, ddd,  $J = 8.4, 6.9, 1.5$  Hz,  $\text{H}^9$ ), 7.08 (1H, dd,  $J = 7.9, 0.8$  Hz,  $\text{H}^{4a}$  or  $\text{H}^{4b}$ ), 6.97 (1H, dd,  $J = 8.4, 1.2$  Hz,  $\text{H}^8$ ), 6.91 (1H, d,  $J = 7.9$  Hz,  $\text{H}^{4a}$  or  $\text{H}^{4b}$ ), 6.80 (1H, td,  $J$

= 7.6, 1.2 Hz, H<sup>3a</sup> or H<sup>3b</sup>), 6.63 – 6.69 (1H, m, H<sup>3a</sup> or H<sup>3b</sup>), 6.57 – 6.63 (2H, m, H<sup>2a</sup> or H<sup>2b</sup>), 6.52 (1H, t, *J* = 2.6 Hz, H<sup>6a</sup> or H<sup>6b</sup>), 6.43 – 6.50 (2H, m, H<sup>10</sup>, H<sup>2a</sup> or H<sup>2b</sup>), 5.98 (1 H, dd, *J* = 7.5, 1.0 Hz, H<sup>1a</sup> or H<sup>1b</sup>), 5.93 (1H, d, *J* = 7.5 Hz, H<sup>1a</sup> or H<sup>1b</sup>).

<sup>19</sup>F{<sup>1</sup>H} NMR (376 MHz, CDCl<sub>3</sub>) δ -138.73 (1F, dd, *J* = 24.9, 5.1 Hz), -143.23 (1F, dd, *J* = 23.3, 6.5 Hz), -152.10 (1F, t, *J* = 21.1 Hz), -159.02 (1F, td, *J* = 7.9 Hz), -162.27 (1F, td, *J* = 21.7, 8.7 Hz).

<sup>13</sup>C{<sup>1</sup>H} NMR (100 MHz, CDCl<sub>3</sub>) δ 181.1, 171.1, 143.6, 142.9, 142.8, 142.6, 142.3, 141.3, 138.5, 138.1, 134.4, 133.5, 133.4, 132.2, 128.9, 125.9, 125.7, 125.5, 125.3, 122.4, 122.3, 120.4, 118.2, 113.5, 110.8, 109.6, 107.3 (2 X C).

### *Cis*-**3.27a**-C<sub>6</sub>F<sub>5</sub>

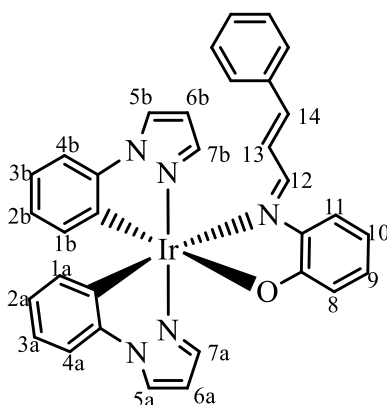
<sup>1</sup>H NMR (400 MHz, CDCl<sub>3</sub>) δ 8.76 (1H, dd, *J* = 5.9, 0.8 Hz, H<sup>5a</sup> or H<sup>5b</sup>), 8.32 (1H, dd, *J* = 5.7, 0.7 Hz, H<sup>5a</sup> or H<sup>5b</sup>), 7.86 – 6.59 (14H, m), 6.37 (1H, dd, *J* = 7.5, 0.8 Hz), 6.23 – 6.21 (1H, m), 6.14 (1H, ddd, *J* = 8.4, 6.3, 2.0 Hz).

<sup>19</sup>F{<sup>1</sup>H} NMR (376 MHz, CDCl<sub>3</sub>) δ -159.64 (bs, 2F), -150.63 (t, *J* = 20.7 Hz), -137.49 (bs, 1F), -135.43 (bs, 1F).

MS (ASAP): Calcd for C<sub>31</sub>H<sub>19</sub>F<sub>5</sub>Ir<sup>193</sup>N<sub>5</sub>O 766.1217; Found *m/z* 766.1254

IR (solid state): ν(C=N)<sub>imine</sub> 1575 cm<sup>-1</sup>

### Complex **3.27b**-Cinnamyl



Complex **3.27b**-Cinnamyl was prepared using dimer **2.17b** (90 mg, 0.088 mmol), ligand **L3.27**-Cinnamyl (46 mg, 0.194 mmol) and Na<sub>2</sub>CO<sub>3</sub> (21 mg, 0.194 mmol) was left to stir for 3 h in dry MeOH (10 ml). After passing through celite, the crude product

was purified using column chromatography (silica) and eluted with DCM:MeOH (10:1) to give a red solid after evaporation of the solvent. (110 mg, 89%).

#### ***Trans*-3.27b-Cinnamyl**

**<sup>1</sup>H NMR** (500 MHz, CDCl<sub>3</sub>) δ 8.50 (1H, d, *J* = 9.5 Hz, H<sup>12</sup>), 8.02 (1H, d, *J* = 2.6 Hz, H<sup>5a</sup> or H<sup>5b</sup>), 8.00 (1H, d, *J* = 2.4 Hz, H<sup>5a</sup> or H<sup>5b</sup>), 7.55 (1H, d, *J* = 1.8 Hz H<sup>7a</sup> or H<sup>7b</sup>), 7.45 (1H, d, *J* = 2.0 Hz, H<sup>7a</sup> or H<sup>7b</sup>), 7.30 – 7.22 (5H, m, H<sup>11</sup>), 7.19 (1H, dd, *J* = 7.9, 0.8 Hz, H<sup>4a</sup> or H<sup>4b</sup>), 7.11 (1H, d, *J* = 7.4 Hz, H<sup>4a</sup> or H<sup>4b</sup>), 7.07 (1H, ddd, *J* = 8.4, 6.9, 1.6 Hz), 7.01 – 6.96 (3 H, m) 6.93 – 6.88 (2H, m, H<sup>14</sup>, H<sup>3a</sup> or H<sup>3b</sup>), 6.85 – 6.80 (2H, m, H<sup>3a</sup> or H<sup>3b</sup>), 6.66 (1H, td, *J* = 7.5, 1.1 Hz, H<sup>2a</sup> or H<sup>2b</sup>), 6.51 (1H, t, *J* = 2.6 Hz, H<sup>6a</sup> or H<sup>6b</sup>), 6.47 (1H, t, *J* = 2.6 Hz, H<sup>6a</sup> or H<sup>6b</sup>), 6.44 (2H, m, H<sup>1a</sup> or H<sup>1b</sup>), 6.13 (1H, dd, *J* = 7.5, 1.1 Hz, H<sup>1a</sup> or H<sup>1b</sup>).

**<sup>13</sup>C{<sup>1</sup>H} NMR** (125 MHz, CDCl<sub>3</sub>) δ 171.0, 158.7 (C<sup>12</sup>), 145.1, 144.1, 143.2, 141.5, 138.0 (C<sup>7a</sup> or C<sup>7b</sup>), 137.7 (C<sup>7a</sup> or C<sup>7b</sup>), 135.5, 135.1, 133.7 (C<sup>1a</sup> or C<sup>1b</sup>), 132.9, 131.6, 130.5, 129.6, 128.5, 128.1, 127.5, 126.1, 125.9, 125.8, 125.5, 122.0, 121.5, 121.0, 117.2, 113.4, 110.9, 110.7, 107.2 (C<sup>6a</sup> or C<sup>6b</sup>), 106.9 (C<sup>6a</sup> or C<sup>6b</sup>).

#### ***Cis*-3.27b-Cinnamyl**

**<sup>1</sup>H NMR** (400 MHz, CDCl<sub>3</sub>) δ 8.03 – 8.00 (2H, m), 7.63 – 6.37 (22H, m), 6.35 (1H, dd, *J* = 7.4, 1.2 Hz, H<sup>1a</sup> or H<sup>1b</sup>), 6.27 (1H, dd, *J* = 7.5, 1.1 Hz, H<sup>1a</sup> or H<sup>1b</sup>).

**MS (ASAP):** Calcd for C<sub>33</sub>H<sub>26</sub>Ir<sup>193</sup>N<sub>5</sub>O 702.1847; Found *m/z* 702.2224.

**IR (solid state):** ν(C=N)<sub>imine</sub> 1574 cm<sup>-1</sup>

## **6.4 Experimental procedures for Chapter 4**

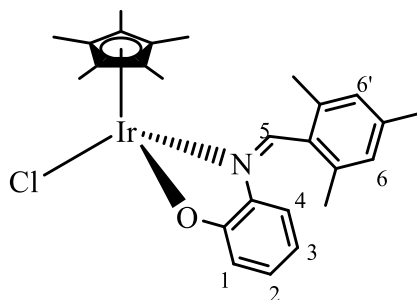
### **General Procedure for the Synthesis of Half-sandwich complexes with N<sup>^</sup>O**

#### **Ligands**

Dichloro-bridged dimers [MCl<sub>2</sub>Cp\*]<sub>2</sub> (**4.14**) (M = Ir, **a**, Rh, **b**)<sup>21</sup> and [RuCl<sub>2</sub>(*p*-cym)]<sub>2</sub> (**4.14c**)<sup>22</sup> were prepared using literature methods. The appropriate dimer **4.14a-c** (0.088 – 0.163 mmol, 70 – 100 mg), the relevant N<sup>^</sup>O ligand **L3.27-R** (R = Mes, Anisyl, Cinnamyl) (2.0 – 2.2 equiv) and Na<sub>2</sub>CO<sub>3</sub> (2.0 – 2.2 equiv) were placed in an evacuated Schlenk tube which was wrapped in aluminium foil to protect it from light and allowed to stir at room temperature under nitrogen atmosphere in dry MeOH (6-8 ml). The

reaction was monitored by  $^1\text{H}$  NMR spectroscopy until completion and the solvent was removed *in vacuo* leaving behind the crude product which was dissolved in DCM (8-12 ml) and passed through celite. The filtrate was reduced in volume and hexane was added to induce precipitation. The precipitate was isolated, washed with hexane and dried *in vacuo*.

### Complex 4.15a-Mes



$[\text{IrCl}_2\text{Cp}^*]_2$  (**4.14a**) (0.088 mmol, 70 mg), ligand **L3.27-Mes** (0.194 mmol, 46 mg) and  $\text{Na}_2\text{CO}_3$  (0.194 mmol, 21 mg) was stirred in dry MeOH (6 ml) in the dark for 2.5 hrs to give complex *cis*-**4.15a-Mes** as a single isomer (orange solid, 70 mg, 68 %).

### *Cis*-4.15a-Mes

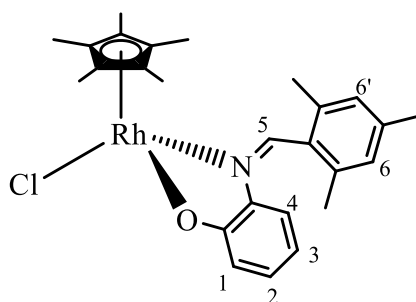
$^1\text{H}$  NMR (400 MHz,  $\text{CDCl}_3$ )  $\delta$  8.70 (1H, s,  $\text{H}^5$ ), 6.95 (1H, s,  $\text{H}^6/\text{H}^{6'}$ ), 6.92 – 6.86 (2H, m,  $\text{H}^1, \text{H}^2$ ), 6.82 (1H, s,  $\text{H}^6/\text{H}^{6'}$ ), 6.42 (1H, dd,  $J = 8.3$  Hz, 1.3 Hz,  $\text{H}^4$ ), 5.98 (1H, ddd,  $J = 8.3, 6.5, 1.7$  Hz,  $\text{H}^3$ ), 2.42 (3H, s, *ortho*-Me), 2.31 (3H, s, *para*-Me), 2.01 (3H, s, *ortho*-Me), 1.67 (15H, s,  $\text{CH}_3(\text{Cp}^*)$ ).

$^{13}\text{C}\{^1\text{H}\}$  NMR (125 MHz,  $\text{CDCl}_3$ )  $\delta$  170.5, 162.5 ( $\text{C}^5$ ), 139.6, 139.0, 136.0, 135.0, 132.1, 130.4, 129.8 ( $\text{C}^6$  or  $\text{C}^{6'}$ ), 128.5 ( $\text{C}^6$  or  $\text{C}^{6'}$ ), 120.3 ( $\text{C}^4$ ), 113.5 ( $\text{C}^3$ ), 84.5 ( $\text{C}(\text{Cp}^*)$ ), 21.2 (*ortho*-C), 20.2 (*para*-C), 19.6 (*ortho*-C), 8.7 ( $\text{CH}_3(\text{Cp}^*)$ ).

**MS (ESI):**  $m/z$  515  $[\text{M}-\text{Cl}-\text{Cp}^*+(\text{MeCN})_2]^+$

**IR (solid state):**  $\nu(\text{C}=\text{N})_{\text{imine}}$  1583  $\text{cm}^{-1}$

## Complex 4.15b-Mes



[RhCl<sub>2</sub>Cp\*]<sub>2</sub> (**4.14b**) (0.113 mmol, 70 mg), ligand **L3.27-Mes** (0.227 mmol, 54 mg) and Na<sub>2</sub>CO<sub>3</sub> (0.227 mmol, 24 mg) was allowed to stir in dry MeOH (7 ml) in the dark for 3 hrs to give a complex *cis*-**4.15b-Mes** as a single isomer (dark red solid 64 mg g, 58 %).

### *Cis*-**4.15b-Mes**

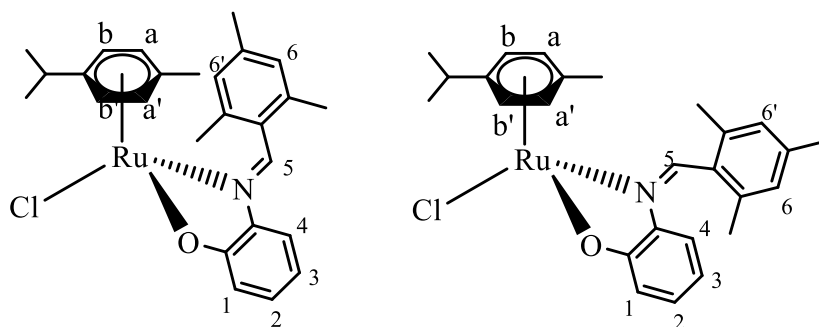
<sup>1</sup>H NMR (400 MHz, CDCl<sub>3</sub>) δ 8.67 (1H, s, H<sup>5</sup>), 6.91 (1H, s, H<sup>6</sup> or H<sup>6'</sup>), 6.89 – 6.86 (2H, m, H<sup>1</sup>, H<sup>2</sup>), 6.76 (1H, s, H<sup>6</sup> or H<sup>6'</sup>), 6.33 (1H, d, *J* = 8.3 Hz, H<sup>4</sup>), 5.95 (1H, ddd, *J* = 8.4 Hz, 5.4 Hz, 2.7 Hz, H<sup>3</sup>), 2.43 (3H, s, *ortho*-Me), 2.29 (3H, s, *para*-Me), 1.89 (3H, s, *ortho*-Me), 1.68 (15H, s, CH<sub>3</sub>(Cp\*)).

<sup>13</sup>C{<sup>1</sup>H} NMR (100 MHz, CDCl<sub>3</sub>): δ 169.4, 162.9 (C<sup>5</sup>), 139.5, 138.1 (C<sup>4</sup>), 135.8, 134.8, 132.1, 129.9 (C<sup>3</sup>, C<sup>4</sup>), 129.7, 128.3, 120.6, 120.2 (C<sup>1</sup> or C<sup>2</sup>), 112.7 (C<sup>1</sup> or C<sup>2</sup>), 92.9 (C(Cp\*)), 21.2 (*ortho*-CH<sub>3</sub>), 20.1 (*para*-CH<sub>3</sub>), 19.5 (*ortho*-CH<sub>3</sub>), 8.69 (CH<sub>3</sub>(Cp\*)),

**MS (ES):** *m/z* 476 [M-Cl]<sup>+</sup>

**IR (solid state):** ν(C=N)<sub>imine</sub> 1581 cm<sup>-1</sup>

### Complex 4.15c-Mes



[RuCl<sub>2</sub>(*p*-Cym)]<sub>2</sub> (**4.14c**) (0.163 mmol 100 mg), ligand **L3.27-Mes** (0.342 mmol, 82 mg) and Na<sub>2</sub>CO<sub>3</sub> (0.342 mmol, 36 mg) was allowed to stir in dry MeOH (7 ml) in the dark for 3 hrs to give a complex **4.15c-Mes** as a *trans:cis* mixture (78:22) (dark red solid 64 mg, 58 %).

#### *Trans*-4.15c-Mes

<sup>1</sup>H NMR (500 MHz, CDCl<sub>3</sub>) δ 9.01 (1H, s, H<sup>5</sup>), 7.31 (1H, dd, *J* = 8.4, 1.2 Hz, H<sup>4</sup>), 7.06 (1H, s, H<sup>6</sup> or H<sup>6'</sup>), 7.04 (1H, s, H<sup>6</sup> or H<sup>6'</sup>), 7.00 (1H, ddd, *J* = 8.4, 6.9, 1.3 Hz, H<sup>1</sup>), 6.92 (1H, dd, *J* = 8.5, 1.3 Hz, H<sup>2</sup>), 6.43 (1H, ddd, *J* = 8.3, 6.9, 1.3 Hz, H<sup>3</sup>), 5.45 (1H, d, *J* = 6.3 Hz, H<sup>b</sup> or H<sup>b'</sup>), 5.18 (1H, d, *J* = 6.3 Hz, H<sup>a</sup> or H<sup>a'</sup>), 4.99 (1H, d, *J* = 5.6 Hz, H<sup>b</sup> or H<sup>b'</sup>), 3.50 (1H, d, *J* = 5.4 Hz, H<sup>a</sup> or H<sup>a'</sup>), 2.75 (1H, sept, *J* = 7.0 Hz, H<sup>7</sup>), 2.50 (3H, s, Me), 2.43 (3H, s, Me), 2.41 (3H, s, Me), 2.00 (3H, s, *p*-CH<sub>3</sub>(*p*-cym)), 1.21 (3H, d, *J* = 7.0 Hz, CH(CH<sub>3</sub>)<sub>2</sub>), 1.07 (3H, d, *J* = 7.0 Hz, CH(CH<sub>3</sub>)<sub>2</sub>)

<sup>13</sup>C{<sup>1</sup>H} NMR (125 MHz, CDCl<sub>3</sub>) δ 169.8, 162.9, 140.1, 137.2, 135.4, 134.1, 133.4, 129.8, 129.7, 128.4, 119.3, 119.6, 114.4, 102.4, 99.1, 84.1, 82.0, 81.3, 80.7, 30.9, 22.2, 22.3, 21.6, 20.1, 19.2, 17.6

MS (ESI): *m/z* 474 [M-Cl]<sup>+</sup>

IR (solid state): ν(C=N)<sub>imine</sub> 1597 cm<sup>-1</sup>

#### *Cis*-4.15c-Mes

<sup>1</sup>H NMR: (500 MHz, CDCl<sub>3</sub>) δ 9.02 (1H, s, H<sup>5</sup>), 6.95 (1H, bs, H<sup>6</sup>), 6.88 – 6.84 (2H, m, H<sup>1</sup>, H<sup>2</sup>), 6.81 (1H, bs, H<sup>6</sup>), 6.42 (1H, d, *J* = 8.5 Hz, H<sup>4</sup>), 5.99 (1H, m, H<sup>3</sup>), 5.48 (1H, d, *J* = 6.0 Hz, H<sup>b</sup> or H<sup>b'</sup>), 5.42 (1H, d, *J* = 6.0 Hz, H<sup>b</sup> or H<sup>b'</sup>), 5.33 (1H, d, *J* = 6.0 Hz, H<sup>a</sup>

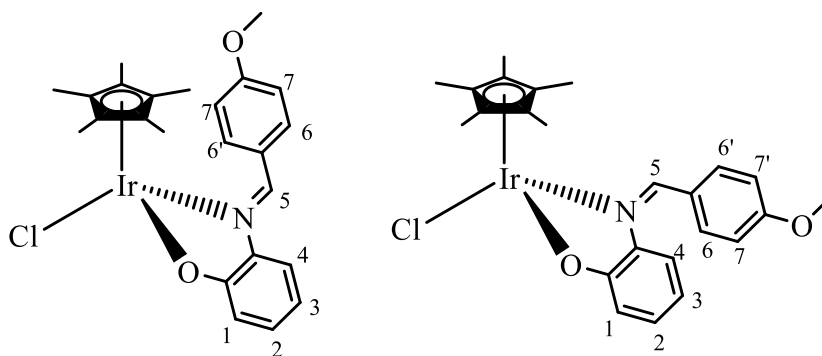
or H<sup>a</sup>), 5.18 (1H, d,  $J = 5.7$  Hz, H<sup>a</sup> or H<sup>a'</sup>), 2.87 (1H, sept,  $J = 6.9$  Hz, H<sup>7</sup>), 2.47 (3H, s, *ortho*-Me), 2.32 (3H, s, *para*-Me), 2.29 (3H, s, *p*-CH<sub>3</sub>(*p*-cym)), 1.96 (3H, s, *ortho*-Me), 1.24 (3H, d  $J = 4.3$  Hz, CH(CH<sub>3</sub>)<sub>2</sub>), 1.22 (3H, d  $J = 4.3$  Hz, CH(CH<sub>3</sub>)<sub>2</sub>).

<sup>13</sup>C{<sup>1</sup>H} NMR (125 MHz, CDCl<sub>3</sub>)  $\delta$  170.5, 162.9, 139.5, 136.9, 135.9, 134.5, 132.4, 129.9, 129.7, 128.4, 119.9, 119.6, 113.4, 101.4, 98.5, 83.1, 81.8, 81.4, 80.9, 30.9, 22.3, 22.3, 21.2, 20.0, 19.6, 18.6

MS (ESI):  $m/z$  474 [M-Cl]<sup>+</sup>

IR (solid state):  $\nu(\text{C=N})_{\text{imine}}$  1597 cm<sup>-1</sup>

### Complex 4.15a-Anisyl



[IrCl<sub>2</sub>Cp\*]<sub>2</sub> (**4.14a**) (0.088 mmol, 70 mg), ligand **L3.27-Anisyl** (0.176 mmol, 46 mg) and Na<sub>2</sub>CO<sub>3</sub> (0.176 mmol, 17 mg) was allowed to stir in dry MeOH (6 ml) in the dark for 3 h to give a *trans*-**4.15a-Anisyl** as a single isomer (red solid 70 mg, 68%). *cis*-**4.15a-Anisyl** was observed after irradiation of the *trans* isomer.

### *Trans*-4.15a-Anisyl

<sup>1</sup>H NMR (400 MHz, CDCl<sub>3</sub>)  $\delta$  8.90 (1H, s, H<sup>5</sup>), 8.42 (2H, d,  $J = 8.8$  Hz, H<sup>6</sup>, H<sup>6'</sup>), 7.38 (1H, d,  $J = 8.0$  Hz, H<sup>4</sup>), 7.03 – 6.97 (4H, m, H<sup>1</sup>, H<sup>2</sup>, H<sup>7</sup>, H<sup>7'</sup>), 6.42 (1H, ddd,  $J = 8.1, 6.3, 2.5$ , H<sup>3</sup>), 3.89 (3H, s, OCH<sub>3</sub>), 1.41 (15H, s, CH<sub>3</sub>(Cp\*)).

<sup>13</sup>C{<sup>1</sup>H} NMR (100 MHz, CDCl<sub>3</sub>)  $\delta$  168.1, 161.3, 158.1, 142.8, 134.2, 129.5, 126.2, 120.7, 116.9, 115.0, 114.3, 92.5 (C(Cp\*)), 55.3 (OCH<sub>3</sub>), 8.8 (CH<sub>3</sub>(Cp\*)).

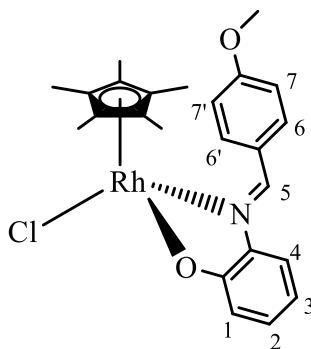
MS (ESI):  $m/z$  595 [M-Cl+MeCN]<sup>+</sup>

IR (solid state):  $\nu(\text{C=N})_{\text{imine}}$  1577 cm<sup>-1</sup>

### *Cis*-4.15a-Anisyl

$^1\text{H NMR}$  (400 MHz,  $\text{CDCl}_3$ )  $\delta$  8.39 (1H, s,  $\text{H}^5$ ), 7.49 (2H, d,  $J = 8.6$  Hz,  $\text{H}^6$ ,  $\text{H}^{6'}$  or  $\text{H}^7$ ,  $\text{H}^{7'}$ ), 7.02 – 6.88 (3H, m), 6.85 (2H, d,  $J = 9.0$ ,  $\text{H}^6$ ,  $\text{H}^{6'}$  or  $\text{H}^7$ ,  $\text{H}^{7'}$ ), 6.08 (1H, ddd,  $J = 8.3$ , 6.3, 2.0,  $\text{H}^2$  or  $\text{H}^3$ ), 3.83 (3H, s,  $\text{OCH}_3$ ), 1.65 (15H, s,  $\text{CH}_3(\text{Cp}^*)$ ).

### Complex 4.15b-Anisyl



$[\text{RhCl}_2\text{Cp}^*]_2$  (**4.14b**) (0.113 mmol, 70 mg), ligand **L3.27-Anisyl** (0.226 mmol, 51 mg) and  $\text{Na}_2\text{CO}_3$  (0.226 mmol, 24 mg) was allowed to stir in dry MeOH (7 ml) in the dark for 3 hrs to give complex *trans*-4.15b-Anisyl as a single isomer (dark red solid 64 mg, 57%).

### *Trans*-4.15b-Anisyl

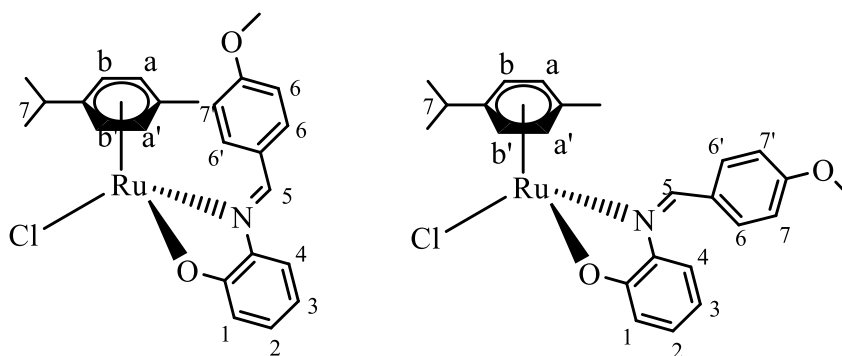
$^1\text{H NMR}$  (400 MHz,  $\text{CDCl}_3$ )  $\delta$  8.88 (1H, s,  $\text{H}^5$ ), 8.52 (2H, d,  $J = 8.7$  Hz,  $\text{H}^6$ ,  $\text{H}^{6'}$ ), 7.34 (1H, bd,  $J = 7.8$  Hz,  $\text{H}^4$ ), 7.03 (2H, d,  $J = 8.9$  Hz,  $\text{H}^7$ ,  $\text{H}^{7'}$ ), 6.98 – 6.93 (2H, m,  $\text{H}^1$ ,  $\text{H}^2$ ), 6.37 (1H, ddd,  $J = 8.2$  Hz, 6.5 Hz, 1.8 Hz,  $\text{H}^3$ ), 3.86 (3H, s,  $\text{OCH}_3$ ), 1.44 (15H, s,  $\text{CH}_3(\text{Cp}^*)$ ).

$^{13}\text{C}\{^1\text{H}\}$  NMR (100 MHz,  $\text{CDCl}_3$ )  $\delta$  168.3, 162.3, 159.1, 141.9, 133.7, 129.5, 126.8, 120.4, 115.9, 114.0, 113.7, 93.5 ( $\text{C}(\text{Cp}^*)$ ), 55.5 ( $\text{OCH}_3$ ), 8.7 ( $\text{CH}_3(\text{Cp}^*)$ ).

**MS (ESI):**  $m/z$  464  $[\text{M}-\text{Cl}]^+$ .

**IR (solid state):**  $\nu(\text{C}=\text{N})_{\text{imine}}$  1570  $\text{cm}^{-1}$

### Complex 4.15c-Anisyl



[RuCl<sub>2</sub>(p-Cym)]<sub>2</sub> (**4.14c**) (0.163 mmol 100 mg.), ligand **L3.27-Mes** (0.342 mmol, 82 mg) and Na<sub>2</sub>CO<sub>3</sub> (0.342 mmol, 36 mg) was allowed to stir in dry MeOH (7 ml) in the dark for 3 hrs to give a complex **4.15c-Mes** as a *trans:cis* mixture (78:22) (dark red solid 64 mg, 58 %).

#### *Trans*-4.15c-Anisyl

<sup>1</sup>H NMR (400 MHz, CDCl<sub>3</sub>) δ 9.04 (1H, s, H<sup>5</sup>), 8.29 (2H, d, *J* = 8.6 Hz, H<sup>6</sup>, H<sup>6'</sup>), 7.27 (1H, d, *J* = 7.7 Hz, H<sup>4</sup>), 7.07 (2H, d, *J* = 8.9 Hz, H<sup>7</sup>, H<sup>7'</sup>), 7.00 – 6.92 (2H, m, H<sup>1</sup>, H<sup>2</sup>), 6.41 (1H, ddd, *J* = 8.5, 6.4, 1.5 Hz, H<sup>3</sup>), 5.37 (1H, d, *J* = 5.8, H<sup>b</sup> or H<sup>b'</sup>), 5.11 (1H, d, *J* = 5.9 Hz, H<sup>a</sup> or H<sup>a'</sup>), 4.72 (1H, d, *J* = 5.8, H<sup>b</sup> or H<sup>b'</sup>), 4.58 (1H, d, *J* = 5.6 Hz, H<sup>a</sup> or H<sup>a'</sup>), 3.93 (3H, s, OCH<sub>3</sub>), 2.61 (1H, sept, *J* = 6.7 Hz, H<sup>7</sup>), 2.25 (3H, s, Me), 1.08 (6H, d, *J* = 6.9 Hz, CH(CH<sub>3</sub>)<sub>2</sub>).

<sup>13</sup>C{<sup>1</sup>H} NMR (100 MHz, CDCl<sub>3</sub>) δ 168.9, 161.7, 158.4, 132.9, 129.9, 129.6, 120.1, 115.1, 114.2, 113.8, 101.3, 100.3, 85.1, 82.6, 81.8, 80.3, 55.6, 30.9, 22.5, 21.9, 18.7.

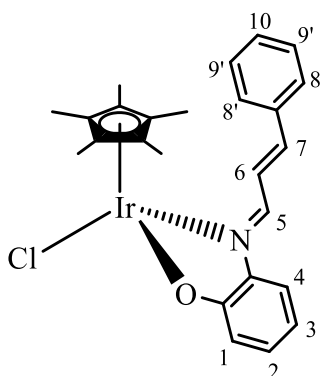
MS (ES): *m/z* 462 [M-Cl]<sup>+</sup>, *m/z* 503 [M+MeCN]<sup>+</sup>

IR (solid state): ν(C=N)<sub>imine</sub> 1577 cm<sup>-1</sup>

#### *Cis*-4.15c-Anisyl

<sup>1</sup>H NMR (500 MHz, CDCl<sub>3</sub>) δ 8.72 (1H, s, H<sup>5</sup>), 7.46 (2H, d, *J* = 8.7 Hz, H<sup>6</sup>, H<sup>6'</sup> or H<sup>7</sup>, H<sup>7'</sup>), 7.00 – 6.87 (3H, m), 6.83 (2H, d, *J* = 8.7 Hz, H<sup>6</sup>, H<sup>6'</sup> or H<sup>7</sup>, H<sup>7'</sup>), 6.08 (1H, t, *J* = 6.4 Hz), 5.49 (1H, br d, *J* = 5.76 Hz), 5.42 (1H, br d, *J* = 5.76 Hz), 5.36 (1H, d, *J* = 5.9 Hz), 5.15 (1H, br d, *J* = 5.96 Hz), 3.82 (3H, s), 2.83 (1H, septet, *J* = 6.8 Hz), 2.29 (3H, s), 2.21 – 2.18 (6H, m, <sup>*i*</sup>Pr).

## Complex 4.15a-Cinnamyl



$[\text{IrCl}_2\text{Cp}^*]_2$  (**4.14a**) (0.126 mmol, 100 mg), ligand **L4.16-Anisyl** (0.265 mmol, 59 mg) and NaOMe (0.265 mmol, 14 mg) was allowed to stir in dry MeOH (8 ml) in the dark for 1 h to give complex *trans*-**4.16a-Cinnamyl** as a single isomer (red solid 141 mg, 89 %).

### *Trans*-**4.16a-Cinnamyl**

$^1\text{H NMR}$  (400 MHz,  $\text{CDCl}_3$ )  $\delta$  8.36 (1H, d,  $J = 9.5$  Hz,  $\text{H}^5$ ), 7.55 – 7.35 (6H, m,  $\text{H}^6$ ,  $\text{H}^8$ ,  $\text{H}^{8'}$ ,  $\text{H}^9$ ,  $\text{H}^{9'}$ ,  $\text{H}^{10}$ ), 7.24 (1H, d,  $J = 8.3, 1.2$  Hz,  $\text{H}^4$ ), 7.13 (1H, d,  $J = 16.0$  Hz,  $\text{H}^7$ ), 7.00 (1H, ddd,  $J = 8.3, 6.9, 1.3$  Hz,  $\text{H}^2$ ), 6.92 (1H, dd,  $J = 8.3, 1.2$ ,  $\text{H}^1$ ), 6.42 (1H, ddd,  $J = 8.1, 6.9, 1.3$ ,  $\text{H}^3$ ), 1.64–8.7 ( $\text{CH}_3(\text{Cp}^*)$ ).

$^{13}\text{C}\{^1\text{H}\}$  NMR (125 MHz,  $\text{CDCl}_3$ )  $\delta$  168.9, 157.98 (C5), 152.4, 145.8 (C7), 142.2, 135.4, 130.5, 130.2 (C2), 129.1, 128.9 (2 x C), 128.1 (2 x C), 119.7 (H1), 115.5 (C4), 114.6 (C3), 85.1 (C(Cp\*)), 8.9 ( $\text{CH}_3(\text{Cp}^*)$ ).

**MS (ESI):**  $m/z$  550  $[\text{M}-\text{Cl}]^+$

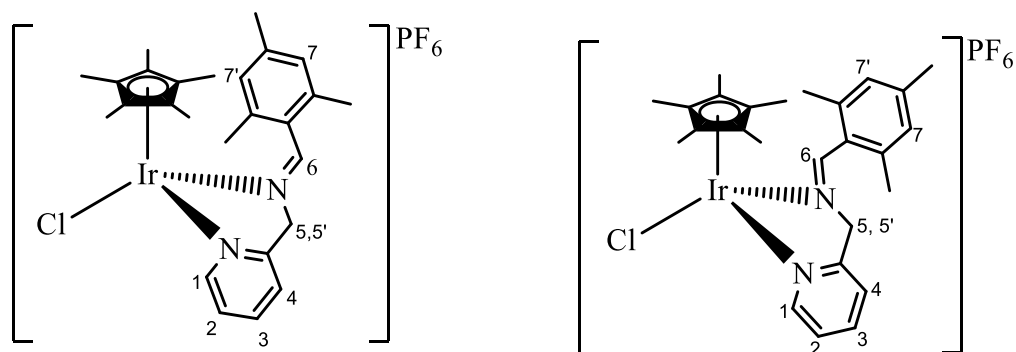
**IR (solid state):**  $\nu(\text{C}=\text{N})_{\text{imine}}$  1575  $\text{cm}^{-1}$

### General Procedure for the synthesis of half-sandwich complexes with N^N ligands

The appropriate dimer **4.14a** or **4.14c** (0.126 – 0.163 mmol, 100 mg), the relevant N^N ligand **L4.16-R** (R = Mes, Anisyl) (2.0 – 2.2 equiv) and  $\text{KPF}_6$  (2.0 – 2.2 equiv) were placed in an evacuated Schlenk tube which was wrapped in aluminium foil to protect it from light and allowed to stir at room temperature under nitrogen atmosphere in dry MeOH (7 ml). The reaction was monitored by  $^1\text{H NMR}$  spectroscopy until completion and the solvent was removed *in vacuo* leaving behind the crude product which was

dissolved in DCM (8-12 ml) and passed through celite. The filtrate was reduced in volume and hexane was added to induce precipitation. The precipitate was isolated, washed with hexane and dried *in vacuo*.

### Complex 4.16a-Mes



[IrCl<sub>2</sub>Cp\*]<sub>2</sub> (**4.14a**) (0.126 mmol, 100 mg), ligand **L4.16-Mes** (0.252 mmol, 65 mg) and KPF<sub>6</sub> (0.252 mmol, 65 mg) was allowed to stir in dry MeOH (7 ml) in the dark for 2 hrs to give complex *trans*-**4.16a-Mes** as a single isomer (yellow solid 163 mg, 87 %).

### *Trans*-4.16a-Mes

<sup>1</sup>H NMR (400 MHz, CDCl<sub>3</sub>) δ 9.33 (1H, s, H<sup>6</sup>), 8.49 (1H, d, *J* = 5.3 Hz, H<sup>1</sup>), 7.95 (1H, td, *J* = 7.7 Hz, 1.3 Hz, H<sup>3</sup>), 7.76 (1H, d, *J* = 7.8 Hz, H<sup>4</sup>), 7.48 (1H, t, *J* = 6.6 Hz, H<sup>2</sup>), 6.90 (2H, s, H<sup>7</sup>, H<sup>7'</sup>), 5.66 (1H, d, *J* = 18.0 Hz, H<sup>5</sup>/H<sup>5'</sup>), 5.54 (1H, d, *J* = 18.0 Hz, H<sup>5</sup>/H<sup>5'</sup>), 2.34 (6H, s, 2 x Me), 2.31 (3H, s, Me), 1.39 (15H, s, CH<sub>3</sub>(Cp\*)).

<sup>13</sup>C{<sup>1</sup>H} NMR (100 MHz, CDCl<sub>3</sub>) δ 177.2, 158.3, 150.5, 141.6, 139.9, 135.4, 135.1, 129.4, 129.3, 128.2, 126.4, 122.4, 88.7 (*C*(Cp\*)), 64.4, 21.3 (*para*-CH<sub>3</sub>), 19.9 (*ortho*-CH<sub>3</sub>), 19.6 (*ortho*-CH<sub>3</sub>), 8.8 (CH<sub>3</sub>(Cp\*)).

MS (ESI): *m/z* 601 [M]<sup>+</sup>.

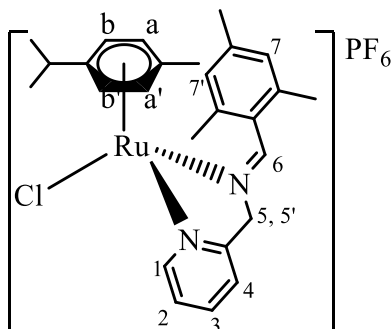
IR (solid state): ν(C=N)<sub>imine</sub> 1607 cm<sup>-1</sup>

### *Cis*-4.16a-Mes

<sup>1</sup>H NMR (400 MHz, CDCl<sub>3</sub>): δ 8.96 (1H, s, H<sup>6</sup>), 8.50 (1H, d, *J* = 5.4 Hz, H<sup>1</sup>), 7.87 (1H, td, *J* = 7.8 Hz, 1.3 Hz, H<sup>3</sup>), 7.51 – 7.46 (2H, m, H<sup>2</sup>, H<sup>4</sup>), 7.03 (1H, s, H<sup>7</sup>/H<sup>7'</sup>), 6.90 (1H, s, H<sup>7</sup>/H<sup>7'</sup>), 5.09 (1H, dd, *J* = 18.6, 2.5 Hz, H<sup>5</sup>/H<sup>5'</sup>), 4.95 (1H, d, *J* = 18.1 Hz, H<sup>5</sup>/H<sup>5'</sup>),

2.37 (3H, s, *ortho*-Me), 2.33 (3H, s, *para*-Me), 2.12 (3H, s, *ortho*-Me), 1.73 (15H, s, Me-(Cp\*)).

### Complex 4.16c-Mes



[RuCl<sub>2</sub>(p-Cym)]<sub>2</sub> (**4.14c**) (0.163 mmol, 100 mg), ligand **L4.16-Mes** (0.359 mmol, 66 mg) and KPF<sub>6</sub> (0.359 mmol, 86 mg) was allowed to stir in dry MeOH (7 ml) in the dark for 3 h to give a crude product **4.16c-Mes**. Purification of complex *trans*-**4.16c-Mes** proved to be difficult therefore a crude yield was recorded (brown solid, 87%).

### *Trans*-4.16c-Mes

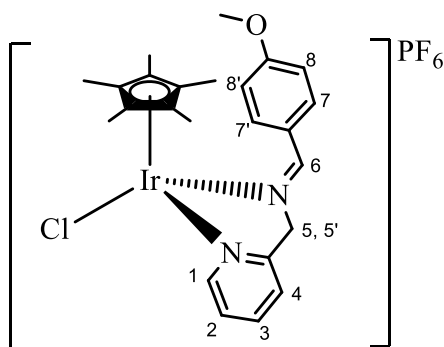
<sup>1</sup>H NMR (400 MHz, CDCl<sub>3</sub>) δ 9.07 – 9.05 (2H, m, H<sup>1</sup>, H<sup>6</sup>), 7.86 (1H, t, *J* = 7.3 Hz, H<sup>3</sup>), 7.50 – 7.46 (2H, m, H<sup>2</sup>, H<sup>4</sup>), 7.06 (1H, s, H<sup>7</sup> or H<sup>7'</sup>), 7.03 (1H, s, H<sup>7</sup> or H<sup>7'</sup>), 5.56 (1H, bs, H<sup>b</sup> or H<sup>b'</sup>), 5.46 (1H, d, *J* = 19.0 Hz, H<sup>5</sup> or H<sup>5'</sup>), 5.34 (1H, d, *J* = 6.2 Hz, H<sup>a</sup> or H<sup>a'</sup>), 5.21 (1H, d, *J* = 19.0 Hz, H<sup>5</sup> or H<sup>5'</sup>), 5.08 (1H, d, *J* = 5.9 Hz, H<sup>b</sup> or H<sup>b'</sup>), 4.28 (1H, bs, H<sup>a</sup> or H<sup>a'</sup>), 2.48 (1H, sept, *J* = 6.9 Hz), 2.43 (3H, s, Me), 2.40 (3H, s, Me), 2.38 (3H, s, Me), 2.05 (3H, s, *p*-cym(Me)), 0.99 (3H, d, *J* = 6.9 Hz), 0.97 (3H, d, *J* = 6.9 Hz).

<sup>13</sup>C{<sup>1</sup>H} NMR (100 MHz, CDCl<sub>3</sub>) δ 179.9 (C<sup>6</sup>), 158.6, 154.4, 141.5, 139.7, 136.4, 135.7, 132.9, 129.2, 128.4, 125.8, 121.2, 84.2(C<sup>b</sup> or C<sup>b'</sup>), 81.5(C<sup>a</sup> or C<sup>a'</sup>), 78.9 (C<sup>b</sup> or C<sup>b'</sup>), 78.2(C<sup>a</sup> or C<sup>a'</sup>), 69.7 (C<sup>5</sup>, C<sup>5'</sup>), 31.6, 31.4, 30.8, 22.7, 22.1, 21.6, 21.3, 20.7, 19.9, 18.5 (*Me*-pcym)

MS (ESI): *m/z* 509 [M]<sup>+</sup>

IR (solid state): ν(C=N)<sub>imine</sub> 1576 cm<sup>-1</sup>

## Complex 4.16a-Anisyl



[IrCl<sub>2</sub>Cp\*]<sub>2</sub> (**4.14a**) (0.126 mmol, 100 mg), ligand **L4.16-Anisyl** (0.252 mmol, 57 mg) and KPF<sub>6</sub> (0.252 mmol, 46 mg) was allowed to stir in dry MeOH (7 ml) in the dark for 2 hrs to give complex *trans*-**4.16a-Anisyl** as a single isomer (yellow solid 160 mg, 87 %).

### *Trans*-**4.16a-Anisyl**

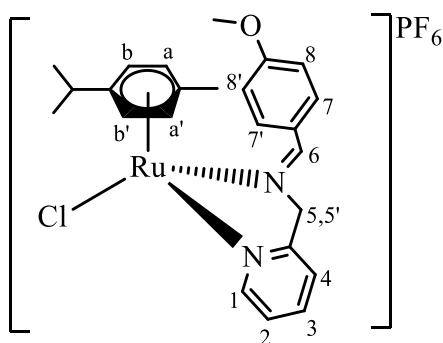
<sup>1</sup>H NMR (400 MHz, CD<sub>3</sub>CN) δ 8.83 (1H, s, H<sup>6</sup>), 8.61 (1H, d, *J* = 5.4 Hz, H<sup>1</sup>), 8.43 (2H, d, *J* = 9.0 Hz, H<sup>7</sup>, H<sup>7'</sup>), 8.06 (1H, td, *J* = 7.8 Hz, 1.4 Hz, H<sup>3</sup>), 7.71 (1H, d, *J* = 7.9 Hz, H<sup>4</sup>), 7.56 (1H, t, *J* = 6.6 Hz, H<sup>2</sup>), 7.10 (2H, d, *J* = 8.7 Hz, H<sup>8</sup>, H<sup>8'</sup>), 5.37 (1H, d, *J* = 17.6 Hz, H<sup>5</sup> or H<sup>5'</sup>), 5.22 (1H, d, *J* = 17.5 Hz, H<sup>5</sup> or H<sup>5'</sup>), 3.91 (3H, s, OCH<sub>3</sub>), 1.52 (15H, s, CH<sub>3</sub>(Cp\*)).

<sup>13</sup>C{<sup>1</sup>H} NMR (100 MHz, CD<sub>3</sub>CN) δ 173.1, 165.4, 152.1, 141.1, 135.1, 127.4, 124.5, 122.0, 115.2, 89.9 (C(Cp\*)), 75.4 (H<sup>6</sup>), 56.6 (OCH<sub>3</sub>), 9.1 (CH<sub>3</sub>(Cp\*)).

MS (ESI): *m/z* 589 [M]<sup>+</sup>.

IR (solid state): ν(C=N)<sub>imine</sub> 1603 cm<sup>-1</sup>

### Complex 4.16c-Anisyl



[RuCl<sub>2</sub>(p-Cym)]<sub>2</sub> (**4.14c**) (0.163 mmol, 100 mg), ligand **L4.16-Anisyl** (0.327 mmol, 74 mg) and KPF<sub>6</sub> (0.327 mmol, 60 mg) was allowed to stir in dry MeOH (7 ml) in the dark for 3 h to give complex *trans*-**4.16c-Anisyl** (golden brown solid 192 mg, 92 %).

#### *Trans*-**4.16c-Anisyl**

<sup>1</sup>H NMR (400 MHz, CDCl<sub>3</sub>) δ 8.93 (1H, d, *J* = 5.5 Hz, H<sup>1</sup>), 8.85 (1H, s, H<sup>6</sup>), 8.41 (2H, *J* = 8.7 Hz, H<sup>7</sup>, H<sup>7'</sup>), 7.88-7.83 (1H, td, m, H<sup>3</sup>), 7.47-7.42 (2H, m, H<sup>2</sup>, H<sup>4</sup>), 7.05 (2H, d, *J* = 8.7 Hz, H<sup>8</sup>, H<sup>8'</sup>), 5.60-5.51 (3H, m, H<sup>b</sup>, H<sup>b'</sup>, H<sup>5</sup>/H<sup>5'</sup>), 5.25 (1H, d, *J* = 18.9 Hz, H<sup>5</sup>/H<sup>5'</sup>), 5.20 (1H, d, *J* = 5.8 Hz, H<sup>a</sup>, H<sup>a'</sup>), 5.12 (1H, d, *J* = 18.9 Hz, H<sup>5</sup>/H<sup>5'</sup>), 3.92 (3H, s, OMe), 2.81 (1H, sept, *J* = 6.9 Hz, H<sup>9</sup>), 2.16 (3H, s, *p*-CH<sub>3</sub>(*p*-cym)), 1.26 (3H, d, *J* = 6.9 Hz, CH(CH<sub>3</sub>)<sub>2</sub>), 1.13 (3H, d, *J* = 6.9 Hz, CH(CH<sub>3</sub>)<sub>2</sub>).

<sup>13</sup>C NMR (100 MHz, CDCl<sub>3</sub>) δ 176.8, 163.4, 158.3, 154.5, 139.5, 133.5, 125.5, 125.7, 120.9, 114.3, 106.9, 101.2, 85.6, 85.4, 84.2, 83.4, 72.1, 55.7 (OCH<sub>3</sub>), 31.1 (CH(CH<sub>3</sub>)<sub>2</sub>), 22.2 (CH(CH<sub>3</sub>)<sub>2</sub>), 18.5 (CH(CH<sub>3</sub>)<sub>2</sub>).

**MS (ESI):** *m/z* 497 [M]<sup>+</sup>

**IR (solid state):** ν(C=N)<sub>imine</sub> 1598 cm<sup>-1</sup>

## 6.5 Bibliography

1. A. D. Becke, *J. Chem. Phys.*, 1997, **107**, 8554-8560.
2. C. Adamo and V. Barone, *J. Comput. Chem.*, 1998, **19**, 418-429.
3. C. Adamo and V. Barone, *J. Chem. Phys.*, 1999, **110**, 6158-6170.
4. Y. Zhao and D. G. Truhlar, *Theor. Chem. Acc.*, 2008, **120**, 215-241.
5. P. J. H. T. H. Dunning Jr., 1976.
6. D. Figgen, K. A. Peterson, M. Dolg and H. Stoll, *J. Chem. Phys.*, 2009, **130**, 164108.
7. R. Bauernschmitt and R. Ahlrichs, *J. Chem. Phys.*, 1996, **104**, 9047-9052.
8. J. S. Sears, T. Koerzdoerfer, C.-R. Zhang and J.-L. Brédas, *J. Chem. Phys.*, 2011, **135**, 151103.
9. E. R. Davidson, *Journal of Computational Physics*, 1975, **17**, 87-94.
10. J. Tomasi, B. Mennucci and R. Cammi, *Chem. Rev.*, 2005, **105**, 2999-3094.
11. J. Weber and G. Hohlneicher, *Molecular Physics*, 2003, **101**, 2125-2144.
12. F. Santoro, A. Lami, R. Improta and V. Barone, *J. Chem. Phys.*, 2007, **126**, 184102.
13. R. D. Gaussian 09, Frisch, M. J.; Trucks, G. W.; Schlegel, H. B.; Scuseria, G. E.; Robb, M. A.; Cheeseman, J. R.; Scalmani, G.; Barone, V.; Mennucci, B.; Petersson, G. A.; Nakatsuji, H.; Caricato, M.; Li, X.; Hratchian, H. P.; Izmaylov, A. F.; Bloino, J.; Zheng, G.; Sonnenberg, J. L.; Hada, M.; Ehara, M.; Toyota, K.; Fukuda, R.; Hasegawa, J.; Ishida, M.; Nakajima, T.; Honda, Y.; Kitao, O.; Nakai, H.; Vreven, T.; Montgomery, J. A., Jr.; Peralta, J. E.; Ogliaro, F.; Bearpark, M.; Heyd, J. J.; Brothers, E.; Kudin, K. N.; Staroverov, V. N.; Keith, T.; Kobayashi, R.; Normand, J.; Raghavachari, K.; Rendel, A.; Burant, J. C.; Iyengar, S. S.; Tomasi, J.; Cossi, M.; Rega, N.; Millam, J. M.; Klene, M.; Knox, J. E.; Cross, J. B.; Bakken, V.; Adamo, C.; Jaramillo, J.; Gomperts, R.; Stratmann, R. E.; Yazyev, O.; Austin, A. J.; Cammi, R.; Pomelli, C.; Ochterski, J. W.; Martin, R. L.; Morokuma, K.; Zakrzewski, V. G.; Voth, G. A.; Salvador, P.; Dannenberg, J. J.; Dapprich, S.; Daniels, A. D.; Farkas, O.; Foresman, J. B.; Ortiz, J. V.; Cioslowski, J.; Fox, D. J. Gaussian, Inc., Wallingford CT, 2013.

14. W. Kohn and L. J. Sham, *Physical Review*, 1965, **140**, A1133-A1138.
15. J. A. Pople, P. M. W. Gill and B. G. Johnson, *Chem. Phys. Lett.*, 1992, **199**, 557-560.
16. J. Tomasi, B. Mennucci and E. Cancès, *Journal of Molecular Structure: THEOCHEM*, 1999, **464**, 211-226.
17. G. Scalmani and M. J. Frisch, *J. Chem. Phys.*, 2010, **132**, 114110.
18. C. Adamo and V. Barone, *J. Chem. Phys.*, 1998, **108**, 664-675.
19. L. Goerigk and S. Grimme, *Journal of Chemical Theory and Computation*, 2011, **7**, 291-309.
20. S. E. Wheeler and K. N. Houk, *Journal of Chemical Theory and Computation*, 2010, **6**, 395-404.
21. R. G. Ball, W. A. G. Graham, D. M. Heinekey, J. K. Hoyano, A. D. McMaster, B. M. Mattson and S. T. Michel, *Inorg. Chem.*, 1990, **29**, 2023-2025.
22. J. Tönnemann, J. Risse, Z. Grote, R. Scopelliti and K. Severin, *Eur. J. Inorg. Chem.*, 2013, **2013**, 4558-4562.

## Crystallography Data for Chapter 2:

### Crystal data and structure refinement for 2.24a-*i*Pr

Identification code	13012
Empirical formula	C <sub>45</sub> H <sub>58</sub> Cl <sub>2</sub> Ir N <sub>3</sub> O
Formula weight	920.04
Temperature	150(2) K
Wavelength	0.71073 Å
Crystal system	Monoclinic
Space group	C2/c
Unit cell dimensions	$a = 27.764(14)$ Å $\alpha = 90^\circ$ $b = 14.918(8)$ Å $\beta = 98.371(9)^\circ$ $c = 18.083(9)$ Å $\gamma = 90^\circ$
Volume	7410(7) Å <sup>3</sup>
Z	8
Density (calculated)	1.649 Mg/m <sup>3</sup>
Absorption coefficient	3.790 mm <sup>-1</sup>
F(000)	3744
Crystal size	0.22 x 0.13 x 0.07 mm <sup>3</sup>
Theta range for data collection	1.48 to 26.00°.
Index ranges	-34 ≤ h ≤ 34, -18 ≤ k ≤ 18, -22 ≤ l ≤ 22
Reflections collected	28190
Independent reflections	7270 [R(int) = 0.1692]
Completeness to theta = 26.00°	99.7 %
Absorption correction	Empirical
Max. and min. transmission	0.831 and 0.520
Refinement method	Full-matrix least-squares on F <sup>2</sup>
Data / restraints / parameters	7270 / 348 / 363
Goodness-of-fit on F <sup>2</sup>	0.929
Final R indices [I > 2σ(I)]	R1 = 0.0725, wR2 = 0.1736
R indices (all data)	R1 = 0.1390, wR2 = 0.1918
Largest diff. peak and hole	2.313 and -2.543 e.Å <sup>-3</sup>

### Crystal data and structure refinement for 2.24a-Dipp

Identification code	13057
Empirical formula	C <sub>43</sub> H <sub>43</sub> Cl <sub>3</sub> Ir N <sub>3</sub> O <sub>2</sub>
Formula weight	932.35
Temperature	150(2) K
Wavelength	0.71073 Å
Crystal system	Triclinic
Space group	P-1
Unit cell dimensions	a = 9.460(3) Å      α = 90.953(5)°. b = 12.796(3) Å      β = 94.117(5)°. c = 15.498(4) Å      γ = 90.670(5)°.
Volume	1870.9(9) Å <sup>3</sup>
Z	2
Density (calculated)	1.655 Mg/m <sup>3</sup>
Absorption coefficient	3.825 mm <sup>-1</sup>
F(000)	932
Crystal size	0.32 x 0.10 x 0.04 mm <sup>3</sup>
Theta range for data collection	2.05 to 26.00°.
Index ranges	-11 ≤ h ≤ 11, -15 ≤ k ≤ 15, -19 ≤ l ≤ 19
Reflections collected	14864
Independent reflections	7274 [R(int) = 0.0710]
Completeness to theta = 26.00°	98.9 %
Absorption correction	Empirical
Max. and min. transmission	0.831 and 0.526
Refinement method	Full-matrix least-squares on F <sup>2</sup>
Data / restraints / parameters	7274 / 0 / 475
Goodness-of-fit on F <sup>2</sup>	0.888
Final R indices [I > 2σ(I)]	R1 = 0.0481, wR2 = 0.0780
R indices (all data)	R1 = 0.0648, wR2 = 0.0823
Largest diff. peak and hole	2.224 and -1.443 e.Å <sup>-3</sup>

### Crystal data and structure refinement for 2.24b-Dipp

Identification code	13059
Empirical formula	C <sub>38</sub> H <sub>37</sub> Cl <sub>3</sub> Ir N <sub>5</sub> O
Formula weight	878.28
Temperature	150(2) K
Wavelength	0.71073 Å
Crystal system	Triclinic
Space group	P-1
Unit cell dimensions	a = 9.447(4) Å      α = 84.814(7)°. b = 11.680(5) Å      β = 78.207(7)°. c = 16.245(7) Å      γ = 81.115(7)°.
Volume	1730.4(13) Å <sup>3</sup>
Z	2
Density (calculated)	1.686 Mg/m <sup>3</sup>
Absorption coefficient	4.129 mm <sup>-1</sup>
F(000)	872
Crystal size	0.29 x 0.20 x 0.10 mm <sup>3</sup>
Theta range for data collection	1.77 to 27.00°.
Index ranges	-11 ≤ h ≤ 12, -14 ≤ k ≤ 14, -20 ≤ l ≤ 20
Reflections collected	14776
Independent reflections	7431 [R(int) = 0.0487]
Completeness to theta = 27.00°	98.4 %
Absorption correction	Empirical
Max. and min. transmission	0.831 and 0.532
Refinement method	Full-matrix least-squares on F <sup>2</sup>
Data / restraints / parameters	7431 / 0 / 446
Goodness-of-fit on F <sup>2</sup>	0.969
Final R indices [I > 2σ(I)]	R1 = 0.0365, wR2 = 0.0715
R indices (all data)	R1 = 0.0439, wR2 = 0.0736
Largest diff. peak and hole	1.562 and -1.257 e.Å <sup>-3</sup>

### Crystallography Data for Chapter 3:

#### Crystal data and structure refinement for 3.27a-Ph

Identification code	16071
Empirical formula	C <sub>36</sub> H <sub>28</sub> Cl <sub>2</sub> Ir N <sub>3</sub> O
Formula weight	781.71
Temperature	150(2) K
Wavelength	0.71073 Å
Crystal system	Triclinic
Space group	P-1
Unit cell dimensions	a = 11.8861(18) Å    α = 99.502(3)° b = 12.1067(18) Å    β = 115.802(2)° c = 12.3851(18) Å    γ = 101.031(3)°
Volume	1511.4(4) Å <sup>3</sup>
Z	2
Density (calculated)	1.718 Mg/m <sup>3</sup>
Absorption coefficient	4.629 mm <sup>-1</sup>
F(000)	768
Crystal size	0.24 x 0.14 x 0.03 mm <sup>3</sup>
Theta range for data collection	1.79 to 26.00°.
Index ranges	-14 ≤ h ≤ 14, -14 ≤ k ≤ 14, -15 ≤ l ≤ 15
Reflections collected	11821
Independent reflections	5863 [R(int) = 0.0741]
Completeness to theta = 26.00°	98.6 %
Absorption correction	Empirical
Max. and min. transmission	0.831 and 0.601
Refinement method	Full-matrix least-squares on F <sup>2</sup>
Data / restraints / parameters	5863 / 0 / 388
Goodness-of-fit on F <sup>2</sup>	0.901
Final R indices [I > 2σ(I)]	R <sub>1</sub> = 0.0441, wR <sub>2</sub> = 0.0757
R indices (all data)	R <sub>1</sub> = 0.0609, wR <sub>2</sub> = 0.0805
Largest diff. peak and hole	2.312 and -1.345 e.Å <sup>-3</sup>

**Crystal data and structure refinement for 3.27b-Ph**

Identification code	14027
Empirical formula	C <sub>32</sub> H <sub>28</sub> Ir N <sub>5</sub> O <sub>2</sub>
Formula weight	706.79
Temperature	150(2) K
Wavelength	0.71073 Å
Crystal system	Triclinic
Space group	P-1
Unit cell dimensions	a = 10.127(4) Å      α = 67.803(7)° b = 11.923(5) Å      β = 86.309(7)° c = 12.173(5) Å      γ = 81.424(7)°
Volume	1345.7(9) Å <sup>3</sup>
Z	2
Density (calculated)	1.744 Mg/m <sup>3</sup>
Absorption coefficient	5.001 mm <sup>-1</sup>
F(000)	696
Crystal size	0.37 x 0.20 x 0.04 mm <sup>3</sup>
Theta range for data collection	1.81 to 27.00°.
Index ranges	-12 ≤ h ≤ 12, -15 ≤ k ≤ 15, -15 ≤ l ≤ 15
Reflections collected	11412
Independent reflections	5783 [R(int) = 0.0611]
Completeness to theta = 27.00°	98.4 %
Absorption correction	Empirical
Max. and min. transmission	0.831 and 0.545
Refinement method	Full-matrix least-squares on F <sup>2</sup>
Data / restraints / parameters	5783 / 0 / 363
Goodness-of-fit on F <sup>2</sup>	0.958
Final R indices [I > 2σ(I)]	R1 = 0.0401, wR2 = 0.0808
R indices (all data)	R1 = 0.0489, wR2 = 0.0834
Largest diff. peak and hole	2.107 and -1.346 e.Å <sup>-3</sup>

### Crystal data and structure refinement for 3.27a-Mes

Identification code	17073
Empirical formula	C <sub>40</sub> H <sub>40</sub> Ir N <sub>3</sub> O <sub>3</sub>
Formula weight	802.95
Temperature	150(2) K
Wavelength	0.71073 Å
Crystal system	Monoclinic
Space group	P2(1)/c
Unit cell dimensions	a = 9.958(4) Å      α = 90° b = 29.451(11) Å    β = 108.267(7)° c = 12.218(5) Å     γ = 90°
Volume	3403(2) Å <sup>3</sup>
Z	4
Density (calculated)	1.567 Mg/m <sup>3</sup>
Absorption coefficient	3.966 mm <sup>-1</sup>
F(000)	1608
Crystal size	0.45 x 0.12 x 0.11 mm <sup>3</sup>
Theta range for data collection	1.38 to 26.00°.
Index ranges	-12 ≤ h ≤ 12, -36 ≤ k ≤ 35, -15 ≤ l ≤ 14
Reflections collected	26230
Independent reflections	6686 [R(int) = 0.0871]
Completeness to theta = 26.00°	100.0 %
Absorption correction	Empirical
Max. and min. transmission	0.837 and 0.378
Refinement method	Full-matrix least-squares on F <sup>2</sup>
Data / restraints / parameters	6686 / 0 / 431
Goodness-of-fit on F <sup>2</sup>	1.013
Final R indices [I > 2σ(I)]	R1 = 0.0524, wR2 = 0.1180
R indices (all data)	R1 = 0.0702, wR2 = 0.1246
Largest diff. peak and hole	4.206 and -2.006 e.Å <sup>-3</sup>

### Crystal data and structure refinement for 3.27b-Mes

Identification code	15132
Empirical formula	C <sub>36</sub> H <sub>36</sub> Cl <sub>2</sub> Ir N <sub>5</sub> O <sub>2</sub>
Formula weight	833.80
Temperature	150(2) K
Wavelength	0.71073 Å
Crystal system	Monoclinic
Space group	P2(1)/n
Unit cell dimensions	a = 9.538(2) Å      α = 90° b = 20.994(5) Å      β = 100.615(4)° c = 16.903(4) Å      γ = 90°
Volume	3326.9(15) Å <sup>3</sup>
Z	4
Density (calculated)	1.665 Mg/m <sup>3</sup>
Absorption coefficient	4.215 mm <sup>-1</sup>
F(000)	1656
Crystal size	0.31 x 0.13 x 0.05 mm <sup>3</sup>
Theta range for data collection	1.56 to 27.00°.
Index ranges	-12 ≤ h ≤ 12, -26 ≤ k ≤ 25, -21 ≤ l ≤ 21
Reflections collected	27529
Independent reflections	7238 [R(int) = 0.0604]
Completeness to theta = 27.00°	99.6 %
Absorption correction	Empirical
Max. and min. transmission	0.831 and 0.519
Refinement method	Full-matrix least-squares on F <sup>2</sup>
Data / restraints / parameters	7238 / 0 / 420
Goodness-of-fit on F <sup>2</sup>	0.942
Final R indices [I > 2σ(I)]	R1 = 0.0294, wR2 = 0.0590
R indices (all data)	R1 = 0.0379, wR2 = 0.0606
Largest diff. peak and hole	1.671 and -0.940 e.Å <sup>-3</sup>

### Crystal data and structure refinement for 3.27b-Anisyl

Identification code	16159
Empirical formula	C <sub>33</sub> H <sub>30</sub> Ir N <sub>5</sub> O <sub>3</sub>
Formula weight	736.82
Temperature	150(2) K
Wavelength	0.71073 Å
Crystal system	Triclinic
Space group	P-1
Unit cell dimensions	a = 9.8638(14) Å     α = 76.416(2)° b = 12.3440(17) Å     β = 83.976(2)° c = 12.6954(18) Å     γ = 67.643(2)°
Volume	1389.4(3) Å <sup>3</sup>
Z	2
Density (calculated)	1.761 Mg/m <sup>3</sup>
Absorption coefficient	4.850 mm <sup>-1</sup>
F(000)	728
Crystal size	0.12 x 0.10 x 0.05 mm <sup>3</sup>
Theta range for data collection	1.65 to 27.00°.
Index ranges	-12 ≤ h ≤ 12, -15 ≤ k ≤ 15, -15 ≤ l ≤ 16
Reflections collected	11860
Independent reflections	5972 [R(int) = 0.0517]
Completeness to theta = 27.00°	98.4 %
Absorption correction	Empirical
Max. and min. transmission	0.831 and 0.678
Refinement method	Full-matrix least-squares on F <sup>2</sup>
Data / restraints / parameters	5972 / 0 / 382
Goodness-of-fit on F <sup>2</sup>	0.879
Final R indices [I > 2σ(I)]	R1 = 0.0358, wR2 = 0.0578
R indices (all data)	R1 = 0.0445, wR2 = 0.0600
Largest diff. peak and hole	1.608 and -1.290 e.Å <sup>-3</sup>

## Crystallography Data for Chapter 4:

### Crystal data and structure refinement for *trans*-4.15a-Cinnamyl

Identification code	17021
Empirical formula	C <sub>26</sub> H <sub>29</sub> Cl <sub>3</sub> Ir N O
Formula weight	670.05
Temperature	150(2) K
Wavelength	0.71073 Å
Crystal system	Monoclinic
Space group	P2(1)/c
Unit cell dimensions	a = 11.149(3) Å      α = 90° b = 14.086(4) Å      β = 106.890(5)° c = 17.208(5) Å      γ = 90°
Volume	2585.9(12) Å <sup>3</sup>
Z	4
Density (calculated)	1.721 Mg/m <sup>3</sup>
Absorption coefficient	5.492 mm <sup>-1</sup>
F(000)	1312
Crystal size	0.29 x 0.16 x 0.13 mm <sup>3</sup>
Theta range for data collection	1.90 to 26.99°.
Index ranges	-14 ≤ h ≤ 14, -17 ≤ k ≤ 17, -21 ≤ l ≤ 21
Reflections collected	21311
Independent reflections	5643 [R(int) = 0.0778]
Completeness to theta = 26.99°	99.9 %
Absorption correction	Empirical
Max. and min. transmission	0.831 and 0.505
Refinement method	Full-matrix least-squares on F <sup>2</sup>
Data / restraints / parameters	5643 / 0 / 294
Goodness-of-fit on F <sup>2</sup>	0.926
Final R indices [I > 2σ(I)]	R1 = 0.0394, wR2 = 0.0705
R indices (all data)	R1 = 0.0559, wR2 = 0.0744
Largest diff. peak and hole	2.086 and -0.912 e.Å <sup>-3</sup>

**Crystal data and structure refinement for *trans*-4.15c-Mes**

Identification code	16057
Empirical formula	C <sub>26</sub> H <sub>30</sub> Cl N O Ru
Formula weight	509.03
Temperature	150(2) K
Wavelength	0.71073 Å
Crystal system	Triclinic
Space group	P-1
Unit cell dimensions	a = 10.872(3) Å      α = 63.706(6)° b = 11.742(3) Å      β = 65.681(5)° c = 11.824(3) Å      γ = 62.832(5)°
Volume	1161.6(5) Å <sup>3</sup>
Z	2
Density (calculated)	1.455 Mg/m <sup>3</sup>
Absorption coefficient	0.807 mm <sup>-1</sup>
F(000)	524
Crystal size	0.19 x 0.10 x 0.07 mm <sup>3</sup>
Theta range for data collection	1.99 to 26.00°.
Index ranges	-13 ≤ h ≤ 13, -14 ≤ k ≤ 14, -14 ≤ l ≤ 14
Reflections collected	9162
Independent reflections	4517 [R(int) = 0.1400]
Completeness to theta = 26.00°	98.7 %
Absorption correction	Empirical
Max. and min. transmission	0.831 and 0.542
Refinement method	Full-matrix least-squares on F <sup>2</sup>
Data / restraints / parameters	4517 / 2 / 287
Goodness-of-fit on F <sup>2</sup>	0.730
Final R indices [I > 2σ(I)]	R1 = 0.0655, wR2 = 0.0953
R indices (all data)	R1 = 0.1622, wR2 = 0.1149
Largest diff. peak and hole	0.506 and -0.616 e.Å <sup>-3</sup>

**Crystal data and structure refinement for *cis*-4.15c-Mes**

Identification code	16004
Empirical formula	C <sub>26</sub> H <sub>30</sub> Cl N O Ru
Formula weight	509.03
Temperature	150(2) K
Wavelength	0.71073 Å
Crystal system	Orthorhombic
Space group	P2(1)2(1)2(1)
Unit cell dimensions	a = 7.231(8) Å      α = 90° b = 9.182(10) Å     β = 90° c = 34.27(4) Å      γ = 90°
Volume	2275(4) Å <sup>3</sup>
Z	4
Density (calculated)	1.486 Mg/m <sup>3</sup>
Absorption coefficient	0.824 mm <sup>-1</sup>
F(000)	1048
Crystal size	0.25 x 0.09 x 0.08 mm <sup>3</sup>
Theta range for data collection	2.30 to 26.00°.
Index ranges	-8<=h<=8, -11<=k<=7, -33<=l<=42
Reflections collected	10736
Independent reflections	4350 [R(int) = 0.3263]
Completeness to theta = 26.00°	98.8 %
Absorption correction	Empirical
Max. and min. transmission	0.831 and 0.184
Refinement method	Full-matrix least-squares on F <sup>2</sup>
Data / restraints / parameters	4350 / 304 / 277
Goodness-of-fit on F <sup>2</sup>	0.993
Final R indices [I>2sigma(I)]	R1 = 0.1156, wR2 = 0.2408
R indices (all data)	R1 = 0.1738, wR2 = 0.2743
Absolute structure parameter	0.35(14)
Largest diff. peak and hole	1.245 and -1.265 e.Å <sup>-3</sup>

**Crystal data and structure refinement for *trans*-4.15c-Anisyl**

Identification code	17016
Empirical formula	C <sub>24</sub> H <sub>26</sub> Cl N O <sub>2</sub> Ru
Formula weight	496.98
Temperature	150(2) K
Wavelength	0.71073 Å
Crystal system	Triclinic
Space group	P-1
Unit cell dimensions	a = 10.998(2) Å      α = 95.326(4)° b = 11.559(3) Å      β = 98.871(4)° c = 17.337(4) Å      γ = 94.441(4)°
Volume	2158.9(8) Å <sup>3</sup>
Z	4
Density (calculated)	1.529 Mg/m <sup>3</sup>
Absorption coefficient	0.870 mm <sup>-1</sup>
F(000)	1016
Crystal size	0.31 x 0.20 x 0.04 mm <sup>3</sup>
Theta range for data collection	1.78 to 26.00°.
Index ranges	-13 ≤ h ≤ 13, -14 ≤ k ≤ 14, -21 ≤ l ≤ 21
Reflections collected	16986
Independent reflections	8391 [R(int) = 0.0612]
Completeness to theta = 26.00°	98.8 %
Absorption correction	Empirical
Max. and min. transmission	0.831 and 0.580
Refinement method	Full-matrix least-squares on F <sup>2</sup>
Data / restraints / parameters	8391 / 0 / 531
Goodness-of-fit on F <sup>2</sup>	0.892
Final R indices [I > 2σ(I)]	R1 = 0.0448, wR2 = 0.0793
R indices (all data)	R1 = 0.0666, wR2 = 0.0851
Largest diff. peak and hole	0.738 and -0.720 e.Å <sup>-3</sup>

**Crystal data and structure refinement for *cis*-4.15c-Anisyl**

Identification code	17020
Empirical formula	C <sub>24</sub> H <sub>26</sub> Cl N O <sub>2</sub> Ru
Formula weight	496.98
Temperature	150(2) K
Wavelength	0.71073 Å
Crystal system	Monoclinic
Space group	P2(1)/c
Unit cell dimensions	a = 11.400(5) Å      α = 90° b = 18.787(8) Å      β = 102.573(8)° c = 10.384(5) Å      γ = 90°
Volume	2170.6(16) Å <sup>3</sup>
Z	4
Density (calculated)	1.521 Mg/m <sup>3</sup>
Absorption coefficient	0.865 mm <sup>-1</sup>
F(000)	1016
Crystal size	0.24 x 0.22 x 0.17 mm <sup>3</sup>
Theta range for data collection	1.83 to 26.00°.
Index ranges	-14 ≤ h ≤ 14, -23 ≤ k ≤ 22, -12 ≤ l ≤ 12
Reflections collected	16770
Independent reflections	4263 [R(int) = 0.1545]
Completeness to theta = 26.00°	99.9 %
Absorption correction	Empirical
Max. and min. transmission	0.831 and 0.383
Refinement method	Full-matrix least-squares on F <sup>2</sup>
Data / restraints / parameters	4263 / 0 / 266
Goodness-of-fit on F <sup>2</sup>	0.925
Final R indices [I > 2σ(I)]	R1 = 0.0631, wR2 = 0.1106
R indices (all data)	R1 = 0.1191, wR2 = 0.1253
Largest diff. peak and hole	0.823 and -0.808 e.Å <sup>-3</sup>

## Postgraduate Activities

### Internal Seminars

- 17<sup>th</sup> December 2014 “*Chemoselective Cross-coupling*” by Dr Allan Watson (University of Strathclyde)
- 28<sup>th</sup> January 2015 “*Electronic Energy Transfer in the Context of Artificial Light-Harvesting Antennae*” by Prof Anthony Harriman (Newcastle University)
- 11<sup>th</sup> September 2015 “*Bright Aspects of Lanthanide Luminescence*” by Prof Jean-Claude Bünzli (Switzerland)
- 2<sup>nd</sup> December 2015 “*New Directions in Catalysis - From Biofuels to Self-Healing Aeroplanes*” by Prof Duncan Wass (University of Bristol)
- 18<sup>th</sup> May 2016 “*Ultrafast Spectroscopy to Measure Molecular Dynamics in Photochemistry and Photobiology*” by Prof Steve Meech (University of East Anglia)
- 25<sup>th</sup> May 2016 “*Metal-organic framework composites and capsules with enhanced properties*” by Dr Darren Bradshaw (University of Southampton)
- 5<sup>th</sup> October 2016 “*Development of radiotracers for PET imaging: from molecular design to production*” by Prof S. J. Archibald (University of Hull)

### Internal Symposia

- 17<sup>th</sup> July 2014 Postgraduate Research Symposia 2014, University of Leicester (Attended)
- 23<sup>rd</sup> January 2015 One Day Symposium on Catalytic C-H Functionalization, University of Leicester (Attended)
- 5<sup>th</sup> April 2017 RSC Organic Division Midlands Meeting 2017, University of Leicester  
Posted presented: “*Elucidating the Origins of EPESS in Cyclometallated Ir(III) Complexes*”
- 4<sup>th</sup> July 2017 Postgraduate Research Symposia 2017, University of Leicester  
Oral presentation: “*Photophysical Properties of Imines in Ir(III) and Ru(II) Complexes*”

## External Symposia

16<sup>th</sup> – 20<sup>th</sup> June 2014

3<sup>rd</sup> Dalton Summer School on Electronic Structural Methods in Inorganic Chemistry, University of Edinburgh

Poster presented: *“Investigations into the cause of Enhanced Phosphorescence Emission in the Solid State (EPESS)”*

20<sup>th</sup> – 21<sup>st</sup> April 2015

*Southern Dalton Meeting*, University of Sussex, Brighton

Poster presented: *“Investigations into the cause of Enhanced Phosphorescence Emission in the Solid State (EPESS)”*

18<sup>th</sup> – 19<sup>th</sup> April 2016

Molecular Photophysics Conference II, University of Newcastle

Poster presented: *“Solid state Luminescence vs Photoisomerisation in Cyclometallated Ir(III) Complexes”*

(Awarded Best Oral Presentation)

16<sup>th</sup> – 17<sup>th</sup> March 2017

York Photochemistry Symposium, University of York

Poster presented: *“Elucidating the Origin of EPESS in Iridium(III) Complexes”*